

Award Number: W81XWH-20-1-0117

TITLE: The Use of High-Quality Chemical Tools to Rescue TBK1 Function and Identify Novel ATP-Competitive Targets in ALS

PRINCIPAL INVESTIGATOR: Dr. Alison Axtman, Ph.D.

CONTRACTING ORGANIZATION: University of North Carolina at Chapel Hill

REPORT DATE: MAY 2022

TYPE OF REPORT: ANNUAL

PREPARED FOR: U.S. Army Medical Research and Development Command  
Fort Detrick, Maryland 21702-5012

DISTRIBUTION STATEMENT: Approved for Public Release;  
Distribution Unlimited

The views, opinions and/or findings contained in this report are those of the author(s) and should not be construed as an official Department of the Army position, policy or decision unless so designated by other documentation.

<b>REPORT DOCUMENTATION PAGE</b>			<i>Form Approved</i> <i>OMB No. 0704-0188</i>		
Public reporting burden for this collection of information is estimated to average 1 hour per response, including the time for reviewing instructions, searching existing data sources, gathering and maintaining the data needed, and completing and reviewing this collection of information. Send comments regarding this burden estimate or any other aspect of this collection of information, including suggestions for reducing this burden to Department of Defense, Washington Headquarters Services, Directorate for Information Operations and Reports (0704-0188), 1215 Jefferson Davis Highway, Suite 1204, Arlington, VA 22202-4302. Respondents should be aware that notwithstanding any other provision of law, no person shall be subject to any penalty for failing to comply with a collection of information if it does not display a currently valid OMB control number. <b>PLEASE DO NOT RETURN YOUR FORM TO THE ABOVE ADDRESS.</b>					
<b>1. REPORT DATE</b> MAY 2022		<b>2. REPORT TYPE</b> Annual Report		<b>3. DATES COVERED</b> 1 April 2021 – 31 MARCH 2022	
<b>4. TITLE AND SUBTITLE</b>  The Use of High-Quality Chemical Tools to Rescue TBK1 Function and Identify Novel ATP-Competitive Targets in ALS			<b>5a. CONTRACT NUMBER</b>		
			<b>5b. GRANT NUMBER</b> W81XWH-20-1-0117		
			<b>5c. PROGRAM ELEMENT NUMBER</b>		
<b>6. AUTHOR(S)</b> Alison Axtman, Thomas Durcan, Lenore Beitel, Sarah Lépine  E-Mail: alison.axtman@unc.edu			<b>5d. PROJECT NUMBER</b>		
			<b>5e. TASK NUMBER</b>		
			<b>5f. WORK UNIT NUMBER</b>		
<b>7. PERFORMING ORGANIZATION NAME(S) AND ADDRESS(ES)</b>  University of North Carolina at Chapel Hill Chapel Hill, NC 27599-5023  McGill University Montreal, Quebec, Canada H3A 0G4			<b>8. PERFORMING ORGANIZATION REPORT NUMBER</b>		
<b>9. SPONSORING / MONITORING AGENCY NAME(S) AND ADDRESS(ES)</b>  U.S. Army Medical Research and Development Command Fort Detrick, Maryland 21702-5012			<b>10. SPONSOR/MONITOR'S ACRONYM(S)</b>		
			<b>11. SPONSOR/MONITOR'S REPORT NUMBER(S)</b>		
<b>12. DISTRIBUTION / AVAILABILITY STATEMENT</b> Approved for Public Release; Distribution Unlimited					
<b>13. SUPPLEMENTARY NOTES</b>					
<b>14. ABSTRACT</b> We are developing chemical tools and biological reagents to interrogate the regulation of kinase-mediated biological pathways as new avenues to reduce the accumulation of toxic protein aggregates in ALS. TDP-43 is the most commonly misfolded and deposited protein in ALS. Failure of the autophagy system is one mechanism that allows proteins like TDP-43 to accrue in aggregates. TBK1 is a human protein kinase that plays an essential role in autophagy and which, through multiple genetic studies, has been confirmed as a protein that exhibits inactivating mutations in ALS patients. We have identified linkable compounds that potently engage TBK1 in cells and several putative TRAF3-recruiting ligands. These are currently being covalently linked to produce the first TBK1-activating activation-targeting chimera (ATTACs). As an alternative approach, we have identified the chemical probes from two distinct chemical series that inhibit casein kinase 2 (CK2), which indirectly activates TBK1. We have and will continue to improve the physical properties of SGC-CK2-1 (from series 1) to make it suitable for <i>in vivo</i> use. In parallel, we have designed and are preparing a CK2 degrader based on these two scaffolds. Furthermore, through development of a novel TDP-43 aggregation assay in stem cell-derived motor neurons, we aim to identify protein kinases that, when modulated, reduce the deposition and/or promote the clearance of misfolded proteins. We have generated motor neurons harboring ALS-relevant mutant TDP-43 and characterized expression of mutant versus wild-type (WT) TDP-43 during differentiation as well as viability of these cells. We have also developed a methodology to quantify the nuclear to cytoplasmic translocation of TDP-43. We have confirmed that mutations in TDP-43 elicit subtle changes in its translocation propensity and phosphorylation.					
<b>15. SUBJECT TERMS</b> ALS, TDP-43, iPSC, TRAF3, TBK1, ATTAC, CK2, chemical probe, CX-4945, pyrazolopyrimidine, naphthyridine					
<b>16. SECURITY CLASSIFICATION OF:</b>			<b>17. LIMITATION OF ABSTRACT</b>	<b>18. NUMBER OF PAGES</b>	<b>19a. NAME OF RESPONSIBLE PERSON</b> USAMRDC
<b>a. REPORT</b> U	<b>b. ABSTRACT</b> U	<b>c. THIS PAGE</b> U			<b>19b. TELEPHONE NUMBER</b> (include area code)
			UU	88	

## Table of Contents

	<u>Page</u>
Introduction.....	4
Body.....	5
Key Research Accomplishments.....	13
Reportable Outcomes.....	15
Conclusion.....	17
References.....	18
Appendices.....	20

# 1, INTRODUCTION

Accumulation of protein and RNA aggregates is a hallmark in amyotrophic lateral sclerosis (ALS) pathology. Misfolded wild-type (WT) and mutant proteins deposit and form aggregates that are toxic to motor neurons (MNs) in ALS patients. The most common protein found in inclusions within the cytoplasm of MNs from ALS patients is transactive response DNA-binding protein 43 (TDP-43).<sup>1</sup> Although only 2% of familial ALS cases are linked to mutations in the TDP-43 gene (TARDBP), TDP-43 positive inclusions are found in nearly 97% of ALS patients, irrespective of whether their disease is familial or sporadic.<sup>2</sup> Protein aggregation is exacerbated in ALS by failure of the autophagy system, allowing accumulation rather than clearance of aggregates. The pathology associated with impaired autophagy in ALS progression supports that identification of target proteins that regulate autophagy would be of therapeutic interest. Loss-of-function mutations in TANK-binding kinase (TBK1) are genetically linked with ALS.<sup>1, 3</sup> TBK1, which is highly expressed in neurons, plays essential roles in both innate immunity and autophagy. Studies related to TBK1 function, pathological findings, and known pathogenic mechanisms in ALS support that autophagy is the major pathway impacted by TBK1 mutations and that targeting this kinase could modify ALS pathology.<sup>3</sup> Chemical tools capable of rescuing or activating TBK1 function, either through directly acting on TBK1 or indirectly modulating TBK1 via inhibition of casein kinase 2 (CK2), could therefore represent novel ALS therapeutics. Through a parallel, unbiased strategy, a small molecule that reduces translocation and/or seeding of TDP-43 in MNs could enable identification of essential aggregation regulators. Targeting protein aggregation and/or autophagy is a novel therapeutic approach for ALS. If successful, this approach would alter the course of disease and slow its progression.

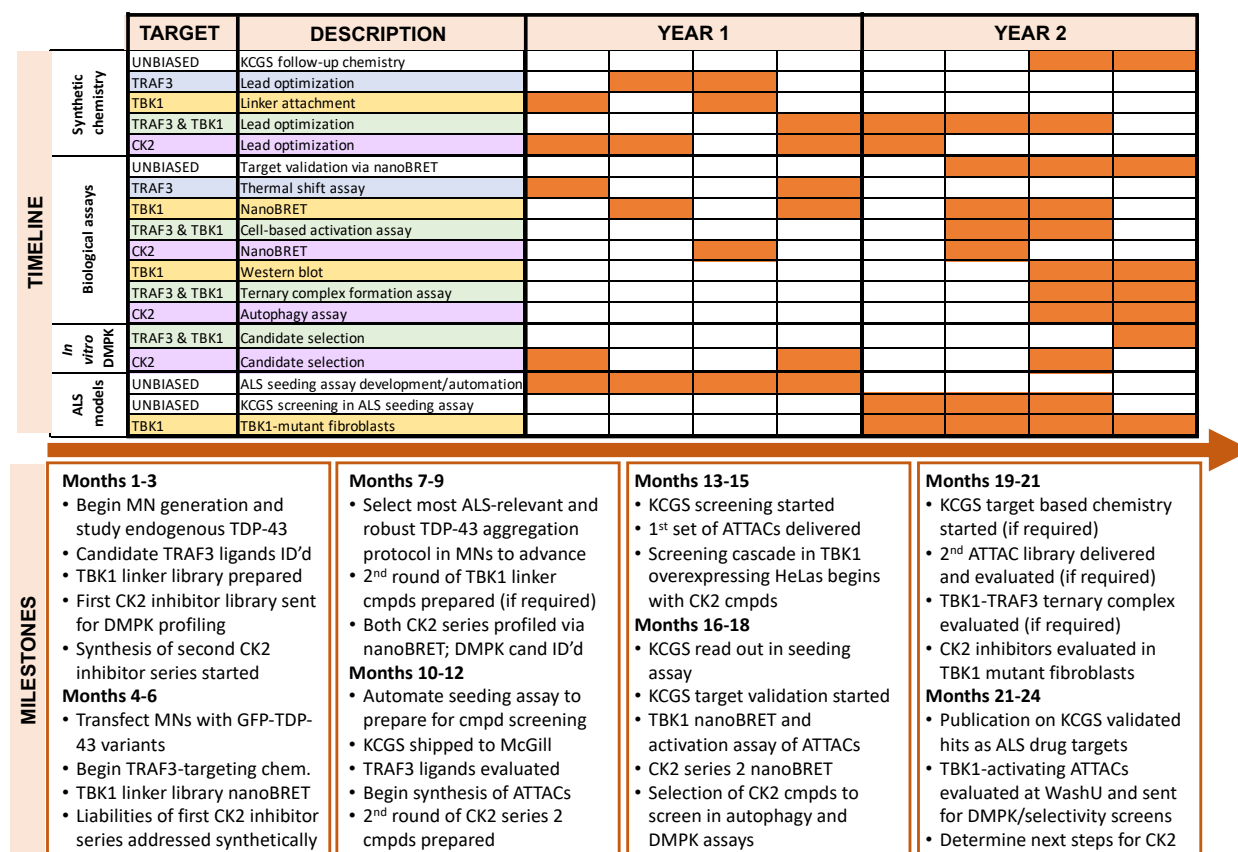


Figure 1. Timelines and milestones for entire award period.

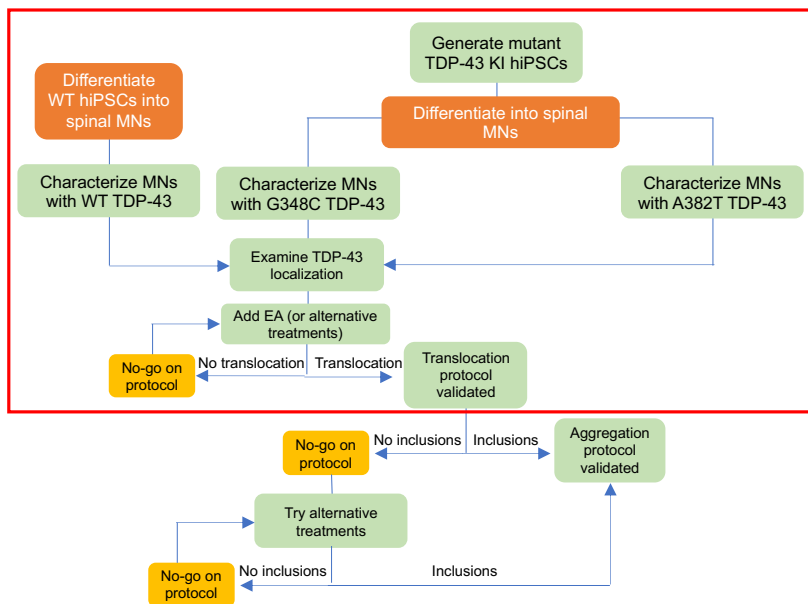


**2. KEYWORDS:**ALS, TDP-43, iPSC, TRAF3, TBK1, ATTAC, CK2, chemical probe, CX-4945, pyrazolopyrimidine, naphthyridine

**BODY**

**3. ACCOMPLISHMENTS, 4. IMPACT, and 5. CHANGES/PROBLEMS:**

In our grant proposal we set out to accomplish the following **Hypothesis or Objective:** *Successful completion of this project will yield several key compounds and biological assays that target essential proteins in ALS-propagating pathways. Discovery of previously untapped biological targets as well as pre-clinical candidates that reduce protein aggregation provide potential to offer new ALS treatment options.* We defined specific aims to enable delivery of the chemical and biological reagents. Our progress can be framed in terms of these aims as well as a defined timeline/milestone Gantt chart provided in the grant proposal (Figure 1).

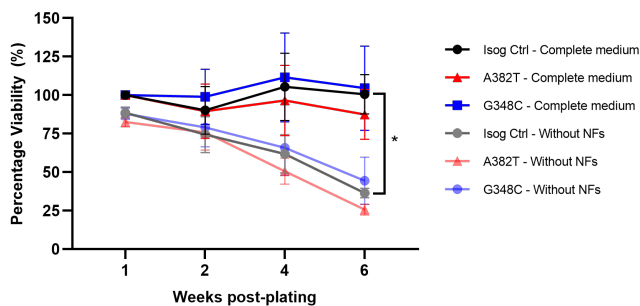


**Aim 1. Screen kinase chemogenomic set (KCGS) to identify new ATP-binding protein targets that reduce seeding of protein aggregates.** In addition to the design and profiling of targeted small molecules in Aims 2 and 3, we will screen our curated set of 188 potent and narrowly selective kinase inhibitors known as KCGS (Kinase Chemogenomic Set). Details related to the development and kinome coverage of KCGS were published during year one of the award period.<sup>4, 5</sup> We plan to screen KCGS in newly developed assays that examine whether TDP-43 translocation and/or aggregation is impacted

**Figure 2.** Aim 2 decision tree with current progress boxed in red, edits to the original workflow in light green boxes

by small molecule kinase inhibitors. Further work on these assays has been one of the focus areas for the second year of the award period.

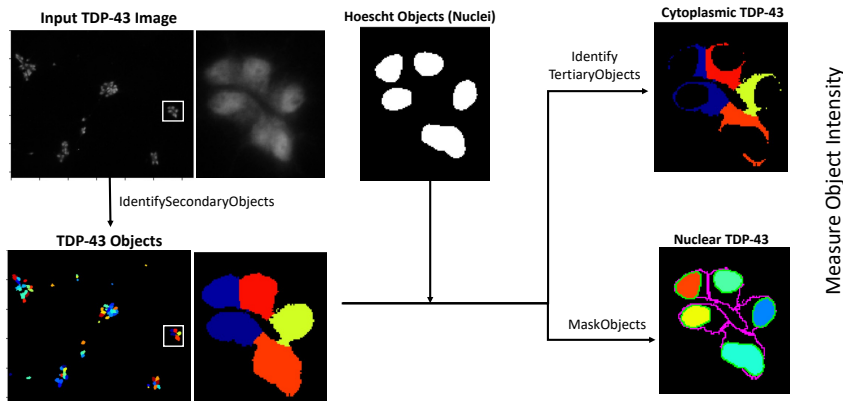
As shown in Figure 2, we have continued to work toward establishment of a TDP-43



**Figure 3.** Glutamate-induced excitotoxicity assay to assess neuronal viability in culture with and without growth factors present (n = 4).

aggregation assay and modified a few steps along the way. Instead of working with GFP-labeled wild-type (WT) or mutant TDP-43, we have opted to use antibodies to visualize unmodified TDP-43. To accomplish this, we knocked-in mutant TDP-43 (G348C or A382T) into human induced pluripotent stem cells (hiPSCs) and differentiated them into spinal MNs and differentiated WT hiPSCs in parallel. During differentiation, cells were stained and analyzed via qPCR for markers of differentiation and imaged for their ability to

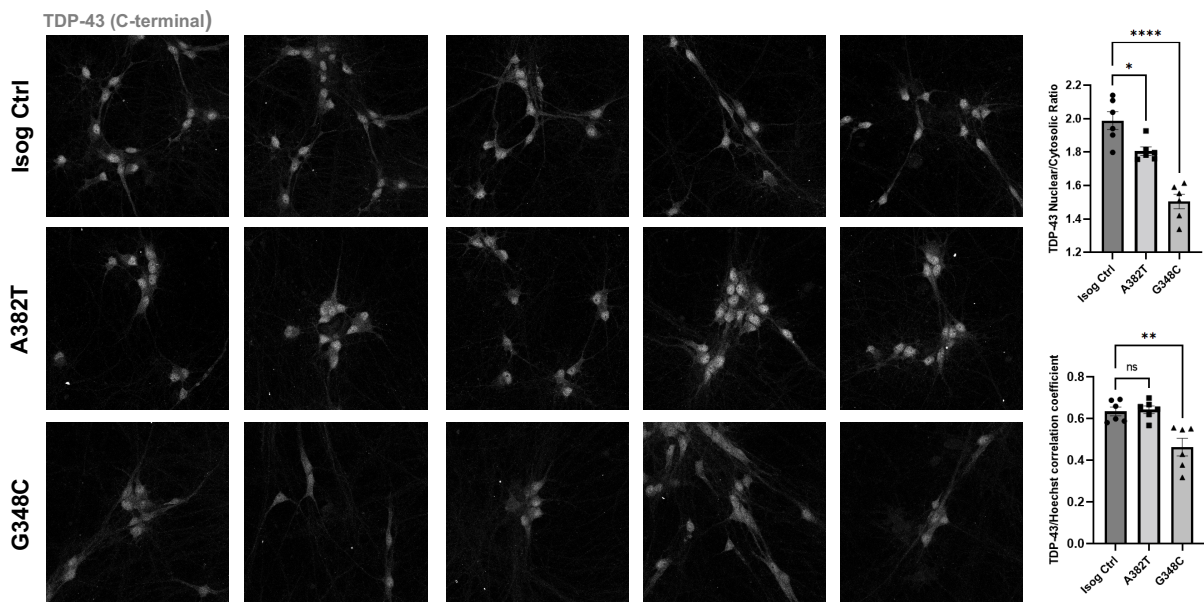
form neuronal networks. TDP-43 transcript and protein levels were also analyzed to look for differences, including in the soluble and insoluble fractions. No differences in WT and mutant TDP-43 expression were noted across genotypes and developmental stages. Moreover, no discernible changes in neuronal viability were observed up to six weeks in culture in the presence or absence of growth factors (Figure 3).



**Figure 4.** Pipeline to quantify TDP-43 translocation.

Next, we monitored localization of TDP-43 in fully differentiated MNs. TDP-43 predominantly resides within the nucleus, binds both DNA and RNA, and plays roles in RNA stabilization, splicing and translational regulation.<sup>6</sup> In ALS, however, TDP-43 translocates from the nucleus into the cytoplasm where it becomes a predominant component of ubiquitinated inclusions.<sup>7, 8</sup>

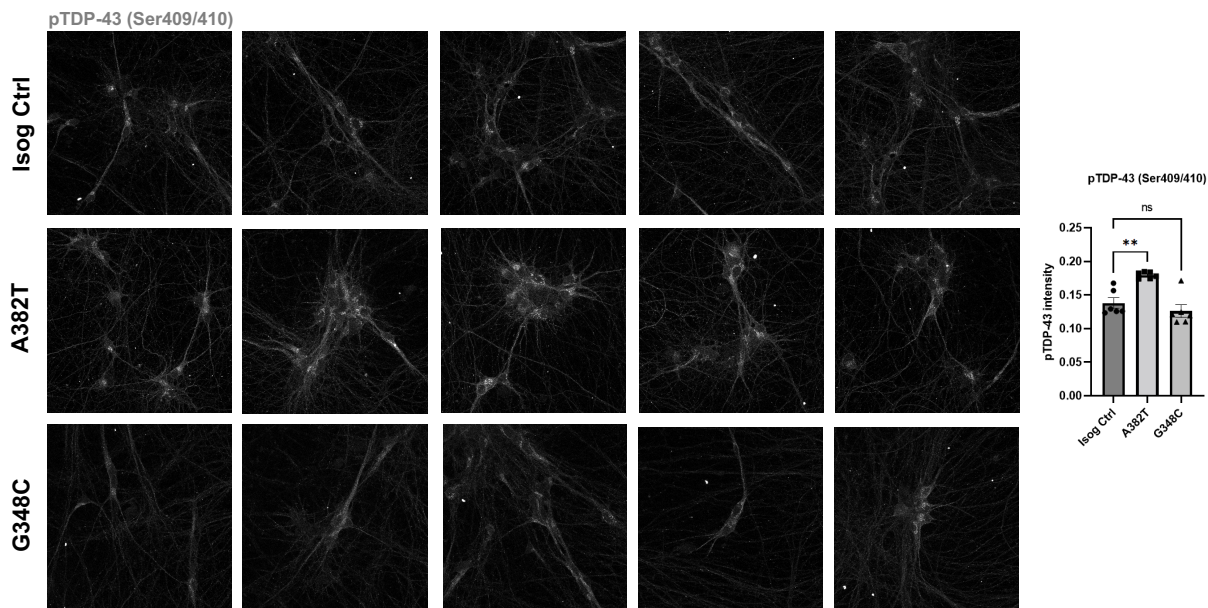
Since TDP-43 mutations are rare, mechanisms like oxidative stress have been implicated as drivers of this nuclear to cytoplasmic translocation.<sup>9</sup> We imaged the localization of WT and mutant TDP-43 with N- and C-terminal antibodies and found both to reside almost exclusively in the nucleus. In our hands, treatment of MNs with ethacrynic acid (EA) induced some TDP-43 translocation (also referred to as mislocalization). No toxicity and some translocation were observed following a 5-hour dose-response (30, 50, and 70  $\mu$ M) EA treatment at these concentrations. Diminished bright nuclear staining induced by EA treatment was interpreted to correlate with TDP-43 moving into the cytoplasm. We also assessed TDP-43 phosphorylation using antibodies for phosphorylated TDP-43, allowing us to quantify phospho-TDP-43 mean intensity and total phospho-TDP-43-positive puncta.



Plotted Mean  $\pm$  SEM, N=1, Individual dots represent the per-image mean values

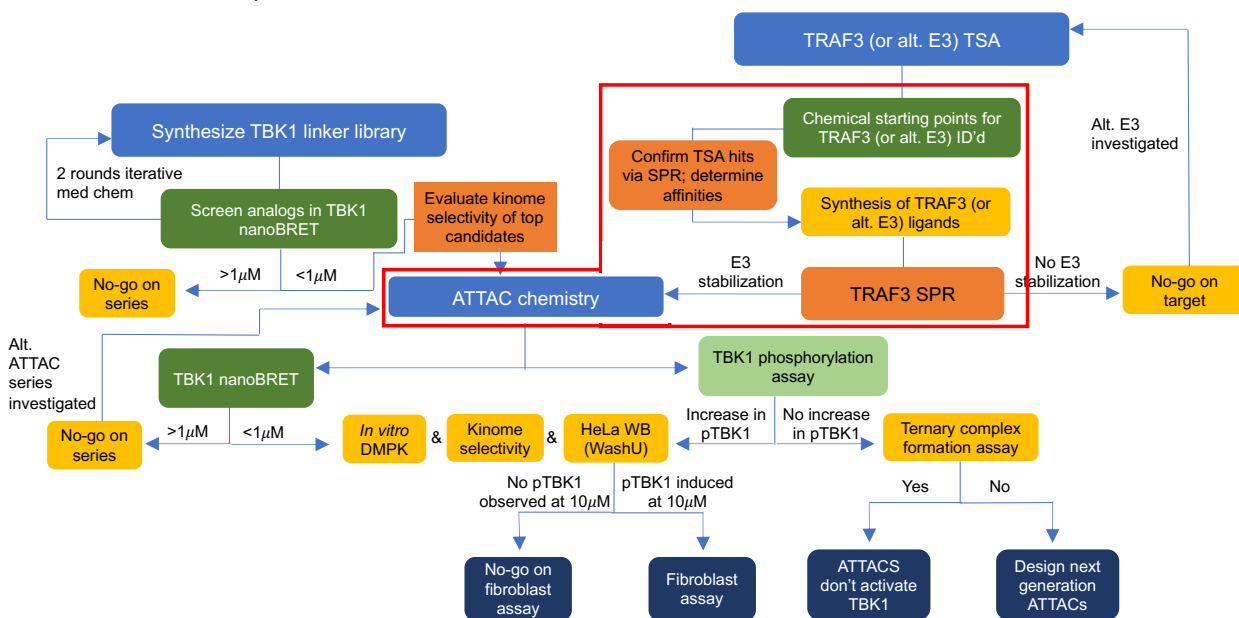
**Figure 5.** Images and quantification of cytoplasmic mislocalization of TDP-43 in mutant MNs (six weeks).

We developed a method to quantify TDP-43 translocation using CellProfiler to identify the TDP-43 staining within the image, subtract out the nucleus (stained with Hoescht), and allow quantification of both cytoplasmic and nuclear TDP-43 (Figure 4). Building on these initial findings and with the image analysis pipeline, we matured MNs for up to six weeks and were able to quantify changes with one of the mutant TDP-43 (G348C) MNs in cytoplasmic translocation (Figure 5) and increased phosphorylation of cytoplasmic TDP-43 observed with the other mutant line (A382T) (Figure 6). MNs are inherently difficult to culture for long periods, so with findings observed at six weeks, small scale assays with compounds will now be assessed for effect on translocation and TDP-43 phosphorylation.



Plotted Mean  $\pm$  SEM, N=1, Individual dots represent the per-image mean values

**Figure 6.** Images and quantification of abundant punctate cytosolic phospho-TDP-43 staining in A382T MNs, but not G348C MNs, when compared with controls.

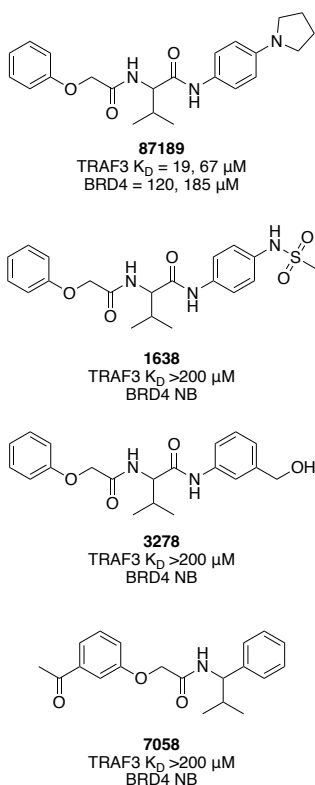


**Figure 7.** Aim 2 decision tree with current progress boxed in red, edit to the original workflow in light green box.

Since the project inception, we have pivoted our strategy along the way, made improvements to the original proposed workflow, and focused on delivering a more physiologically relevant and robust assay because of these modifications.

**Aim 2. Develop a TBK1-activating activation-targeting chimera (ATTAC).** As a departure from traditional small molecule kinase screening campaigns that aim to identify *inhibitors* of substrate phosphorylation, we are developing compounds that *promote* TBK1 phosphorylation. Phosphorylation of TBK1 activates it. One type of ubiquitination (UbK63) has been described to activate protein kinases, including TBK1.<sup>10-12</sup> As UbK63 is a known activation step for TBK1, we hypothesize that a heterobifunctional molecule can be designed to promote UbK63 and thus activate TBK1. To explore this hypothesis, we are preparing novel ATTACs that link a potent TBK1-targeting inhibitor and a ligand for an E3 ligase responsible for UbK63 of TBK1 (TRAF3).

As shown in Figure 7, assembly of ATTACs relies on development of the warhead that recruits TBK1 and a ligand for TRAF3. During year 1, we modified and published a series of cell-active, pyrimidine-based inhibitors of TBK1, which have been published as a preprint and in *J Med Chem*.<sup>13, 14</sup> In parallel, lead compounds

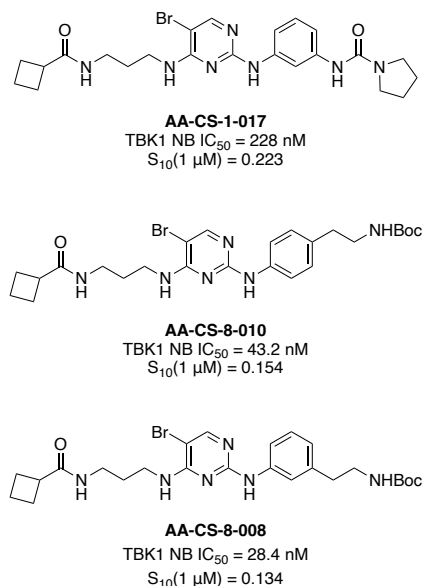


**Figure 9.** Structures and associated data for TRAF3 ligands after second round of SPR studies.

were modified to probe where

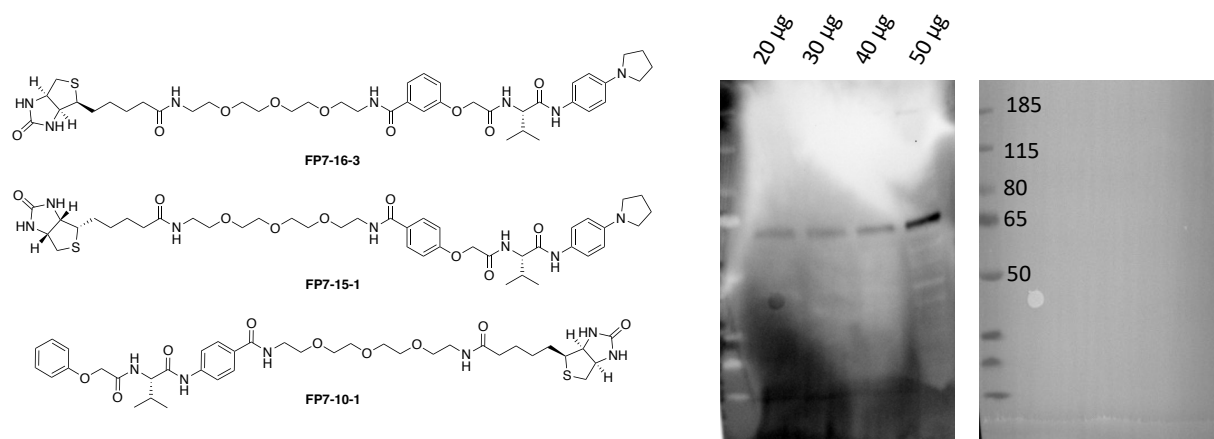
a linker could be attached without compromising cellular target engagement of TBK1. Since many exemplars within the library of 33 analogs retained cellular target engagement of TBK1, we profiled the kinome-wide selectivity of several. While none of the analogs were found to be particularly selective, AA-CS-8-008 and AA-CS-8-010 represented more potent and selective analogs than their parent (AA-CS-1-017) and were elected as the best candidates for advancement (Figure 8). AA-CS-8-008 and AA-CS-8-010 are being prepared on a larger scale to enable ATTAC assembly.

For the TRAF3-targeting warhead, during year 1 we established a relationship with a reputable SPR vendor who was able to assess binding to our TRAF3 truncate versus to BRD4, another E3 ligase, in parallel. From this SPR screening effort, we identified compound **87189** (Figure 9) that binds dose-dependently to TRAF3 with an apparent  $K_D = 19 \mu\text{M}$  and more weakly to BRD4 ( $K_D \sim 120 \mu\text{M}$ ). To follow-up on this result, we screened lead compound **87189** via SPR against two additional proteins from diverse classes to determine whether this compound is a promiscuous compound that binds many proteins. The results indicate that **87189** could be more promiscuous but did not deter its use for TRAF3. In parallel, we revisited our fragment library and identified 15 close analogs of **87189** that had not been screened via SPR. Rather than investing in additional synthetic efforts, these 15 analogs and 6 additional analogs that bear slight structural modifications were screened via SPR to generate structure-activity relationships. In this second study, compound **87189** was found to bind dose-dependently to TRAF3 with an apparent  $K_D = 67 \mu\text{M}$  and



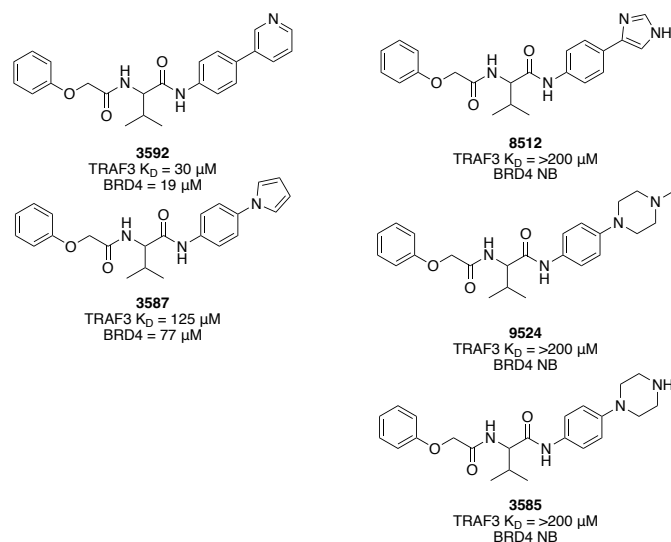
**Figure 8.** Structures and associated data for TBK1 inhibitors selected for ATTAC preparation.

more weakly to BRD4 ( $K_D = 185 \mu\text{M}$ ). Three additional analogs (**1638**, **3278**, and **7058**) were found to bind weakly to TRAF3 with  $K_D$  values outside the assay range ( $>200 \mu\text{M}$ ) with no apparent binding to the BRD4 surface (Figure 9). The remaining 18 compounds were found to bind weakly to TRAF3 and BRD4 (8 analogs,  $K_D$  values  $>200 \mu\text{M}$ ) or not bind either protein surface (10 analogs).



**Figure 10.** Structures of TRAF3 PD ligands and TRAF3 antibody titration results in U87MG cells.

Given the promising results observed with compound **87189**, we prepared a small library of ligands based on **87189** to be used in pulldown (PD) experiments. We intended to validate the SPR results using this orthogonal method. These biotinylated ligands (Figure 10) were prepared and a TRAF3 antibody obtained. PD experiments were attempted initially using SH-SY5Y cell lysate ( $30 \mu\text{g}$ ), streptavidin-conjugated dynabeads, and TRAF3 antibody #4729 from CST. No TRAF3 was identified in the lysate or pulled down by the ligands in Figure 10. Based on better published expression of TRAF3, we tried U87MG cell lysate and did a titration experiment with a new TRAF3 antibody (rabbit mAb #61095 from CST) versus our original antibody. As shown in Figure 10, the new antibody was able to detect TRAF3 ( $\sim 60 \text{ kDa}$ ). The original antibody was still not able to detect TRAF3 in U87MG cell lysate. With a validated TRAF3 antibody, we can reattempt PD experiments in SH-SY5Y and U87MG cell lysate. This validated antibody might also prove useful in exploratory experiments with our ATTACs.



**Figure 11.** Structures and associated data for TRAF3 ligands after third round of SPR studies.

Based on the results from the second library of TRAF3 ligands, we decided to synthesize a final library of close analogs of **87189**. We designed and prepared 24 novel analogs and resynthesized fresh powder of **87189**. Sixteen of these analogs were modified at a single position. The remaining eight analogs were prepared with a fixed chiral center at the position bearing the isopropyl group. SPR analysis of these 25 analogs revealed that three analogs (**8512**, **9524**, and **3585**) bind weakly to TRAF3 with fast “on-off” kinetics and do not bind to BRD4 (Figure 11). Two analogs (**3592** and **3587**) bind to both TRAF3 and BRD4 with  $K_D$  values within the assay range and were suggested to bind non-specifically to protein surfaces





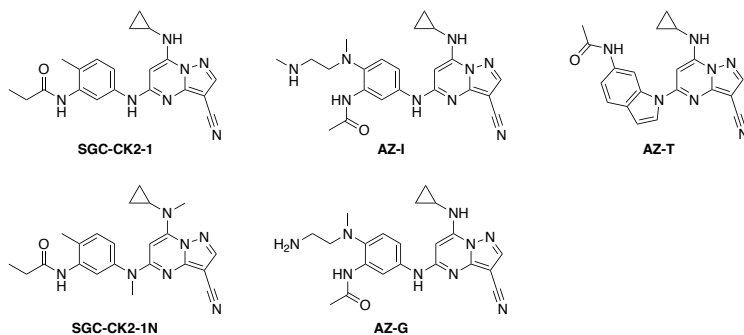
as a key regulator of neuronal function, has increased interest in the exploration of CK2 inhibition for the treatment of neurodegenerative disorders, including AD, PD and ALS.<sup>19-22</sup>

CK2 was demonstrated to be an essential regulator of TBK1 activation at steady state and during viral infection. In response to viral infection, knockdown of CK2 (shCK2 $\alpha$ ) or genetic ablation of its kinase activity led to TBK1 hyperactivation and interferon induction. This regulation of TBK1 by CK2 is indirect, mediated by proteins to be defined.<sup>23</sup> Since S403 phosphorylation of p62 is mediated by TBK1, TBK1 may be recruited to compensate for loss of CK2 and execute this essential phosphorylation to mediate autophagy.<sup>24</sup> Importantly, a small molecule CK2 inhibitor (TBB)

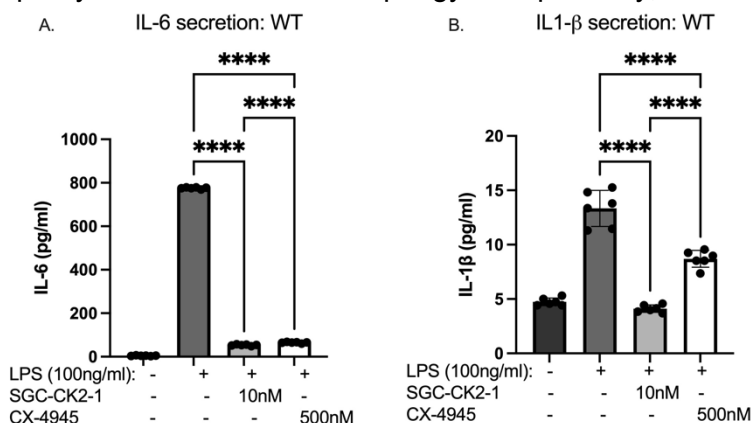
resulted in time- and dose-dependent TBK1 activation and interferon induction in two human cell lines *without* co-stimulation or viral infection.<sup>23</sup> TBB is not the best choice of inhibitor to study CK2 given its lack of potency (1.6  $\mu$ M) and limited knowledge surrounding its selectivity and toxicity.<sup>25</sup> Recognizing a need for the development of high quality chemical tools to study CK2, we synthesized two CK2 chemical probes from orthogonal chemical series (Figure 12). These probes were developed to help interrogate the mechanism of TBK1 activation via CK2 inhibition, how CK2 inhibition

influences TBK1-mediated autophagy, and whether CK2 inhibitors could become ALS therapeutics. SGC-CK2-1 (Figure 14) emerged from our “series 1” in Figure 12.<sup>26, 27</sup> Recently, we have found that this compound blunts a neuroinflammatory response in microglia and outperforms a widely used CK2 inhibitor (CX-4945) when directly compared (Figure 13). This finding could represent another relevant and beneficial outcome of CK2 inhibition in ALS patients. A paper that summarizes this work is in the revisions stage at *Front Mol Neurosci*.

We evaluated the developability of SGC-CK2-1, the entire library from which it was selected, and its negative control compound (SGC-CK2-1N, Figure 14) during year one and found this series to demonstrate suboptimal logD values, kinetic solubility in aqueous buffer, and mouse liver microsomal stability. Evaluation of *in vivo* PK properties when CD-1 mice were dosed at 10 mg/kg IP confirmed that our chemical probe, and the analogs from the same chemical series, did not demonstrate suitable PK properties for *in vivo* use due to quick



**Figure 14.** Structures of chemical probe, negative control, and analogs from pyrazolopyrimidine series (series 1 in Aim 3 Workflow).

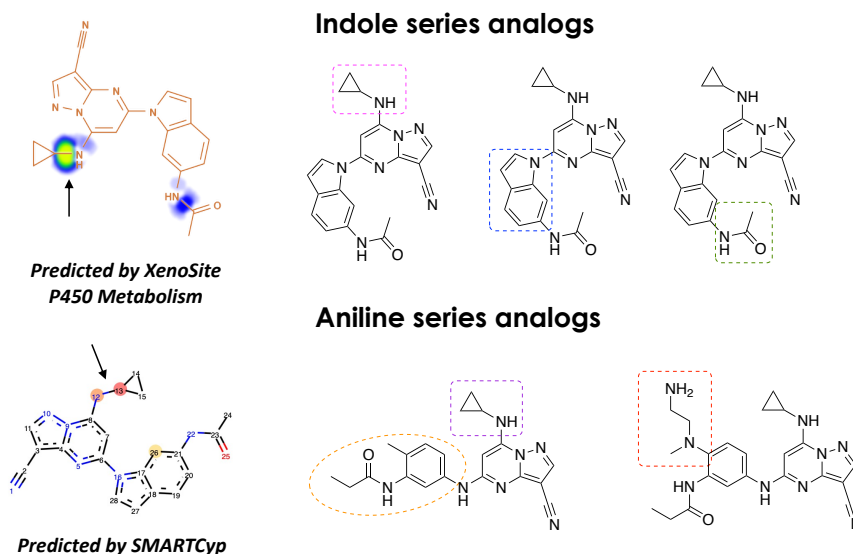


**Figure 13.** SGC-CK2-1 reduces pro-inflammatory cytokine secretion more effectively than CX-4945 in stem cell derived microglia (MGLs). MGLs were stimulated with LPS and simultaneously treated with either SGC-CK2-1 or CX-4945 for 24 hours. In all conditions, SGC-CK2-1 was more effective at inhibiting both IL-6 and IL-1 $\beta$  cytokine secretion into the culture media than CX-4945. These data represent three independent differentiations. \*\*\*\*  $p \leq 0.0001$ ; \*\*\*  $p = 0.0006$ ; \*\*  $p = 0.0024$ ; Error bars indicate the mean  $\pm$  SD.

metabolism. To try to improve the *in vivo* stability of the pyrazolopyrimidines while maintaining those parts of each scaffold that make essential interactions with CK2, we modified both the Aniline (SGC-CK2-1, AZ-G, and AZ-I in Figure 14) and Indole (AZ-T in Figure 14) scaffolds in parallel (Figure 15). Two computational models predicted that the 7-position

cyclopropyl amine was a site of P450 metabolism and thus a potential metabolic liability (Figure 15).<sup>28, 29</sup>

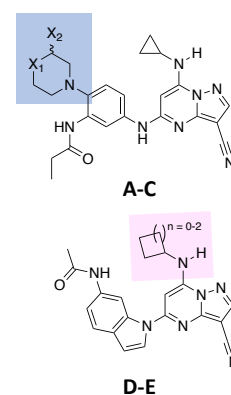
More than 100 analogs have been synthesized with different structural modifications to address sites of metabolic liabilities. Figure 16 highlights five promising analogs and associated data from this library with the structural modifications aimed at addressing liabilities colored pink or blue.



**Figure 15.** Sites of metabolism and analog design strategy.

These analogs are potent in the CK2 $\alpha'$  NanoBRET assay (IC<sub>50</sub> values <400 nM) and exhibit good kinome-wide selectivity scores ( $S_{10}(1 \mu\text{M}) < 0.02$ ). Importantly, they also demonstrate improved mouse liver microsomal stability and kinetic solubility versus SGC-CK2-1. Many members of our library with promising microsomal stability have been advanced to *in vivo* PK studies in mice, which are being done collaboratively with Takeda. Synthetic efforts are ongoing to further improve our pyrazolopyrimidine series based on the data collected and deliver a suitable compound for use *in vivo*. With respect to series 1, we have several candidate inhibitors that will be evaluated by our collaborators at Washington University in St Louis (WUSTL). In parallel, we have synthetic plans to convert SGC-CK2-1 into a CK2 degrader that will allow us to further probe the role of CK2 in driving ALS pathology.

Compound	CK2 $\alpha'$ NB IC <sub>50</sub> (nM)	Kinome-wide selectivity score: $S_{10}(1 \mu\text{M})$	Mouse Liver Microsomal Stability (% remaining, T=30 min)	Kinetic Solubility ( $\mu\text{g/mL}$ )
A	17	0.017 (7)	86.2	55.19
B	216	0.007 (3)	88.5	87.64
C	16	0.01 (4)	83.2	95.71
D	382	0.02 (8)	100.8	1.71
E	104	0.017 (7)	77.7	1.36
SGC-CK2-1	16	0.007 (3)	40.5	1.37



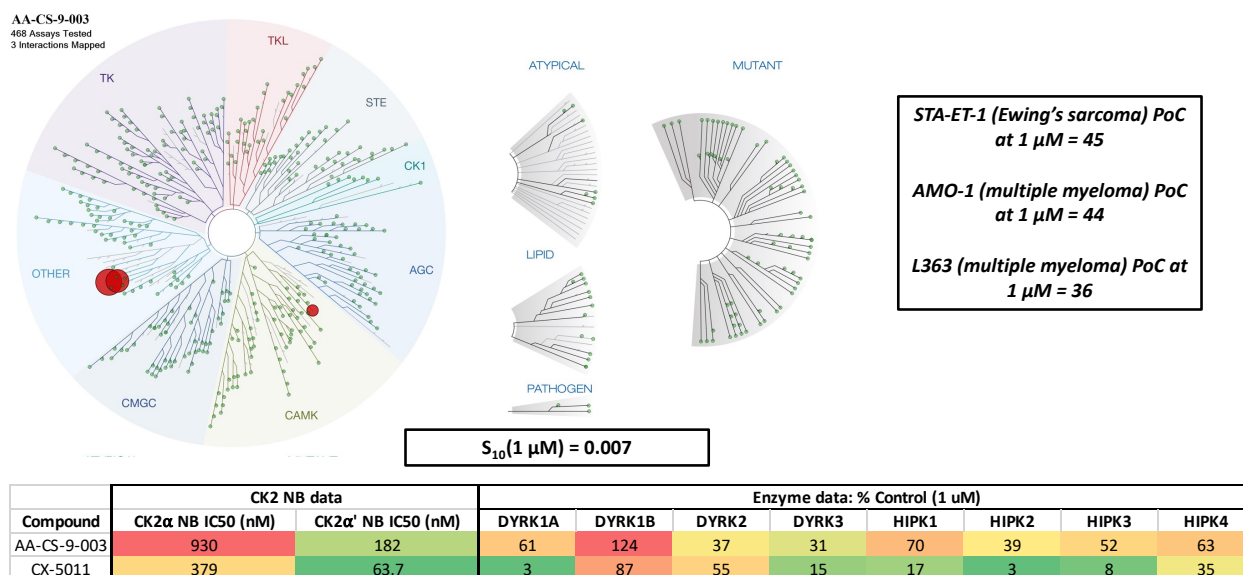
**Figure 16.** Promising analogs from pyrazolopyrimidine series (series 1).

For series 2, we prepared some exemplified and non-exemplified analogs around the CX-4945 and CX-5011 scaffolds and evaluated them in the CK2 $\alpha'$  and CK2 $\alpha$  NanoBRET assays. A few analogs demonstrated solubility problems. Based on the promiscuity of CX-4945, we explored the selectivity of these compounds for CK2 through profiling the entire library of 23 compounds against highly homologous CMGC kinases from the DYRK and HIPK sub-families at 1  $\mu\text{M}$  to generate % control values. These data indicated that our naphthyridine analogs are less selective than pyrazolopyrimidine leads and likely inhibit many kinases if broadly profiled.



We selected ten analogs from series 2 to send for kinome-wide profiling based on the enzymatic panel results.

Based on documented antiproliferative activity of CX-4945, we collaboratively profiled the entire library as well as CX-4945 and CX-5011 (25 compounds in total) against a panel of Ewing's sarcoma and multiple myeloma cell lines and found they were not broadly antiproliferative. The STA-ET-1 Ewing's sarcoma cell line was the most sensitive of the cell lines tested. Of the multiple myeloma cell lines tested, only two (AMO-1 and L363) of the six cell lines tested were responsive to the 25 naphthyridines in series 2. We have not improved on the potency and/or selectivity of a non-exemplified member of our first library (AA-CS-9-003) through continued analog synthesis (Figure 17). We have identified a chemical probe from series 2 that is a viable back-up for the pyrazolopyrimidines and will also be advanced to studies at Washington University in St Louis (WUSTL). A suitable negative control is being prepared, additional data collected, co-crystallography attempted with our collaborators at SGC Frankfurt, and a manuscript drafted around this compound. We have designed a degrader based on AA-CS-9-003 that will be synthesized to support studies aimed at discerning the roles of CK2 in driving ALS biology.



**Figure 17.** Data collected for probe compound AA-CS-9-003, an analog of CX-5011 (series 2).

We have delivered on most of our initially proposed timeline and milestones with respect to this Aim (Figure 12). The delays posed by COVID-19 have set back advancement of compounds to WUSTL. We will continue to move through workflow outlined in Figure 12, which, like Aim 2, was slightly altered to include Western blotting for pTBK1 instead of the originally proposed TBK1 activation assay. Upon completion of degraders based on series 1 and 2, these bifunctional molecules will also be shared with WUSTL and the scientific community.

## Key Research Accomplishments

### Aim 1

- Published pre-print and peer-reviewed publication in *Int J Mol Sci* about KCGS
- Generated human induced pluripotent stem cells with two ALS-relevant mutant forms of TDP-43 incorporated: G348C and A382T that were successfully used to generate spinal motor neurons
- Characterized transcript and protein levels of mutant versus WT TDP-43 during differentiation, with RNAseq analysis of five replicates across both mutant and control

MNs completed, leading to the identification of a number of genes altered across mutant and control lines

- Characterized localization of mutant versus WT TDP-43 in spinal motor neurons without and with treatment with ethacrynic acid
- Demonstrated translocation and phosphorylation is associated with mutations in TDP-43 with maturation of MN cultures
- No changes in MN viability observed with TDP-43 mutations
- Developed methodology to allow quantification of TDP-43 translocation

## Aim 2

- Identified several potent TBK1 inhibitors that permeate cells and engage TBK1 in a cellular target engagement assay
- Published pre-print and peer-reviewed publication in *J Med Chem* about this series
- Confirmed GSK8612 to be the best available TBK1 inhibitor in terms of cellular potency and kinome-wide selectivity
- Found that GSK8612 was not tolerant of incorporation of a linker without significant losses in TBK1 cellular target engagement potency
- Prioritized several analogs with linkers attached that maintain potent TBK1 cellular target engagement and demonstrated improved kinome-wide selectivity versus the corresponding parent compound
- Selected and scaled up two TBK1-targeting warheads with linker attached (AA-CS-8-008 and AA-CS-8-010) to enable ATTAC assembly
- Identified several putative TRAF6 ligands via thermal shift assay
- Identified several putative TRAF3 ligands via thermal shift assay
- Confirmed dose-dependent binding of a small molecule ligand (**87189**) to TRAF3 with an apparent  $K_D = 19/67 \mu\text{M}$  and some demonstrated binding selectivity over E3 ligase BRD4 ( $n = 2$ )
- Identified a ligand (**3592**) that binds TRAF3 with an apparent  $K_D = 30 \mu\text{M}$  but also binds to BRD4
- Identified several additional weakly binding TRAF3 ligands that show some selectivity for TRAF3 versus BRD4 via SPR
- Validated a commercially available TRAF3 antibody
- Designed linkable versions of **87189** and **3592** for scale-up to be used in ATTAC assembly

## Aim 3

- Delivered best available chemical probe targeting CK2 from series one: SGC-CK2-1
- Published pre-print and publication in *Cell Chem Biol* about SGC-CK2-1
- Validated that selective CK2 inhibition is not toxic to the majority of cancer cell lines or primary cells
- Demonstrated that SGC-CK2-1 blunts a neuroinflammatory response in stem cell derived microglia and outperforms clinical CK2 agent CX-4945
- Submitted microglia work for publication in *Front Cell Neurosci* (in revisions stage)
- Determined that SGC-CK2-1 has sub-optimal developability properties and requires improvement to be a useful *in vivo* tool compound
- Confirmed that, while it demonstrates improved mouse liver microsomal stability versus SGC-CK2-1, Aniline I suffers from poor kinome-wide selectivity that precludes its use as a high-quality CK2 tool compound
- Prepared more than 100 pyrazolopyrimidine analogs (series 1) to address metabolic liabilities and improve *in vivo* stability

- Delivered several potent CK2 inhibitors that engage CK2 in cells, retain excellent kinome-wide selectivity, and demonstrate improved mouse liver microsomal stability and kinetic solubility versus SGC-CK2-1
- Selected a subset of pyrazolopyrimidine-based CK2 inhibitors for evaluation of *in vivo* mouse PK
- Designed a CK2 degrader based on SGC-CK2-1 to begin synthesizing
- Determined that naphthyridines based on CX-4945 (series 2) suffer from poor solubility in DMSO, while those based around CX-5011 demonstrate slightly better solubility
- Confirmed that naphthyridine analogs designed around CX-4945 and CX-5011 demonstrate potent engagement of CK2 in cells, but suffer from sub-optimal selectivity when profiled against highly homologous CMGC kinase families as well as more broadly
- Demonstrated that series 2 naphthyridines are not broadly antiproliferative when tested against 12 Ewing's sarcoma and multiple myeloma cell lines
- Selected a chemical probe from the naphthyridine series: AA-CS-9-003
- Designed a suitable negative control compound to be offered with this chemical probe
- Sent AA-CS-9-003 for attempted co-crystallography at SGC Frankfurt
- Designed a CK2 degrader based on AA-CS-9-003 to begin synthesizing
- Selected lead compounds from series 1 and 2 to be profiled at Washington University in St Louis

## 6. PRODUCTS:

### Reportable Outcomes

#### Manuscripts, abstractions, presentations

##### A. Manuscripts and published abstracts

1. Drewry, D. H.; Annor-Gyamfi, J. K.; Wells, C. I.; Pickett, J. E.; Dederer, V.; Preuss, F.; Mathea, S.; Axtman, A. D. Identification of pyrimidine-based lead compounds for understudied kinases implicated in driving neurodegeneration. *J Med Chem* **2022**, *65*, 2, 1313–1328; doi: 10.1021/acs.jmedchem.1c00440.
2. Axtman, A. D. Characterizing the role of the dark kinome in neurodegenerative disease – A mini review. *Biochim Biophys Acta Gen Subj* **2021**, *1865*, 130014; doi: 10.1016/j.bbagen.2021.130014.
3. Wells, C.; Drewry, D. H.; Pickett, J. E.; Tjaden, A.; Krämer, A.; Müller, S.; Gyenis, L.; Menyhart, D.; Litchfield, D. W.; Knapp, S.; Axtman, A. D. Development of a potent and selective chemical probe for the pleiotropic kinase CK2. *Cell Chem Biol* **2021**, *28*, 546-558.e10; doi.org/10.1016/j.chembiol.2020.12.013.
4. Wells, C. I.; Al-Ali, H.; Andrews, D. M.; Asquith, C. R. M.; Axtman, A. D.; Dikic, I.; Ebner, D.; Elkins, J.; Ettmayer, P.; Fischer, C.; Frederiksen, M.; Futrell, R. E.; Gray, N. S.; Hatch, S. B.; Knapp, S.; Lücking, U.; Michaelides, M.; Mills, C. E.; Müller, S.; Owen, D.; Picado, A.; Saikatendu, K. S.; Schröder, M.; Stolz, A.; Tellechea, M.; Turunen, B. J.; Vilar, S.; Wang, J.; Zuercher, W. J.; Willson, T. M.; Drewry, D. H. The Kinase Chemogenomic Set (KCGS): An open science resource for kinase vulnerability identification. *Int J Mol Sci* **2020**, *22*, 566; doi: 10.3390/ijms22020566.
5. Wells, C.; Drewry, D. H.; Pickett, J. E.; Tjaden, A.; Krämer, A.; Knapp, S.; Menyhart, D.; Gyenis, L.; Litchfield, D. W.; Axtman, A. D. Development of the first selective chemical probe for the pleiotropic kinase CK2, an emerging target in neurodegenerative disease. *Alzheimer's Dement* **2020**, *16*, e12278; doi: 10.1002/alz.12278.
6. Lindsley, C. W.; Axtman, A. D. NeuroChat with Research Assistant Professor Alison Axtman. *ACS Chem Neurosci* **2020**, *11*, 2783–2785; doi: 10.1021/acchemneuro.0c00548.

7. Krahn, A. I.; Wells, C.; Drewry, D. H.; Beitel, L. K.; Durcan, T. M.; Axtman, A. D. Defining the neural kinome: strategies and opportunities for small molecule drug discovery to target neurodegenerative diseases. *ACS Chem Neurosci* **2020**, *11*, 1871–1886; doi: 10.1021/acchemneuro.0c00176.

## B. Preprints

1. Yang, X.; Dickmader, R. J.; Bayati, A.; Taft-Benz, S. A.; Smith, J. L.; Madden, E.; Brown, J. W.; Lenarcic, E. M.; Yount, B. L.; Chang, E.; Axtman, A. D.; Baric, R. S.; Heise, M. T.; McPherson, P. S.; Moorman, N. J.; Willson, T. M. Host kinase CSNK2 is a target for inhibition of pathogenic  $\beta$ -coronaviruses including SARS-CoV-2. *BioRxiv* **2022**, doi: 10.1101/2022.01.03.474779.
2. Drewry, D.; Annor-Gyamfi, J. K.; Wells, C.; Pickett, J. E.; Axtman, A. Strategy for Lead Identification for Understudied Kinases. *ChemRxiv* **2021**, 14195207; doi: 10.26434/chemrxiv.14195207.v1.
3. Wells, C.; Drewry, D. H.; Pickett, J. E.; Tjaden, A.; Krämer, A.; Müller, S.; Gyenis, L.; Menyhart, D.; Litchfield, D. W.; Knapp, S.; Axtman, A. D. Development of a potent and selective chemical probe for the pleiotropic kinase CK2. *Cell Press Sneak Peek* **2020**; doi: <https://ssrn.com/abstract=3732376>.
4. Wells, C.; Drewry, D. H.; Pickett, J. E.; Axtman, A. D. SGC-CK2-1: the first selective chemical probe for the pleiotropic kinase CK2. *ChemRxiv* **2020**, 12296180; doi: 10.26434/chemrxiv.12296180.
5. Krahn, A. I.; Wells, C.; Drewry, D. H.; Beitel, L. K.; Durcan, T. M.; Axtman, A. D. Defining the neural kinome: strategies and opportunities for small molecule drug discovery to target neurodegenerative diseases. *BioRxiv* **2020**, doi: 10.1101/2020.04.01.020206.
6. Wells, C.; Al-Ali, H.; Andrews, D. M.; Asquith, C. R. M.; Axtman, A. D.; Chung, M.; Dikic, I.; Ebner, D.; Elkins, J.; Ettmayer, P.; Fischer, C.; Frederiksen, M.; Gray, N. S.; Hatch, S.; Knapp, S.; Lee, S.; Lücking, U.; Michaelides, M.; Mills, C. E.; Müller, S.; Owen, D.; Picado, A.; Ramadan, K.; Saikatendu, K. S.; Schröder, M.; Stolz, A.; Tellechea, M.; Treiber, D. K.; Turunen, B. J.; Vilar, S.; Wang, J.; Zuercher, W. J.; Willson, T. M.; Drewry, D. H. The Kinase Chemogenomic Set (KCGS): An open science resource for kinase vulnerability identification. *BioRxiv* **2019**, 886523; doi: 10.1101/886523.

## C. Oral presentations

- March 2022:* “Casein kinase 2: Not understudied, but still dark”  
St. Jude Children’s Research Hospital, virtual
- February 2022:* “Development of a chemical probe for CK2 enables illumination of its function”  
Emory University, virtual
- July 2021:* “Development of Chemical Probes for Kinases Implicated in Neurodegeneration”  
Innovations and Transformation in Pharmaceutical Sciences 2021, virtual
- March 2021:* “Characterizing the Role of the Dark Proteome in Neurodegenerative Disease” SGC Board Meeting, virtual
- November 2020:* “Design of the first selective chemical probe for the pleiotropic kinase CK2” Target 2035 kick-off webinar, virtual
- November 2020:* “Casein kinase 2 (CK2): Not understudied but still dark”  
CBMC Faculty Research Update Meeting, virtual
- October 2020:* “Progress on Chemical Tools and Role of IDG Dark Kinases in Neurodegeneration” Kinase-DRGC meeting, virtual
- October 2020:* “Opportunities for Small Molecule Drug Discovery within the Neural Kinome” ATOM-IDG symposium, virtual

April 2020: “CSNK2A1/2 (CK2) probe”  
SGC Chemical Probes Joint Management Committee meeting, virtual

#### **D. Poster presentations**

February 2021: “Illumination of CK2 uncovers new roles in cell biology”  
IDG Face-to-Face Annual Meeting, virtual

December 2020: “Development of the first selective chemical probe for the pleiotropic kinase CK2, an emerging target in neurodegenerative disease”  
CSHL Neurodegenerative Diseases: Biology & Therapeutics, virtual

November 2020: “Development of the first selective chemical probe for the pleiotropic kinase CK2, an emerging target in neurodegenerative disease”  
Alzheimer’s Association International Conference Neuroscience Next, virtual

September 2020: “Identification of novel kinase targets in ALS”  
19<sup>th</sup> Annual NEALS Meeting, virtual

#### **Funding applied for based on work supported by this training grant**

##### **A. Received**

1. Clinical NIH Loan Repayment Program award through the National Institute on Aging (Axtman)

##### **B. Applied for**

1. Renewal application for Clinical NIH Loan Repayment Program award through the National Institute on Aging (Axtman)- due November 18, 2021
2. “Use of iPSC-based model systems to interrogate novel protein targets that drive neurodegeneration” 2021 NYSCF- Robertson Neuroscience Investigator Award- due February 17, 2021
3. “Optimization of a potent and cell active CK2 chemical probe for use in Alzheimer’s disease” NIH PAR-21-029 Discovery of in vivo Chemical Probes for the Nervous System (R01 Clinical Trial Not Allowed)- due February 5, 2021
4. “Design and evaluation of first-in-class chimeric molecules in 3D ALS co-culture models” NIH Director’s Transformative Research Awards (R01); NOSI: Common Fund ALS-related Transformative Research Award- due September 30, 2020
5. “Strategies to activate kinases in pursuit of novel small molecule therapeutics for neurodegenerative diseases” New Innovator Award (DP2)- due August 21, 2020

#### **Employment or research opportunities applied for and/or received based on experience/training supported by this grant**

1. Promotion to Research Associate Professor, effective April 1, 2021 (Axtman)
2. Promotion to Associate Professor, effective February 14, 2021 (Durcan)
3. Guest Associate Editors for a co-listed special topic in *Front Cell Neurosci* and *Front Mol Neurosci*: “The Next Generation of Tools and Technologies for Studying Human Neurons in a Dish” (Axtman and Durcan)
4. Promoted to Medicinal Chemistry Core Lead Principal Investigator for NIA-funded TREAT-AD program, effective January 2022 (Axtman)

## **7. PARTICIPANTS & OTHER COLLABORATING ORGANIZATIONS**

#### **Personnel receiving pay from the research effort**

Alison Axtman (UNC)- PI  
Carrow Wells (UNC)- Research Associate  
Jeffery Smith (UNC)- Research Associate

Anna Franco (McGill)- Research Associate  
Mathilde Chaineau (McGill)- Research Associate  
Andrea Krahn (McGill)- Research Associate  
Timothy Miller (WUSTL)- co-I  
Cindy Ly (WUSTL)- co-PI

### **Personnel working on the project but not receiving pay from the research effort**

Thomas Durcan (McGill)- co-PI  
Sarah Lepine (McGill)- Graduate Student

### **Conclusions**

Despite setbacks incurred due circumstances out of our control (COVID-19 and crisis in Ukraine), we have delivered on many of our milestones. We have pivoted in strategy where necessary to produce a very robust and relevant portfolio of deliverables. The many significant research accomplishments as well as notable reportable outcomes highlight our measurable and impactful progress. We will continue to be productive as a team beyond the award period. We aim to provide the research community with useful chemical and biological reagents for use in their own studies in hopes that better therapies for ALS patients will be realized.

### **References**

- (1) Freischmidt, A.; Wieland, T.; Richter, B.; Ruf, W.; Schaeffer, V.; Muller, K.; Marroquin, N.; Nordin, F.; Hubers, A.; Weydt, P.; et al. Haploinsufficiency of TBK1 causes familial ALS and fronto-temporal dementia. *Nat Neurosci* **2015**, *18*, 631-636. DOI: 10.1038/nn.4000.
- (2) Chen-Plotkin, A. S.; Lee, V. M.; Trojanowski, J. Q. TAR DNA-binding protein 43 in neurodegenerative disease. *Nat Rev Neurol* **2010**, *6*, 211-220. DOI: 10.1038/nrneurol.2010.18.
- (3) Oakes, J. A.; Davies, M. C.; Collins, M. O. TBK1: A new player in ALS linking autophagy and neuroinflammation. *Mol Brain* **2017**, *10*, 5. DOI: 10.1186/s13041-017-0287-x.
- (4) Wells, C. I.; Al-Ali, H.; Andrews, D. M.; Asquith, C. R. M.; Axtman, A. D.; Dikic, I.; Ebner, D.; Etmayer, P.; Fischer, C.; Frederiksen, M.; et al. The kinase chemogenomic set (KCGS): An open science resource for kinase vulnerability identification. *Int J Mol Sci* **2021**, *22*, 566. DOI: 10.3390/ijms22020566.
- (5) Wells, C. I.; Hassan, A.-A.; Andrews, D. M.; Asquith, C. R. M.; Axtman, A. D.; Chung, M.; Dikic, I.; Ebner, D.; Elkins, J. M.; Etmayer, P.; et al. The kinase chemogenomic set (KCGS): An open science resource for kinase vulnerability identification. *BioRxiv* **2019**, 10.1101/2019.1112.1122.886523. DOI: 10.1101/2019.12.22.886523.
- (6) Buratti, E.; Baralle, F. E. Multiple roles of TDP-43 in gene expression, splicing regulation, and human disease. *Front Biosci* **2008**, *13*, 867-878. DOI: 10.2741/2727.
- (7) Arai, T.; Hasegawa, M.; Akiyama, H.; Ikeda, K.; Nonaka, T.; Mori, H.; Mann, D.; Tsuchiya, K.; Yoshida, M.; Hashizume, Y.; et al. TDP-43 is a component of ubiquitin-positive tau-negative inclusions in frontotemporal lobar degeneration and amyotrophic lateral sclerosis. *Biochem Biophys Res Commun* **2006**, *351*, 602-611. DOI: 10.1016/j.bbrc.2006.10.093.
- (8) Neumann, M.; Sampathu, D. M.; Kwong, L. K.; Truax, A. C.; Micsenyi, M. C.; Chou, T. T.; Bruce, J.; Schuck, T.; Grossman, M.; Clark, C. M.; et al. Ubiquitinated TDP-43 in frontotemporal lobar degeneration and amyotrophic lateral sclerosis. *Science* **2006**, *314*, 130-133. DOI: 10.1126/science.1134108.
- (9) Iguchi, Y.; Katsuno, M.; Takagi, S.; Ishigaki, S.; Niwa, J.; Hasegawa, M.; Tanaka, F.; Sobue, G. Oxidative stress induced by glutathione depletion reproduces pathological modifications of TDP-43 linked to TDP-43 proteinopathies. *Neurobiol Dis* **2012**, *45*, 862-870. DOI: 10.1016/j.nbd.2011.12.002.

- (10) Mohapatra, B.; Ahmad, G.; Nadeau, S.; Zutshi, N.; An, W.; Scheffe, S.; Dong, L.; Feng, D.; Goetz, B.; Arya, P.; et al. Protein tyrosine kinase regulation by ubiquitination: Critical roles of Cbl-family ubiquitin ligases. *Biochim Biophys Acta* **2013**, *1833*, 122-139. DOI: 10.1016/j.bbamcr.2012.10.010.
- (11) Nazio, F.; Carinci, M.; Cecconi, F. ULK1 ubiquitylation is regulated by phosphorylation on its carboxy terminus. *Cell Cycle* **2017**, *16*, 1744-1747. DOI: 10.1080/15384101.2017.1361063.
- (12) Nguyen, L. K.; Kolch, W.; Kholodenko, B. N. When ubiquitination meets phosphorylation: A systems biology perspective of EGFR/MAPK signalling. *Cell Commun Signal* **2013**, *11*, 52. DOI: 10.1186/1478-811x-11-52.
- (13) Drewry, D.; Annor-Gyamfi, J.; Wells, C.; Pickett, J.; Dederer, V.; Preuss, F.; Mathea, S.; Axtman, A. Identification of pyrimidine-based lead compounds for understudied kinases implicated in driving neurodegeneration. *J Med Chem* **2022**, *65*, 1313-1328. DOI: 10.1021/acs.jmedchem.1c00440.
- (14) Drewry, D.; Annor-Gyamfi, J. K.; Wells, C.; Pickett, J. E.; Axtman, A. Strategy for Lead Identification for Understudied Kinases. *ChemRxiv* **2021**, *14195207*; doi: 10.26434/chemrxiv.14195207.v1.
- (15) Lamark, T.; Kirkin, V.; Dikic, I.; Johansen, T. NBR1 and p62 as cargo receptors for selective autophagy of ubiquitinated targets. *Cell Cycle* **2009**, *8*, 1986-1990. DOI: 10.4161/cc.8.13.8892.
- (16) Matsumoto, G.; Wada, K.; Okuno, M.; Kurosawa, M.; Nukina, N. Serine 403 phosphorylation of p62/SQSTM1 regulates selective autophagic clearance of ubiquitinated proteins. *Mol Cell* **2011**, *44*, 279-289. DOI: 10.1016/j.molcel.2011.07.039.
- (17) Herhaus, L.; Dikic, I. Expanding the ubiquitin code through post-translational modification. *EMBO Rep* **2015**, *16*, 1071-1083. DOI: 10.15252/embr.201540891.
- (18) Pierre, F.; Chua, P. C.; O'Brien, S. E.; Siddiqui-Jain, A.; Bourbon, P.; Haddach, M.; Michaux, J.; Nagasawa, J.; Schwaebe, M. K.; Stefan, E.; et al. Discovery and SAR of 5-(3-chlorophenylamino)benzo[c][2,6]naphthyridine-8-carboxylic acid (CX-4945), the first clinical stage inhibitor of protein kinase CK2 for the treatment of cancer. *J Med Chem* **2011**, *54*, 635-654. DOI: 10.1021/jm101251q.
- (19) Perez, D. I.; Gil, C.; Martinez, A. Protein kinases CK1 and CK2 as new targets for neurodegenerative diseases. *Med Res Rev* **2011**, *31*, 924-954. DOI: 10.1002/med.20207.
- (20) Castello, J.; Ragnauth, A.; Friedman, E.; Rebholz, H. CK2—an emerging target for neurological and psychiatric disorders. *Pharmaceuticals* **2017**, *10*, 7. DOI: 10.3390/ph10010007.
- (21) Cozza, G.; Pinna, L. A.; Moro, S. Kinase CK2 inhibition: An update. *Curr Med Chem* **2013**, *20*, 671-693. DOI: 10.2174/092986713804999312.
- (22) Guerra, B.; Issinger, O. G. Protein kinase CK2 in human diseases. *Curr Med Chem* **2008**, *15*, 1870-1886. DOI: 10.2174/092986708785132933.
- (23) Du, M.; Liu, J.; Chen, X.; Xie, Y.; Yuan, C.; Xiang, Y.; Sun, B.; Lan, K.; Chen, M.; James, S. J.; et al. Casein kinase II controls TBK1/IRF3 activation in IFN response against viral infection. *J Immunol* **2015**, *194*, 4477-4488. DOI: 10.4049/jimmunol.1402777.
- (24) Matsumoto, G.; Shimogori, T.; Hattori, N.; Nukina, N. TBK1 controls autophagosomal engulfment of polyubiquitinated mitochondria through p62/SQSTM1 phosphorylation. *Hum Mol Genet* **2015**, *24*, 4429-4442. DOI: 10.1093/hmg/ddv179.
- (25) Sarno, S.; Reddy, H.; Meggio, F.; Ruzzene, M.; Davies, S. P.; Donella-Deana, A.; Shugar, D.; Pinna, L. A. Selectivity of 4,5,6,7-tetrabromobenzotriazole, an ATP site-directed inhibitor of protein kinase CK2 ('casein kinase-2'). *FEBS Lett* **2001**, *496*, 44-48. DOI: 10.1016/S0014-5793(01)02404-8.
- (26) Wells, C. I.; Drewry, D. H.; Pickett, J. E.; Tjaden, A.; Krämer, A.; Müller, S.; Gyenis, L.; Menyhart, D.; Litchfield, D. W.; Knapp, S.; et al. Development of a potent and selective chemical probe for the pleiotropic kinase CK2. *Cell Chem Biol* **2021**, *28*, 546-558.e510. DOI: 10.1016/j.chembiol.2020.12.013.

(27) Wells, C.; Drewry, D. H.; Pickett, J. E.; Axtman, A. D. SGC-CK2-1: The first selective chemical probe for the pleiotropic kinase CK2. *ChemRxiv* **2020**, 10.26434/chemrxiv.12296180.v12296181.

(28) Matlock, M. K.; Hughes, T. B.; Swamidass, S. J. Xenosite server: A web-available site of metabolism prediction tool. *Bioinformatics* **2014**, *31*, 1136-1137. DOI: 10.1093/bioinformatics/btu761.

(29) Rydberg, P.; Gloriam, D. E.; Zaretski, J.; Breneman, C.; Olsen, L. Smartcyp: A 2D method for prediction of cytochrome p450-mediated drug metabolism. *ACS Med Chem Lett* **2010**, *1*, 96-100. DOI: 10.1021/ml100016x.

**8. SPECIAL REPORTING REQUIREMENTS:** not applicable

## 9. APPENDICES

Attached are copies of the following:

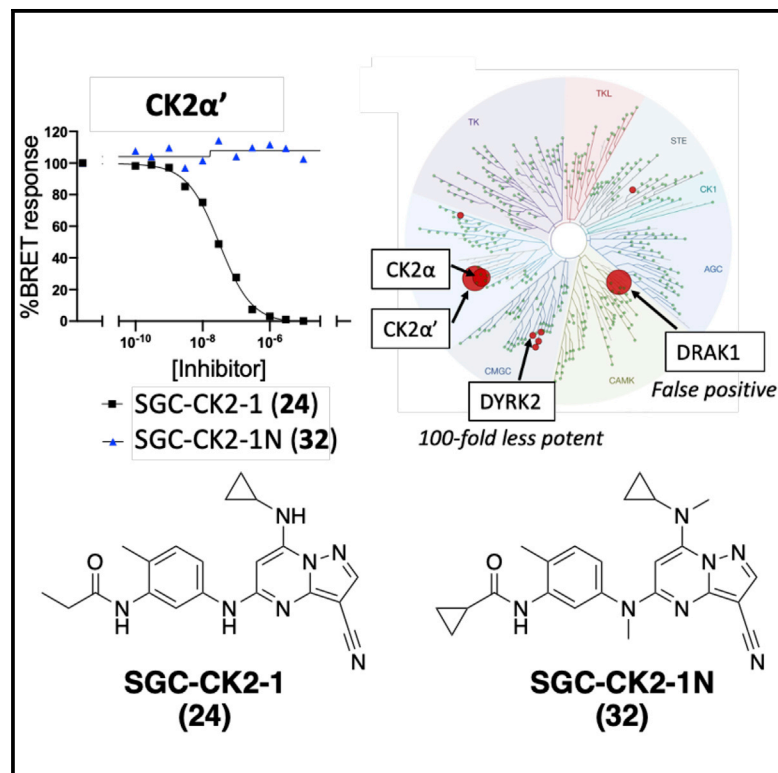
1. Wells, C.; Drewry, D. H.; Pickett, J. E.; Tjaden, A.; Krämer, A.; Müller, S.; Gyenis, L.; Menyhart, D.; Litchfield, D. W.; Knapp, S.; Axtman, A. D. Development of a potent and selective chemical probe for the pleiotropic kinase CK2. *Cell Chem Biol* **2021**, *28*, 546-558.e10; doi.org/10.1016/j.chembiol.2020.12.013.
2. Wells, C. I.; Al-Ali, H.; Andrews, D. M.; Asquith, C. R. M.; Axtman, A. D.; Dikic, I.; Ebner, D.; Elkins, J.; Etmayer, P.; Fischer, C.; Frederiksen, M.; Futrell, R. E.; Gray, N. S.; Hatch, S. B.; Knapp, S.; Lücking, U.; Michaelides, M.; Mills, C. E.; Müller, S.; Owen, D.; Picado, A.; Saikatendu, K. S.; Schröder, M.; Stolz, A.; Tellechea, M.; Turunen, B. J.; Vilar, S.; Wang, J.; Zuercher, W. J.; Willson, T. M.; Drewry, D. H. The Kinase Chemogenomic Set (KCGS): An open science resource for kinase vulnerability identification. *Int J Mol Sci* **2020**, *22*, 566; doi: 10.3390/ijms22020566.
3. Drewry, D. H.; Annor-Gyamfi, J. K.; Wells, C. I.; Pickett, J. E.; Dederer, V.; Preuss, F.; Mathea, S.; Axtman, A. D. Identification of pyrimidine-based lead compounds for understudied kinases implicated in driving neurodegeneration. *J Med Chem* **2022**, *65*, 2, 1313–1328; doi: 10.1021/acs.jmedchem.1c00440.
4. Axtman, A. D. Characterizing the role of the dark kinome in neurodegenerative disease – A mini review. *Biochim Biophys Acta Gen Subj* **2021**, *1865*, 130014; doi: 10.1016/j.bbagen.2021.130014.



# Cell Chemical Biology

## Development of a potent and selective chemical probe for the pleiotropic kinase CK2

### Graphical Abstract



### Authors

Carrow I. Wells, David H. Drewry, Julie E. Pickett, ..., David W. Litchfield, Stefan Knapp, Alison D. Axtman

### Correspondence

alison.axtman@unc.edu

### In Brief

Many papers have detailed the function(s) of casein kinase 2 (CK2). Characterization of CK2, however, has been confounded by the use of suboptimal inhibitors. Wells et al. have identified the best available chemical tool to use in illuminating the essential roles of this pleiotropic kinase.

### Highlights

- We developed a potent, selective, and cell-active chemical probe for CK2
- We identified a negative control compound to be used with the CK2 probe
- Our selective chemical probe (SGC-CK2-1) is not broadly antiproliferative
- SGC-CK2-1 is the best available chemical tool to define the roles of CK2 in cells



## Article

# Development of a potent and selective chemical probe for the pleiotropic kinase CK2

Carrow I. Wells,<sup>1,2,7</sup> David H. Drewry,<sup>1,2,7</sup> Julie E. Pickett,<sup>1,2</sup> Amelie Tjaden,<sup>3,4</sup> Andreas Krämer,<sup>3,4</sup> Susanne Müller,<sup>3,4</sup> Laszlo Gyenis,<sup>5</sup> Daniel Menyhart,<sup>5</sup> David W. Litchfield,<sup>5,6</sup> Stefan Knapp,<sup>3,4</sup> and Alison D. Axtman<sup>1,2,8,\*</sup>

<sup>1</sup>Structural Genomics Consortium (SGC), UNC Eshelman School of Pharmacy, University of North Carolina at Chapel Hill (UNC-CH), Chapel Hill, NC 27599, USA

<sup>2</sup>Division of Chemical Biology and Medicinal Chemistry, UNC Eshelman School of Pharmacy, UNC-CH, Chapel Hill, NC 27599, USA

<sup>3</sup>Institute for Pharmaceutical Chemistry, Johann Wolfgang Goethe-University, Max-von-Laue-Str. 9, 60438 Frankfurt am Main, Germany

<sup>4</sup>Structural Genomics Consortium, Buchman Institute for Life Sciences, Johann Wolfgang Goethe-University, Max-von-Laue-Str. 15, 60438 Frankfurt am Main, Germany

<sup>5</sup>Department of Biochemistry, Schulich School of Medicine & Dentistry, University of Western Ontario, London, Ontario, N6A 5C1, Canada

<sup>6</sup>Department of Oncology, Schulich School of Medicine & Dentistry, University of Western Ontario, London, Ontario, N6A 5C1, Canada

<sup>7</sup>These authors contributed equally

<sup>8</sup>Lead contact

\*Correspondence: [alison.axtman@unc.edu](mailto:alison.axtman@unc.edu)

<https://doi.org/10.1016/j.chembiol.2020.12.013>

## SUMMARY

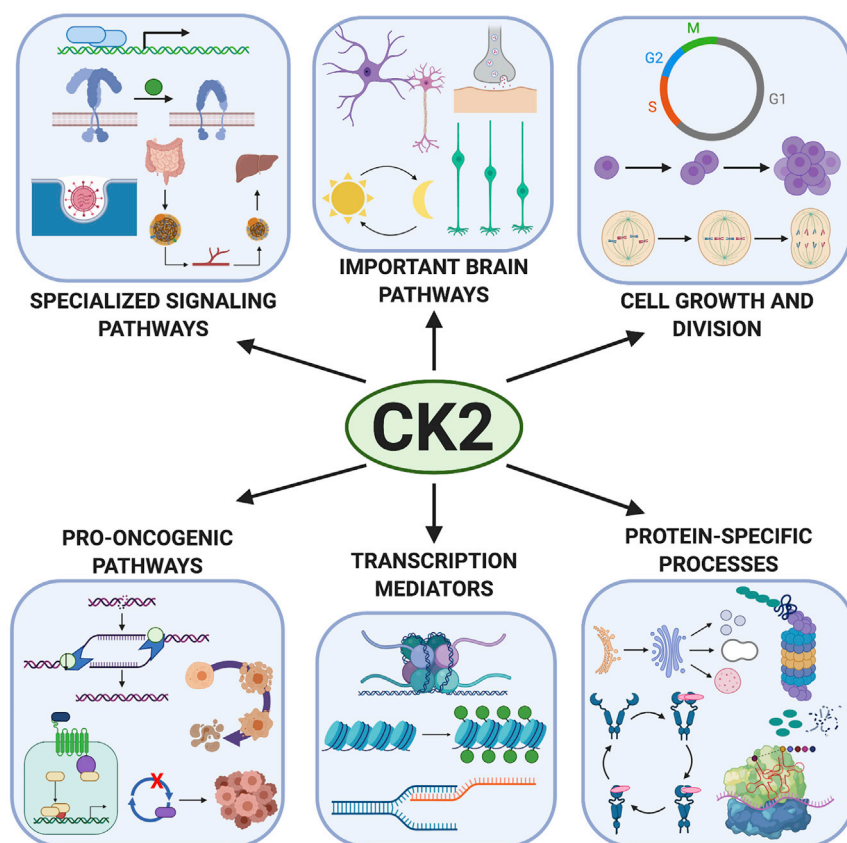
Building on the pyrazolopyrimidine CK2 (casein kinase 2) inhibitor scaffold, we designed a small targeted library. Through comprehensive evaluation of inhibitor selectivity, we identified inhibitor 24 (SGC-CK2-1) as a highly potent and cell-active CK2 chemical probe with exclusive selectivity for both human CK2 isoforms. Remarkably, despite years of research pointing to CK2 as a key driver in cancer, our chemical probe did not elicit a broad antiproliferative phenotype in >90% of >140 cell lines when tested in dose-response. While many publications have reported CK2 functions, CK2 biology is complex and an available high-quality chemical tool such as SGC-CK2-1 will be indispensable in deciphering the relationships between CK2 function and phenotypes.

## INTRODUCTION

Protein phosphorylation is one of the most common and important post-translational modifications, playing a key role in signal transduction (Ardito et al., 2017). Protein kinases catalyze this reaction, phosphorylating a specific substrate and causing a conformational change that affects protein function (Plattner and Bibb, 2012; Röhm et al., 2020). One protein kinase, CK2 (casein kinase 2 [CSNK2]) has been implicated in the phosphorylation of hundreds of cellular proteins with >10% of the phosphoproteome matching the consensus sequence for CK2 phosphorylation (Meggio and Pinna, 2003; Salvi et al., 2009). Via genetic and biochemical studies in a variety of experimental models, CK2 has been found to be both constitutively active and ubiquitously expressed, making it important in many biological processes (Figure 1 and Table S1) (Ahmed et al., 2002; Meggio and Pinna, 2003; Nuñez de Villavicencio-Diaz et al., 2017; Rabalski et al., 2016). CK2 exists as a tetrameric complex made up of two catalytic subunits, designated CK2 $\alpha$  (encoded by the CSNK2A1 gene) and CK2 $\alpha'$  (encoded by the CSNK2A2 gene), and two regulatory subunits, CK2 $\beta$  (Litchfield, 2003). Given the reported involvement of CK2 in a multitude of pathways, selective chemical probes would be indispensable tools for deciphering its complex roles in biological processes (Ahmed et al., 2002).

Although CK2 biology has been well-studied, reflected by >1,000 PubMed references to the human gene, selective and potent inhibitors of CK2 have remained elusive. As shown in Figure 2A, some early reported compounds that bound to CK2 originate from such diverse chemical scaffolds as benzotriazoles (TBB, 4,5,6,7-tetrabromobenzotriazole and TMCB, 4,5,6,7-tetrabromo-2-dimethylamino-1-carboxymethyl-benzimidazole) to thienopyrimidines (TTP 22) to natural product-like flavonoids (fisetin) (Golub et al., 2011; Lolli et al., 2012; Szyszka et al., 1995). TBB was published as a CK2 inhibitor in 1995 and demonstrated modest selectivity for CK2 over CK1 (casein kinase 1) (Szyszka et al., 1995). Evaluation of this compound against a panel of 33 (Sarno et al., 2001) and 70 (Pagano et al., 2008) kinases showed however that, while maintaining reasonable selectivity, it did inhibit several other kinases with >90% inhibition at a screening concentration of 10  $\mu$ M (DYRK1A, DYRK2, DYRK3, HIPK2, and PIM1-3). In 2010, the compound CX-4945 (silmitasertib) was published, which has since become the most commonly employed CK2 inhibitor. Silmitasertib received orphan drug status in the US for treatment of advanced cholangiocarcinoma and has entered clinical testing in oncology (Gowda et al., 2017; Siddiqui-Jain et al., 2010). Given its antiproliferative activity in several different cancer cell lines, this inhibitor has been advanced and is currently being evaluated in clinical





**Figure 1. Summary of biological pathways mediated by CK2**

tency for CK2 (Figure 2B). They further evaluate this series for both mechanistic and phenotypic endpoints, including pS129-AKT levels and antiproliferative activity (Chuaqui et al., 2013; Dowling et al., 2012, 2013, 2016). While the compounds are potent, the lead structure (17) has considerable off-target kinase activity (HIPK1–4, DAPK1–3, DYRK2, and BMPR1B), resulting in the need for further modification of this scaffold for probe development (Dowling et al., 2016). Due to its relatively favorable kinome-wide selectivity profile as well as its good cellular potency, we started our CK2 chemical probe project utilizing this promising starting point (17).

## RESULTS

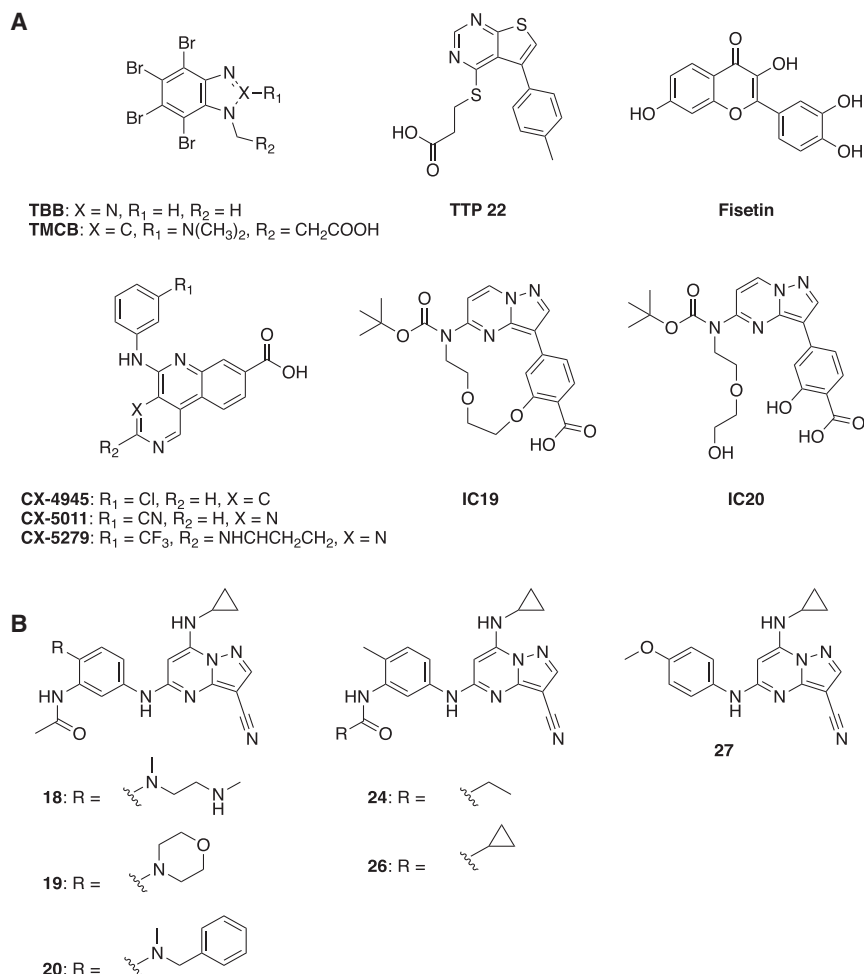
### Design and synthesis of pyrazolopyrimidine inhibitors of CK2

Based on the published data for pyrazolopyrimidines targeting CK2, we prepared a small library of compounds. We opted to

resynthesize a subset of the published molecules so we could further characterize their selectivity and cell activity and also expand into unexplored chemical space by designing and preparing an additional six analogs not described in these papers. Table 1 shows the structures and corresponding CK2 enzymatic activity for the subset of previously exemplified molecules that we resynthesized for further characterization. Three of these compounds (17, 22, 29) had been previously reported to have narrow selectivity profiles when screened at Ambit/DiscoverX in panels of 324 (29) or 402 (17 and 22) kinases. The remaining three compounds are close structural analogs with potent enzymatic activity, but for which limited selectivity data had been reported (Chuaqui et al., 2013; Dowling et al., 2012, 2013, 2016). Figure 2B shows the compounds we designed based upon surveying the literature for structures and corresponding data. Structure–activity relationships were developed, and compounds designed that incorporated minor structural changes (18, 24, 26) and some slightly larger structural perturbations (19, 20, 27). Analogs 19 and 20 were designed with groups at a position that has proven tolerant to a wide variety of structural modifications from methyl to alkyldiamine chains (Table 1). The morpholine (19) and benzylamine (20) are bulkier than previously exemplified groups and would explore the spatial tolerance of this portion of the pocket. Analog 27 is devoid of the acetamide that is present in all previously exemplified compounds (Table 1). This modest change is expected to affect binding, as the acetamide has been shown to engage in a network of hydrogen bonds in previously solved and our own solved structures (Dowling et al., 2016). All analogs were prepared

trials for several oncology indications, basal cell carcinoma, multiple myeloma, cholangiocarcinoma, breast cancer, and medulloblastoma, all listed as active or recruiting trials on [clinicaltrials.gov](http://clinicaltrials.gov) (Pierre et al., 2011). Recently, silmitasertib emerged as a candidate for severe acute respiratory syndrome coronavirus 2 (SARS-CoV-2), as pharmacological inhibition of CK2 was found to result in antiviral efficacy (Bouhaddou et al., 2020). Despite being fairly narrow spectrum and displaying modest kinome-wide selectivity, CX-4945 does significantly inhibit other kinases with  $IC_{50}$  (half maximal inhibitory concentration) values well below 100 nM, including CDK1, CLK1–CLK3, DAPK3, DYRK1A, DYRK1B, DYRK3, FLT3, HIPK3, PIM1, and TBK1 (Kim et al., 2014, 2016; Pierre et al., 2011). Thus, the off-target activities of this inhibitor confound results when trying to attribute target to function to phenotype. Efforts have aimed at improving the selectivity of CX-4945, producing benzonaphthyrindine analogs such as CX-5011, CX-5033, and CX-5279 that display improved selectivity versus CX-4945 (Figure 2A) (Battistutta et al., 2011). Recently, a series of acyclic/macrocylic pyrazolo[1,5-a]pyrimidines (Figure 2A, IC20 and IC19) was published that demonstrates excellent selectivity *in vitro*. However, the required introduction of a carboxylic acid group resulted in modest, low micromolar cellular activity (Krämer et al., 2020).

Given both the biological importance of this target and lack of selective inhibitors, we recognized the need for a CK2 chemical probe to enable accurate elucidation of its biological effects. Three recent publications from scientists at AstraZeneca disclose a series of pyrazolopyrimidines with nanomolar (nM) po-



**Figure 2. Structures of reported and synthesized pyrazolopyrimidine CK2 inhibitors**

(A) Structures of literature-reported CK2 inhibitors used in studies aimed at interrogating CK2 function.

(B) Structures of non-exemplified pyrazolopyrimidines synthesized.

with the other molecules in the set (Table 2 and Figure 3C). Of note, our compounds were significantly more selective than CX-4945, currently the most frequently utilized CK2 inhibitor in the literature (Figure 3C). CX-4945 has an  $S_{10}(1\mu\text{M}) = 0.069$  with 28 kinases >90% (%, percent inhibition) (Figure S1) and compound **24**, for example, has an  $S_{10}(1\mu\text{M}) = 0.007$  with only three kinases >90%. By comparison, in smaller assay panels (94 wild-type human kinases) and tested at a lower concentration, CX-4945, CX-5011, CX-5033, and CX-5279 had  $S_{10}(0.5\mu\text{M}) = 0.064, 0.032, 0.053,$  and  $0.021$ , respectively. While it is difficult to compare selectivity scores since the assay panels contain different kinase constructs and were evaluated using different assay platforms and compound concentrations, clearly the more recently generated benzimidazopyrimidines are more selective than CX-4945 (Battistutta et al., 2011).

In parallel, we assessed the cellular penetrance and target engagement of all compounds using the CK2 $\alpha$  and CK2 $\alpha'$

using convergent chemistry and, where possible, utilizing previously reported synthetic routes (Dowling et al., 2012, 2013, 2016). Key transformations, including nucleophilic aromatic substitution and Buchwald-Hartwig amination, allowed preparation of all analogs. Detailed routes are included in the Supplemental Information (Scheme S1).

### Modulation of pyrazolopyrimidines yields inhibitors with exclusive selectivity for CK2 and potent in cell target engagement

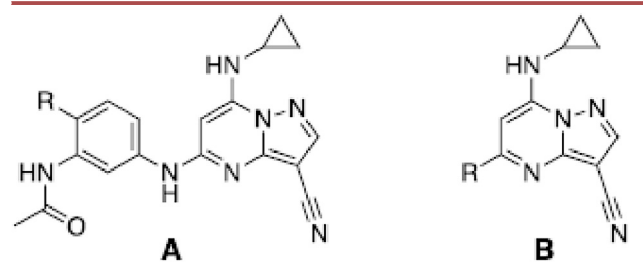
Upon preparation of the analogs shown in Table 1 and Figure 2B, the compound set was sent to Eurofins DiscoverX to be profiled against 403 wild-type human kinases using their scanMAX platform to characterize kinome-wide selectivity. Table 2 summarizes our findings related to the cellular potency and kinome-wide selectivity of the compounds we prepared. The selectivity score ( $S_{10}(1\mu\text{M})$ ) is calculated by dividing the number of inhibited kinases having an experimental value greater than 90% inhibition (I) by the total number of tested kinases. A low  $S_{10}(1\mu\text{M})$  value reflects high compound selectivity whereas a high  $S_{10}(1\mu\text{M})$  value represents poor selectivity (Bosc et al., 2017). From the entire set of compounds, four of our six non-exemplified pyrazolopyrimidines from Figure 2B (**20**, **24**, **26**, and **27**) exhibited higher kinome-wide selectivity compared


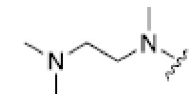
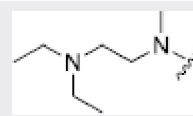
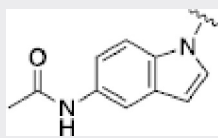
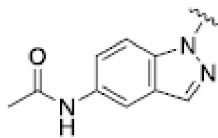
nanoBRET assays in HEK-293 cells. Given the high sequence similarity of the active sites of CK2 $\alpha$  and CK2 $\alpha'$ , we did not anticipate preferential binding to one versus the other (Lozeman et al., 1990). The nanoBRET assay relies upon bioluminescence resonance energy transfer (BRET) between CK2 $\alpha$ -Nluc or CK2 $\alpha'$ -Nluc, each tagged with nanoluciferase (Nluc), and a tracer with a red-shifted fluorophore appended. Our analogs, which compete with the tracer for binding to the active site, were introduced in a dose-dependent manner and BRET was plotted versus concentration, allowing us to calculate a target engagement  $IC_{50}$  value (Vasta et al., 2017). Our entire series was active in the CK2 $\alpha$  and CK2 $\alpha'$  cellular target engagement assays with several inhibitors exhibiting single digit nanomolar potencies (Figure S3). As expected, no significant difference in potency was observed between the two CK2 subunits. Nine of the pyrazolopyrimidines demonstrated CK2 $\alpha'$  nanoBRET in cell target engagement  $IC_{50}$  values less than or equal to 20 nM. The remaining three compounds were less potent in the nanoBRET assays, especially compounds **26** and **27**, which demonstrated micromolar  $IC_{50}$  values. CX-4945, for comparison, was shown to have a CK2 $\alpha'$  nanoBRET  $IC_{50} = 45$  nM.

Off-target kinase inhibition was evaluated for the subset of very selective compounds that inhibited three or fewer kinases. Follow-up was carried out in dose-response using an



**Table 1. Reported CK2 inhibitors and biochemical activity**



Cmpd	Scaffold	R	Reported CK2 IC <sub>50</sub> (nM)
17	A		<3
15	A		<3
16	A		9
22	A	CH <sub>3</sub>	<3
29	B		10
31	B		26

(Chuaqui et al., 2013; Dowling et al., 2012, 2013, 2016).

enzymatic and/or nanoBRET assay corresponding to each of the wild-type off-target kinases that inhibited >60% in the DiscoverX scanMAX panel. All enzymatic assays were carried out at the  $K_m$  of ATP for the respective kinase. Table 2 lists the kinases inhibited >60% for **20**, **24**, **26**, and **27**. While the selectivity of all four analogs satisfy our chemical probe criteria (Asquith et al., 2019), the most potent compound in the CK2 nanoBRET assays (**24**) was chosen as the chemical probe candidate (Figure 3D). As shown in Table 2, DYRK2 was the only significant off-target kinase to demonstrate an IC<sub>50</sub> value < 1  $\mu$ M. Of note, the potency of **24** in the CK2 $\alpha$  and CK2 $\alpha'$  enzymatic assays was such that 100-fold selectivity for CK2 over DYRK2, its most potently inhibited off-target kinase, was observed. Since it seemed to be a common off target of compounds in our library, all analogs in Table 2 were tested in the DYRK2 nanoBRET assay. Only **17** was found to be active at <1  $\mu$ M against DYRK2 in cells (Figure S4, IC<sub>50</sub> = 160 nM). An IC<sub>50</sub> value of 3.7  $\mu$ M was determined for **24** in the DYRK2 nanoBRET assay (Figure S4). Impressively, the 100-fold selectivity for CK2 over DYRK2 in the respective enzymatic assays was maintained in the cell-based system.

### Global methylation of nitrogens results in the identification of a negative control

With our chemical probe identified, we shifted our attention to furnishing a negative control compound that could be used in tandem in biological experiments. A negative control compound is structurally similar to the probe yet devoid of activity at the primary target and is useful to add rigor to the conclusion that a phenotypic response is due to the target in question. If the negative control is active in the phenotypic assay, the response is likely due to an off target. Given its modest CK2 activity in the nanoBRET assay, narrow selectivity profile, and structural similarity to **24**, **26** was chosen as a chemical starting point from which to synthesize a negative control. To convert **26** to a structurally similar negative control, we methylated the aniline that connects the 5-position of the pyrazolopyrimidine core to the aryl side chain as well as the 7-position pyrazolopyrimidine aniline bearing a cyclopropyl ring. These methylations were designed to interrupt key interactions between the pyrazolopyrimidine scaffold and the CK2 ATP binding site, thus abolishing binding affinity. As shown in Scheme S1, **26** was globally methylated using methyl iodide, the various products were separated, and structural assignments made via spectroscopy. Compound **32** was profiled to determine both its kinome-wide selectivity and cellular target engagement of CK2 $\alpha'$ . Based on no inhibition of any kinases >80% at 1  $\mu$ M and no cellular activity in the CK2 $\alpha'$  nanoBRET assay up to 10  $\mu$ M, **32** (SGC-CK2-1N) was chosen as the negative control: a structurally related compound that lacks CK2 affinity. In addition to a lack of cellular activity, **32** was also found to be devoid of CK2 $\alpha$  and CK2 $\alpha'$  potency in the corresponding enzymatic assays (Table 2).

### SGC-CK2-1 assumes a canonical ATP-competitive binding mode

The CK2-targeting pyrazolopyrimidines from which our non-exemplified compounds were designed bind in the ATP site of CK2. X-ray crystallographic structures have been reported for **15**, **17**, and **22** (Dowling et al., 2016). To determine how our compounds bind relative to these, we solved structures corresponding to compounds **24** and **29**. Compound **24** (SGC-CK2-1) was chosen since it was the nominated chemical probe, while compound **29** represents a structurally different inhibitor with good kinome-wide selectivity and potency in the CK2 $\alpha$  and CK2 $\alpha'$  nanoBRET assays. Through solving the structures of diverse compounds, we hoped to maximize our information learned about the plasticity of the CK2 ATP binding pocket. As shown in Figures 3A and 3B, compounds **24** and **29**, similar to **15**, **17**, and **22**, act as type I kinase inhibitors and occupy the ATP pocket exclusively. All compounds adopt nearly identical orientations and make similar interactions. In agreement with previously solved structures, the backbone of H115 and V116 in the hinge makes key hydrogen bonds with the pyrazolopyrimidine core and 7-cyclopropylamine. The 3-carbonitrile interacts via a water molecule with a network of hydrogen bonds that includes the oxygen and nitrogen of the propionamide in **24** and the acetamide in **15**, **17**, **22**, and **29**. Our structures show that key interactions are made with the DWG (D, aspartic acid, W, tryptophan, and G, glycine)-motif (D175),  $\alpha$ C helix (E81), and K68 as part of this hydrogen bond network. These structures also support that the methyl groups on negative control **32** likely disrupt a hydrogen bond with V116 in the hinge

**Table 2. Potency and selectivity of CK2-targeting pyrazolopyrimidines**

Cmpd	S <sub>10</sub> (1 μM)	# kinases >90%l at 1 μM	CK2α NB IC <sub>50</sub> (nM)	CK2α' NB IC <sub>50</sub> (nM)	Wild-type kinases >90%l at 1 μM (%)	Enzymatic IC <sub>50</sub> values (nM)	Wild-type kinases >35%l at 1 μM (%)	Off-target IC <sub>50</sub> or enzymatic assay values (nM)
<b>17</b>	0.042	17	5.3	4.4	Figure S2	NT <sup>a</sup>		
<b>15</b>	0.02	8	2.7	1.3	Figure S2	NT <sup>a</sup>		
<b>16</b>	0.012	5	15	7.6	Figure S2	NT <sup>a</sup>		
<b>22</b>	0.032	13	3.2	1.8	Figure S2	NT <sup>a</sup>		
<b>29</b>	0.015	6	11	3.9	Figure S2	NT <sup>a</sup>		
<b>31</b>	0.027	11	94	20	Figure S2	NT <sup>a</sup>		
<b>18</b>	0.025	10	3.3	2.6	Figure S2	NT <sup>a</sup>		
<b>19</b>	0.025	10	67	15	Figure S2	NT <sup>a</sup>		
<b>20</b>	0.005	2	280	130	CSNK2A2 (100) CSNK2A1 (96.7)	CSNK2A2: 94 CSNK2A1: 91		
<b>24</b>	0.007	3	36	16	CSNK2A2 (100) DRAK1 (100) CSNK2A1 (99.5)	CSNK2A2: 2.3 DRAK1: >10,000 CSNK2A1: 4.2	DYRK2 (86) PLK4 (77) HIPK2 (74) MEK5 (72) HIPK1 (68) HIPK3 (66)	DYRK2: 440 PLK4: >10,000 HIPK2: 3400 MEK5: 0%l at 1 μM HIPK1: 3,700 HIPK3: 8,100
<b>26</b>	0.002	1	7,700	2,700	CSNK2A2 (100)	CSNK2A2: 120	CSNK2A1 (80) SGK1 (68) SGK3 (67)	CSNK2A1: 150 SGK1: >10,000 SGK3: >10,000
<b>27</b>	0.007	3	2,200	1,000	CSNK2A2 (99.3) CLK2 (97.6) PHKG2 (95.6)	CSNK2A2: 240 CLK2: 2995 PHKG2: >10,000	CAMK2A (84) SGK1 (73) CHEK2 (72) BLK (67) DAPK3 (66) SGK3 (65) DYRK2 (63)	CAMK2A: >10,000 SGK1: 3,600 CHEK2: >10,000 BLK: >10,000 DAPK3: >10,000 SGK3: >10,000 DYRK2: 720
<b>32</b>	0.00	0	NT	>10,000	None >90% CSNK2A2 (35) CSNK2A1 (0)	CSNK2A1: >10,000 CSNK2A2: >10,000		
CX-4945	0.069	28	340	45	Figure S1	NT <sup>a</sup>		

<sup>a</sup>NT: compound not tested.

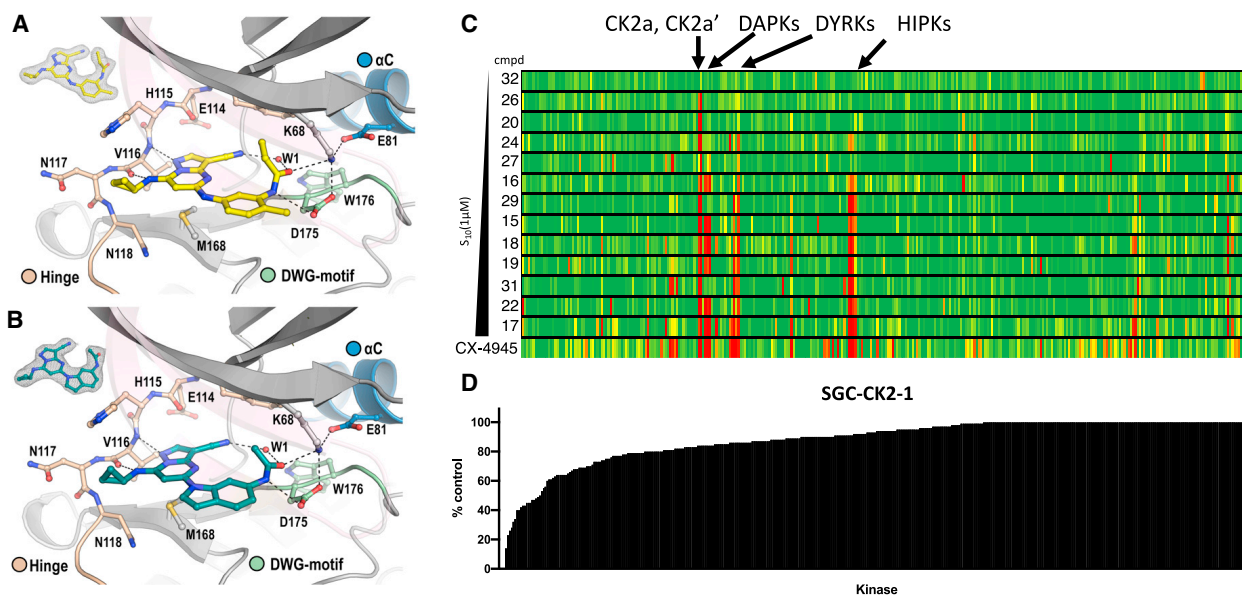
region of the ATP binding pocket as well as change the binding orientation due to steric clash with the ATP site in the region of M168 such that other key interactions cannot be maintained. In Figure 3A, the pyrazolopyrimidine core and pendant aryl ring are co-planar. The addition of a methyl group is proposed to rotate the aryl ring such that the two rings will not maintain co-planarity, thus preventing many key hydrogen interactions from being made with aryl ring substituents.

### Selective CK2 inhibition results in narrow antiproliferative activity in cancer cell lines

Multiple studies link CK2 inhibition to a reduction of proliferation for a range of cancer cells. We wanted to see if the antiproliferative activity held for our non-exemplified compounds, especially SGC-CK2-1, which has enhanced selectivity. Our working hypothesis was that a narrower set of cell lines would be responsive to a more selective compound and highlight true dependencies on CK2. Based upon reports that the previously exemplified pyrazolopyrimidines in our library inhibited the growth of HCT-116 colorectal carcinoma cells and that **17** exhibited a high level of activity as a monotherapy in HCT-116 xenografts (Dowling et al., 2016),

we evaluated the antiproliferative activity of our entire library in this colon cancer cell line. Table S2 shows the previously reported cytotoxicity data in HCT-116 cells alongside the data we collected following 72 h of continuous treatment. Compounds that had previously been reported as cell growth inhibitors demonstrated antiproliferative activity in our hands as well. This was also true of the non-selective CK2 inhibitor CX-4945 (Pierre et al., 2011). Our non-exemplified analogs (**18**, **19**, **20**, **24**, **26**, and **27**) showed variable growth inhibition. Our negative control (**32**) did not demonstrate antiproliferative activity. Remarkably, the most selective compounds, **20**, **24**, **26**, and **27**, demonstrated no antiproliferative activity in this assay.

Driven by our findings with respect to HCT-116 proliferation, we expanded our exploration of the antiproliferative activity of the chemical probe **24**. CK2 inhibition has been linked with suppressing glioblastoma invasiveness as well as pro-survival signaling pathways and growth (Pencheva et al., 2017; Zheng et al., 2013). As these published studies employed U-87 MG cells, we tested the antiproliferative activity of **24** in this glioblastoma cell line after 72 h of continuous compound treatment. As was observed in HCT-116 cells, **24** demonstrated no antiproliferative



**Figure 3. X-ray crystallographic structure of human CK2 $\alpha$  in complex with pyrazolopyrimidines and kinome-wide selectivity of the library** (A) and (B) **24** (A, PDB: 6Z83) is shown in yellow and **29** (B, PDB: 6Z84) in teal stick representation, respectively. The hinge region is colored brown, the  $\alpha$ C helix blue, the DWG motif green, and water molecules are shown as red spheres. The pink P loop was made transparent for better view of the interaction. Hydrogen bonds are indicated as black dashed lines. The insert on the upper left corner of each panel shows the electron density map ( $2F_o - F_c$ ) of the bound ligand contoured at  $1\sigma$ . (C) Heatmap of kinome-wide selectivity of all analogs and CX-4945, ranked from most (top) to least (bottom) selective, when profiled against 403 wild-type kinases at  $1\mu\text{M}$  in the DiscoverX scanMAX platform. (D) Kinome-wide selectivity of SGC-CK2-1 (**24**) displayed as % control and ranked from most (left) to least (right) inhibited when profiled against 403 wild-type kinases at  $1\mu\text{M}$  in the DiscoverX scanMAX platform.

activity when tested up to a concentration of  $10\mu\text{M}$ . We also investigated whether **24** could activate caspase 3/7 in U-87 MG cells (Rahnel et al., 2017). At multiple time points, no caspase 3/7 activation was observed when tested up to a concentration of  $10\mu\text{M}$ .

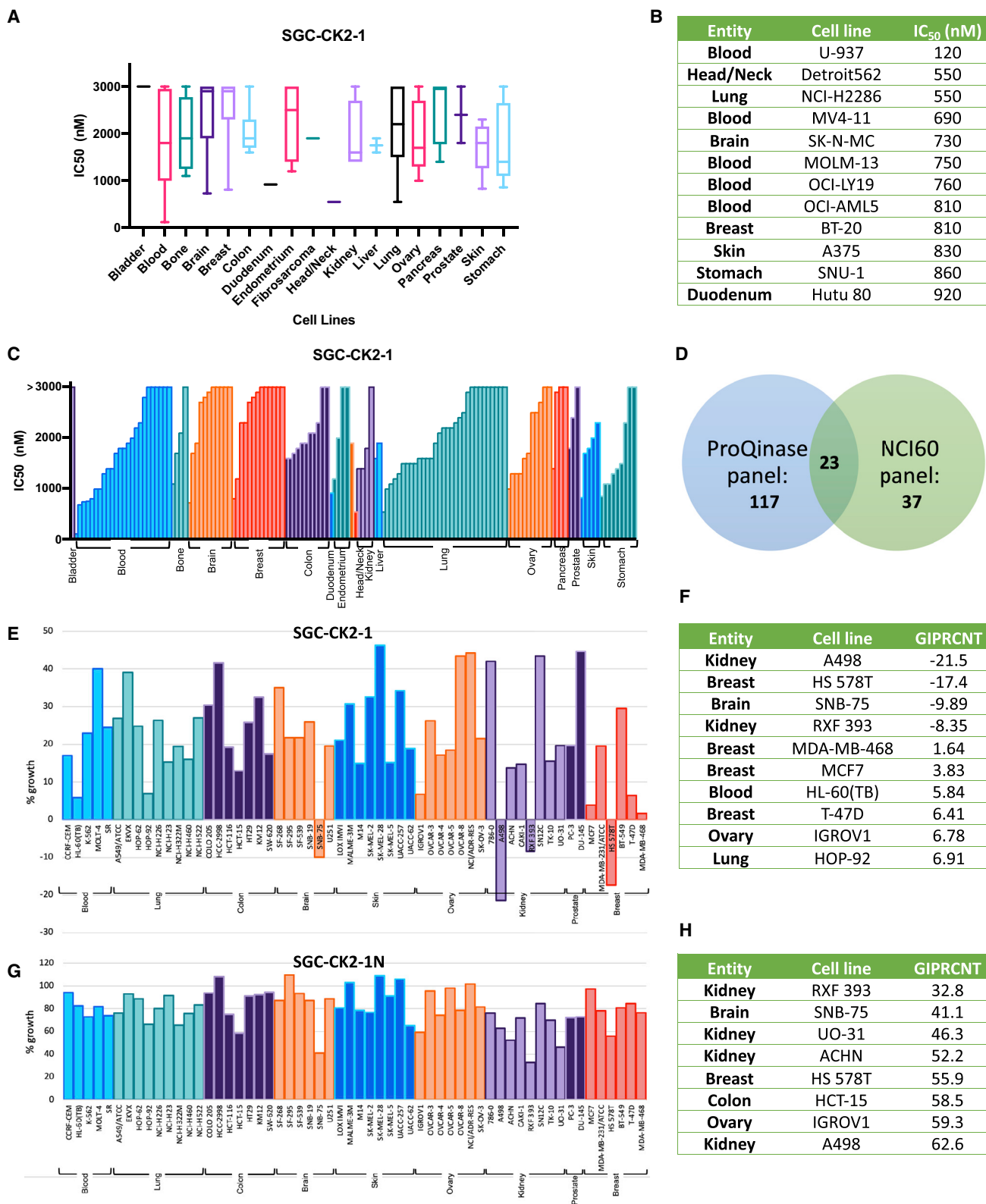
Motivated by the lack of antiproliferative activity of SGC-CK2-1 (**24**) in HCT-116 and U-87 MG cells, we opted to further profile this compound in multiple large panels of cancer cell lines (Figure 4). We profiled **24** against 140 cancer cell lines in eight-point dose-response. Remarkably, we found that **24** only inhibited cell proliferation below  $500\text{ nM}$  in one cell line, a pro-monocytic, human histiocytic lymphoma line U-937 (Figures 4A and 4B). Figure 4C and Table S3 contain antiproliferative results for all 140 cell lines tested. In parallel, we profiled SGC-CK2-1 (**24**) and SGC-CK2-1N (**32**) using the NCI60 panel at  $10\mu\text{M}$  (Figures 4E–4H) (Shoemaker, 2006). As shown in Figure 4D and Table S3, 23 cell lines are shared in common between the 140 and NCI60 panels. We profiled SGC-CK2-1 in 176 distinct cancer cell lines in total. SGC-CK2-1 elicited minor lethality (8%–22%) in A498, HS 578T, RXF 393, and SNB-75 cells and inhibited growth >90% in an additional six cell lines at the single  $10\mu\text{M}$  dose (Figures 4E and 4F). SGC-CK2-1N was devoid of significant antiproliferative activity (Figures 4G and 4H).

### SGC-CK2-1 potently modulates downstream cellular activity

With a chemical probe in hand that possesses exquisite kinase selectivity, binds to CK2 in cells, and does not elicit widespread

antiproliferative activity, we sought to verify that this target engagement with CK2 leads to the expected inhibition of downstream phosphorylation events mediated by CK2. To explore the impact of SGC-CK2-1 (**24**) on known downstream CK2 targets we treated HCT-116 cells in dose-response for either 3 h or 24 h. We opted to use HCT-116 cells since they had been used previously in exploring downstream phosphorylation in response to pyrazolopyrimidine-based CK2 inhibitors and to probe whether CK2 is inhibited in these cells despite the lack of evidence of any antiproliferative activity when treated with of SGC-CK2-1 (**24**) (Dowling et al., 2016). CK2 has been shown to phosphorylate AKT at serine 129 (S129), leading to multiple direct and indirect consequences, and phosphorylation at this site has been used to confirm CK2 is active (Di Maira et al., 2005; Girardi and Ruzzone, 2015; Zanin et al., 2012). As shown in Figures 5A and 5B, we observed a dose-dependent decrease in AKT S129 phosphorylation due to treatment of HCT-116 cells at both time points, confirming that CK2 inhibition by **24** results in disruption of its downstream signaling inside the cell. This finding is in alignment with previously reported CK2 inhibitors.

Additional studies targeted at studying CK2 downstream signaling were performed using EIF2S2, a known substrate and interacting partner for CK2, as a biomarker for CK2 inhibition (Llorens et al., 2003). These analyses were performed using human osteosarcoma (U2OS) cells engineered to express wild-type CK2 $\alpha$  or a double mutant of CK2 $\alpha$  (designated DM, harboring V66A/I174A substitutions) under the control of tetracycline. Both wild-type and DM CK2 $\alpha$  incorporate HA epitope tags



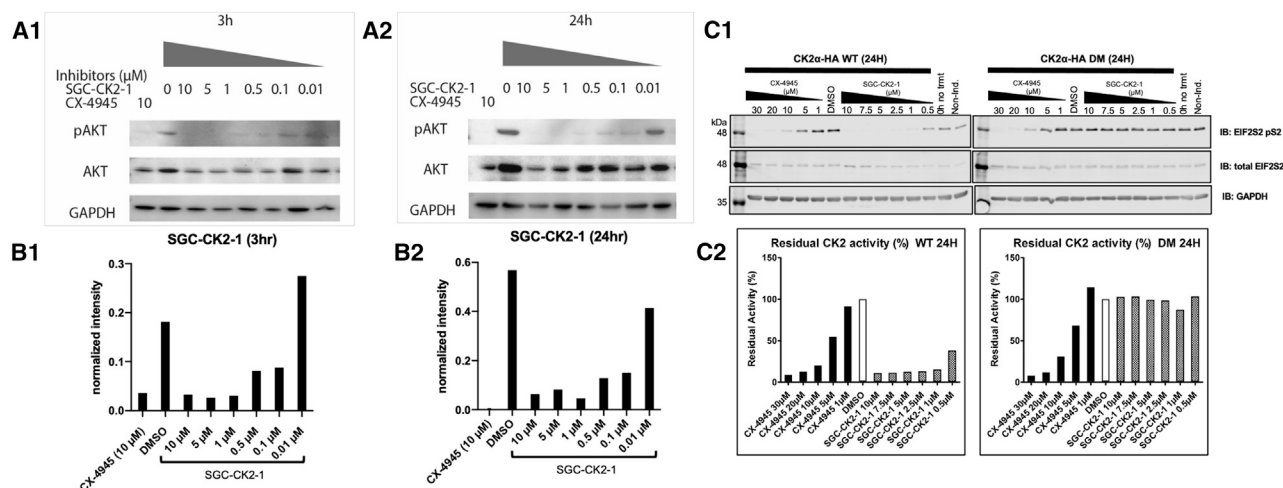
**Figure 4. SGC-CK2-1 (24) evaluated for antiproliferative activity**

(A) Potency data for 140 cell lines grouped by origin.

(B) Growth inhibited cell lines within 140 panel with an IC<sub>50</sub> value < 1 μM.

(legend continued on next page)





**Figure 5. Western blot analysis and quantification in response to SGC-CK2-1 (24)**

(A) Western blot for HCT-116 cell protein extracts (20  $\mu$ g) treated with decreasing doses of SGC-CK2-1 and CX-4945 as positive control (from left to right: CX-4945 10  $\mu$ M, DMSO 0.1%, SGC-CK2-1 10  $\mu$ M, 5  $\mu$ M, 1  $\mu$ M, 0.5  $\mu$ M, 0.1  $\mu$ M, and 0.01  $\mu$ M). The inhibition of phosphorylated AKT (S129) and AKT1 was analyzed after 3 h (A1) and 24 h (A2) of inhibitor treatment. Glyceraldehyde-3-phosphate dehydrogenase (GAPDH) was used as a loading control.

(B) Intensity levels of phosphorylated AKT (S129) normalized against GAPDH loading control of western blot analysis after 3 h (B1) and 24 h (B2) of compound treatment.

(C) Phosphorylation of EIF2S2 in FT-U2OS cells expressing wild-type (WT) or DM, V66A/I174A) CK2 $\alpha$ . Expression of exogenous CK2 $\alpha$  was induced with tetracycline for 48 h and cells were then treated for 24 h with decreasing doses of CX-4945 or SGC-CK2-1: CX-4945 (30, 20, 10, 5, 1  $\mu$ M), SGC-CK2-1 (10, 7.5, 5, 2.5, 1, 0.5  $\mu$ M). As controls, cells were also subjected to treatment with DMSO (vehicle control) or were analyzed either without induction of exogenous CK2 $\alpha$  or without any treatment as indicated. (C1) Phosphorylation of EIF2S2 was assessed by immunoblot analysis (top panels) together with analysis of total levels of EIF2S2 (middle panels) and GAPDH (bottom panels) as loading controls. (C2) Residual CK2 activity reflects phosphorylation of EIF2S2 expressed as the percentage of the level of phosphorylation detected in the absence of the inhibitor.

to enable detection. Mutations in the DM (V66A/I174A) are within the ATP binding site and abolish binding of high-affinity type I inhibitors. While dose-dependent inhibition of EIF2S2 pS2 was observed in the case of wild-type CK2 $\alpha$ -HA, SGC-CK2-1 did not affect phosphorylation of EIF2S2 in the cells harboring the DM CK2 $\alpha$ -HA (Figure 5C). This is in contrast to CX-4945, which exhibited dose-dependent inhibition of EIF2S2 pS2 in cells with wild-type and DM CK2 $\alpha$ -HA. Of note, SGC-CK2-1 demonstrated robust inhibition of CK2 and its downstream signaling at a concentration at least 10 $\times$  less than CX-4945.

## DISCUSSION

While it was anticipated that the minor structural changes to the pyrazolopyrimidine lead structure would result in compounds of similar potency and selectivity to their progenitors, analogs with more significant structural changes were designed to probe the pocket and determine which interactions were favorable and what changes might lead to enhanced selectivity. Comparison of the CK2 nanoBRET data corresponding with analogs **19** and **20** with that generated for analogs **15–18**, **22**, and **24** confirm that the portion of the binding pocket that accommodates the

morpholine (**19**) or benzylamine (**20**) is also sensitive to changes in steric bulk. While the other analogs bear a methyl or alkyldiamine group, incorporation of the bulkier morpholine and especially the benzylamine results in significant loss in CK2 cellular target engagement. These data support that cyclic side chains at this position do not increase affinity for CK2.

An interesting observation was made in examining the structures of **22**, **24**, and **26** and their corresponding biological data. While the difference in structures is only a methyl group (acetamide in **22** and propionamide in **24**), **24** inhibits considerably fewer off-target kinases than **22**. This finding is supported by our follow-up data in Table 2 for **24**, and the data provided in the original publication for **22**. CK2, DYRK1–3, HIPK1–3, and DAPK1–3 were all inhibited with residual activity <45% at 0.1  $\mu$ M, supporting our finding that **22** is less selective than **24** (Dowling et al., 2013). While our X-ray crystallography structures of **24** and **29**, like those solved for other pyrazolopyrimidines, support that the CK2 $\alpha$  ATP pocket has space to accommodate the homologated amide, it appears that other kinases may not be as tolerant. This part of the CK2 $\alpha$  pocket is only moderately tolerant, as there is a 10-fold loss in CK $\alpha$  cellular target engagement in moving from **22** to **24** and a significant 200-fold loss in

(C) Proliferation data as IC<sub>50</sub> values for all 140 cancer cell lines profiled.

(D) Overlapping cell lines in antiproliferative panels.

(E) NCI60 results for SCG-CK2-1 when tested at 10  $\mu$ M. Bars above zero indicate growth inhibition, while bars below zero indicate lethality.

(F) Cell lines with growth inhibited percentage (GIPRCNT) < 10 when treated with 10  $\mu$ M SGC-CK2-1.

(G) NCI60 results for SCG-CK2-1N when tested at 10  $\mu$ M. All bars reflect growth inhibition.

(H) Cell lines with GIPRCNT < 65 when treated with 10  $\mu$ M SGC-CK2-1N.

moving from **24** to **26**. So changing from acetamide to propionamide to cyclopropanecarboxamide, while subtly different in structure, results in significantly reduced CK2 cellular target engagement as well as number of kinases inhibited in broad profiling ( $S_{10}$  score, Table 2). We propose that modifying this part of the pyrazolopyrimidine scaffold and/or accessing this part of the ATP binding site may be key to building in selectivity for CK2 versus other kinases.

The exquisite selectivity of **24** for CK2 was explored from a structural perspective. CK2 shares closest structural homology with the DYRKs, HIPKs, CLKs, and SPRKs within the CMGC subfamily. The main differences between CK2 and DYRK family members are in the hinge (H115 in CK2 $\alpha$  or Y116 in CK2 $\alpha'$  versus M/L in DYRKs) and key hydrophobic contact in  $\beta$ -sheet 7 (M163 in CK2 $\alpha$  or M164 in CK2 $\alpha'$  versus L/V in DYRKs). We hypothesize that the larger xDFG/pre-DFG residue (I174 for CK2 $\alpha$  or I175 for CK2 $\alpha'$  versus V for DYRK1A/B) also contributes to better binding to CK2, a strategy that has been used by others in the field to impart selectivity (Martin et al., 2012; Rudolph et al., 2015; Schröder et al., 2020; Tong et al., 2013). This hypothesis is further supported by our studies with DM CK2 $\alpha$  (Figure 5C), in which I174 is mutated to A174. Since critical interactions with V66 are not observed (Figures 3 and S6), the I174A mutation seems responsible for obliteration of SGC-CK2-1 binding to CK2 $\alpha$ , demonstrating the sensitivity of SGC-CK2-1 to subtle changes in the CK2 $\alpha$  ATP binding site. The overlay of **24** bound to CK2 versus DYRK2 and DYRK1A (Figure S6) shows improved hydrophobic contacts in the case of CK2. It is also interesting to note that we do not observe any CLK family inhibition despite their high structural homology. CLK family kinases are often an off target of CK2 inhibitors, including CX-4945.

We found that the most selective compounds, **20**, **24**, **26**, and **27**, demonstrated no antiproliferative activity in our HCT-116 antiproliferation assay. Since these compounds were found to only inhibit CK2 $\alpha$  and CK2 $\alpha'$ , a working hypothesis is that the antiproliferative activity exhibited by less selective compounds was likely due to inhibition of an off-target kinase or combination of kinases and not due solely to inhibition of CK2. From examination of the inhibition profiles of the most potent inhibitors of proliferation in HCT-116 cells, **15**, **17**, **18**, and **22**, potent inhibition (>80%) of DAPK1–3, DYRK2, HIPK1–3, and RPS6KA4 at 1  $\mu$ M in the DiscoverX binding assay emerged (Figure S5). Our follow-up  $K_d$  determinations at DiscoverX for **17** confirmed that it potently inhibits all of these kinases with values <8 nM. Compounds **20**, **24**, **26**, **27**, and **32** were devoid of activity for these same kinases (<50% for most) at 1  $\mu$ M in the DiscoverX binding assay, while the remainder of compounds tested showed less consistent potent inhibition of these same kinases. We followed up on off-target kinases potently inhibited in the DiscoverX panel using the corresponding enzymatic assays run at the  $K_m$  of ATP for the compounds that inhibit proliferation of HCT-116 cells (**15**, **17**, **18**, and **22**). Although the binding data implicate several kinases, published and collected enzymatic data point to inhibition of DAPKs as driving the antiproliferative activity (Figure S5) (Dowling et al., 2016). The most potent antiproliferative agents in the series (**17** and **18**) demonstrate significant inhibition of both DAPK2 and DAPK3 in addition to CK2 ( $IC_{50}$  values <130 nM). Antiproliferative activity is reduced with less potent inhibition of DAPK2 and/or DAPK3 by **15** and especially **22**. The

DAPK family has been reported to have effects on cell proliferation (Elbadawy et al., 2018). Furthermore, dual DAPK1 and DAPK3 inhibition has been shown to result in HCT-116 apoptosis (Elbadawy et al., 2018; Farag and Roh, 2019). We hypothesize that inhibiting a combination of DAPK1–3 and CK2 may be causing the antiproliferative effects that we are observing with our most potent growth inhibitors (**15**, **17**, **18**, and **22**).

Anti-tumor drugs are known to display different anti-proliferative efficacy depending on the cell lines used in the assay. We have shown that SGC-CK2-1 (**24**) does not demonstrate significant antiproliferative activity against a panel of 140 different cancer cell lines originating from 18 different locations within the body. The most sensitive cell line, U937, is a human myeloid leukemia cell line. An association between CK2 inhibition and leukemia has been previously reported, with higher expression levels of CK2 being associated with a poorer prognosis (Kim et al., 2007). It was gratifying to see no significant antiproliferative activity elicited by SGC-CK2-1N in the NCI60 panel. Cell lines that demonstrated some lethality in response to SGC-CK2-1 in the NCI60 panel include one brain cancer cell line (SNB-75), two kidney cell lines (A498 and RXF 393), and one breast cancer cell line (HS 578T). Of note, two of these four were the most inhibited (>58%, Figure 4H) cell lines by SGC-CK2-1N (SNB-75 and RXF 393), so there is clearly some sensitivity to the scaffold that is not related to CK2 inhibition. A498 cells were also included in the 140-cell line panel. While an  $IC_{50}$  = 1.8  $\mu$ M was determined for growth inhibition in these cells in the larger panel study, 10  $\mu$ M SGC-CK2-1 induced some cell death. The last cell line that demonstrated lethality in response to SGC-CK2-1 (HS 578T) is a breast cancer cell line that has been shown to overexpress CK2 and depend on CK2 for its survival (Romieu-Mourez et al., 2001, 2002). Other cancer cell lines in common between the two panels that demonstrated >93% growth inhibition in response to 10  $\mu$ M SGC-CK2-1 include HL-60, MCF7, MDA-MB-468, and T-47D ( $IC_{50}$  values 1.2–2.8  $\mu$ M). Generally, we found leukemia (HL-60 and U937) and breast (MCF7, MDA-MB-468, T-47D, and HS 578T) cancer cells to be most responsive to our chemical probe in terms of proliferation.

In general, we found no correlation between CK2 expression and sensitivity of a particular cell line to our chemical probe. One hypothesis that could explain why our compound does not affect proliferation in nearly all of these diverse hyperproliferating cell lines is that they have evolved to shunt around CK2 control of processes such as DNA damage repair and p53 activation (Rabalski et al., 2016). One reported role of CK2 is DNA damage cell cycle checkpoint control, while another related role is regulation of p53 function (McKendrick et al., 1999; Montenarh, 2016). If cancer cells are able to circumvent these regulatory pathways to promote their survival and growth, they become less sensitive to CK2 inhibition. Subcellular localization of CK2 has also been described as key to its function and certain sub-populations may be more critical for survival/viability, adding another layer of complexity to CK2 biology (Faust and Montenarh, 2000).

Using the same experimental context (same cell line and same dose range), we confirmed the inability of SGC-CK2-1 (**24**) to counteract proliferation of HCT-116 cells despite suppression of endogenous CK2 activity. While the literature strongly supports that CK2 drives proliferation and oncogenesis as a

pro-survival protein kinase overexpressed in cancer (Chua et al., 2017; Di Maira et al., 2019; Trembley et al., 2009), our results challenge this paradigm. The use of CK2 inhibitors with suboptimal kinome-wide selectivity has added to this notion, through ascribing results to CK2 that are likely due to off-target kinase inhibition. Our studies have demonstrated that SGC-CK2-1 is more selective and potent in cellular target engagement as well as inhibition of downstream signaling elicited by CK2 $\alpha$  (generally the predominant catalytic subunit of CK2) than CX-4945 and that it lacks the antiproliferative effects that have been reported for CX-4945 and have motivated its use in clinical trials for multiple oncological indications (Chon et al., 2015; Eroglu et al., 2020; Siddiqui-Jain et al., 2010; Zakharia et al., 2019). While inhibition of CK2 $\alpha$  by either SGC-CK2-1 or CX-4945 can be prevented by expression of a V66A/I174A DM of CK2 $\alpha$ , phosphorylation is recovered (or inhibition is prevented) nearly completely by SGC-CK2-1. These experiments demonstrate that SGC-CK2-1 more efficiently inhibits CK2 than CX-4945, as a 10 times lower concentration is required to elicit the same response. That inhibition by SGC-CK2-1 is more effectively prevented with the CK2 mutant supports that SGC-CK2-1 yields a much “cleaner” analysis of CK2-dependent effects within cells. Reduction of CK2 activity via knockout of CK2 $\alpha$  has been found to significantly enhance the cytotoxicity of approved chemotherapeutics so a combination strategy may prove fruitful when using SGC-CK2-1 in a cancer context (Di Maira et al., 2019).

In addition to its potential applications in deciphering the biological roles of CK2 at the cellular level, a highly selective probe for CK2 may also have important implications related to CK2 as a potential therapeutic target. For example, CK2 is highly expressed in the brain and has been implicated in the molecular pathology of neurodegenerative diseases (Castello et al., 2017). The non-toxic nature our selective CK2 probe suggests that CK2 inhibition could be a viable approach for treating disorders of the brain. Roles for CK1 and CK2 have recently been discovered in the molecular pathology of different neurodegenerative disorders, such as Alzheimer disease (AD), Parkinson disease (PD), amyotrophic lateral sclerosis (ALS), and frontotemporal dementia (FTD) (Perez et al., 2011). CK2 has been shown to be involved in the neuroinflammatory response in AD mediated by astrocytes, to co-localize with  $\alpha$ -synuclein in Lewy bodies in PD patient brains, and to contribute to the formation of TDP-43 aggregates in ALS and FTD (Hasegawa et al., 2008; Rosenberger et al., 2016; Ryu et al., 2008). In addition, the recent finding that host cell CK2 activity is hijacked by SARS-CoV-2 indicates that a non-toxic inhibitor of CK2 could be a valuable antiviral agent (Bouhaddou et al., 2020). Overall, the identification of specific, non-toxic inhibitors of CK2, like SGC-CK2-1, could represent a therapeutic option to treat neurodegenerative diseases and viral infections.

## SIGNIFICANCE

**We have described the design, synthesis, and biological evaluation of a series of pyrazolopyrimidines as selective inhibitors of CK2 $\alpha$  and CK2 $\alpha'$ . We have demonstrated that our probe is CK2 active using three orthogonal assay formats: binding assay at DiscoverX, radiometric enzyme assay at Eurofins, and nanoBRET cellular target engagement assays.**

**Compound 24 (SGC-CK2-1) emerged as our chemical probe candidate. This compound outperforms all published inhibitors in terms of kinome-wide selectivity. When combined with its potent cellular activity and confirmed inhibition of downstream CK2 signaling, our chemical probe represents a high-quality tool to interrogate CK2 biology. Importantly, this confirmed inhibitor of CK2 does not elicit significant antiproliferative activity when broadly profiled. This is in stark contrast to widely studied and less selective inhibitors of CK2 and opens the door to exploring the roles of CK2 beyond oncology, such as in the areas of neuroscience and virology. With so many putative substrates, CK2 is clearly a pleiotropic kinase. Additional studies aided by this chemical probe and the negative control are underway that aim to deconvolute CK2 biology and refine its roles in key disease-propagating pathways.**

## STAR★METHODS

Detailed methods are provided in the online version of this paper and include the following:

- KEY RESOURCES TABLE
- RESOURCE AVAILABILITY
  - Lead Contact
  - Materials Availability
  - Data and Code Availability
- EXPERIMENTAL MODEL AND SUBJECT DETAILS
  - Cell lines
- METHOD DETAILS
  - General information for chemical synthesis
  - Kinome screening
  - *In vitro* kinase radiometric kinase profiler and LANCE assays
  - NanoBRET measurements
  - HCT-116 and U-87 MG 72hr AlamarBlue cell proliferation assay
  - Caspase-Glo 3/7 assay
  - ProKinase broad tumor cell line profiling
  - NCI60 profiling
  - HCT-116 western blot analyses
  - U2OS western blot analyses
  - Crystallography Methods
- QUANTIFICATION AND STATISTICAL ANALYSIS
  - Statistical analysis
- ADDITIONAL RESOURCES

## SUPPLEMENTAL INFORMATION

Supplemental information can be found online at <https://doi.org/10.1016/j.chembiol.2020.12.013>.

## ACKNOWLEDGMENTS

Constructs for NanoBRET measurements of CK2 $\alpha$ , CK2 $\alpha'$ , and DYRK2 were kindly provided by Promega. Drs. Koshlap and Picado provided NMR support and helped with structural confirmation of **32**. We thank the Department of Chemistry Mass Spectrometry Core Laboratory at UNC for their assistance with mass spectrometry analysis. We used the TREEspot kinase interaction mapping software to prepare the kinome trees in our Table of Contents graphic and Supplemental Information: <http://treespot.discoverx.com>. Figure 1 was

created with [Biorender.com](https://biorender.com). We thank PharmAdvance for synthetic support. We also thank the beamline scientists at the Swiss Light Source (CH) for their great support during data collection and the NCI for performing proliferation studies (NCI60).

The SGC is a registered charity (number 1097737) that receives funds from AbbVie, Bayer Pharma AG, Boehringer Ingelheim, Canada Foundation for Innovation, Eshelman Institute for Innovation, Genome Canada, Genentech, Innovative Medicines Initiative (EU/EFPIA) (ULTRA-DD grant no. 115766), Janssen, Merck KGaA Darmstadt Germany, MSD, Novartis Pharma AG, Ontario Ministry of Economic Development and Innovation, Pfizer, São Paulo Research Foundation-FAPESP, Takeda, and Wellcome (106169/ZZ14/Z). Research reported in this publication was supported in part by the NC Biotech Center Institutional Support Grant 2018-IDG-1030, NIH 1U24DK116204, DOD ALSRP award AL190107, and NC Policy Collaboratory at UNC-CH with funding from the NC Coronavirus Relief Fund established and appropriated by the NC General Assembly. Research was also supported by funding from the Canadian Institutes of Health Research (agency no. 37854) and the Natural Sciences and Engineering Research Council of Canada (RGPIN/04186-2014).

#### AUTHOR CONTRIBUTIONS

Conceptualization, C.I.W., D.H.D., and A.D.A.; Validation, C.I.W., S.K., L.G., D.W.L., and A.D.A.; Formal Analysis, C.I.W., A.K., and L.G.; Investigation, C.I.W., J.E.P., A.T., A.K., D.M., L.G., and A.D.A.; Resources C.I.W., S.K., D.W.L., and A.D.A.; Writing – Original Draft, C.I.W. and A.D.A.; Writing – Review & Editing, all authors; Visualization, C.I.W., A.T., A.K., L.G., and A.D.A.; Supervision, C.I.W., S.M., S.K., L.G., D.W.L., and A.D.A.; Project Administration, A.D.A.; Funding Acquisition, A.D.A.

#### DECLARATION OF INTERESTS

The authors declare no competing interests.

Received: November 5, 2020

Revised: November 30, 2020

Accepted: December 22, 2020

Published: January 22, 2021

#### REFERENCES

- Ahmed, K., Gerber, D.A., and Cochet, C. (2002). Joining the cell survival squad: an emerging role for protein kinase CK2. *Trends Cell Biol.* *12*, 226–230.
- Ardito, F., Giuliani, M., Perrone, D., Troiano, G., and Lo Muzio, L. (2017). The crucial role of protein phosphorylation in cell signaling and its use as targeted therapy. *Int J. Mol. Med.* *40*, 271–280.
- Asquith, C.R.M., Berger, B.-T., Wan, J., Bennett, J.M., Capuzzi, S.J., Crona, D.J., Drewry, D.H., East, M.P., Elkins, J.M., Fedorov, O., et al. (2019). SGC-GAK-1: a chemical probe for cyclin G associated kinase (GAK). *J. Med. Chem.* *62*, 2830–2836.
- Banerjee, S., Wei, T., Wang, J., Lee, J.J., Gutierrez, H.L., Chapman, O., Wiley, S.E., Mayfield, J.E., Tandon, V., Juarez, E.F., et al. (2019). Inhibition of dual-specificity tyrosine phosphorylation-regulated kinase 2 perturbs 26S proteasome-addicted neoplastic progression. *Proc. Natl. Acad. Sci. U S A* *116*, 24881–24891.
- Battistutta, R., Cozza, G., Pierre, F., Papinutto, E., Lolli, G., Sarno, S., O'Brien, S.E., Siddiqui-Jain, A., Haddach, M., Anderes, K., et al. (2011). Unprecedented selectivity and structural determinants of a new class of protein kinase CK2 inhibitors in clinical trials for the treatment of cancer. *Biochemistry* *50*, 8478–8488.
- Bosc, N., Meyer, C., and Bonnet, P. (2017). The use of novel selectivity metrics in kinase research. *BMC Bioinformatics* *18*, 17.
- Bouhaddou, M., Memon, D., Meyer, B., White, K.M., Rezelj, V.V., Correa Marrero, M., Polacco, B.J., Melnyk, J.E., Ulferts, S., Kaake, R.M., et al. (2020). The global phosphorylation landscape of SARS-CoV-2 infection. *Cell* *182*, 685–712.
- Castello, J., Ragnauth, A., Friedman, E., and Rebholz, H. (2017). CK2—an emerging target for neurological and psychiatric disorders. *Pharmaceuticals* *10*, 7.
- Chon, H.J., Bae, K.J., Lee, Y., and Kim, J. (2015). The casein kinase 2 inhibitor, CX-4945, as an anti-cancer drug in treatment of human hematological malignancies. *Front. Pharmacol.* *6*, 70.
- Chua, M.M.J., Ortega, C.E., Sheikh, A., Lee, M., Abdul-Rassoul, H., Hartshorn, K.L., and Dominguez, I. (2017). CK2 in cancer: cellular and biochemical mechanisms and potential therapeutic target. *Pharmaceuticals* *10*, 18.
- Chuaqui, C.E., Dowling, J.E., Lyne, P., Pontz, T., and Ye, Q. (2013). 3-cyano-5-aryl-amino-7-cycloalkylaminopyrrolo[1, 5 - a]pyrimidine derivatives and their use as antitumor agents, *WO2013144532A1* (AstraZeneca UK Limited).
- Davis, M.I., Hunt, J.P., Herrgard, S., Ciceri, P., Wodicka, L.M., Pallares, G., Hocker, M., Treiber, D.K., and Zarrinkar, P.P. (2011). Comprehensive analysis of kinase inhibitor selectivity. *Nat. Biotechnol.* *29*, 1046–1051.
- Di Maira, G., Gentilini, A., Pastore, M., Caligiuri, A., Piombanti, B., Raggi, C., Rovida, E., Lewinska, M., Andersen, J.B., Borgo, C., et al. (2019). The protein kinase CK2 contributes to the malignant phenotype of cholangiocarcinoma cells. *Oncogenesis* *8*, 61.
- Di Maira, G., Salvi, M., Arrigoni, G., Marin, O., Sarno, S., Brustolon, F., Pinna, L.A., and Ruzzene, M. (2005). Protein kinase CK2 phosphorylates and upregulates Akt/PKB. *Cell Death Differ.* *12*, 668–677.
- Dowling, J.E., Alimzhanov, M., Bao, L., Block, M.H., Chuaqui, C., Cooke, E.L., Denz, C.R., Hird, A., Huang, S., Larsen, N.A., et al. (2013). Structure and property based design of pyrazolo[1,5-a]pyrimidine inhibitors of CK2 kinase with activity in vivo. *ACS Med. Chem. Lett.* *4*, 800–805.
- Dowling, J.E., Alimzhanov, M., Bao, L., Chuaqui, C., Denz, C.R., Jenkins, E., Larsen, N.A., Lyne, P.D., Pontz, T., Ye, Q., et al. (2016). Potent and selective CK2 kinase inhibitors with effects on wnt pathway signaling in Vivo. *ACS Med. Chem. Lett.* *7*, 300–305.
- Dowling, J.E., Chuaqui, C., Pontz, T.W., Lyne, P.D., Larsen, N.A., Block, M.H., Chen, H., Su, N., Wu, A., Russell, D., et al. (2012). Potent and selective inhibitors of CK2 kinase identified through structure-guided hybridization. *ACS Med. Chem. Lett.* *3*, 278–283.
- Elbadawy, M., Usui, T., Yamawaki, H., and Sasaki, K. (2018). Novel functions of death-associated protein kinases through mitogen-activated protein kinase-related signals. *Int. J. Mol. Sci.* *19*, 3031.
- Emsley, P., and Cowtan, K. (2004). Coot: model-building tools for molecular graphics. *Acta Crystallogr. D Biol. Crystallogr.* *60*, 2126–2132.
- Eroglu, Z., Cowey, C.L., Soong, J., McCormick, D., Fan, P., Chen, J., Elgendy, M., Jang, S., and Chang, A.L.S. (2020). A phase I study of CX-4945 administered orally twice daily to patients with advanced basal cell carcinoma. *J. Clin. Oncol.* *38*, TPS10080.
- Farag, A.K., and Roh, E.J. (2019). Death-associated protein kinase (DAPK) family modulators: current and future therapeutic outcomes. *Med. Res. Rev.* *39*, 349–385.
- Faust, M., and Montenarh, M. (2000). Subcellular localization of protein kinase CK2. A key to its function? *Cell Tissue Res.* *307*, 329–340.
- Gandin, V., Masvidal, L., Cargnello, M., Gyenis, L., McLaughlan, S., Cai, Y., Tenkerian, C., Morita, M., Balanathan, P., Jean-Jean, O., et al. (2016). mTORC1 and CK2 coordinate ternary and eIF4F complex assembly. *Nat. Commun.* *7*, 11127.
- Girardi, C., and Ruzzene, M. (2015). CK2 function in the regulation of akt pathway. In *Protein Kinase CK2 Cellular Function in Normal and Disease States*, vol 12, K. Ahmed, O.G. Issinger, and R. Szyszka, eds. (Springer), pp. 125–140.
- Golub, A.G., Bdzhola, V.G., Briukhovetska, N.V., Balanda, A.O., Kukhareno, O.P., Kotey, I.M., Ostrynska, O.V., and Yarmoluk, S.M. (2011). Synthesis and biological evaluation of substituted (thieno[2,3-d]pyrimidin-4-ylthio)carboxylic acids as inhibitors of human protein kinase CK2. *Eur. J. Med. Chem.* *46*, 870–876.
- Gowda, C., Sachdev, M., Muthusami, S., Kapadia, M., Petrovic-Dovat, L., Hartman, M., Ding, Y., Song, C., Payne, J.L., Tan, B.H., et al. (2017). Casein



- kinase II (CK2) as a therapeutic target for hematological malignancies. *Curr. Pharm. Des.* **23**, 95–107.
- Gyenis, L., Duncan, J.S., Turowec, J.P., Bretner, M., and Litchfield, D.W. (2011). Unbiased functional proteomics strategy for protein kinase inhibitor validation and identification of bona fide protein kinase substrates: application to identification of EEF1D as a substrate for CK2. *J. Proteome Res.* **10**, 4887–4901.
- Hasegawa, M., Arai, T., Nonaka, T., Kametani, F., Yoshida, M., Hashizume, Y., Beach, T.G., Buratti, E., Baralle, F., Morita, M., et al. (2008). Phosphorylated TDP-43 in frontotemporal lobar degeneration and amyotrophic lateral sclerosis. *Ann. Neurol.* **64**, 60–70.
- Haynes, K.A., and Silver, P.A. (2011). Synthetic reversal of epigenetic silencing. *J. Biol. Chem.* **286**, 27176–27182.
- Kabsch, W. (2010). Xds. *Acta Crystallogr. D Biol. Crystallogr.* **66**, 125–132.
- Kim, H., Choi, K., Kang, H., Lee, S.-Y., Chi, S.-W., Lee, M.-S., Song, J., Im, D., Choi, Y., and Cho, S. (2014). Identification of a novel function of CX-4945 as a splicing regulator. *PLoS One* **9**, e94978.
- Kim, H., Lee, K.-S., Kim, A.-K., Choi, M., Choi, K., Kang, M., Chi, S.-W., Lee, M.-S., Lee, J.-S., Lee, S.-Y., et al. (2016). A chemical with proven clinical safety rescues Down-syndrome-related phenotypes in through DYRK1A inhibition. *Dis. Model. Mech.* **9**, 839–848.
- Kim, J.S., Eom, J.I., Cheong, J.W., Choi, A.J., Lee, J.K., Yang, W.I., and Min, Y.H. (2007). Protein kinase CK2alpha as an unfavorable prognostic marker and novel therapeutic target in acute myeloid leukemia. *Clin. Cancer Res.* **13**, 1019–1028.
- Krämer, A., Kurz, C.G., Berger, B.-T., Celik, I.E., Tjaden, A., Greco, F.A., Knapp, S., and Hanke, T. (2020). Optimization of pyrazolo[1,5-a]pyrimidines lead to the identification of a highly selective casein kinase 2 inhibitor. *Eur. J. Med. Chem.* **208**, 112770.
- Lebedev, A.A., Vagin, A.A., and Murshudov, G.N. (2008). Model preparation in MOLREP and examples of model improvement using X-ray data. *Acta Crystallogr. D Biol. Crystallogr.* **64**, 33–39.
- Lechner, C., Flasshoff, M., Falke, H., Preu, L., Loac, N., Meijer, L., Knapp, S., Chaikwad, A., and Kunick, C. (2019). [b]-Annulated halogen-substituted indoles as potential DYRK1A inhibitors. *Molecules* **24**, 4090.
- Litchfield, D.W. (2003). Protein kinase CK2: structure, regulation and role in cellular decisions of life and death. *Biochem. J.* **369**, 1–15.
- Llorens, F., Roher, N., Miró, F.A., Sarno, S., Ruiz, F.X., Meggio, F., Plana, M., Pinna, L.A., and Itarte, E. (2003). Eukaryotic translation-initiation factor eIF2beta binds to protein kinase CK2: effects on CK2alpha activity. *Biochem. J.* **375**, 623–631.
- Lolli, G., Cozza, G., Mazzorana, M., Tibaldi, E., Cesaro, L., Donella-Deana, A., Meggio, F., Venerando, A., Franchin, C., Sarno, S., et al. (2012). Inhibition of protein kinase CK2 by flavonoids and tyrostatins. A structural insight. *Biochemistry* **51**, 6097–6107.
- Lozeman, F.J., Litchfield, D.W., Piening, C., Takio, K., Walsh, K.A., and Krebs, E.G. (1990). Isolation and characterization of human cDNA clones encoding the alpha and the alpha' subunits of casein kinase II. *Biochemistry* **29**, 8436–8447.
- Martin, M.P., Zhu, J.-Y., Lawrence, H.R., Pireddu, R., Luo, Y., Alam, R., Ozcan, S., Sebt, S.M., Lawrence, N.J., and Schönbrunn, E. (2012). A novel mechanism by which small molecule inhibitors induce the DFG flip in aurora A. *ACS Chem. Biol.* **7**, 698–706.
- McKendrick, L., Milne, D., and Meek, D. (1999). Protein kinase CK2-dependent regulation of p53 function: evidence that the phosphorylation status of the serine 386 (CK2) site of p53 is constitutive and stable. *Mol. Cell Biochem* **191**, 187–199.
- Meggio, F., and Pinna, L.A. (2003). One-thousand-and-one substrates of protein kinase CK2? *FASEB J.* **17**, 349–368.
- Montenarh, M. (2016). Protein kinase CK2 in DNA damage and repair. *Transl Cancer Res.* **5**, 49–63.
- Núñez de Villavicencio-Díaz, T., Rabalski, A.J., and Litchfield, D.W. (2017). Protein kinase CK2: intricate relationships within regulatory cellular networks. *Pharmaceuticals* **10**, 27.
- Pagano, M.A., Bain, J., Kazimierczuk, Z., Sarno, S., Ruzzene, M., Di Maira, G., Elliott, M., Orzeszko, A., Cozza, G., Meggio, F., et al. (2008). The selectivity of inhibitors of protein kinase CK2: an update. *Biochem. J.* **415**, 353–365.
- Pencheva, N., de Gooijer, M.C., Vis, D.J., Wessels, L.F.A., Wurdinger, T., van Tellingen, O., and Bernards, R. (2017). Identification of a druggable pathway controlling glioblastoma invasiveness. *Cell Rep.* **20**, 48–60.
- Perez, D.I., Gil, C., and Martinez, A. (2011). Protein kinases CK1 and CK2 as new targets for neurodegenerative diseases. *Med. Res. Rev.* **31**, 924–954.
- Pierre, F., Chua, P.C., O'Brien, S.E., Siddiqui-Jain, A., Bourbon, P., Haddach, M., Michaux, J., Nagasawa, J., Schwaebel, M.K., Stefan, E., et al. (2011). Discovery and SAR of 5-(3-chlorophenylamino)benzo[c][2,6]naphthyridine-8-carboxylic acid (CX-4945), the first clinical stage inhibitor of protein kinase CK2 for the treatment of cancer. *J. Med. Chem.* **54**, 635–654.
- Plattner, F., and Bibb, J.A. (2012). Chapter 25 - serine and threonine phosphorylation. In *Basic Neurochemistry*, Eighth Edition, S.T. Brady, G.J. Siegel, R.W. Albers, and D.L. Price, eds. (Academic Press), pp. 467–492.
- Rabalski, A.J., Gyenis, L., and Litchfield, D.W. (2016). Molecular pathways: emergence of protein kinase CK2 (CSNK2) as a potential target to inhibit survival and DNA damage response and repair pathways in cancer cells. *Clin. Cancer Res.* **22**, 2840–2847.
- Rahnel, H., Viht, K., Lavogina, D., Mazina, O., Haljasorg, T., Enkvist, E., and Uri, A. (2017). A selective biligand inhibitor of CK2 increases caspase-3 activity in cancer cells and inhibits platelet aggregation. *ChemMedChem* **12**, 1723–1736.
- Röhm, S., Krämer, A., and Knapp, S. (2020). Function, structure and topology of protein kinases. In *Topics in Medicinal Chemistry* (Springer), pp. 1–24.
- Romieu-Mourez, R., Landesman-Bollag, E., Seldin, D.C., and Sonenshein, G.E. (2002). Protein kinase CK2 promotes aberrant activation of nuclear factor- $\kappa$ B, transformed phenotype, and survival of breast cancer cells. *Cancer Res.* **62**, 6770–6778.
- Romieu-Mourez, R., Landesman-Bollag, E., Seldin, D.C., Traish, A.M., Mercurio, F., and Sonenshein, G.E. (2001). Roles of IKK kinases and protein kinase CK2 in activation of nuclear factor- $\kappa$ B in breast cancer. *Cancer Res.* **61**, 3810–3818.
- Rosenberger, A.F.N., Morrema, T.H.J., Gerritsen, W.H., van Haastert, E.S., Snkhchyan, H., Hilhorst, R., Rozemuller, A.J.M., Scheltens, P., van der Vies, S.M., and Hoozemans, J.J.M. (2016). Increased occurrence of protein kinase CK2 in astrocytes in Alzheimer's disease pathology. *J. Neuroinflamm* **13**, 4.
- Rudolph, J., Aliagas, I., Crawford, J.J., Mathieu, S., Lee, W., Chao, Q., Dong, P., Rouge, L., Wang, W., Heise, C., et al. (2015). Leveraging the pre-DFG residue thr-406 to obtain high kinase selectivity in an aminopyrazole-type PAK1 inhibitor series. *ACS Med. Chem. Lett.* **6**, 711–715.
- Ryu, M.Y., Kim, D.W., Arima, K., Mouradian, M.M., Kim, S.U., and Lee, G. (2008). Localization of CKII beta subunits in Lewy bodies of Parkinson's disease. *J. Neurol. Sci.* **266**, 9–12.
- Salvi, M., Sarno, S., Cesaro, L., Nakamura, H., and Pinna, L.A. (2009). Extraordinary pleiotropy of protein kinase CK2 revealed by weblogo phospho-proteome analysis. *Biochim. Biophys. Acta* **1793**, 847–859.
- Sarno, S., Reddy, H., Meggio, F., Ruzzene, M., Davies, S.P., Donella-Deana, A., Shugar, D., and Pinna, L.A. (2001). Selectivity of 4,5,6,7-tetrabromobenzotriazole, an ATP site-directed inhibitor of protein kinase CK2 ('casein kinase-2'). *FEBS Lett.* **496**, 44–48.
- Schröder, M., Bullock, A.N., Fedorov, O., Bracher, F., Chaikwad, A., and Knapp, S. (2020). DFG-1 residue controls inhibitor binding mode and affinity, providing a basis for rational design of kinase inhibitor selectivity. *J. Med. Chem.* **63**, 10224–10234.
- Shoemaker, R.H. (2006). The NCI60 human tumour cell line anticancer drug screen. *Nat. Rev. Cancer* **6**, 813–823.
- Siddiqui-Jain, A., Drygin, D., Streiner, N., Chua, P., Pierre, F., O'Brien, S.E., Bliesath, J., Omori, M., Huser, N., Ho, C., et al. (2010). CX-4945, an orally bioavailable selective inhibitor of protein kinase CK2, inhibits prosurvival and angiogenic signaling and exhibits antitumor efficacy. *Cancer Res.* **70**, 10288–10298.
- Szyska, R., Grankowski, N., Felczak, K., and Shugar, D. (1995). Halogenated benzimidazoles and benzotriazoles as selective inhibitors of protein-kinases

- CK I and CK II from *Saccharomyces cerevisiae* and other sources. *Biochem. Biophys. Res. Commun.* **208**, 418–424.
- Tong, Y., Stewart, K.D., Florjancic, A.S., Harlan, J.E., Merta, P.J., Przytulinska, M., Soni, N., Swinger, K.K., Zhu, H., Johnson, E.F., et al. (2013). Azaindole-based inhibitors of Cdc7 kinase: impact of the pre-DFG residue, val 195. *ACS Med. Chem. Lett.* **4**, 211–215.
- Trembley, J.H., Wang, G., Unger, G., Slaton, J., and Ahmed, K. (2009). Protein kinase CK2 in health and disease: CK2: a key player in cancer biology. *Cell Mol. Life Sci.* **66**, 1858–1867.
- Vagin, A.A., Steiner, R.A., Lebedev, A.A., Potterton, L., McNicholas, S., Long, F., and Murshudov, G.N. (2004). REFMAC5 dictionary: organization of prior chemical knowledge and guidelines for its use. *Acta Crystallogr. D Biol. Crystallogr.* **60**, 2184–2195.
- Vasta, J.D., Corona, C.R., Wilkinson, J., Zimprich, C.A., Hartnett, J.R., Ingold, M.R., Zimmerman, K., Machleidt, T., Kirkland, T.A., Huwiler, K.G., et al. (2017). Quantitative, wide-spectrum kinase profiling in live cells for assessing the effect of cellular ATP on target engagement. *Cell Chem. Biol.* **25**, 206–214.
- Wells, C., Couñago, R.M., Limas, J.C., Almeida, T.L., Cook, J.G., Drewry, D.H., Elkins, J.M., Gileadi, O., Kapadia, N.R., Lorente-Macias, A., et al. (2019). SGC-AAK1-1: a chemical probe targeting AAK1 and BMP2K. *ACS Med. Chem. Lett.* **11**, 340–345.
- Zakharia, K., Miyabe, K., Wang, Y., Wu, D., Moser, C.D., Borad, M.J., and Roberts, L.R. (2019). Preclinical in vitro and in vivo evidence of an antitumor effect of CX-4945, a casein kinase II inhibitor, in cholangiocarcinoma. *Transl Oncol.* **12**, 143–153.
- Zanin, S., Borgo, C., Girardi, C., O'Brien, S.E., Miyata, Y., Pinna, L.A., Donella-Deana, A., and Ruzzene, M. (2012). Effects of the CK2 inhibitors CX-4945 and CX-5011 on drug-resistant cells. *PLoS One* **7**, e49193.
- Zheng, Y., McFarland, B.C., Drygin, D., Yu, H., Bellis, S.L., Kim, H., Bredel, M., and Benveniste, E.N. (2013). Targeting protein kinase CK2 suppresses prosurvival signaling pathways and growth of glioblastoma. *Clin. Cancer Res.* **19**, 6484–6494.

STAR★METHODS

KEY RESOURCES TABLE

Reagent or Resource	Source	Identifier
<b>Antibodies</b>		
pS129 AKT1	Abcam	Cat# ab133458; RRID: AB_10895993
AKT1	Cell Signaling Technology	Cat# 2920; RRID: AB_1147620
GAPDH	Invitrogen	Cat# MA5-15738; RRID: AB_10977387
GAPDH	Millipore	Cat# MAB374; RRID: AB_2107445
EIF2S2 pS2	YenZym	N/A
Total-EIF2S2	Novus	Cat# H00008894-M09; RRID: AB_1236902
IRDye® 800CW Goat anti-Rabbit IgG Secondary Antibody	LICOR	Cat# 926-32211; RRID: AB_621843
IRDye® 680RD Goat anti-Mouse IgG Secondary Antibody	LICOR	Cat# 926-68070; RRID: AB_10956588
Anti-mouse HRP-linked	Cell Signaling Technology	Cat# 7076; RRID: AB_330924
Anti-rabbit HRP-linked	Cell Signaling Technology	Cat# 7074; RRID: AB_2099233
<b>Bacterial and Virus Strains</b>		
E. Coli BL21 Rosetta DE3	Novagen	Cat# 70954
<b>Chemicals, Peptides, and Recombinant Proteins</b>		
FuGENE HD	Promega	Cat# E2311
Opti-MEM reduced serum medium, no phenol red	Gibco	Cat# 11058021
Dulbecco's Modified Eagle Medium (DMEM)	Gibco	Cat# 11965
Fetal bovine serum (FBS)	Corning	Cat #35-010-CV
AlamarBlue	Invitrogen	Cat# DAL1100
McCoy's 5A media	Corning	Cat# 10-050-CV
Minimal essential medium (MEM)	Gibco	Cat# 11090-081
DMEM w/ High Glucose and L-Glutamine; w/o Sodium Pyruvate, L-Arg, and L-Lys	Wisent	Cat# 319-119-CL
Premium Dialyzed FBS, US Origin	Wisent	Cat# 080-950
Blasticidin S HCl	Wisent	Cat# 400-190-EM
Hygromycin B	Wisent	Cat# 450-141-IG
Penicillin-Streptomycin	Thermo (Gibco)	Cat# 15140-122
Arginin L-Arginine-HCl (non-labeled)	Sigma-Aldrich	Cat# A4599-100G
L-Lysin-HCl (non-labeled)	Sigma-Aldrich	Cat# L7039-100G
L-Proline	Sigma-Aldrich	Cat# P8865-100G
CX-4945 (Silmitasertib)	MedKoo	Cat# 200843
Dimethyl Sulfoxide	Fisher	Cat# BP231-1
<b>Critical Commercial Assays</b>		
CK2a1 NanoBRET	Promega	Cat# NV2981
CK2a2 NanoBRET	Promega	Cat# NV1191
Caspase-Glo 3/7 Assay System	Promega	Cat# G8090
<b>Deposited Data</b>		
CK2 alpha bound to chemical probe SGC-CK2-1 generated	This paper	6Z83
CK2 alpha bound to chemical probe SGC-CK2-1 derivative generated	This paper	6Z84
DYRK2 crystal structure used in analysis	<a href="#">Banerjee et al., 2019</a>	6K0J

(Continued on next page)

**Continued**

Reagent or Resource	Source	Identifier
DYRK1A crystal structure used in analysis	Lechner et al., 2019	6T6A
All associated data for SGC-CK2-1 and SGC-CK2-1N	This paper	<a href="https://www.thesgc.org/chemical-probes/SGC-CK2-1">https://www.thesgc.org/chemical-probes/SGC-CK2-1</a>
<b>Experimental Models: Cell Lines</b>		
HEK-293	ATCC	Cat# CRL-1573
HCT-116	ATCC	Cat# CCL-247
U-87 MG	ATCC	Cat# HTB-14
Flp-In™ T-REx U2OS	(Haynes and Silver, 2011)	N/A
<b>Software and Algorithms</b>		
GraphPad Prism 8.2.0	GraphPad Software, Inc.	<a href="http://www.graphpad.com">http://www.graphpad.com</a>
CCP4 suite (includes used Programs: AIMLESS, REFMAC5, MOLREP and Coot)	Collaborative Computational Project No. 4	<a href="https://www.ccp4.ac.uk/">https://www.ccp4.ac.uk/</a>
XDS	MPI Heidelberg	<a href="http://xds.mpimf-heidelberg.mpg.de/">http://xds.mpimf-heidelberg.mpg.de/</a>
PYMOL	Schrödinger Inc	<a href="https://pymol.org/2/">https://pymol.org/2/</a>
Image Lab Software 6.1	Bio-Rad	<a href="https://www.bio-rad.com/de-de/product/image-lab-software?ID=KRE6P5E8Z">https://www.bio-rad.com/de-de/product/image-lab-software?ID=KRE6P5E8Z</a>

**RESOURCE AVAILABILITY****Lead Contact**

Further information and requests for resources and reagents should be directed to and will be fulfilled by the Lead Contact, Alison Axtman ([alison.axtman@unc.edu](mailto:alison.axtman@unc.edu)).

**Materials Availability**

SGC-CK2-1 and SGC-CK2-1N can be requested at <https://www.thesgc.org/chemical-probes/SGC-CK2-1>. All other compounds can be requested through contacting the Lead Contact.

**Data and Code Availability**

The accession numbers for the crystal structures reported in this paper are PDB: 6Z83 and PDB: 6Z84. Original data have been deposited for SGC-CK2-1 and SGC-CK2-1N to <https://www.thesgc.org/chemical-probes/SGC-CK2-1>.

**EXPERIMENTAL MODEL AND SUBJECT DETAILS****Cell lines****HCT-116**

Human colorectal carcinoma cells; diploid; male (adult). Cells were purchased from ATCC and were cultured in McCoy's 5a Medium (Corning) supplemented with 10% fetal bovine serum (FBS, Corning). Cells were incubated in 5% CO<sub>2</sub> at 37C. Cell lines were passaged every 72 hours with trypsin and not allowed to reach confluency.

**HEK293**

Human embryonic kidney cells; hypotriploid; female (fetal). Cells were purchased from ATCC and grown in Dulbecco's Modified Eagle's medium (DMEM, Gibco) supplemented with 10% (v/v) fetal bovine serum (FBS, Corning). Cells were incubated in 5% CO<sub>2</sub> at 37C. Cell lines were passaged every 72 hours with trypsin and not allowed to reach confluency.

**U-87 MG**

Human glioblastoma astrocytoma cells; hypodiploid; female. Cells were purchased from ATCC and were cultured in MEM (Gibco) supplemented with 10% FBS (Corning). Cells were incubated in 5% CO<sub>2</sub> at 37C. Cell lines were passaged every 72 hours with trypsin and not allowed to reach confluency.

**U2OS**

Human osteosarcoma U2OS cells expressing the tetracycline responsible element of Flp-In™ T-REx system (FT-U2OS, gift from Karmella Haynes, Arizona State University, (Haynes and Silver, 2011)) were cultured in Dulbecco's Modified Eagle's medium without sodium pyruvate, L-Arg, and L-Lys (DMEM, Wisent) supplemented with 10% of 10 kDa cut-off fetal bovine serum (Wisent), 100 µg/mL streptomycin, 100 units/mL penicillin (Thermo), 15 µg/mL blasticidin (Wisent), and 150 µg/mL hygromycin

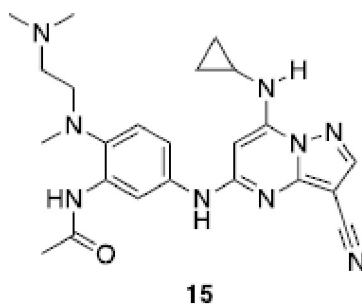


B (Wisent). The cell media was also supplemented with 0.398 mM L-Arg, 0.274 mM L-Lys, and 3.47 mM L-Pro. The cells were grown at 37°C with 5% CO<sub>2</sub> in 10 cm dishes (TPP, FroggBio) or in 6-well plates (Greiner Bio-One). Following the recommendations of Flp-In™ T-REx cell line development of ThermoFisher Scientific (<http://www.thermofisher.com/>), we developed cell lines stably expressing the wild-type CSNK2A1-HA (WT) or the inhibitor resistant forms of double mutant (DM, V66A/I174A) of the kinase with tight tetracycline regulation. The exogenous CSNK2A1 has a C-terminal HA tag to be able to distinguish from the endogenous kinase. The cell lines were induced 48h prior to inhibitor treatment with 1 μg/mL tetracycline and were kept induced during the inhibitor treatment. Cells were challenged in two independent experiment with a range of inhibitor concentrations as indicated in the figures.

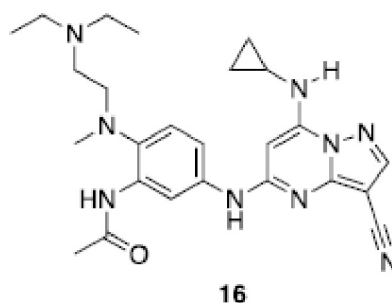
## METHOD DETAILS

### General information for chemical synthesis

Reagents were purchased from commercial suppliers and used without further purification. Unless otherwise stated, temperatures are given in degrees Celsius (°C); operations were carried out at room or ambient temperature (“rt” or “RT”), typically a range of from about 18–25°C; evaporation of solvent was carried out using a rotary evaporator under reduced pressure (typically 4.5–30 mm Hg) with a bath temperature of up to 60°C; the course of reactions was typically followed by thin layer chromatography (TLC); products exhibited satisfactory <sup>1</sup>H-NMR and/or microanalytical data; and the following conventional abbreviations are also used: L (liters), mL (milliliters), mmol (millimoles), g (grams), mg (milligrams), min (minutes), and h (hours). Reactions were conducted under a blanket of nitrogen unless otherwise stated. Compounds were visualized under UV lamp (254 nm). <sup>1</sup>H and <sup>13</sup>C NMR spectra were collected in DMSO-*d*<sub>6</sub>, acetonitrile-*d*<sub>4</sub>, chloroform-*d*, or methanol-*d*<sub>4</sub> and recorded on Varian Inova 400 or Bruker Avance 300 or 700 MHz spectrometers. Peak positions are given in parts per million (ppm) downfield from tetramethylsilane as the internal standard, in some cases; J values are expressed in hertz. Purity was assessed via analytical HPLC using an Agilent SB- C18 3.5 μm column (150 x 4.6 mm) with a 90%/10% gradient of water (0.02% TFA)/methanol as the mobile phase (flow rate = 0.8 mL/min) monitored at a wavelength of 254 nm at 30°C. Reaction schemes and procedures can be found in [Supplemental Information Scheme S1](#).

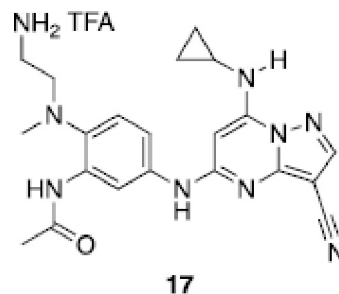


The analytical data for **15** matches that previously reported (Dowling et al., 2016); <sup>1</sup>H NMR (300 MHz, methanol-*d*<sub>4</sub>) δ 8.19 (d, *J* = 2.4 Hz, 1H), 8.08 (s, 1H), 7.77 (m, 1H), 7.25 (d, *J* = 8.7 Hz, 1H), 6.03 (s, 1H), 3.03 (m, 2H), 2.63 (m, 4H), 2.45 (m, 2H), 2.30 (s, 6H), 2.20 (s, 3H), 0.89 (m, 2H), 0.74 (d, *J* = 3.9 Hz, 2H); HRMS-ESI (*m/z*): [M + H]<sup>+</sup> calcd for C<sub>23</sub>H<sub>30</sub>N<sub>9</sub>O, 448.26; found 448.35; Purity (HPLC): 95.4%. Appearance: yellow solid.

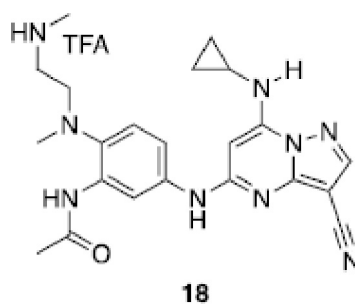


The analytical data for **16** matches that previously reported (Dowling et al., 2016); <sup>1</sup>H NMR (300 MHz, chloroform-*d*) δ 9.78 (s, 1H), 8.37 d, *J* = 2.1 Hz, 1H), 7.99 (s, 1H), 7.46 (d, *J* = 7.8 Hz, 1H), 7.24 (m, 1H), 7.05 (s, 1H), 6.33 (s, 1H), 6.02 (s, 1H),

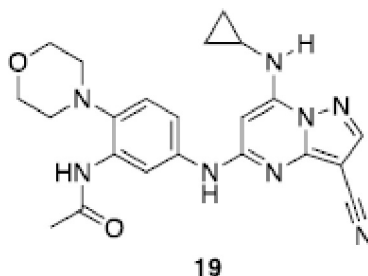
2.87 (t,  $J = 5.1$  Hz, 2H), 2.69 (s, 3H), 2.62 (m, 5H), 2.49 (t,  $J = 5.1$  Hz, 2H), 2.20 (s, 3H), 1.04 (t,  $J = 7.2$  Hz, 6H), 0.94 (d,  $J = 7.8$  Hz, 2H), 0.74 (m, 2H); HRMS-ESI ( $m/z$ ):  $[M + H]^+$  calcd for  $C_{25}H_{34}N_9O$ , 476.29; found 476.35; Purity (HPLC): 99.1%. Appearance: yellow solid.



The analytical data for **17** matches that previously reported (Dowling et al., 2016);  $^1H$  NMR (300 MHz, methanol- $d_4$ )  $\delta$  8.09 (s, 1H), 8.01 (d,  $J = 2.1$  Hz, 1H), 7.82 (d,  $J = 8.7$  Hz, 1H), 7.22 (d,  $J = 8.7$  Hz, 1H), 5.99 (s, 1H), 3.30 (m, 2H), 3.08 (m, 2H), 2.63 (t,  $J = 3.6$  Hz, 4H), 2.23 (s, 3H), 0.90 (m, 2H), 0.74 (m, 2H); HRMS-ESI ( $m/z$ ):  $[M + H]^+$  calcd for  $C_{21}H_{26}N_9O$ , 420.23; found 420.26; HRMS-ESI ( $m/z$ ):  $[M + Na]^+$  calcd for  $C_{21}H_{25}N_9NaO$ , 442.21; found 442.21; Purity (HPLC): 95.5%. Appearance: yellow solid.

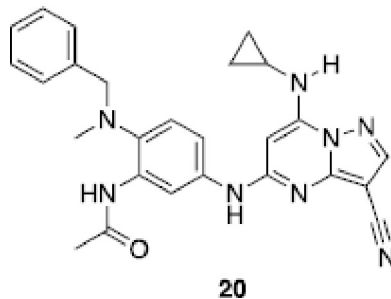


$^1H$  NMR (300 MHz, methanol- $d_4$ )  $\delta$  8.09 (s, 1H), 7.92 (d,  $J = 2.4$  Hz, 1H), 7.80 (dd,  $J = 2.4, 6.3$  Hz, 1H), 7.23 (d,  $J = 8.7$  Hz, 1H), 5.98 (s, 1H), 3.31 (m, 2H), 3.12 (m, 2H), 2.68 (s, 6H), 2.64 (m, 1H), 2.21 (s, 3H), 0.90 (m, 2H), 0.74 (m, 2H);  $^{13}C$  NMR (176 MHz, DMSO- $d_6$ )  $\delta$  168.8, 157.8, 156.9, 150.9, 148.2, 145.0, 137.0, 133.7, 121.8, 115.3, 114.9, 112.6, 76.4, 51.3, 45.6, 42.7, 32.5 (2C), 24.4, 23.3, 6.5 (2C); HRMS-ESI ( $m/z$ ):  $[M + H]^+$  calcd for  $C_{22}H_{28}N_9O$ , 434.24; found 434.26; Purity (HPLC): 96.3%. Appearance: yellow solid.

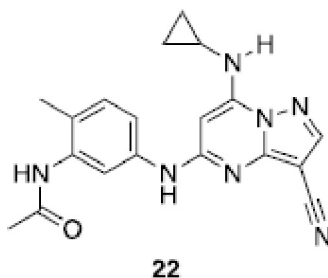


$^1H$  NMR (300 MHz, chloroform- $d$ )  $\delta$  8.58 (s, 1H), 8.34 (d,  $J = 2.1$  Hz, 1H), 8.00 (s, 1H), 7.54 (d,  $J = 6.9$  Hz, 1H), 7.22 (d,  $J = 8.7$  Hz, 1H), 6.94 (s, 1H), 6.35 (s, 1H), 5.99 (s, 1H), 3.89 (t,  $J = 4.5$  Hz, 4H), 2.89 (t,  $J = 4.5$  Hz, 4H), 2.67 (m, 1H), 2.23 (s, 3H), 0.91 (m, 2H), 0.77 (m, 2H);  $^{13}C$  NMR (176 MHz, DMSO- $d_6$ )  $\delta$  168.4, 157.0, 151.0, 148.3, 145.2, 137.4, 136.6, 133.1, 120.5, 115.4, 115.0, 112.9, 76.4,

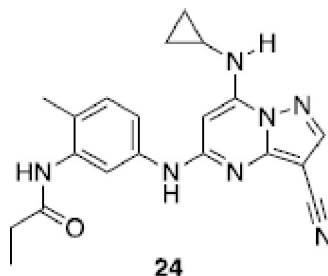
66.6 (4C), 52.2, 24.3, 23.4, 6.7 (2C); HRMS-ESI ( $m/z$ ):  $[M + H]^+$  calcd for  $C_{22}H_{25}N_8O_2$ , 433.21; found 433.24; Purity (HPLC): 99.2%. Appearance: yellow solid.



$^1H$  NMR (300 MHz, chloroform- $d$ )  $\delta$  8.60 (s, 1H), 8.30 (d,  $J = 2.4$  Hz, 1H), 8.00 (s, 1H), 7.50 (d,  $J = 8.4$  Hz, 1H), 7.33 (m, 6H), 6.89 (s, 1H), 6.33 (s, 1H), 5.99 (s, 1H), 3.95 (s, 2H), 2.66 (s, 4H), 2.12 (s, 3H), 0.89 (m, 2H), 0.76 (m, 2H);  $^{13}C$  NMR (176 MHz, DMSO- $d_6$ )  $\delta$  168.3, 157.0, 151.0, 148.3, 145.1, 138.3, 137.6, 136.4, 133.5, 128.8 (2C), 128.3 (2C), 127.2, 121.6, 115.0 (2C), 113.0, 76.4, 60.3 (2C), 42.1, 24.3, 23.4, 6.7 (2C); HRMS-ESI ( $m/z$ ):  $[M + H]^+$  calcd for  $C_{26}H_{27}N_8O$ , 467.23; found 467.34; Purity (HPLC): 96.6%. Appearance: yellow solid.

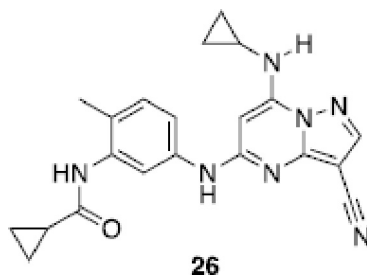


The analytical data for **22** matches that previously reported (Dowling et al., 2013);  $^1H$  NMR (300 MHz, DMSO- $d_6$ )  $\delta$  9.61 (s, 1H), 9.26 (s, 1H), 8.34 (s, 1H), 8.21 (s, 1H), 7.64 (m, 2H), 7.15 (d,  $J = 8.4$  Hz, 1H), 6.01 (s, 1H), 2.59 (m, 1H), 2.16 (s, 3H), 2.07 (s, 3H), 0.79 (m, 2H), 0.70 (m, 2H); HRMS-ESI ( $m/z$ ):  $[M + H]^+$  calcd for  $C_{19}H_{20}N_7O$ , 362.17; found 361.95; HRMS-ESI ( $m/z$ ):  $[M + Na]^+$  calcd for  $C_{19}H_{19}N_7NaO$ , 384.15; found 384.22; Purity (HPLC): 99.4%. Appearance: yellow solid.

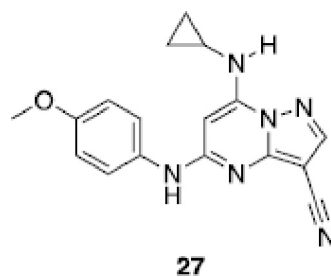


$^1H$  NMR (300 MHz, DMSO- $d_6$ )  $\delta$  9.61 (s, 1H), 9.21 (s, 1H), 8.34 (s, 1H), 8.22 (s, 1H), 7.68 (s, 1H), 7.62 (d,  $J = 7.5$  Hz, 1H), 7.15 (d,  $J = 8.4$  Hz, 1H), 6.01 (s, 1H), 2.59 (m, 1H), 2.34 (q,  $J = 7.5$  Hz, 2H), 2.16 (s, 3H), 1.11 (t,  $J = 7.5$  Hz, 3H), 0.80 (m, 2H), 0.72 (m, 2H);  $^{13}C$  NMR (176 MHz, DMSO- $d_6$ )  $\delta$  172.1, 157.1, 151.0, 148.4, 145.2, 138.2, 136.7, 130.4, 125.5, 116.6 (2C), 115.0, 76.4, 76.2, 29.2, 23.4, 17.3, 10.2, 6.6 (2C); HRMS-ESI ( $m/z$ ):  $[M + H]^+$  calcd for  $C_{20}H_{22}N_7O$ , 376.19;

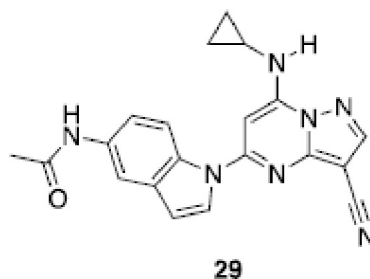
found 376.24; HRMS-ESI ( $m/z$ ):  $[M + Na]^+$  calcd for  $C_{20}H_{21}N_7NaO$ , 398.17; found 398.24; Purity (HPLC): 98.5%. Appearance: yellow solid.



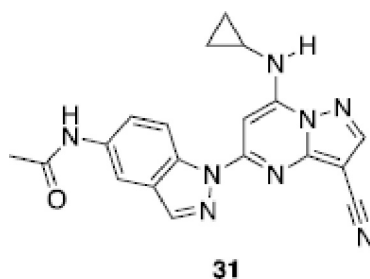
$^1H$  NMR (300 MHz, DMSO- $d_6$ )  $\delta$  9.60 (s, 1H), 9.49 (s, 1H), 8.34 (s, 1H), 8.22 (s, 1H), 7.70 (s, 1H), 7.62 (d,  $J = 7.5$  Hz, 1H), 7.15 (d,  $J = 8.4$  Hz, 1H), 6.00 (s, 1H), 2.58 (m, 1H), 2.19 (s, 3H), 1.91 (m, 1H), 0.78 (m, 6H), 0.71 (m, 2H);  $^{13}C$  NMR (176 MHz, DMSO- $d_6$ )  $\delta$  171.7, 157.0, 151.0, 148.4, 145.2, 138.2, 136.7, 130.4, 125.0, 116.4, 116.3, 115.0, 76.4, 76.3, 23.4, 17.4, 14.1, 7.1 (2C), 6.6 (2C); HRMS-ESI ( $m/z$ ):  $[M + H]^+$  calcd for  $C_{21}H_{22}N_7O$ , found 388.19; found 388.27; Purity (HPLC): 97.1%. Appearance: yellow solid.



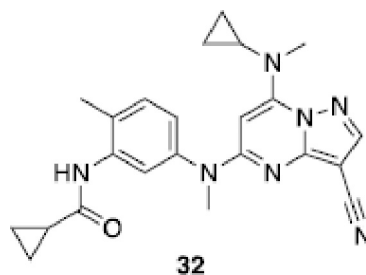
$^1H$  NMR (300 MHz, chloroform- $d$ )  $\delta$  7.98 (s, 1H), 7.32 (d,  $J = 8.7$  Hz, 2H), 6.95 (d,  $J = 8.7$  Hz, 2H), 6.79 (s, 1H), 6.31 (s, 1H), 5.73 (s, 1H), 3.84 (s, 3H), 2.56 (m, 1H), 0.84 (m, 2H), 0.71 (m, 2H);  $^{13}C$  NMR (176 MHz, DMSO- $d_6$ )  $\delta$  157.0, 154.9, 151.1, 148.2, 145.0, 133.3, 121.5, 115.0, 114.0 (3C), 76.1, 75.8, 55.2, 23.3, 6.5 (2C); HRMS-ESI ( $m/z$ ):  $[M + H]^+$  calcd for  $C_{17}H_{17}N_6O$ , 321.15; found 321.22; Purity (HPLC): 99.5%. Appearance: yellow solid.



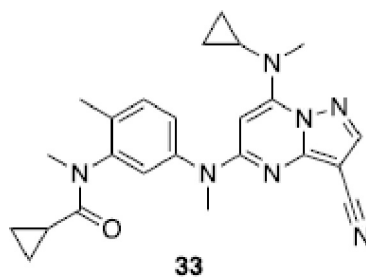
The analytical data for **29** matches that previously reported (Dowling et al., 2012);  $^1H$  NMR (300 MHz, DMSO- $d_6$ )  $\delta$  10.03 (s, 1H), 9.06 (s, 1H), 8.87 (s, 1H), 8.65 (s, 1H), 8.05 (d,  $J = 3.6$  Hz, 1H), 7.58 (d,  $J = 8.4$  Hz, 1H), 7.24 (dd,  $J = 1.2, 8.4$  Hz, 1H), 6.80 (s, 1H), 6.77 (m, 1H), 2.85 (m, 1H), 2.07 (s, 3H), 0.98 (m, 2H), 0.82 (m, 2H); HRMS-ESI ( $m/z$ ):  $[M + Na]^+$  calcd for  $C_{20}H_{17}N_7NaO$ , 394.14; found 393.98; Purity (HPLC): 97.2%. Appearance: yellow solid.



The analytical data for **31** matches that previously reported (Dowling et al., 2012);  $^1\text{H}$  NMR (300 MHz, DMSO- $d_6$ )  $\delta$  10.28 (s, 1H), 9.19 (s, 1H), 8.99 (s, 1H), 8.65 (s, 1H), 8.46 (s, 1H), 7.82 (d,  $J = 8.7$  Hz, 1H), 7.47 (dd,  $J = 1.2, 8.7$  Hz, 1H), 7.16 (s, 1H), 2.50 (m, 1H), 2.12 (s, 3H), 0.91 (m, 2H), 0.81 (m, 2H); HRMS-ESI ( $m/z$ ):  $[\text{M} + \text{H}]^+$  calcd for  $\text{C}_{19}\text{H}_{17}\text{N}_8\text{O}$ , 373.15; found 373.15; HRMS-ESI ( $m/z$ ):  $[\text{M} + \text{Na}]^+$  calcd for  $\text{C}_{19}\text{H}_{16}\text{N}_8\text{NaO}$ , 395.13; found 395.15; Purity (HPLC): 97.2%. Appearance: yellow solid.



**32:**  $^1\text{H}$  NMR (400 MHz, acetonitrile- $d_3$ )  $\delta$  8.08 (s, 1H), 8.03 (s, 1H), 7.75 (s, 1H), 7.31 (d,  $J = 8.1$  Hz, 1H), 7.07 (dd,  $J = 2.3, 5.7$  Hz, 1H), 5.81 (s, 1H), 3.48 (s, 3H), 3.32 (s, 3H), 2.39 (m, 1H), 2.30 (s, 3H), 1.78 (m, 1H), 0.87 (m, 2H), 0.81 (m, 2H), 0.65 (m, 2H), 0.51 (m, 2H);  $^{13}\text{C}$  NMR (176 MHz, acetonitrile- $d_3$ )  $\delta$  173.2, 159.9 (2C), 154.2, 152.7, 145.4, 143.9, 138.7, 132.4, 123.7, 122.7, 115.8, 84.5, 77.4, 40.5, 38.8, 34.7, 17.9, 15.4, 9.1 (2C), 7.9 (2C); HRMS-ESI ( $m/z$ ):  $[\text{M} + \text{H}]^+$  calcd for  $\text{C}_{23}\text{H}_{26}\text{N}_7\text{O}$ , 416.22; found 416.22; Purity (LCMS): >95%.



$^1\text{H}$  NMR (400 MHz, acetonitrile- $d_3$ )  $\delta$  8.05 (s, 1H), 7.46 (d,  $J = 8.0$  Hz, 1H), 7.32 (m, 2H), 5.78 (s, 1H), 3.51 (s, 3H), 3.34 (s, 3H), 3.16 (s, 3H), 2.41 (m, 1H), 2.29 (s, 3H), 1.27 (m, 3H), 0.82 (m, 2H), 0.64 (m, 2H), 0.53 (m, 2H);  $^{13}\text{C}$  NMR (176 MHz, acetonitrile- $d_3$ ) 173.6, 159.8, 154.1, 152.9, 145.5, 145.0, 144.9, 136.2, 133.3, 127.8, 127.5, 115.7, 84.2, 77.4, 40.6, 38.9, 36.4, 34.7, 17.3, 12.5, 9.2, 9.1, 8.5, 8.0; HRMS-ESI ( $m/z$ ):  $[\text{M} + \text{H}]^+$  calcd for  $\text{C}_{24}\text{H}_{28}\text{N}_7\text{O}$ , 430.24; found 430.23; Purity (LCMS): >95%.

### Kinome screening

The scanMAX assay was used to assess the selectivity of each compound at 1  $\mu\text{M}$  at Eurofins DiscoverX Corporation as a commercial assay service. This assay platform screens against 403 wild-type human kinases providing percent inhibition values. This method has been previously described (Davis et al., 2011).

### In vitro kinase radiometric kinase profiler and LANCE assays

Eurofins kinase enzymatic radiometric assays were carried out at the  $K_m$  of ATP in dose-response (9-pt curve in duplicate) for each kinase for which it was offered. The CSNK2A1/CK2 $\alpha$  (14-445KP) and CSNK2A2/CK2 $\alpha'$  (14-689KP) assays were both carried out at 10  $\mu\text{M}$ . The peptide substrate used for CSNK2A1/CK2 $\alpha$  and CSNK2A2/CK2 $\alpha'$  was RRRDDSDDDD. Eurofins kinase enzymatic LANCE assay was carried out at the  $K_m$  of ATP for MEK5 at a single concentration (10  $\mu\text{M}$ ) in duplicate. Details about the substrate used, protein constructs, controls, and assay protocol for each kinase assay can be found at <https://www.eurofinsdiscoveryservices.com>.

### NanoBRET measurements

Constructs for NanoBRET measurements of CK2 $\alpha$ , CK2 $\alpha'$ , and DYRK2 were kindly provided by Promega. NanoBRET assays were executed as described previously (Wells et al., 2019).

Example protocol for CK2 $\alpha'$ : The C-terminal Nanoluciferase (NL)/ CK2 $\alpha'$  fusion (CK2 $\alpha'$ -NL) was encoded in pFN32K expression vector, including flexible Gly-Ser-Ser-Gly linkers between NL and CK2 $\alpha'$  (Promega). For cellular NanoBRET target engagement experiments, a 10  $\mu\text{g}/\text{mL}$  solution of DNA in Opti-MEM without serum was made containing 9  $\mu\text{g}/\text{mL}$  of Carrier DNA (Promega) and 1  $\mu\text{g}/\text{mL}$  of CK2 $\alpha'$ -NL for a total volume of 1.05 mL. To this solution was then added 31.5  $\mu\text{L}$  of FuGENE HD (Promega) to form a lipid:DNA complex. The solution was then mixed by inversion 8 times and incubated at room temperature for 20 min. The resulting transfection complex (1.082 mL) was then gently mixed with 21 mL of HEK-293 cells (ATCC) suspended at a density of  $2 \times 10^5$  cells/mL in DMEM (Gibco) + 10% FBS (Corning). This solution was then dispensed (100  $\mu\text{L}$ ) into 96-well tissue culture treated plates (Corning #3917) followed by incubation (37°C / 5% CO $_2$ ) for 24 hours.

After 24 hours the media was removed and replaced with 85  $\mu\text{L}$  of room temperature Opti-MEM without phenol red. NanoBRET Tracer K5 (Promega) was used at a final concentration of 1.0  $\mu\text{M}$  as previously determined to be the optimal concentration in a titration experiment. A total of 5  $\mu\text{L}$  per well (20x working stock of NanoBRET Tracer K5 [20  $\mu\text{M}$ ] in Tracer Dilution Buffer (Promega N291B)) was added to all wells, except the “no tracer” control wells. All test compounds were prepared initially as concentrated (10 mM) stock solutions in 100% DMSO (Sigma), and then diluted in Opti-MEM media (99%) to prepare 1% DMSO working stock solutions. A total of 10  $\mu\text{L}$  per well of the 10-fold test compound stock solutions (final assay concentration of 0.1% DMSO) were added. For “no compound” and “no tracer” control wells, a total of 10  $\mu\text{L}$  per well of Opti-MEM plus DMSO (9  $\mu\text{L}$  Opti-MEM with 1  $\mu\text{L}$  DMSO) was added for a final concentration of 1% DMSO. 96-well plates containing cells with NanoBRET Tracer K5 and test compounds (100  $\mu\text{L}$  total volume per well) were equilibrated (37°C / 5 % CO<sub>2</sub>) for 2 hours.

After 2 hours the plates were cooled to room temperature for 15 min. To measure NanoBRET signal, NanoBRET NanoGlo substrate (Promega) at a ratio of 1:166 to Opti-MEM media in combination with extracellular NanoLuc Inhibitor (Promega) diluted 1:500 (10  $\mu\text{L}$  [30 mM stock] per 5 mL Opti-MEM plus substrate) were combined to create a 3X stock solution. A total of 50  $\mu\text{L}$  of the 3X substrate/extracellular NL inhibitor were added to each well. The plates were read within 10 min on a GloMax Discover luminometer (Promega) equipped with 450 nm BP filter (donor) and 600 nm LP filter (acceptor), using 0.3 s integration time according to the “NanoBRET 618” protocol.

Test compounds were evaluated at eleven concentrations in competition with NanoBRET Tracer K5 in HEK-293 cells transiently expressing the NL-CK2 $\alpha$  or CK2 $\alpha'$  fusion protein. Raw milliBRET (mBRET) values were obtained by dividing the acceptor emission values (600 nm) by the donor emission values (450 nm), and then multiplying by 1000. Averaged control values were used to represent complete inhibition (no tracer control: Opti-MEM + DMSO only) and no inhibition (tracer only control: no compound, Opti-MEM + DMSO + Tracer K5 only) and were plotted alongside the raw mBRET values. The data with n=3 biological replicates was first normalized and then fit using Sigmoidal, 4PL binding curve in Prism Software (version 8, GraphPad, La Jolla, CA, USA). All error bars are based on n=3 and are +/- standard error (SE).

#### HCT-116 and U-87 MG 72hr AlamarBlue cell proliferation assay

This assay was performed as previously described (Dowling et al., 2016). Briefly, this is a fluorometric assay to determine cell viability upon dosing with CK2 inhibitors as compared to vehicle control (DMSO) and staurosporine (control). Specifically, the system incorporates a resazurin-based reagent that upon entering living cells is reduced causing both a change in color and an increase in fluorescence. The CK2 inhibitors were evaluated in both HCT-116 and U-87 MG cells. For each compound a GI<sub>50</sub> (Growth Inhibition Concentration 50%) was calculated, using the fluorescence corresponding with cells treated for 72hrs with 10  $\mu\text{M}$  staurosporine as the assay minimum (positive control) and DMSO vehicle as the maximum (negative control). HCT-116 and U-87 MG cells were seeded at 2500 cells/well in Costar Flat bottomed 96 well plates (Black wall/clear bottom) in 90  $\mu\text{L}$  of phenol-red free McCoy's 5a (HCT-116) or MEM (U-87 MG) with 10% FBS and incubated overnight in 37°C, 5% CO<sub>2</sub>. Compound plates were then treated with 1  $\mu\text{L}$  of 100X compound (10 pt dose response) and incubated for 72hrs at 37°C, 5% CO<sub>2</sub>. The AlamarBlue reagent (Thermo) was then added to each well (10  $\mu\text{L}$ ) incubated for 4hrs at 37°C, 5% CO<sub>2</sub>. Fluorescence was measured at 535 nm (excitation) and 590 nm (emission) using a GloMax plate reader.

#### Caspase-Glo 3/7 assay

This assay was performed according to manufacturer instructions (Promega G8090). Briefly U-87 MG cells were plated in a Corning white walled flat bottom plate (cat # 3917) at a density of 20,000 cells/well. Cells were plated in all wells except for the no cell control wells. After the cells adhered to the plate, they were treated with compound for 16 hours. After 16 hours to each well was added 100 $\mu\text{L}$  of Caspase 3/7 glo reagent. The plate was mixed at 300rpm for 30sec. The plate was allowed to incubate at room temperature for 30 min, and then the plate was read. Compound **24** did not demonstrate significant Caspase 3/7 activation.

#### ProQinase broad tumor cell line profiling

Analysis of the impact of SGC-CK2-1 on the proliferation of 140 tumor cell lines was carried out at ProQinase. The IC<sub>50</sub> values were determined for SGC-CK2-1 and reference compound bortezomib in parallel. Compound treatment of cells started one day after seeding with a final DMSO concentration of 0.1% and was performed by nanodrop-dispensing using a Tecan Dispenser. 0.1% DMSO (solvent) and staurosporine (10  $\mu\text{M}$ ) served as high control (100% viability) and low control (0% viability), respectively. SGC-CK2-1 was dosed with effective concentrations between 3  $\mu\text{M}$  and 0.9 nM, with 3-fold dilutions in between. Bortezomib was dosed with effective concentrations between 1  $\mu\text{M}$  and 0.3 nM, with 3-fold dilutions in between.

Cells were cultured in different recommended media, which varied by cell line. For the assays, cells were seeded in white cell culture-treated flat and clear bottom multi-well plates and incubated at 37°C overnight before compounds were added. After incubation for 72h at 37°C at 5% or 10% CO<sub>2</sub> dependent on the medium, cell plates were equilibrated to room temperature for one hour, CellTiterGlo reagent (Promega) was added and luminescence was measured approximately an hour later using a luminometer.

Raw data were converted into percent cell viability relative to the high and low control, which were set to 100% and 0%, respectively. IC<sub>50</sub> calculation was performed using GraphPad Prism software with a variable slope sigmoidal response fitting model using 0% viability as bottom constraint and 100% viability as top constraint.



### NCI60 profiling

SGC-CK2-1 and SGC-CK2-1N were profiled against 59 cancer cells lines at a single dose of 10  $\mu$ M as has been described previously (Shoemaker, 2006). The one-dose data was reported as a mean graph of the percent growth of treated cells. A value was also reported, corresponding to the growth relative to the no-drug control and relative to the time zero number of cells. This allowed for detection of both growth inhibition (values between 0 and 100) and lethality (values less than 0).

### HCT-116 western blot analyses

HCT-116 cells (ATCC® CCL-247™) were cultured in McCoy's 5A plus L-Glutamine medium (Gibco) supplemented by 10 % FBS (Gibco) and Penicillin/Streptomycin (Gibco). 200,000 cells per well (6-well tissue culture plate) were incubated at 37°C and 5% CO<sub>2</sub> for 24h prior to inhibitor treatment. The inhibitors were diluted to a 1000x fold assay concentration in DMSO and further diluted in culture medium. Successively, the medium of the cells was aspirated and replaced with the medium containing the inhibitor dilutions. Cells were treated for 3h or 24h, washed with PBS and lysed (50 mM Tris pH 8, 150 mM NaCl, 1% NP40, 20 mM NaF, 2 mM Na<sub>3</sub>VO<sub>4</sub>, 2 mM beta-phosphoglycerol, 1x protease inhibitor (Merck)) on ice. The total amount of protein was determined by BCA assay (Pierce, Thermo Fisher Scientific).

Samples were analyzed on a precast 4-12% Bis-Tris gradient gel (Criterion XT, Bio-Rad). Proteins were blotted by a Trans-Blot Turbo Semi-dry blotter (Bio-Rad) on a PVDF membrane (Bio-Rad). The membranes were blocked with 5% bovine serum albumin (Roth) and subsequently incubated with either anti-AKT1 antibody (Akt (pan) 40D4 mouse mAb, SignalingTechnology), anti-phosphoAKT1 antibody (Rb mAb to AKT1 (phospho S129) EPR6150, ab133458, Abcam) and anti-GAPDH (Invitrogen, GA1R, MA5-15738) as a loading control followed by an HRP-conjugated anti-mouse (anti-AKT1 antibody, GAPDH antibody) or anti-rabbit (anti-phosphoAKT1 antibody) antibody and Clarity™ Western ECL substrate (Bio-Rad) on a ChemiDoc XRS+ system (Bio-Rad). Intensity levels of the different bands were determined using the Image Lab Software 6.1 (Bio-Rad). In total, two independent biological repeats of the experiment were performed.

### U2OS western blot analyses

Immunoblotting was done as described previously (Gyenis et al., 2011). Briefly, antibody incubations with primary antibodies were performed with the indicated dilutions in 3% BSA in TBST (contains 0.05% Tween 20) for rabbit antibodies or PBST (contains 0.1% Tween 20) for mouse antibodies. Incubations with secondary antibodies were performed with 1% BSA in TBST or PBST for secondary antibodies. Phosphospecific antibodies detecting pS2 of EIF2S2 (used at 1:10,000) are rabbit polyclonal antibodies (Gandin et al., 2016). For EIF2S2 pS2 signal normalization we immunoblotted with total EIF2S2 (1:500, Novus). The anti-Glyceraldehyde-3-Phosphate Dehydrogenase (GAPDH), clone 6C5 (1:1,000, Millipore) antibody was used as a loading control to ensure equal loading. The EIF2S2 pS2/total EIF2S2 normalized signal was used to calculate residual CSNK2 activity with the signal for DMSO treatment considered to be 100% kinase activity. Infrared IRDye-labeled antibodies (1:10,000, LiCor) were used for immunoblot visualization and quantification was performed on the LiCor Odyssey Infrared Imaging System with the Odyssey V3.0 and Image Studio Lite Ver 5.2 software.

### Crystallography Methods

#### Expression and purification

Expression and purification were performed as described previously (Krämer et al., 2020). Briefly, transformed BL21(DE3) cells were grown in Terrific Broth medium containing 50 mg/mL kanamycin. Protein expression was induced at an OD<sub>600</sub> of 2 by using 0.5 mM isopropyl-thio-galactopyranoside (IPTG) at 18°C for 12 hours. Cells expressing His<sub>6</sub>-tagged CK2 $\alpha$  were lysed in lysis buffer containing 50 mM HEPES pH 7.5, 500 mM NaCl, 25 mM imidazole, 5% glycerol, and 0.5 mM Tris(2-carboxyethyl)phosphine (TCEP) by sonication. After centrifugation, the supernatant was loaded onto a Nickel-Sepharose column equilibrated with 30 mL lysis buffer. The column was washed with 60 mL lysis buffer. Proteins were eluted by an imidazole step gradient (50, 100, 200, 300 mM). Fractions containing protein were pooled together and dialyzed overnight using 1L of final buffer (25 mM HEPES pH 7.5, 500 mM NaCl, 0.5 mM TCEP) at 4°C. Additionally, TEV protease was added (protein:TEV 1:20 molar ratio) to remove the tag. The next day the protein solution was loaded onto Nickel-Sepharose column beads again to remove the TEV protease and cleaved Tag. The combined flow through fraction and the wash fraction (25 mM imidazole) containing the protein was concentrated to approximately 4-5 mL and loaded onto Superdex 75 16/60 Hi-Load gel filtration column equilibrated with final buffer. The protein was concentrated to approximately 9 mg/mL.

#### Crystallization

CK2 $\alpha$  was crystallized using the sitting-drop vapor diffusion method by mixing protein (9 mg/mL) and well solutions in 2:1, 1:1, and 1:2 ratios. The reservoir solution contained 0.2 M ammonia sulfate, 0.1 M bis-tris pH 5.5 and 23-26% (v/v) PEG 3350. Complex structures were achieved by soaking the apo crystals for at least 24h with the desired inhibitor dissolved in reservoir solution. Final concentration of the inhibitor was 0.5 mM.

#### Data collection, structure solution and refinement

Diffraction data were collected at beamline X06DA (Villigen, CH) at a wavelength of 1.0 Å at 100 K. The reservoir solution supplemented with 20% ethylene glycol was used as cryoprotectant. Data were processed using XDS (Kabsch, 2010) and scaled with aimless. The PDB structure with the accession code 3PE2 (Battistutta et al., 2011) was used as an initial search MR model using the program MOLREP (Lebedev et al., 2008). The final model was built manually using Coot (Emsley and Cowtan, 2004) and refined with REFMAC5 (Vagin et al., 2004).

**QUANTIFICATION AND STATISTICAL ANALYSIS****Statistical analysis**

Statistical tests and the associated error bars are identified in the corresponding figure legends. Typical replicate numbers describe the number of technical replicates analyzed in a single experiment. GraphPad Prism 8.2.0 software was used for analyses.

**ADDITIONAL RESOURCES**

All associated data for SGC-CK2-1 and SGC-CK2-1N has been deposited at <https://www.thesgc.org/chemical-probes/SGC-CK2-1>.





Article

# The Kinase Chemogenomic Set (KCGS): An Open Science Resource for Kinase Vulnerability Identification

Carrow I. Wells <sup>1</sup>, Hassan Al-Ali <sup>2,3</sup>, David M. Andrews <sup>4</sup>, Christopher R. M. Asquith <sup>1</sup>, Alison D. Axtman <sup>1</sup>, Ivan Dikic <sup>5,6,7</sup>, Daniel Ebner <sup>8</sup>, Peter Ettmayer <sup>9</sup>, Christian Fischer <sup>10</sup>, Mathias Frederiksen <sup>11</sup>, Robert E. Futrell <sup>1</sup>, Nathanael S. Gray <sup>12,13</sup>, Stephanie B. Hatch <sup>14</sup>, Stefan Knapp <sup>6,15,16</sup>, Ulrich Lücking <sup>17</sup>, Michael Michaelides <sup>18</sup>, Caitlin E. Mills <sup>19</sup>, Susanne Müller <sup>6,15,16</sup>, Dafydd Owen <sup>20</sup>, Alfredo Picado <sup>1</sup>, Kumar S. Saikatendu <sup>21</sup>, Martin Schröder <sup>6,15,16</sup>, Alexandra Stolz <sup>5,6,15</sup>, Mariana Tellechea <sup>5,6,15</sup>, Brandon J. Turunen <sup>22</sup>, Santiago Vilar <sup>3</sup>, Jinhua Wang <sup>12,13</sup>, William J. Zuercher <sup>1</sup>, Timothy M. Willson <sup>1</sup> and David H. Drewry <sup>1,\*</sup>

- <sup>1</sup> Structural Genomics Consortium, UNC Eshelman School of Pharmacy, University of North Carolina at Chapel Hill, Chapel Hill, NC 27599, USA
- <sup>2</sup> The Miami Project to Cure Paralysis, Peggy and Harold Katz Family Drug Discovery Center, Sylvester Comprehensive Cancer Center, Departments of Neurological Surgery and Medicine, University of Miami Miller School of Medicine, Miami, FL 33136, USA
- <sup>3</sup> TruVitech LLC, Miami, FL 33136, USA
- <sup>4</sup> AstraZeneca, Darwin Building, Cambridge Science Park, Cambridge CB4 0WG, UK
- <sup>5</sup> Institute of Biochemistry 2, Faculty of Medicine, Goethe University Frankfurt, Theodor-Stern-Kai 7, 60438 Frankfurt am Main, Germany
- <sup>6</sup> Buchmann Institute for Molecular Life Sciences, Goethe University Frankfurt, Max-von-Laue-Str. 15, 60438 Frankfurt am Main, Germany
- <sup>7</sup> Max Planck Institute of Biophysics, Max-von-Laue-Str. 3, 60438 Frankfurt am Main, Germany
- <sup>8</sup> Nuffield Department of Medicine, Target Discovery Institute, University of Oxford, Oxford OX3 7FZ, UK
- <sup>9</sup> Boehringer Ingelheim RCV GmbH & Co KG, 1121 Vienna, Austria
- <sup>10</sup> MSD, 33 Avenue Louis Pasteur, Boston, MA 02115, USA
- <sup>11</sup> Novartis Institutes for BioMedical Research, Novartis Campus, 4056 Basel, Switzerland
- <sup>12</sup> Department of Biological Chemistry and Molecular Pharmacology, Harvard Medical School, Boston, MA 02115, USA
- <sup>13</sup> Department of Cancer Biology, Dana-Farber Cancer Institute, Boston, MA 02215, USA
- <sup>14</sup> MRC Oxford Institute for Radiation Oncology, Department of Oncology, University of Oxford, Roosevelt Drive, Oxford OX3 7XB, UK
- <sup>15</sup> Structural Genomics Consortium, Buchmann Institute for Molecular Life Sciences, Goethe University Frankfurt, Max-von-Laue-Straße 15, 60438 Frankfurt am Main, Germany
- <sup>16</sup> Institute for Pharmaceutical Chemistry, Johann Wolfgang Goethe-University, Max-von-Laue-Str. 9, 60438 Frankfurt am Main, Germany
- <sup>17</sup> Bayer Pharma AG, Drug Discovery, Müllerstrasse 178, 13353 Berlin, Germany
- <sup>18</sup> Oncology Discovery, AbbVie, 1 North Waukegan Road, North Chicago, IL 60064, USA
- <sup>19</sup> Laboratory of Systems Pharmacology, Department of Systems Biology, Harvard Medical School, Boston, MA 02115, USA
- <sup>20</sup> Discovery Network Group, Pfizer Medicine Design, Cambridge, MA 02139, USA
- <sup>21</sup> Global Research Externalization, Takeda California, Inc., 9625 Towne Center Drive, San Diego, CA 92121, USA
- <sup>22</sup> GlaxoSmithKline, Chemical Biology, 1250 S Collegeville Rd, Collegeville, PA 19426, USA
- \* Correspondence: David.Drewry@unc.edu



**Citation:** Wells, C.I.; Al-Ali, H.; Andrews, D.M.; Asquith, C.R.M.; Axtman, A.D.; Dikic, I.; Ebner, D.; Ettmayer, P.; Fischer, C.; Frederiksen, M.; et al. The Kinase Chemogenomic Set (KCGS): An Open Science Resource for Kinase Vulnerability Identification. *Int. J. Mol. Sci.* **2021**, *22*, 566. <https://doi.org/10.3390/ijms22020566>

Received: 8 December 2020

Accepted: 29 December 2020

Published: 8 January 2021

**Publisher's Note:** MDPI stays neutral with regard to jurisdictional claims in published maps and institutional affiliations.



**Copyright:** © 2021 by the authors. Licensee MDPI, Basel, Switzerland. This article is an open access article distributed under the terms and conditions of the Creative Commons Attribution (CC BY) license (<https://creativecommons.org/licenses/by/4.0/>).

**Abstract:** We describe the assembly and annotation of a chemogenomic set of protein kinase inhibitors as an open science resource for studying kinase biology. The set only includes inhibitors that show potent kinase inhibition and a narrow spectrum of activity when screened across a large panel of kinase biochemical assays. Currently, the set contains 187 inhibitors that cover 215 human kinases. The kinase chemogenomic set (KCGS), current Version 1.0, is the most highly annotated set of selective kinase inhibitors available to researchers for use in cell-based screens.

**Keywords:** protein kinase; kinase inhibitor; chemogenomic set; phenotypic screening; small molecules; KCGS; drug discovery; druggable genome; understudied kinase

## 1. Introduction

The protein kinases have emerged as one of the most productive families of drug targets in the 21st century. Over 60 small molecule kinase inhibitors have been approved by the FDA since 2001 for the treatment of cancer, inflammation, and fibrosis [1]. Many of these drugs, specifically those that are used in oncology, owe their efficacy to inhibition of multiple kinases [2]. For some targets second- and third-generation inhibitors have been designed to block the activity of mutant kinases that cause drug resistance after first line therapy. Collectively these drugs target only a small fraction of the 500+ human kinases. We and others have proposed that the remaining kinases represent an untapped trove of new drug targets [3–5].

Despite the concerted efforts of academic and industrial scientists over the past 25 years, the vast majority of the human kinases remain understudied. Various bibliographic analyses show that, similar to many other protein families, 90% of the research effort has been expended on <20% of the kinases [6]. Initiatives such as the NIH-sponsored Illuminating the Druggable Genome (IDG) program have sought to change this dynamic by making available high-quality data sets and research tools for the “dark” kinases [7]. The availability of a set of potent and selective inhibitors of the understudied kinases could greatly aid the study of their biology and uncover new targets for drug development.

An ever-growing number of kinase inhibitors are commercially available. Many of these compounds have advanced to clinical studies and may be useful for investigators seeking to repurpose kinase drugs for a secondary indication but they do little to expand the number of new kinase targets [8]. Notably, the commercially available kinase inhibitors vary widely in the amount and depth of annotation provided. Their vendors typically list the primary target of each inhibitor and perhaps a handful of off-targets but only rarely provide kinase selectivity profiles. Although the amount of kinase profiling data that can be found in public databases is growing [9], for many compounds broad profiling is either unavailable or described in a multitude of assay formats in the supporting information that accompanies a primary publication. While commercially available kinase sets contain valuable inhibitors of the well-studied kinases, they do little to provide tools to expand research across the breadth of the kinome.

The public availability of a high-quality chemical probe for every understudied kinase would be an ideal way to embolden researchers to explore the therapeutic potential of each kinase target [10]. However, the development of potent and selective chemical probes for over 500 kinases would be an insurmountable task using current resources and technologies. A chemogenomic set [11] of kinase inhibitors provides a practical solution to the problem [12]. The majority of kinase inhibitors, by virtue of competing with the common cofactor adenosine triphosphate (ATP) in a highly conserved binding site, invariably show some cross-activity on multiple kinases. Landmark studies by Bristol-Myers Squibb and GlaxoSmithKline scientists showed that kinome-wide profiling could identify inhibitors with collateral activity on the understudied kinases [13,14]. Building on these observations, the kinase inhibitor sets PKIS [15] and PKIS2 [16] were assembled as collections of published kinase inhibitors using the principles that chemical diversity and the inclusion of multiple exemplars of each chemotype would increase the breadth of kinase coverage and aid analysis of phenotypic screening data [17]. Both sets have found widespread use in the research community and demonstrated that repurposed inhibitors from past projects could be used to probe the biology of the kinase they were made to target and their off-targets as well. However, the full kinase profile of each inhibitor in PKIS and PKIS2 was not known in advance of their selection, and as a result both sets contained many inhibitors that were either too promiscuous (inhibition of too many kinases) or lacked sufficient target potency to be useful contributors to a chemogenomic set [18]. In spite of this limitation, PKIS and PKIS2 contained many valuable inhibitors for a broad set of understudied kinases. Encouraged by these results, we proposed a community experiment to build an optimized kinase chemogenomic set (KCGS) to cover every human kinase [16].

Each inhibitor would have its full kinome profile determined in advance and only those compounds that met a prespecified potency and selectivity would be added to KCGS.

From the start, we chose to make KCGS an open science experiment. All of the compound structures and associated kinase inhibition and selectivity data would be made publicly available. KCGS would be distributed under a Material Trust Agreement (Supplementary File S1) that supported its use as a public resource and prevented the recipients from blocking other researchers from using the set [19]. Eight pharmaceutical companies answered the call to donate kinase inhibitors from their internal compound collections to the effort. Many but not all of these companies were current partners in the Structural Genomics Consortium (SGC) [20]. In addition, several leading academic groups contributed compounds to the initiative. To date, over 1200 kinase inhibitors have been profiled as candidates for inclusion into KCGS. Here, we present the first version of KCGS as well as its initial characterization and examples of its use in cell-based assays. The set will be broadly useful to the scientific community for phenotypic screening to identify the roles of various kinases in biology and disease.

## 2. Results

### 2.1. Compound Selection

Candidate kinase inhibitors were received from GlaxoSmithKline, Pfizer, Takeda, Abbvie, MSD, Bayer, Boehringer Ingelheim, and AstraZeneca. In addition, Vertex gave permission to include their commercially available inhibitors. Academic laboratories that donated inhibitors were Cancer Research UK, Nathanael Gray, and multiple SGC sites. In total, 250 new inhibitors were donated to the initiative as candidates to complement the 950 inhibitors of PKIS and PKIS2.

At the outset, we selected the DiscoverX scanMAX assay to profile all kinase inhibitors donated to the initiative [21]. The scanMAX assay provided kinase binding data on 401 wild type human kinases (Table 1), which was at the time the broadest coverage by any single assay panel [22]. All kinase inhibitors were profiled at a concentration of 1  $\mu$ M. Using a cut-off of 10% activity remaining (PoC, equivalent to 90% inhibition), an activity profile was determined for each inhibitor and a selectivity index ( $S_{10}$ ) was calculated as the fraction of kinases meeting the cut-off. Compounds with an  $S_{10}$  (1  $\mu$ M) < 0.04 were initially selected for consideration for inclusion in KCGS. For these compounds, we performed full-dose response experiments in order to determine  $K_D$  values for all kinases with PoC < 10% in the scanMAX experiment.

**Table 1.** Kinase coverage by kinase chemogenomic set (KCGS) version 1. The human kinases are divided into 10 subfamilies [23]. Kinases: the number of human kinases in each subfamily. Assays: the number of kinases in the DiscoverX scanMAX panel. KCGS: The number of kinases covered by an inhibitor. %: The percentage of kinases screened that are covered by an inhibitor.

	Kinases	Assays	KCGS	%
AGC	63	46	20	43
Atypical	34	7	5	71
CAMK	74	58	28	48
CK1	12	8	3	38
CMGC	64	60	37	62
Lipid	20	13	10	77
Other	81	51	26	51
STE	47	42	13	31
TK	90	81	54	67
TKL	43	35	19	54
Total	215	401	528	54

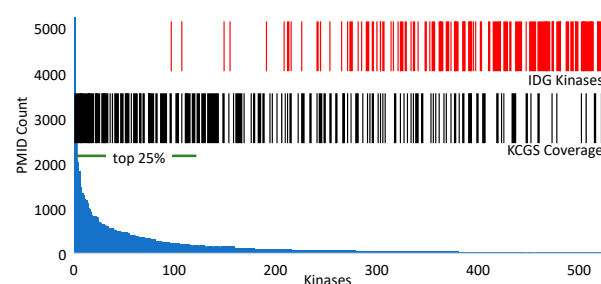
For inclusion in KCGS, an inhibitor was selected if the DiscoverX assay panel showed  $K_D$  < 100 nM on its target kinase and  $S_{10}$  (1  $\mu$ M) < 0.025 in a full panel kinase screen [16].

For inhibitors from PKIS, the assay data from the Nanosyn screening panel of 230 kinases was used to calculate the selectivity index in lieu of submitting the compounds to scanMAX. For inhibitors from PKIS2 and the newly donated compounds, the data from the DiscoverX scanMAX panel of 401 kinases was used to calculate the selectivity index. Compounds that met the inclusion criteria were manually triaged to maximize the coverage of the human kinome. Our aspirational goal was to include two unique chemotypes for each kinase and care was taken not to over-represent kinases that had been more heavily studied (such as EGFR, MAPK14, and GSK3B). For the poorly studied dark kinases, there was often only one or two compounds to select that met the inclusion criteria. Finally, in those cases where two compounds had equivalent kinase profiles, preference was given to inclusion of the chemotype with fewer exemplars in the set. Using these guidelines, version 1.0 of KCGS was assembled with a total of 187 kinase inhibitors. Summary information for each inhibitor is contained in Table S1 and the full kinase profiles can be accessed at [www.randomactsofkinase.org](http://www.randomactsofkinase.org).

## 2.2. Kinase Coverage

The set covered a total of 215 human kinases, which was more than 50% of the full scanMAX assay panel (Tables 1 and S2). Across the branches of the kinome, broad coverage was found in the TK family (67%) and CMGC family (62%). While KCGS appears to cover 71% of the atypical kinases, only a small fraction of these kinases have assays in the scanMAX panel. Lower coverage was obtained for the CK1 (38%) and STE (31%) families. In total, 114 kinases were covered by two or more inhibitors, while the remaining 98 kinases have only one useful inhibitor in the current set (Table S1). Ideally, every kinase would be covered by inhibitors from multiple chemotypes to aid analysis of phenotypic screening data. This remains a goal for future expansion of the set.

Despite the tractability of kinases as drug targets, the majority of the kinome is poorly annotated and remains dark with respect to its role in human biology, in part due to a paucity of reagents. The NIH IDG initiative has nominated 162 dark kinases (Figure 1 and Table S2) for development of chemical and biological tools in an effort to seed research on these understudied proteins [7]. KCGS contains inhibitors of 37 of the IDG dark kinases (Table S2), which may be useful as initial chemical tools to study these kinases. These KCGS compounds can also be used as starting points for development of high-quality chemical probes as the biological function of their kinase targets becomes better understood and the investment in additional optimization is warranted. We utilized a recent data set [24,25] annotated to human protein-coding genes and their genetic relevance to look at the frequency of PubMed publications on individual kinases. Figure 1 depicts the publication counts for kinases covered by KCGS. The set contains inhibitors of most of the more highly studied (top 25%) kinases, but importantly it also contains inhibitors that cover some of the darkest kinases. Future expansion of KCGS will focus on filling the gaps in coverage of the dark kinases.



**Figure 1.** Analysis of kinase coverage in KCGS by publication frequency. The blue histogram indicates the number of publications for each kinase in PubMed (Table S2) [24,25] ordered by frequency with the top 25% noted by the horizontal bar. The red vertical bars indicate the 162 poorly studied dark kinases nominated by the NIH Illuminating the Druggable Genome (IDG) initiative [7]. The black vertical bars indicate the 215 kinases covered by an inhibitor in KCGS version 1.

### 2.3. Chemotype Analysis

To aid analysis of screening data and to support future expansion of KCGS, a method was developed to assign each inhibitor to a specific chemotype based on the chemical structure of its hinge-binding moiety. To accomplish this, 119 known kinase hinge-binder substructures were defined manually and codified using SMILES (Simplified Molecular Input Line Entry System) arbitrary target specification (SMARTS) [26]. To resolve issues where an inhibitor could be assigned to multiple bins, SMARTS were given a priority order. Kinase inhibitors that lacked an obvious hinge-binding group were grouped separately into an additional SMARTS bin. Applying this analysis to the 187 KCGS inhibitors, the compounds were found to occupy 67 of the 120 SMARTS bins (Figure 2A and Table S3). Nine of the bins contained six or more inhibitors, 27 bins had two to five members, and 31 bins contained only one exemplar. The nine most highly populated SMARTS bins contain well-known kinase inhibitor scaffolds, such as indazoles, oxindoles, quinazolines, quinolines, and pyrimidines. Six KCGS compounds that lack an obvious hinge-binder group were placed in the “other” bin. They include an allosteric PAK inhibitor and two allosteric MEK inhibitors. For bins containing multiple exemplars, the individual inhibitors often showed activity on kinases located in several different branches of the kinome. For example, the 13 oxindoles in KCGS showed a cluster of activity on CMGC kinases, but they also inhibited TK, TKL, and STE kinases (Figure 2B). While the oxindole chemotype has been found in many highly promiscuous kinase inhibitors, the inclusion of several oxindoles in KCGS demonstrated that this chemotype can also produce highly selective kinase inhibitors by judicious optimization of the molecules. KCGS contained nine exemplars in the 4-anilino-quinazolines bin (Figure 2C). Six FDA-approved kinase inhibitors that target EGFR and ERBB2 also fall into this bin. However, the SMARTS analysis highlights that modification of the 4-anilino-quinazoline chemotype can also generate inhibitors with activity on several adjacent kinase subfamilies.

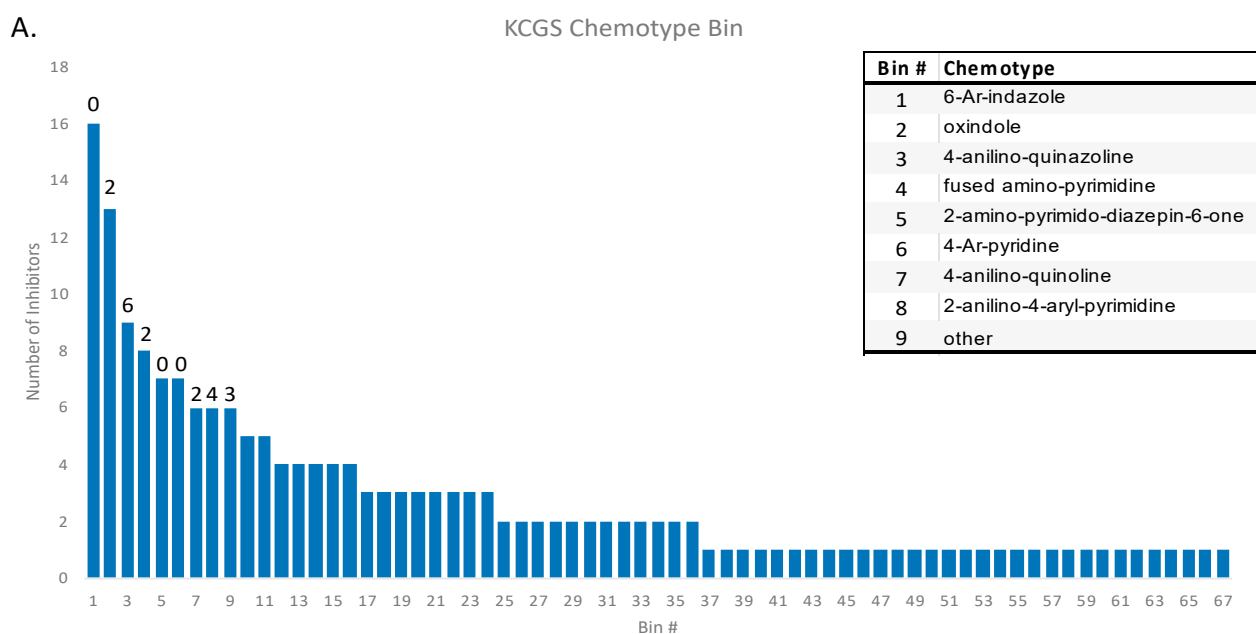
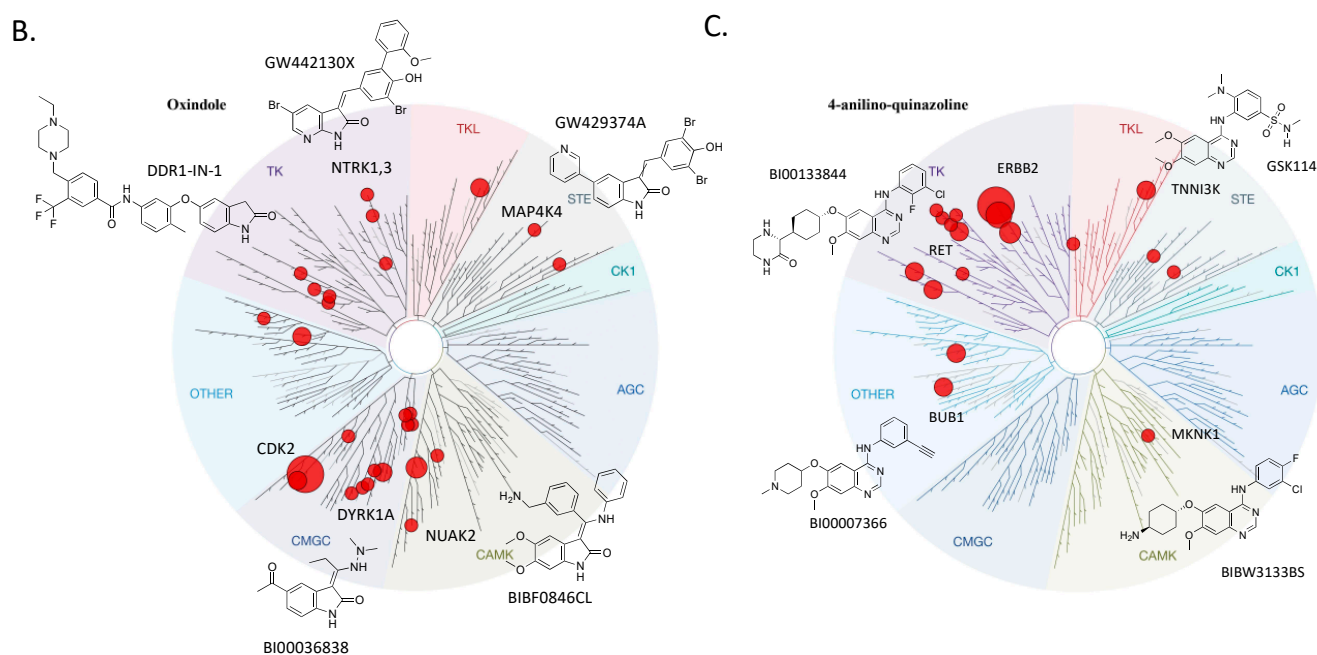


Figure 2. Cont.



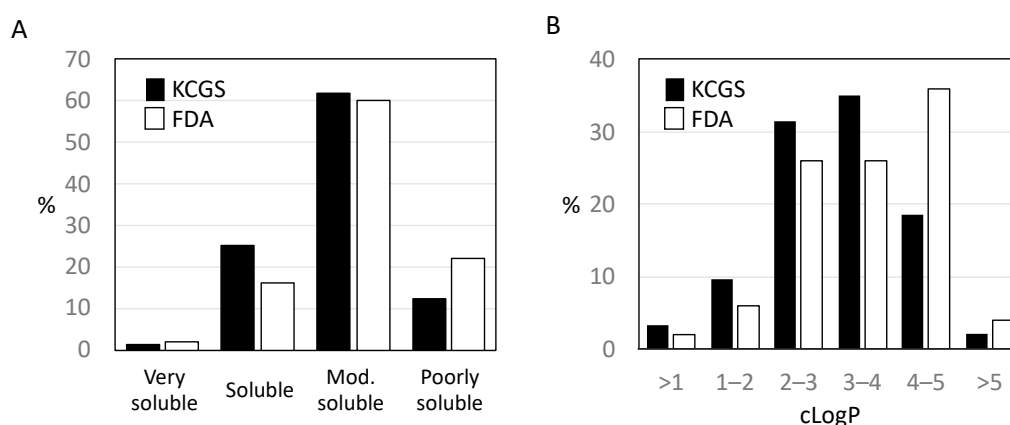


**Figure 2.** KCGS contains inhibitors from 67 distinct chemotypes. (A) This graph displays the number of inhibitors in each SMILES arbitrary target specification (SMARTS) bin. The numbers above the left-most 9 bars represent the number of FDA approved kinase inhibitors in these chemotype bins at the time the manuscript was written. The inset provides names of the 9 most highly populated bins. (B) Tree plot of the human kinases with each subfamily uniquely shaded. Kinases covered by a member of the oxindole SMARTS bin are displayed as red dots, scaled by the number of compounds inhibiting a specific kinase. Representative chemical structures from the oxindole SMARTS bin are shown. (C) Kinases covered by the 4-anilino-quinazoline SMARTS bin with representative chemical structures. (# = number).

#### 2.4. Calculated Properties

All of the inhibitors in KCGS were originally the product of medicinal chemistry projects to target specific kinases. As such, many of them had been optimized with an eye on physicochemical properties and cellular activity. To evaluate the overall quality of the set, the calculated properties of each inhibitor from KCGS were determined in SwissADME [27] and compared to a set of 52 FDA-approved kinase inhibitors [28]. SMILES strings representing each inhibitor were input into SwissADME to generate the predicted solubility and calculated lipophilicity (Table S1). For predicted solubility, the inhibitors were binned into four categories ranging from poorly to very soluble. The solubility profile of both inhibitor sets was similar (Figure 3A). The majority of compounds were predicted to be moderately soluble or better for both KCGS (88%) and the FDA-approved inhibitors (78%). LogP is a common measure of lipophilicity and is considered a critical factor in assessing the drug-like properties of small molecules [29]. The SwissADME consensus logP (cLogP), which is the arithmetic mean of five calculated values (XLOGP3, WLOGP, MLOGP, SILICOS-IT, and iLOGP), was used to compare KCGS to the FDA-approved kinase inhibitors. The results showed that KCGS clogP values trended towards lower lipophilicity than the FDA-approved drugs, with 65% of the KCGS inhibitors falling between cLogP 2 and 4 and proportionally fewer inhibitors with cLogP > 4 (Figure 3B). Overall, these calculations support the premise that the inhibitors in KCGS have physical properties that render them well-suited for use in cell-based assays.





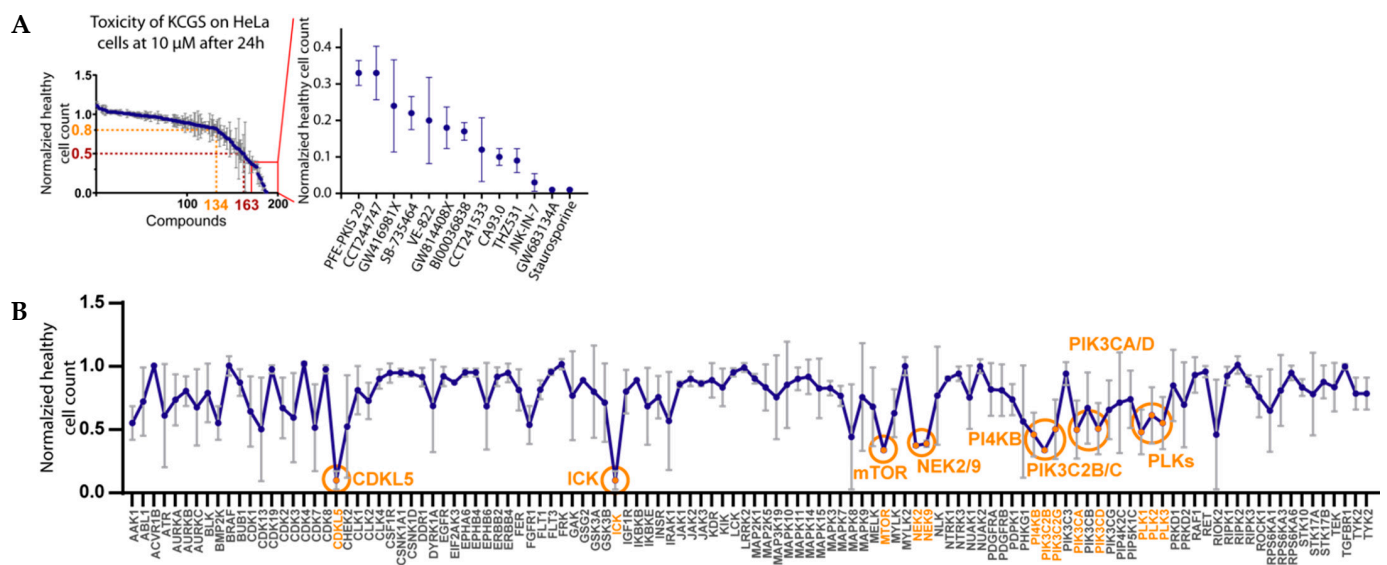
**Figure 3.** Calculated properties. (A) Predicted solubility of the KCGS compounds (black) compared to 52 FDA-approved kinase inhibitors (white) split into four categories and shown as percentage of the set. (B) Hydrophobicity analysis of the KCGS compounds (black) using SwissADME compared to the FDA-approved kinase inhibitors (white) split into six ranges of cLogP and shown as percentage of the set.

### 2.5. Chemogenomic Screening

To format KCGS for distribution to a large number of researchers, 10 mM DMSO stock solutions of the 187 inhibitors were aliquoted into 384-well format plates. Then, 1  $\mu$ L of each inhibitor was dispensed to each well of the plate using an Echo 550 acoustic dispenser for accurate delivery. This 1  $\mu$ L/10 mM volume provides sufficient compound to run 100 assays at a 1  $\mu$ M inhibitor concentration in 96-well format and 200 assays in a 384-well format (assuming 100 and 50  $\mu$ L working volume, respectively, see Supplementary File S2). KCGS was delivered with a plate map that delineates compound identification numbers as well as the kinase profile for each compound (Table S1). Based on the kinase selectivity profile of the inhibitors, 1  $\mu$ M is the recommended screening concentration for chemogenomic experiments to support hit identification and target deconvolution. Screening at higher concentrations will likely complicate data interpretation due to additional undocumented off-target activity of the inhibitors. To aid with hit follow-up, additional quantities of each inhibitor were available from the SGC-UNC for full-dose response and secondary assays.

### 2.6. Cell Toxicity

To facilitate the use of KCGS in cell-based assays, we determined the acute toxicity of the individual inhibitors at a high dose (10  $\mu$ M) in HeLa cells. After 24 h treatment, high content imaging [30,31] was used to measure healthy cell count as well as the percent of necrotic and apoptotic cells, which identified those inhibitors that exhibited varying degrees of toxicity (Figure 4 and Table S4). In total, 134 of the kinase inhibitors had little or no effect on total cell count. A total of 43 of the inhibitors reduced cell count by 20% or more. The most toxic compounds that decreased cell count by >67% are highlighted in Figure 4A. The cell toxicity displayed by these compounds may be due to their inhibition of kinases that affect cell division or cell viability, either as a primary or secondary target. Among the compounds with the largest effect on cell count were inhibitors of kinases involved in cell cycle progression, checkpoint regulation, and cell division including the CDKs (GW416981X, THZ531, BI00036838), AURKC (GW814408X), ATR (VE-822), and CHK1/2 (CCT244747, CCT241533). Other compounds with significant toxicities in HeLa cells at the 10  $\mu$ M dose were GW683134A, a type II inhibitor of KDR, KIT and TEK, and PFE-PKIS 29, a very potent (<10 nM) inhibitor of mTOR and several lipid kinases including all isoforms of PI3K.

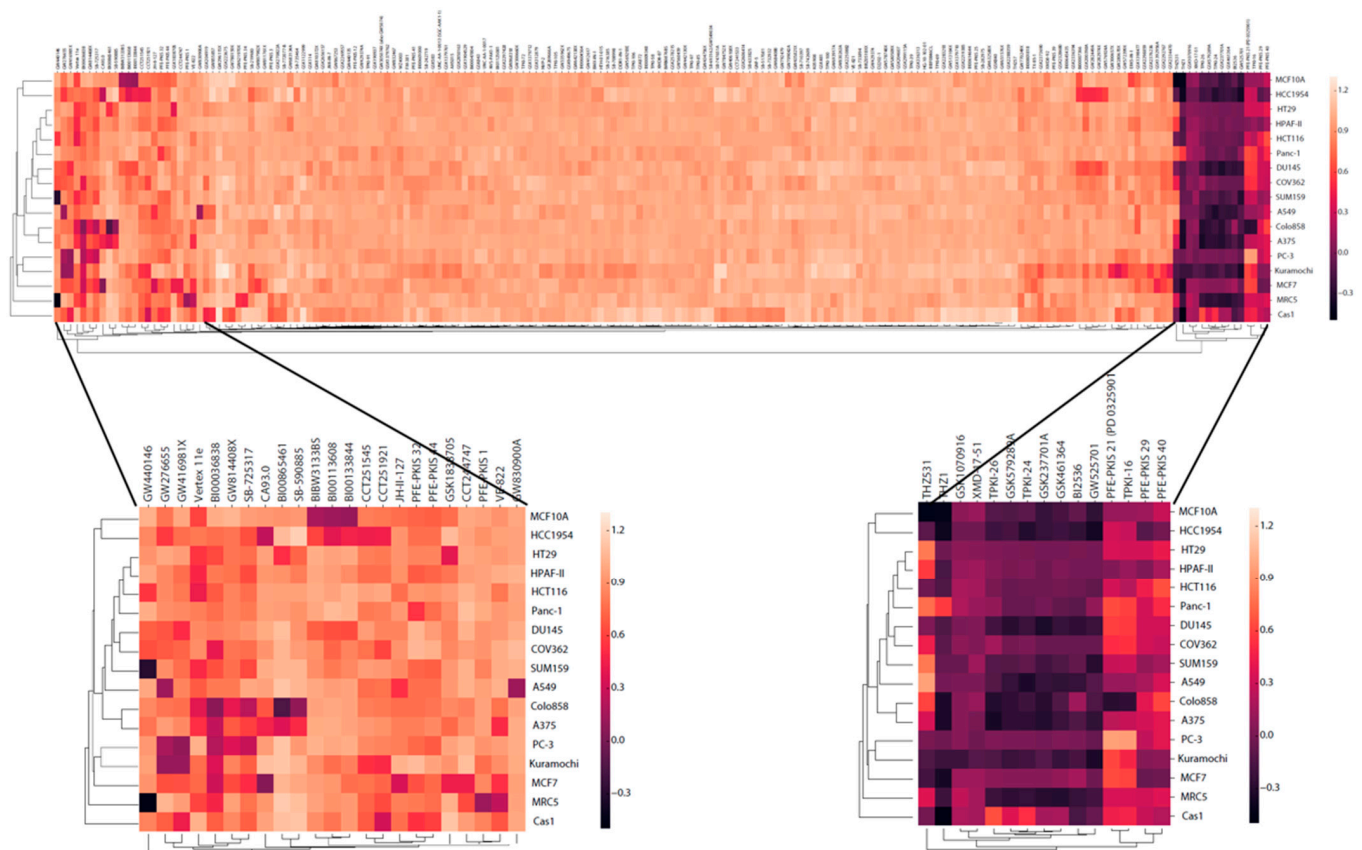


**Figure 4.** Cell toxicity assessment. (A) Effects of KCGS compounds at 10  $\mu\text{M}$  on HeLa cells after 24 h. Measurements were made in triplicate with standard errors shown. Shown is the normalized healthy cell count with highlighted thresholds of 0.8 (80% healthy cells) and 0.5 (50% healthy cells). The panel on the right side displays the compounds with the greatest effect on healthy cell count in HeLa cells. (B) Averaged toxicity measured by normalized healthy cell count for every target covered by two or more chemotypes. Highlighted are target kinases that show a significantly lower healthy cell count than the DMSO control.

To gain further insight into kinases associated with cell toxicity, we performed an analysis of every kinase that is covered in KCGS by two or more distinct chemotypes (Figure 4B). Several kinases were identified whose inhibition resulted in a significantly lower healthy cell count. Several inhibitors of the polo-like kinases (PLKs) showed toxicity, as did inhibitors of the PIK3C and PI4KB lipid kinases. The apparent toxicity of NEK2/NEK9 inhibition by GSK579289, GSK461364, GSK579289, and GSK237701 may also be attributed to the collateral PLK inhibition of these compounds at the high concentration that the assay was performed at. The apparent toxicity of inhibition of the dark kinases CDKL5 and ICK by JNK-IN-7 and BI00036838 may also be due to the inhibition of the other kinase targets of these two inhibitors (Table S1).

### 2.7. Cell Growth

To further document the effect of KCGS on cell viability, we performed assays for cell growth [32] in 16 immortalized cell lines that were selected to cover breast, ovarian, prostate, colorectal, lung, skin, brain, and pancreatic cancers (Table S5). Nonmalignant breast and lung cell lines were included for comparison. Using a 1  $\mu\text{L}$  aliquot of KCGS (10 mM in DMSO), the set was screened in duplicate across the 18 cell lines at a compound concentration of 1  $\mu\text{M}$ . The effects on cell growth, viability and cell cycle were determined after 72 h treatment using high-throughput microscopy [33]. Growth rate (GR) inhibition values, employed to account for variable division times, were computed [34]. GR values below zero are indicative of net cell loss whereas values between zero and one can result from growth arrest or a combination of cell death and proliferation over the assay duration. Therefore, the fraction of dead cells and the cell cycle distribution of the live cells were determined (Table S6). One cell line (SW1783) did not grow under the assay conditions and was excluded from analyses (Table S6). The effect of KCGS across the remaining 17 cell lines is depicted in Figure 5.

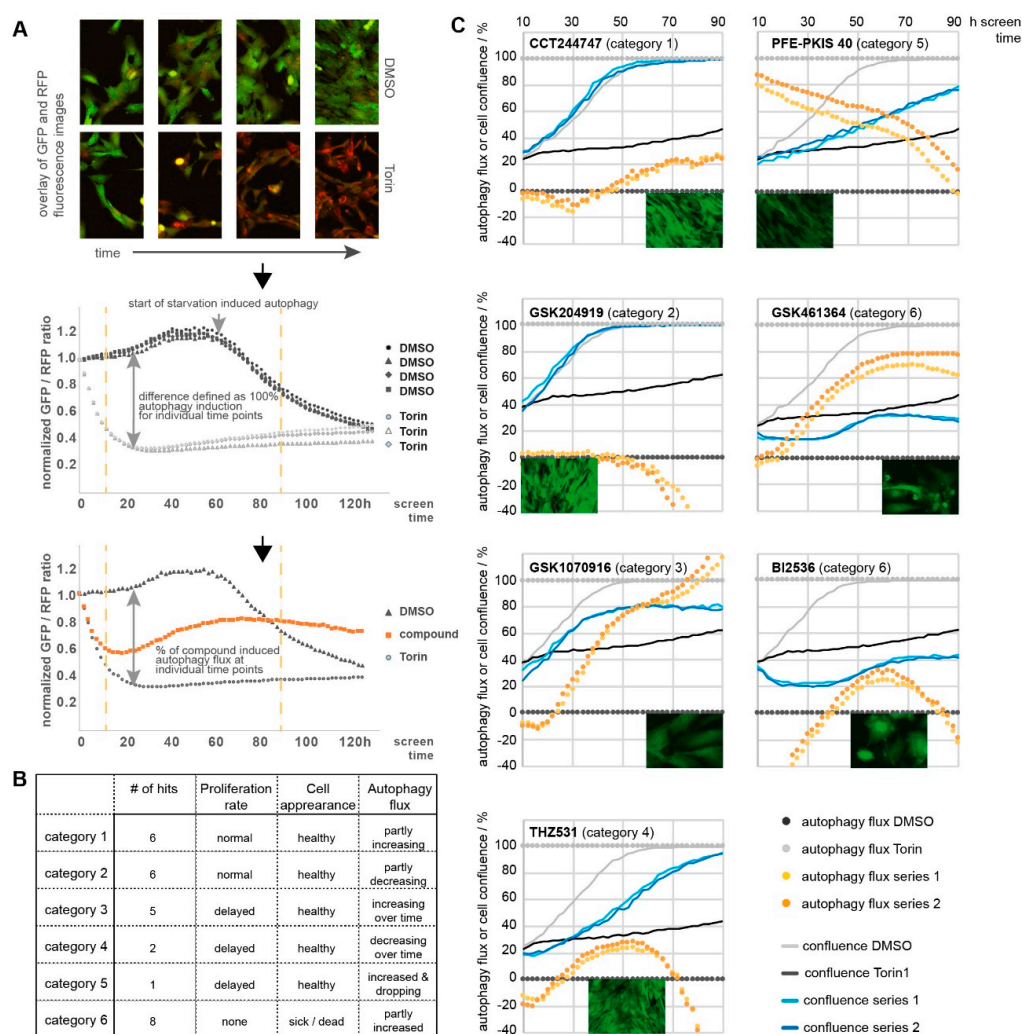


**Figure 5.** The kinase inhibitors in KCGS have different effects on cell growth across a wide range of lines. Normalized growth rate (GR) inhibition values were determined at 72 h post compound treatment. Each row displays data from a single cell line. Each column displays data from a single compound. GR is colored from  $-0.5$  in black to  $1.3$  in yellow. The expanded views display data for compounds that showed cell-line selective decrease in GR and relatively cell-line independent effects, respectively.

Analysis of GR across the 17 cell lines identified three categories of kinase inhibitors. The first category included the majority of inhibitors in KCGS that showed no discernable effect on cell growth, with GR values within 10% of the DMSO control. The second category containing 15 inhibitors showed a  $>30\%$  decrease in GR across most of the cell lines. Six of these compounds (TPKI-24, TPKI-26, GSK461364, GSK579289A, GSK237701A, and BI2536) have PLK inhibitory activity, two are allosteric MEK inhibitors (PFE-PKIS 21 and TPKI-16), and two are inhibitors of aurora kinases (XMD-17-51 and GSK1070916). Notably, only two of these inhibitors (THZ531 and PFE-PKIS 29) were shown to be cytotoxic at a higher concentration in the HeLa cell experiment. The third category contained 23 inhibitors that showed cell line-dependent effects on GR. Six of these compounds (GW416981, BI00036838, GW814408X, SGK-GAK-1 (CA93.0), CCT244747, and VE-882) have been identified as toxic to HeLa cells, but when tested at  $1 \mu\text{M}$  across a wider range of lines their effects were now shown to be dependent on other cellular factors and not intrinsic to the compounds alone. Based on the annotation of these compounds, inhibition of several kinases was highlighted as being responsible for cell line-dependent effects. These kinases include multiple CDK isozymes, GAK, BRAF, and BLK. Determination of whether selective inhibition of these kinases would have potential therapeutic utility in specific cancers will require confirmatory follow-up studies such as CRISPR dropout screens and screening of alternate inhibitors of the same targets. However, these data highlight the power of screening a chemically and biologically diverse chemogenomic set of kinase inhibitors to determine how they perturb a simple cell phenotype.

## 2.8. Kinases Linked to Autophagy

Autophagy is a central mechanism that helps maintain cellular homeostasis. Autophagy is activated in response to different stress conditions such as starvation, protein aggregation, oxidative stress, bacterial infection, inhibition of the TOR1 pathway, and others [35,36]. To determine the effect of kinases on autophagic flux, the KCGS library was screened at 1  $\mu\text{M}$  concentration in RPE1 cells stably expressing the autophagic flux reporter construct GFP-LC3B-RFP-LC3B $\Delta\text{C}$  [37] (Figure 6). The cells were monitored in a time-dependent manner so that the ratio of GFP/RFP intensity ratio represented the level of autophagic flux. The averaged GFP/RFP ratio was subsequently normalized to time point 0 h in order to facilitate easy visualization of differences to the autophagy control compounds Torin1 (inducer) and Torin1 plus Bafilomycin A (inhibitor and deacidifier of lysosomes) compared to the DMSO vehicle control (Table S7).



**Figure 6.** Autophagic flux assay. Compounds (1  $\mu\text{M}$ ) were analyzed for their effect on autophagy flux in RPE1 cells stably expressing the general autophagy flux reporter GFP-LC3B-RFP-LC3B $\Delta\text{C}$ . Phase contrast as well as fluorescent images (GFP, RFP) were taken at indicated time points. (A) Ratio of the GFP/RFP signal correlating with high (Torin1; defined as 100%) and low (DMSO; defined as 0%) autophagy flux. Compound-induced changes in autophagic flux are represented as percentage of this difference. Small black arrows indicate assay workflow (B) Hits are defined as compounds showing > 20% aberration of the GFP/RFP ratio compared in five or more consecutive time points and categorized according to their cell proliferation rate as well as visual appearance. (# = number) (C) Examples of compounds with an effect on autophagic flux. Cell confluence is presented as percentage of covered growth area. Visual appearance of cells and cell confluence were ascertained by examining fluorescent images of the GFP channel at 96 h screen time. Graphs contain the individual average of experiments run in triplicate at two different times.



As expected, DMSO-treated cells had a stable level of autophagic flux until nutrients in the media were depleted and they entered a starvation-induced phase of autophagy induction. In contrast, the GFP/RFP ratio of Torin1-treated cells rapidly decreased within the first screening hours and stayed low over the complete time period of the five-day screening. Of note, treatment with Torin I caused an arrest of cell proliferation but no cell death. Confluence analysis was based on phase contrast images corresponding to the cell-covered area of each well. In this assay, cell health can only be assessed based on visual appearance of the cells and cell proliferation.

Hits were defined as compounds that showed >20% aberration of the GFP/RFP ratio in at least five or more consecutive time points, equivalent to a 10 h assay window. Hits were grouped in six categories based on the increase or decrease in proliferation rate, cell appearance and autophagy flux, respectively (detailed in Figure 6). Category 1 hits included GW416981X, a potent CDK1–3 inhibitor. The CDK inhibitors roscovitine and purvalanol have previously been shown to induce autophagy [38]. Likewise, CHK1 inhibition, represented by the category 1 hit CCT244747, has previously been linked to autophagy induction [39]. However, we also identified several new potential kinase targets for autophagy. For example, GSK204919, a potent dual PRKD1/2 inhibitor, caused a reduction in autophagic flux. The role of PRKD in autophagy has not been well-documented. Additional studies are required to link the observed autophagy reduction to PRKD inhibition rather than another kinase target of GSK204919 (e.g., JAK). Categories 3 and 5 compounds contained inhibitors of kinases known to induce autophagy, such as GSK1070916 (an aurora kinase [40] inhibitor) and PFE-PKIS 40 (a PI3K and mTOR [41] inhibitor). Notably, the RPE-1 cells used in the screen did not show any reduction in cell proliferation at 1  $\mu$ M PFE-PKIS 40, despite its toxicity at 10  $\mu$ M in HeLa cells (see above). The behavior of the category 4 compounds THZ531 (CDK inhibitor) and PFE-PKIS 29 (mTOR inhibitor) likely resulted from overlap of autophagy induction with cell toxicity as already identified in the cell health and cell growth assays. Most of the compounds in category 6 have also been identified in the cell growth assays, including several inhibitors with activity on PLK (TPKI-24, TPKI-26, GSK461364, GSK579289A, GSK237701A, and BI2536), a kinase known to regulate both autophagy as well as mitosis [42].

### 3. Discussion

KCGS version 1.0 is currently the best publicly available set of well-annotated potent and selective kinase inhibitors. All of the inhibitors have narrow selectivity profiles as ascertained from screening across an assay panel covering the majority of the human protein kinases. The set can be obtained by any investigator who agrees to the open science principles of not restricting its use by others and also promises to publish the results of their screen (Supplementary File S1). This manuscript describes the chemical structure and kinase annotation of all of the inhibitors in the current set. We recognize that there is additional room for improvement in the breadth (more kinases) and depth (more chemotypes per kinase) of kinase coverage and in the biological annotation of the set. However, initial characterization of KCGS in phenotypic screens confirmed the utility of the set for chemogenomic exploration of kinase signaling. Screening across 18 cell lines identified a subset of compounds that selectively inhibit their growth. Some of these compounds point to dark kinases that have received little attention as potential drug targets. A screen for autophagy uncovered additional kinase pathways that warrant further exploration. The narrow spectrum kinase activity of the individual inhibitors and the accompanying annotation supports rapid identification of target kinases for additional studies. While the compounds are generally nontoxic, we recommend that KCGS is screened at a maximum concentration of 1  $\mu$ M in cells to minimize the potential for inhibition of additional kinases or off-target toxicity.

Several ongoing activities will support KCGS, which remains as the best publicly available set of kinase inhibitors. One such activity was obtaining screening data on all KCGS compounds in the same assay format. This would ensure that results were

comparable and offers the possibility of providing new kinase coverage. With about a quarter of the set originating in PKIS, which was only screened at Nanosyn, we had an opportunity to further profile these compounds in another 200 kinase assays by utilizing DiscoverX scanMAX. This screening was recently performed at a screening concentration of 1  $\mu$ M (Table S8) for direct comparison to previously published data [15]. For some compounds, we identified new kinase binding partners in the additional assays while for others we did not. For example, GSK270822A and GSK299115A, both amino indazoles, were previously identified as ROCK1 inhibitors when profiled at Nanosyn [15]. When screened more broadly, these compounds were also found to bind to ROCK2, JAK2, JAK3, TYK2, NUA2, and LATS2  $\geq$  25 PoC. All these results need to be verified as true positives via Kd determination and this work is ongoing. The addition of ROCK2 is perhaps not surprising due to its homology to ROCK1. The inhibition of NUA2, if confirmed, provides another chemotype to use to study the biology of this understudied kinase. GW814408X is a KCGS compound that based on original PKIS data only demonstrated potent binding to a single kinase (AURKC). Upon further screening, this compound was found to inhibit a number of other kinases. We will determine Kd values for new kinase hits for all KCGS version 1.0 compounds discovered with this new screening. If compounds fall outside our desired selectivity window, they will be replaced in future releases.

Currently, 51% of the screenable kinome, as defined by the DiscoverX scanMAX, is covered by KCGS version 1.0 for a total of 215 human kinases. Over 100 of these kinases were selectively inhibited by two or more chemotypes in the set. Our originally stated goal was to cover all human kinases with two or more chemotypes, so additional inhibitors are still required for those kinases that are covered by only single chemotype. There are an additional 250 “gap kinases” where we are still seeking an inhibitor that meets our minimal potency and selectivity criteria for inclusion in the set. For many of the gap kinases that are routinely screened in the DiscoverX scanMAX, identification of a nonpromiscuous inhibitor is the primary challenge but may be achievable through iterative medicinal chemistry to improve selectivity. Additionally, there are over 50 human kinases for which robust biochemical screening assays are not readily accessible in any format. For these kinases, it is not yet known if useful inhibitors already exist in the current set or among molecules that are in the public domain. Many of these dark kinases are difficult to express and purify or represent pseudokinases with little or no catalytic activity. Development of new screening formats or assay methodologies will be required to identify a complete set of inhibitors for the whole kinome.

One limitation to the design and selection of the inhibitors in KCGS was the use of potency and selectivity data from cell-free biochemical assays. The activity of kinase inhibitors in cells can be affected the binding of other cellular components to the kinase. In addition, some inhibitors may be less potent in cells if they are not efficient at crossing the cell membrane. However, the provenance of compounds included in KCGS, either from lead optimization programs in the pharmaceutical industry or the product of academic chemical probe development projects, suggests that most of them are likely to be cell active. In fact, the profile of physical properties across KCGS is as good if not better than a set of 52 FDA-approved kinase inhibitor drugs. Regardless, it is not uncommon for kinase inhibitors to demonstrate lower potency in cells than in cell-free assays. A recent advance in the application of NanoBRET technology to measure the target engagement of kinase inhibitors in living cells has provided a method to study this issue [43]. NanoBRET assays have now been developed for 133 of the human kinases that are inhibited by the molecules in KCGS version 1.0. By using these NanoBRET assays, we have begun the process of annotating each of the inhibitors in KCGS for its activity against its corresponding target kinase in live cells. These data will aid the deconvolution of phenotypic screening data of KCGS and identify kinases for which inhibitors with improved cell activities will be required in future releases.

The inhibitors in KCGS were sourced from multiple industrial and academic laboratories in a conscientious effort to maximize both the number of chemotypes (chemical



diversity) and the breadth of kinase coverage (biological diversity). While the core of the set is still composed of molecules that were published by GlaxoSmithKline chemists, KCGS version 1.0 contains inhibitors that originated from the laboratories of four pharmaceutical companies and three academic laboratories. We continue to seek new inhibitors to add to KCGS that represent either a new chemotype or an inhibitor of a gap kinase. To this end, we have completed profiling of molecules that have been donated by three additional companies as well as molecules synthesized in our laboratories and by academic collaborators. Inhibitors representing new chemotypes that increase the depth of coverage on many kinases will be made available as a supplemental set (KCGS version 1.1). Identification of potent and selective inhibitors of the gap kinases represents a more formidable yet surmountable challenge. We continue to welcome donations of candidate inhibitors of these kinases from industrial and academic laboratories to support expansion of the KCGS. All donor laboratories, in return, receive copies of the full KCGS set and the satisfaction of contributing to the goal of maintaining the best publicly available set of a high-quality kinase inhibitors.

#### 4. Materials and Methods

##### 4.1. KCGS

The current version of KCGS is available in 1  $\mu$ L aliquots of a 10 mM DMSO solution at [www.sgc-unc.org/request-kcgs/](http://www.sgc-unc.org/request-kcgs/).

##### 4.2. Kinase Assays

Compounds were screened at 1  $\mu$ M using the KINOMEScan technology in the scan-MAX assay panel of 401 wild-type human kinases and  $S_{10}$  was calculated as previously described [16]. Compounds with  $S_{10} < 0.04$  were submitted for  $K_D$  measurement on kinases with POC < 20%. Compounds with  $K_D < 100$  nM and  $S_{10}$  (1  $\mu$ M) < 0.025 were selected as candidates for inclusion in KCGS.

##### 4.3. Chemotype Binning

Each molecular substructure or bin representing the desired hinge-binder was manually codified in SMARTS language [26] and were given a priority order. Each molecule in KCGS was represented as a SMILES code. The SMARTS search was performed using Open Babel [44] to generate an .smi file to associate the SMILES code of each molecule with a specific SMARTS bin. All .smi files were processed in MATLAB [45] to create a compound-SMART matrix. Compounds with multiple matches were assigned to bin that corresponded to the highest priority SMARTS.

##### 4.4. Cytotoxicity Assays

A triple staining high content screen was performed as previously described [30,31]. HeLa cells exposed to KCGS compounds at 10  $\mu$ M for 24 h were stained with the three dyes: Hoechst 33342 (1  $\mu$ M), Yo-Pro 3 (1  $\mu$ M) and Annexin V (0.3  $\mu$ L per well) for 1 h. Cellular fluorescence was measured using the CQ1 high content imaging system (Yokogawa, Sugarland, TX, USA) with the following setup parameters: Brightfield transmitted light at 70% for 50 ms; Hoechst 33342 was excited by 100 ms exposure; Ex 405 nm/Em 447/60 nm, Yo-Pro 3 by 100 ms exposure; Ex 561 nm/Em 617/73 nm and Annexin V (Alexa 488, ThermoFisher, Waltham, MA, USA) by 50 ms exposure; Ex 488 nm/Em 525/50 nm. All data were analyzed by the Pathfinder software and four categories for cells were designated: healthy cells, early apoptosis, late apoptosis, and necrosis. Each category was calculated as a percentage for every inhibitor. Cell nuclei were classified as either healthy, pyknotic, or fragmented.

##### 4.5. Cell Growth Assays

The KCGS library compounds were arrayed in a 384-well plate at a concentration of 1 mM. Four breast cell lines, (SUM159, MCF7, MCF10A (nonmalignant), and HCC1954),

and two each of ovarian (COV362 and KURAMOCHI), prostate (PC-3 and DU145), colorectal (HT29 and HCT116), lung (A549 and MRC-5), melanoma (COLO858 and A375), glioblastoma (Cas1 and SW1783), and pancreatic (Panc-1 and HPAF-II) cancer cell lines were maintained in their recommended growth media at 37 °C in 5% CO<sub>2</sub>, and were seeded in 384-well CellCarrier plates (Perkin Elmer, Waltham, MA, USA) at the densities listed in Table S5. Cells were allowed to adhere for 24 h and treated in duplicate with the KCGS library by pin transfer for a final concentration of 1 µM. Cells were stained and fixed at the time of pin transfer and following 72 h of treatment. Cells were pulsed for one hour with EdU (Lumiprobe, Hunt Valley, MD, USA) and stained with 1:2000 LIVE/DEAD Far Red Dead Cell Stain (LDR) (Thermo Fisher Scientific, Waltham, MA, USA). Cells were then fixed with 3.7% formaldehyde (Sigma Aldrich, St. Louis, MO, USA) for 30 min and permeabilized with 0.5% Triton X-100 in PBS. The EdU was labeled with cy3-azide (Lumiprobe, Hunt Valley, MD, USA) for 30 min. The cells were then blocked for one hour with Odyssey blocking buffer (LI-COR, Lincoln, NE, USA), and stained overnight at 4 °C with 2 µg/mL Hoechst 33342 (Sigma Aldrich, St. Louis, MO, USA) and a 1:1000 dilution of anti-phospho-histone H3 (pHH3) Alexa 488 (Ser10, clone D2C8) conjugated antibody (Cell Signaling Technologies, Danvers, MA, USA). Fixed cells were imaged with a 10x objective using an IXM-C microscope and analyzed using MetaXpress software (Molecular Devices, San Jose, CA, USA). Nuclei were segmented based on their Hoechst signals. DNA content, defined by the total Hoechst intensity within the nuclear mask, was used to identify cells in the G1 and G2 phases of the cell cycle. The average LDR, EdU and phospho-histone H3 intensities within the nuclear masks were determined and used to classify cells as dead, in S phase or in M phase, respectively. Cells with intermediate DNA content and no EdU signal were classified as S phase dropout cells. Live cell counts were normalized to DMSO-treated controls on the same plates to yield normalized growth rate inhibition (GR) values as described previously [32].

#### 4.6. Autophagy Assays

RPE1 cells (1500 cells/well in 50 µL DMEM/F12, 10% FBS, and 1% P/S) stably expressing the GFP-LC3-RFP-LC3ΔC autophagy flux reporter [37] were seeded in 384-well plates and grown for approximately 18 h. In total, 50 µL media with 2× compound concentration were added and plates were subsequently placed and monitored in an IncuCyte® (Sartorius, Bohemia, NY, USA) instrument. Cells were scanned at indicated times for phase contrast and fluorescence intensity (GFP and RFP) to obtain information about confluence and autophagic flux, respectively. Hits are defined as compounds showing > 20% aberration of the GFP/RFP ratio compared to the control compounds DMSO (0.1%) and Torin1 (250 nM) in at least 5 or more consecutive time points (equivalent to 10 h screening time). Compounds were tested in triplicate and the complete screen was performed twice.

## 5. Conclusions and Future Directions

The KCGS is the largest fully annotated set of selective small molecule kinase inhibitors that is accessible to the biomedical scientific community to explore the involvement of kinases in a broad range of human pathologies and cellular pathways. The library is available in an arrayed 384-well format to support phenotypic screening in academic screening facilities and well-equipped laboratories to conduct target identification, mechanistic, synergy, synthetic lethality, and repurposing screens. Biological annotation of a common set of diverse kinase inhibitors will deepen our understanding of the role of kinases in cell signaling and may uncover new targets for drug discovery programs and precursors to new medicines.

Importantly, the set is a key resource supporting the expansion of the druggable genome. For example, kinases have been shown to play a pivotal role in many aspects of cancer physiopathology and have been a highly productive protein family for the treatment of several cancers [46,47]. A highly annotated small molecule library can be employed to comprehensively investigate the role of kinases in cancer biology. Indeed, the

Target Discovery Institute (TDI), a collaborative cell-based phenotypic screening facility established at the University of Oxford, Nuffield Department of Medicine, to identify more tractable biological targets for potential drug development, has used the KCGS in a range of cancer screens, including combinatorial screens with proteins involved in DNA repair including ATM, SPRTN, FancD2, SETD2, and KMT2D, and pathways involved in ubiquitin-mediated proteolysis, and mRNA dysregulation. The TDI also plans to employ the KCGS library in future combinatorial screens with temazolamide and radiotherapy (ionizing radiation) in glioblastomas. This research has generated its first manuscript from a screen which revealed a striking synthetic lethality between Chk1 inhibition and cyclin F loss [48]. Additionally, several of these ongoing projects have generated very encouraging validated primary hits and, although they will require vigorous follow-up validation, the results highlight the great utility and potential of the KCGC library to uncover novel anticancer targets.

Finally, it is important to acknowledge the potential for employing the KCGS in even more diverse disease-relevant phenotypic screening campaigns across additional human pathologies. Although kinases are heavily targeted in cancer treatment, kinases have also been implicated as causative genes in amyotrophic lateral sclerosis [49], the pathogenesis of Parkinson's Disease [50], and cardiac dysfunction [51], to name a few. By providing open access to the KCGS to a diverse range of biomedical research scientists, the potential to accelerate drug target discovery, identify novel kinase mechanisms, and identify kinase vulnerabilities beyond cancer therapeutics is greatly increased.

**Supplementary Materials:** Supplementary materials can be found at <https://www.mdpi.com/1422-0067/22/2/566/s1>.

**Author Contributions:** Conceptualization, C.I.W., H.A.-A., D.M.A., A.D.A., P.E., C.F., M.F., S.K., U.L., M.M., S.M., D.O., K.S.S., W.J.Z., T.M.W. and D.H.D.; methodology, C.I.W., W.J.Z., T.M.W. and D.H.D.; software, H.A.-A. and S.V.; validation, C.I.W., I.D., D.E., S.K., S.M. and D.H.D.; formal analysis, C.I.W., I.D., D.E., S.B.H., S.K., C.E.M., S.M., M.S., A.S., M.T., S.V. and D.H.D.; investigation, C.R.M.A., S.B.H., C.E.M., M.S., A.S., S.V. and J.W.; resources, D.M.A., P.E., C.F., M.F., N.S.G., U.L., M.M., D.O., K.S.S. and B.J.T.; data curation, C.I.W., A.D.A., R.E.F., W.J.Z. and D.H.D.; writing—original draft preparation, C.I.W., S.M., S.V., T.M.W. and D.H.D.; writing—review and editing, all authors; visualization, C.I.W., C.E.M., M.S. and D.H.D.; supervision, H.A.-A., I.D., D.E., S.K., S.M., T.M.W. and D.H.D.; project administration, C.I.W., A.P., T.M.W. and D.H.D.; funding acquisition, T.M.W. and D.H.D. All authors have read and agreed to the published version of the manuscript.

**Funding:** The Structural Genomics Consortium is a registered charity (no: 1097737) that receives funds from AbbVie; Bayer Pharma AG; Boehringer Ingelheim; Canada Foundation for Innovation; Eshelman Institute for Innovation; Genentech, Genome Canada through Ontario Genomics Institute (OGI-196); EU/EFPIA/OICR/McGill/KTH/Diamond Innovative Medicines Initiative 2 Joint Undertaking (EUbOPEN grant no: 875510); Janssen, Merck KGaA, Merck Sharp and Dohme, Novartis Pharma AG; Pfizer, São Paulo Research Foundation-FAPESP, Takeda and the Wellcome Trust. Additional funding for the SGC-UNC was provided by The Eshelman Institute for Innovation, UNC Lineberger Comprehensive Cancer Center, PharmAlliance, and National Institutes of Health (1R44TR001916-02, 1R01CA218442-01, and 1U24DK116204-01). Support for C.I.W. and D.H.D. also provided by the Foundation for Food and Agriculture Research (FFAR), project A18-2129-S001. Support for I.D. and A.S. provided by DFG, German Research Foundation project 2591307 SFB1177.

**Data Availability Statement:** Data is contained within the article or supplementary materials.

**Acknowledgments:** Daniel Ebner and Stephanie B. Hatch would like to acknowledge and thank Vincenzo D'Angiolella, Anderson Ryan, Sarah Blagden, Kristijan Ramadan, Peter McHugh and Tim Humphrey from the University of Oxford, Department of Oncology for their support and hard work in developing and producing the anticancer screening campaigns highlighted in the future direction section of this manuscript. Construction of the KCGS has been highly collaborative and intricate, with contributions large and small from many people. We value and acknowledge the contributions of the many scientists who have made this possible, offered guidance and suggestions, and who indeed will help us continue to improve the set. This list includes Mirra Chung, Jonathan Elkins, Dan Treiber, many scientists in the SGC, and of course the recipients of KCGS and the previous iterations

of our chemogenomic sets PKIS and PKIS2. These end users have provided valuable feedback that guides our work. Their creative use of the sets provides inspiration to continue down this path so that with ever improving tools the scientific community can link targets to phenotypes and to disease, and through these collaborative efforts identify new targets that will lead to medicines for patients.

**Conflicts of Interest:** The funders (Eshelman Institute for Innovation, AstraZeneca, Boehringer Ingelheim, Novartis Institute for Biomedical Research, Bayer Pharma, AbbVie, Pfizer Inc., Takeda California, Inc., MSD) provided support in the form of salaries for authors (Eshelman Institute for Innovation—D.H.D., C.I.W., A.D.A., W.J.Z., T.M.W.; AstraZeneca—D.M.A.; Novartis Institute for Biomedical Research—M.F.; Bayer Pharma—U.L.; AbbVie—M.M.; Pfizer Inc.—D.O.; Takeda California, Inc.—K.S.S.; MSD—C.F.), but did not play a role in the study design, data collection and analysis, decision to publish, or preparation of the manuscript. N.S.G. is a founder, science advisory board member (SAB) and equity holder in Gatekeeper, Syros, Petra, C4, Allorion, Jengu, B2S and Soltego (board member). The specific roles of all authors are articulated in the author contributions section.

## References

1. Roskoski, R., Jr. FDA-Approved Small Molecule Protein Kinase Inhibitors. Available online: <http://www.brimr.org/PKI/PKIs.htm> (accessed on 1 December 2020).
2. Morphy, R. Selectively nonselective kinase inhibition: Striking the right balance. *J. Med. Chem.* **2010**, *53*, 1413–1437. [[CrossRef](#)] [[PubMed](#)]
3. Ferguson, F.M.; Gray, N.S. Kinase inhibitors: The road ahead. *Nat. Rev. Drug Discov.* **2018**, *17*, 353–377. [[CrossRef](#)] [[PubMed](#)]
4. Knapp, S.; Arruda, P.; Blagg, J.; Burley, S.; Drewry, D.H.; Edwards, A.; Fabbro, D.; Gillespie, P.; Gray, N.S.; Kuster, B.; et al. A public-private partnership to unlock the untargeted kinome. *Nat. Chem. Biol.* **2013**, *9*, 3–6. [[CrossRef](#)] [[PubMed](#)]
5. Fedorov, O.; Muller, S.; Knapp, S. The (un)targeted cancer kinome. *Nat. Chem. Biol.* **2010**, *6*, 166–169. [[CrossRef](#)]
6. Edwards, A.M.; Isserlin, R.; Bader, G.D.; Frye, S.V.; Willson, T.M.; Yu, F.H. Too many roads not taken. *Nature* **2011**, *470*, 163–165. [[CrossRef](#)]
7. Oprea, T.I.; Bologa, C.G.; Brunak, S.; Campbell, A.; Gan, G.N.; Gaulton, A.; Gomez, S.M.; Guha, R.; Hersey, A.; Holmes, J.; et al. Unexplored therapeutic opportunities in the human genome. *Nat. Rev. Drug Discov.* **2018**, *17*, 377. [[CrossRef](#)]
8. Klaeger, S.; Heinzlmeier, S.; Wilhelm, M.; Polzer, H.; Vick, B.; Koenig, P.A.; Reinecke, M.; Ruprecht, B.; Petzoldt, S.; Meng, C.; et al. The target landscape of clinical kinase drugs. *Science* **2017**, *358*. [[CrossRef](#)]
9. Christmann-Franck, S.; van Westen, G.J.; Papadatos, G.; Beltran Escudie, F.; Roberts, A.; Overington, J.P.; Domine, D. Unprecedentedly Large-Scale Kinase Inhibitor Set Enabling the Accurate Prediction of Compound-Kinase Activities: A Way toward Selective Promiscuity by Design? *J. Chem. Inf. Model.* **2016**, *56*, 1654–1675. [[CrossRef](#)]
10. Arrowsmith, C.H.; Audia, J.E.; Austin, C.; Baell, J.; Bennett, J.; Blagg, J.; Bountra, C.; Brennan, P.E.; Brown, P.J.; Bunnage, M.E.; et al. The promise and peril of chemical probes. *Nat. Chem. Biol.* **2015**, *11*, 536–541. [[CrossRef](#)]
11. Jones, L.H.; Bunnage, M.E. Applications of chemogenomic library screening in drug discovery. *Nat. Rev. Drug Discov.* **2017**, *16*, 285–296. [[CrossRef](#)]
12. Gautam, P.; Jaiswal, A.; Aittokallio, T.; Al-Ali, H.; Wennerberg, K. Phenotypic Screening Combined with Machine Learning for Efficient Identification of Breast Cancer-Selective Therapeutic Targets. *Cell Chem. Biol.* **2019**, *26*, 970–979.e974. [[CrossRef](#)] [[PubMed](#)]
13. Bamborough, P.; Drewry, D.; Harper, G.; Smith, G.K.; Schneider, K. Assessment of chemical coverage of kinome space and its implications for kinase drug discovery. *J. Med. Chem.* **2008**, *51*, 7898–7914. [[CrossRef](#)] [[PubMed](#)]
14. Posy, S.L.; Hermsmeier, M.A.; Vaccaro, W.; Ott, K.H.; Todderud, G.; Lippy, J.S.; Trainor, G.L.; Loughney, D.A.; Johnson, S.R. Trends in Kinase Selectivity: Insights for Target Class-Focused Library Screening. *J. Med. Chem.* **2011**, *54*, 54–66. [[CrossRef](#)] [[PubMed](#)]
15. Elkins, J.M.; Fedele, V.; Szklarz, M.; Abdul Azeez, K.R.; Salah, E.; Mikolajczyk, J.; Romanov, S.; Sepetov, N.; Huang, X.-P.; Roth, B.L.; et al. Comprehensive characterization of the Published Kinase Inhibitor Set. *Nat. Biotech.* **2016**, *34*, 95–103. [[CrossRef](#)] [[PubMed](#)]
16. Drewry, D.H.; Wells, C.I.; Andrews, D.M.; Angell, R.; Al-Ali, H.; Axtman, A.D.; Capuzzi, S.J.; Elkins, J.M.; Etmayer, P.; Frederiksen, M.; et al. Progress towards a public chemogenomic set for protein kinases and a call for contributions. *PLoS ONE* **2017**, *12*, e0181585. [[CrossRef](#)]
17. Drewry, D.H.; Wells, C.I.; Zuercher, W.J.; Willson, T.M. A Perspective on Extreme Open Science: Companies Sharing Compounds without Restriction. *SLAS Discov.* **2019**, *24*, 505–514. [[CrossRef](#)]
18. Moret, N.; Clark, N.A.; Hafner, M.; Wang, Y.; Lounkine, E.; Medvedovic, M.; Wang, J.; Gray, N.; Jenkins, J.; Sorger, P.K. Cheminformatics Tools for Analyzing and Designing Optimized Small-Molecule Collections and Libraries. *Cell Chem. Biol.* **2019**, *26*, 765–777.e763. [[CrossRef](#)]
19. Edwards, A.; Morgan, M.; Al Chawaf, A.; Andrusiak, K.; Charney, R.; Cynader, Z.; ElDessouki, A.; Lee, Y.; Moeser, A.; Stern, S.; et al. A trust approach for sharing research reagents. *Sci. Transl. Med.* **2017**, *9*. [[CrossRef](#)]
20. The Structural Genomics Consortium. Available online: [www.thesgc.org](http://www.thesgc.org) (accessed on 1 December 2019).



21. Fabian, M.A.; Biggs, W.H., 3rd; Treiber, D.K.; Atteridge, C.E.; Azimioara, M.D.; Benedetti, M.G.; Carter, T.A.; Ciceri, P.; Edeen, P.T.; Floyd, M.; et al. A small molecule-kinase interaction map for clinical kinase inhibitors. *Nat. Biotechnol.* **2005**, *23*, 329–336. [CrossRef]
22. DiscoverX. scanMAX. Available online: <https://www.discoverx.com/services/drug-discovery-development-services/kinase-profiling/kinomescan/scanmax> (accessed on 1 December 2019).
23. Manning, G.; Whyte, D.B.; Martinez, R.; Hunter, T.; Sudarsanam, S. The Protein Kinase Complement of the Human Genome. *Science* **2002**, *298*, 1912–1934. [CrossRef]
24. Zwick, M.; Kraemer, O.; Carter, A.J. Dataset of the frequency patterns of publications annotated to human protein-coding genes, their protein products and genetic relevance. *Data Brief* **2019**, *25*, 104284. [CrossRef] [PubMed]
25. Carter, A.J.; Kraemer, O.; Zwick, M.; Mueller-Fahrnow, A.; Arrowsmith, C.H.; Edwards, A.M. Target 2035: Probing the human proteome. *Drug Discov. Today* **2019**, *24*, 2111–2115. [CrossRef] [PubMed]
26. DAYLIGHT Chemical Information Systems. Available online: [www.daylight.com/dayhtml/doc/theory/theory.smarts.html](http://www.daylight.com/dayhtml/doc/theory/theory.smarts.html) (accessed on 1 December 2019).
27. Daina, A.; Michielin, O.; Zoete, V. SwissADME: A free web tool to evaluate pharmacokinetics, drug-likeness and medicinal chemistry friendliness of small molecules. *Sci. Rep.* **2017**, *7*, 42717. [CrossRef] [PubMed]
28. Roskoski, R., Jr. Properties of FDA-approved small molecule protein kinase inhibitors. *Pharmacol. Res.* **2019**, *144*, 19–50. [CrossRef]
29. Varma, M.V.; Obach, R.S.; Rotter, C.; Miller, H.R.; Chang, G.; Steyn, S.J.; El-Kattan, A.; Troutman, M.D. Physicochemical space for optimum oral bioavailability: Contribution of human intestinal absorption and first-pass elimination. *J. Med. Chem.* **2010**, *53*, 1098–1108. [CrossRef]
30. Montenegro, R.C.; Clark, P.G.; Howarth, A.; Wan, X.; Ceroni, A.; Siejka, P.; Nunez-Alonso, G.A.; Monteiro, O.; Rogers, C.; Gamble, V.; et al. BET inhibition as a new strategy for the treatment of gastric cancer. *Oncotarget* **2016**, *7*, 43997–44012. [CrossRef]
31. Howarth, A.; Schroder, M.; Montenegro, R.C.; Drewry, D.H.; Sailem, H.; Millar, V.; Muller, S.; Ebner, D.V. HighVia—A Flexible Live-Cell High-Content Screening Pipeline to Assess Cellular Toxicity. *SLAS Discov.* **2020**, *25*, 801–811. [CrossRef]
32. Hafner, M.; Niepel, M.; Chung, M.; Sorger, P.K. Growth rate inhibition metrics correct for confounders in measuring sensitivity to cancer drugs. *Nat. Methods* **2016**, *13*, 521–527. [CrossRef]
33. Mills, C.; Gerosa, L. Optimized Experimental and Analytical Tools for Reproducible Drug-Response Studies. Available online: [http://lincs.hms.harvard.edu/wordpress/wp-content/uploads/2018/06/DoseResponseNanocourse\\_2018\\_Final.pdf](http://lincs.hms.harvard.edu/wordpress/wp-content/uploads/2018/06/DoseResponseNanocourse_2018_Final.pdf) (accessed on 1 December 2019).
34. Hafner, M.; Niepel, M.; Subramanian, K.; Sorger, P.K. Designing Drug-Response Experiments and Quantifying their Results. *Curr. Protoc. Chem. Biol.* **2017**, *9*, 96–116. [CrossRef]
35. Stolz, A.; Putyrski, M.; Kutle, I.; Huber, J.; Wang, C.; Major, V.; Sidhu, S.S.; Youle, R.J.; Rogov, V.V.; Dotsch, V.; et al. Fluorescence-based ATG8 sensors monitor localization and function of LC3/GABARAP proteins. *EMBO J.* **2017**, *36*, 549–564. [CrossRef]
36. Dikic, I.; Elazar, Z. Mechanism and medical implications of mammalian autophagy. *Nat. Rev. Mol. Cell Biol.* **2018**, *19*, 349–364. [CrossRef] [PubMed]
37. Kaizuka, T.; Morishita, H.; Hama, Y.; Tsukamoto, S.; Matsui, T.; Toyota, Y.; Kodama, A.; Ishihara, T.; Mizushima, T.; Mizushima, N. An Autophagic Flux Probe That Releases an Internal Control. *Mol. Cell* **2016**, *64*, 835–849. [CrossRef] [PubMed]
38. Ozfiliz-Kilbas, P.; Sarikaya, B.; Obakan-Yerlikaya, P.; Coker-Gurkan, A.; Arisan, E.D.; Temizci, B.; Palavan-Unsal, N. Cyclin-dependent kinase inhibitors, roscovitine and purvalanol, induce apoptosis and autophagy related to unfolded protein response in HeLa cervical cancer cells. *Mol. Biol. Rep.* **2018**, *45*, 815–828. [CrossRef] [PubMed]
39. Zhou, Z.R.; Yang, Z.Z.; Wang, S.J.; Zhang, L.; Luo, J.R.; Feng, Y.; Yu, X.L.; Chen, X.X.; Guo, X.M. The Chk1 inhibitor MK-8776 increases the radiosensitivity of human triple-negative breast cancer by inhibiting autophagy. *Acta Pharmacol. Sin.* **2017**, *38*, 513–523. [CrossRef]
40. Liu, Z.; Wang, F.; Zhou, Z.W.; Xia, H.C.; Wang, X.Y.; Yang, Y.X.; He, Z.X.; Sun, T.; Zhou, S.F. Alisertib induces G2/M arrest, apoptosis, and autophagy via PI3K/Akt/mTOR- and p38 MAPK-mediated pathways in human glioblastoma cells. *Am. J. Transl. Res.* **2017**, *9*, 845–873. [PubMed]
41. Wang, Y.; Zhang, H. Regulation of Autophagy by mTOR Signaling Pathway. *Adv. Exp. Med. Biol.* **2019**, *1206*, 67–83. [CrossRef]
42. Li, Z.Y.; Zhang, X. Kinases Involved in Both Autophagy and Mitosis. *Int. J. Mol. Sci.* **2017**, *18*, 1884. [CrossRef]
43. Vasta, J.D.; Corona, C.R.; Wilkinson, J.; Zimprich, C.A.; Hartnett, J.R.; Ingold, M.R.; Zimmerman, K.; Machleidt, T.; Kirkland, T.A.; Huwiler, K.G.; et al. Quantitative, Wide-Spectrum Kinase Profiling in Live Cells for Assessing the Effect of Cellular ATP on Target Engagement. *Cell Chem. Biol.* **2018**, *25*, 206–214.e211. [CrossRef]
44. Open Babel: The Open Source Chemistry Toolbox. Available online: <http://openbabel.org/> (accessed on 1 December 2019).
45. MATLAB. Available online: <https://www.mathworks.com/products/matlab.html> (accessed on 1 December 2019).
46. Bhullar, K.S.; Lagaron, N.O.; McGowan, E.M.; Parmar, I.; Jha, A.; Hubbard, B.P.; Rupasinghe, H.P.V. Kinase-Targeted cancer therapies: Progress, challenges and future directions. *Mol. Cancer* **2018**, *17*, 48. [CrossRef]
47. Kannaiyan, R.; Mahadevan, D. A comprehensive review of protein kinase inhibitors for cancer therapy. *Expert. Rev. Anticancer Ther.* **2018**, *18*, 1249–1270. [CrossRef]
48. Burdova, K.; Yang, H.B.; Faedda, R.; Hume, S.; Chauhan, J.; Ebner, D.; Kessler, B.M.; Vendrell, I.; Drewry, D.H.; Wells, C.I.; et al. E2F1 proteolysis via SCF-cyclin F underlies synthetic lethality between cyclin F loss and Chk1 inhibition. *EMBO J.* **2019**, *38*. [CrossRef] [PubMed]

49. Guo, W.; Vandoorne, T.; Steyaert, J.; Staats, K.A.; Van Den Bosch, L. The multifaceted role of kinases in amyotrophic lateral sclerosis: Genetic, pathological and therapeutic implications. *Brain* **2020**, *143*, 1651–1673. [[CrossRef](#)] [[PubMed](#)]
50. Guttuso, T., Jr.; Andrzejewski, K.L.; Lichter, D.G.; Andersen, J.K. Targeting kinases in Parkinson's disease: A mechanism shared by LRRK2, neurotrophins, exenatide, urate, nilotinib and lithium. *J. Neurol. Sci.* **2019**, *402*, 121–130. [[CrossRef](#)] [[PubMed](#)]
51. Singh, R.M.; Cummings, E.; Pantos, C.; Singh, J. Protein kinase C and cardiac dysfunction: A review. *Heart Fail. Rev.* **2017**, *22*, 843–859. [[CrossRef](#)]



## Identification of Pyrimidine-Based Lead Compounds for Understudied Kinases Implicated in Driving Neurodegeneration

David H. Drewry, Joel K. Annor-Gyamfi, Carrow I. Wells, Julie E. Pickett, Verena Dederer, Franziska Preuss, Sebastian Mathea, and Alison D. Axtman\*

Cite This: *J. Med. Chem.* 2022, 65, 1313–1328

Read Online

ACCESS |



Metrics &amp; More

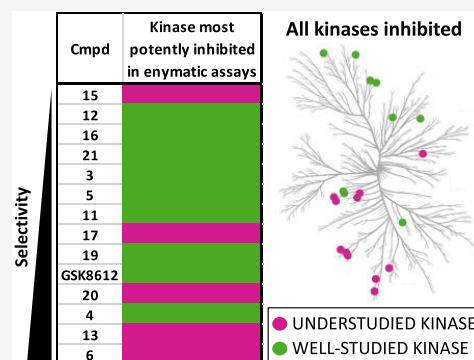


Article Recommendations



Supporting Information

**ABSTRACT:** The pyrimidine core has been utilized extensively to construct kinase inhibitors, including eight FDA-approved drugs. Because the pyrimidine hinge-binding motif is accommodated by many human kinases, kinome-wide selectivity of resultant molecules can be poor. This liability was seen as an advantage since it is well tolerated by many understudied kinases. We hypothesized that nonexemplified aminopyrimidines bearing side chains from well-annotated pyrimidine-based inhibitors with off-target activity on understudied kinases would provide us with useful inhibitors of these lesser studied kinases. Our strategy paired mixing and matching the side chains from the 2- and 4-positions of the parent compounds with modifications at the 5-position of the pyrimidine core, which is situated near the gatekeeper residue of the binding pocket. Utilizing this approach, we imparted improved kinome-wide selectivity to most members of the resultant library. Importantly, we also identified potent biochemical and cell-active lead compounds for understudied kinases like DRAK1, BMP2K, and MARK3/4.



## INTRODUCTION

Pyrimidines represent an important building block in the medicinal chemistry arsenal. Compounds bearing a pyrimidine core have proven to be bioactive and exhibit diverse pharmacology, including anticonvulsant, analgesic, sedative, antidepressive, antipyretic, anti-inflammatory, antiviral, anti-HIV, antimicrobial, and antitumor activities.<sup>1</sup> Pyrimidines are very useful as kinase scaffolds that employ a nitrogen to make key hydrogen bonds with the conserved hinge region found in nearly all human kinases. Aminopyrimidines substituted with an NH in the 2-position can make an additional hydrogen bond with the kinase hinge. To date, eight FDA-approved kinase inhibitors employ a pyrimidine as the key kinase hinge-binding motif.<sup>2</sup>

The work we describe here stems from the synergistic convergence of two separate interests that were satisfied through diversification of the pyrimidine scaffold. The first of these interests centers around the generation and use of kinase inhibitors as tools to build deeper understanding of signaling in neurodegenerative disease. TBK1, a kinase with links to amyotrophic lateral sclerosis (ALS), frontotemporal dementia (FTD), Huntington's disease, and Alzheimer's disease (AD), is potently inhibited by several pyrimidine-bearing compounds.<sup>3–12</sup> A second interest of ours is identification of high-quality tool molecules for understudied kinase targets. Our pursuit of this interest relies on parallel chemical tool and kinase assay development, efforts that are supported in part by the NIH Illuminating the Druggable Genome (IDG) program.

The IDG program aims to catalyze the characterization of all proteins through stimulating research around those that are most poorly studied.<sup>13</sup> One arm of the IDG program supports illumination of the dark kinome, which includes development of high-quality chemical tools for these understudied kinases. As we examined the data available for literature pyrimidine-based TBK1 inhibitors, we noticed a range of understudied kinases that were also inhibited by these compounds.

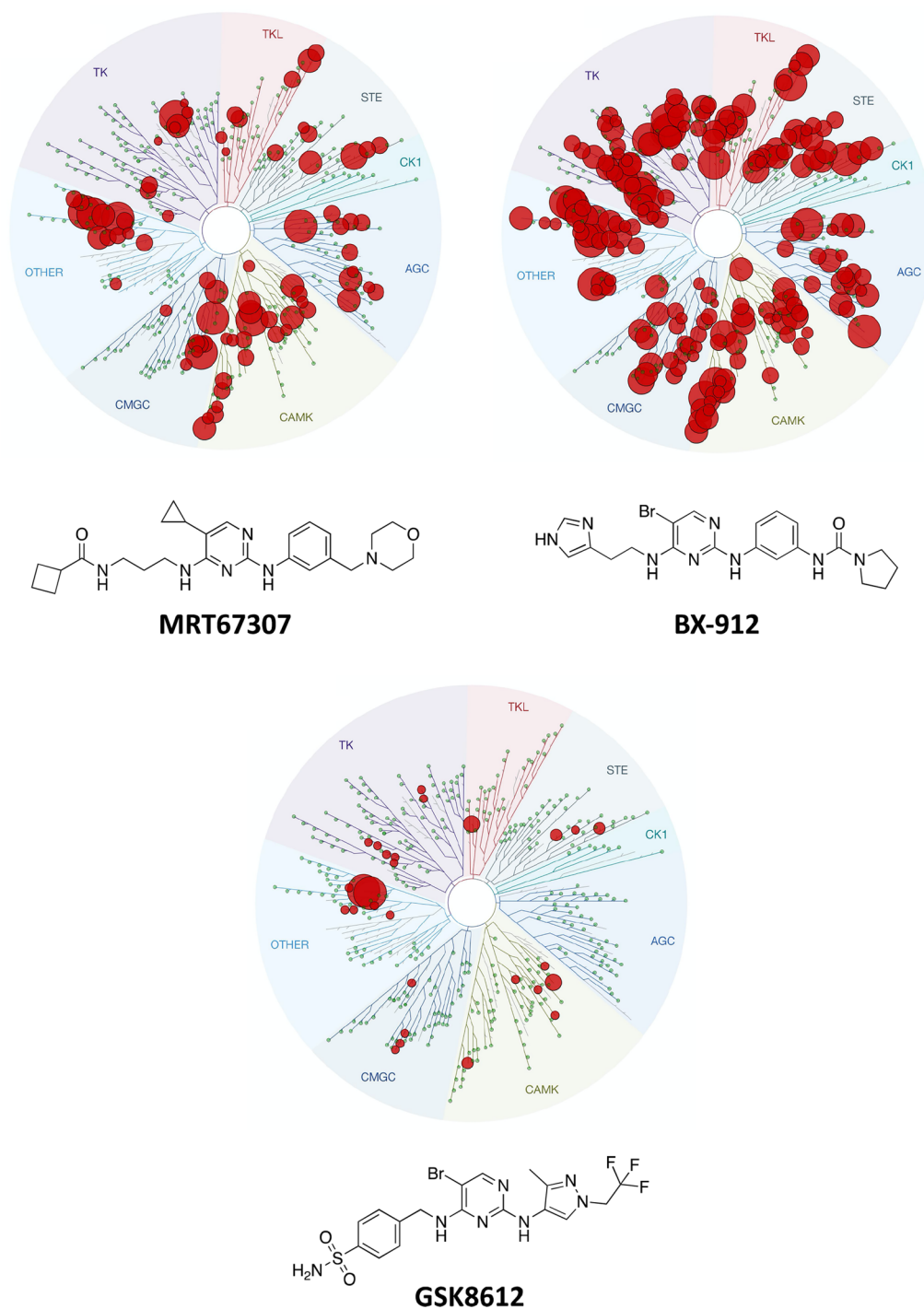
Several of the understudied kinases inhibited by pyrimidines also have been genetically implicated in driving neurodegenerative diseases. The MARK family of kinases, for example, phosphorylates tau protein in its repeat domain and thereby regulates its affinity for microtubules, affecting the aggregation of tau into neurofibrillary tangles. Observations of AD brains show a strong correlation between cognitive dysfunction and cortical neurofibrillary tangle density.<sup>14–16</sup> Mutations in tau have also been shown to cause a form of FTD.<sup>16</sup> Furthermore, with a characterized role in dendrite branching and spine development, understudied kinase AAK1 is suggested to play a role in several neurodegenerative disorders, including AD and ALS.<sup>14,17,18</sup>

**Special Issue:** New Horizons in Drug Discovery - Understanding and Advancing Kinase Inhibitors

**Received:** March 10, 2021

**Published:** August 1, 2021



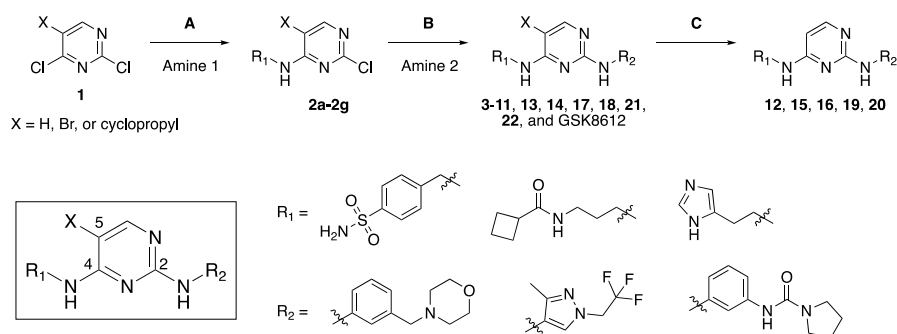


**Figure 1.** Structures and broad selectivity profiling of aminopyrimidines that served as the basis for library design. All WT kinases inhibited > 90% at 10  $\mu\text{M}$  by MRT67307 and BX-912 and all WT kinases inhibited > 65% at 1  $\mu\text{M}$  by GSK8612 are shown.

Figure 1 shows the structures and kinome-wide profiling data generated at DiscoverX (*scanMAX* or *KINOMEScan*) for three TBK1-targeting aminopyrimidines.<sup>19</sup> The data for TBK1 inhibitors MRT67307 and BX-912 (designed for PDK1 but potent inhibitor of TBK1) are already in the literature (LINCS database).<sup>20–24</sup> These two compounds were screened at 10  $\mu\text{M}$  (Figure 1). GSK8612 was recently disclosed by GlaxoSmithKline as a potent and selective TBK1 inhibitor.<sup>25</sup> We opted to survey the kinome-wide selectivity of GSK8612 at DiscoverX at 1  $\mu\text{M}$  (Figure 1). While the screening concentrations are different, it is apparent that these scaffolds

differentially and potently inhibit many kinases across the kinome and that selectivity can be augmented through structural changes.

Several kinases potently inhibited by aminopyrimidines like BX-912, MRT67307, and/or GSK8612 are members of the IDG nominated list of dark kinases. Thus, this scaffold was considered an excellent starting point from which to design high-quality chemical tools. Development of these tools will enable elucidation of the function of those kinases that have suffered from a dearth of characterization, including those on the IDG list. High-quality chemical tools will also enable

Scheme 1. Library Design and Preparation Strategy<sup>a</sup>

<sup>a</sup>Step A: Pyrimidine 1, amine 1, DIPEA, ethanol,  $-10\text{ }^{\circ}\text{C}$  to  $50\text{ }^{\circ}\text{C}$ . Step B: Aminopyrimidine 2, amine 2, dioxane  $\times$  HCl, butanol,  $80\text{ }^{\circ}\text{C}$ . Step C: Aminopyrimidine X, 5% Pd/C, H<sub>2</sub>, TEA, methanol, r.t.

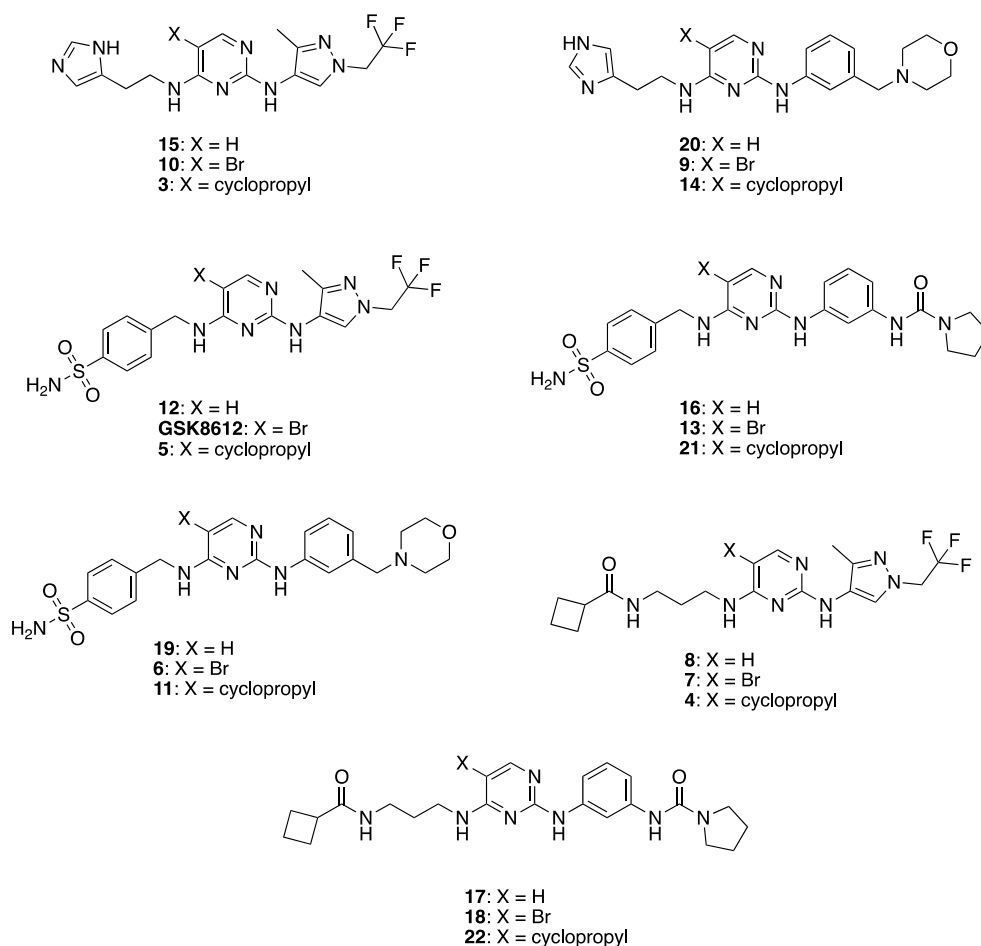


Figure 2. Library of aminopyrimidine analogs prepared.

further characterization of kinase-mediated signaling in neurodegenerative disease and facilitate the validation of therapeutic hypotheses.

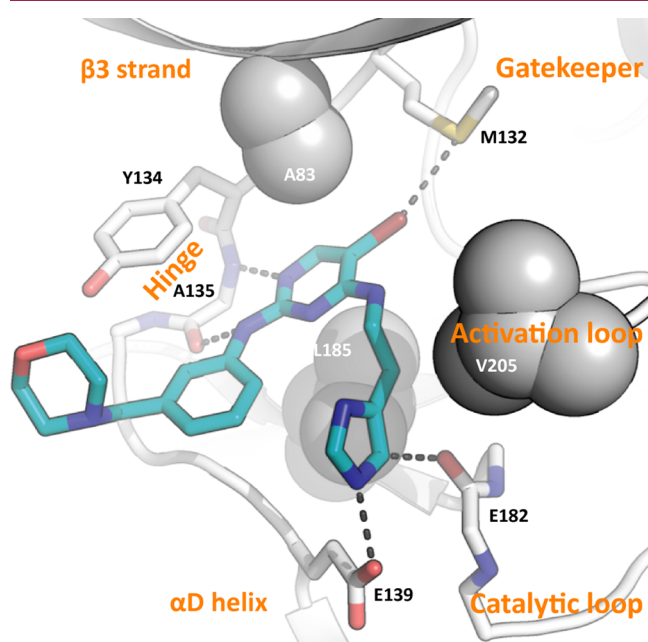
## RESULTS AND DISCUSSION

**Compound Design and Synthesis.** Our library design involved mixing and matching the side chains and cores from published aminopyrimidine inhibitors MRT67307, BX-912, and GSK8612 to furnish 21 total analogs. Specifically, we paired mixing and matching the side chains from the 2- and 4-positions of the parent compounds with modifications at the 5-position of the pyrimidine core as shown in Scheme

1. Seven final compounds were prepared with X = H, seven with X = Br, and seven with X = cyclopropyl (Figure 2). Analogs of BX-912 and MRT67307 (and the parent compounds themselves) that varied only at the 5-position (box in Scheme 1) were not prepared. A great deal of effort has been dedicated to making close structural analogs of these two compounds, and we did not want our work to be redundant. Since it was not commercially available at the time and the most selective of the parent scaffolds, GSK8612 and variants with X = H and cyclopropyl were all synthesized. The method used to prepare these analogs is outlined in Scheme 1. Briefly, taking advantage of the inherent reactivity of 2,4-dichloropyr-

imidines, iterative nucleophilic aromatic displacements were executed, and specific brominated compounds (GSK8612, **6**, **9**, **10**, and **13**) were subsequently dehalogenated to furnish all final compounds.

We had several expected outcomes from our strategy of mixing and matching the side chains and cores from well exemplified pyrimidine-based inhibitors. First, we intended to develop more narrowly selective compounds by incorporating these distinct side chains and 5-position modifications into new compounds. Next, we wanted to generate preliminary structure–activity relationships (SAR) for several understudied kinases. In doing so, we aimed to leverage these scaffolds with known inhibitory activity of dark kinases to identify more optimal chemical starting points for development of high-quality chemical tools. Finally, we wanted to develop focused SAR around the 5-position (box in Scheme 1), which has not been systematically investigated in the literature yet and is proposed to play a key role in dictating both potency and selectivity due to its proximity to the kinase gatekeeper residue (Figure 3).



**Figure 3.** Structural studies support optimization for understudied MARK kinases. X-ray crystallography structure of human MARK3 in complex with aminopyrimidine **9**. Compound **9** (PDB code: 7PIL) is shown in teal stick representation. The kinase structural elements mediating the binding are labeled in orange. Parts of the G-rich loop, including I62, were made transparent to provide a better view of the interactions. Key interactions are indicated as dashed lines.

**Targeted Kinase Inhibition Profiling.** We selected a small panel of representative kinases against which to profile our library of 21 aminopyrimidine analogs. These kinases include some of the original targets for which pyrimidine-based inhibitors were prepared (JAK2, IKK $\epsilon$ , TBK1, and ULK1), a more well-studied kinase that is potently inhibited by many analogs within this structural class (AURKB), and several understudied kinases, many of which are both on the IDG list (AAK1, BMP2K, DRAK1–2, MARK1–4, MLK1, MLK3, and NUA1) and of interest in the neuroscience space.<sup>14,15,17,26–29</sup> We profiled our aminopyrimidine series and the parent aminopyrimidines that influenced our design against this

kinase panel at a single concentration (1  $\mu$ M) in radiometric enzymatic assays at Eurofins at the  $K_m = \text{ATP}$  for each kinase. Table S1 shows the results of this study, where % control is reported for each compound for each kinase and lower values indicate greater inhibition. The column labeled “no. kinases  $\leq 10$  PoC in enzyme panel” in Table 1 captures the number of kinases in this 16-member panel inhibited  $\geq 90\%$  by each compound.

**Table 1. Kinase Panel Profiling of Aminopyrimidine Library**

compound	no. kinases $\leq 10$ PoC in enzyme panel	$S_{10}$ (1 $\mu$ M) <sup>b</sup>	no. kinases with PoC < 10 <sup>c</sup>
3	0	0.005	2
4	1	0.027	11
5	1	0.005	2
6	4	0.047	19
7	7	0.154	62
8	0	0.002	1
9	13	0.233	94
10	0	0.069	28
11	1	0.007	3
12	0	0.002	1
13	4	0.03	12
14	6	0.067	27
15	0	0	0
16	0	0.002	1
17	0	0.007	3
18	16	0.223	90
19	0	0.007	3
20	1	0.022	9
21	1	0.002	1
22	9	0.074	30
MRT67307	12	N.T. <sup>a</sup>	N.T. <sup>a</sup>
MRT68921	13	N.T. <sup>a</sup>	N.T. <sup>a</sup>
BX-795	16	N.T. <sup>a</sup>	N.T. <sup>a</sup>
BX-912	14	N.T. <sup>a</sup>	N.T. <sup>a</sup>
GSK8612	1	0.02	8

<sup>a</sup>N.T.: not tested. <sup>b</sup> $S_{10}$  (1  $\mu$ M): Percentage of screened kinases with PoC values < 10 at 1  $\mu$ M. <sup>c</sup>Number of kinases with PoC values < 10 at 1  $\mu$ M.

We found that, with the exception of two analogs (compounds **9** and **18**), all compounds in our library inhibited fewer kinases in this custom kinase panel than published compounds BX-912, BX-795 (analog of BX-912), MRT67307, and MRT68921 (analog of MRT67307).<sup>20–23</sup> In most cases, we demonstrated a significant decrease in the number of kinases potentially inhibited by our aminopyrimidine analogs. This becomes more meaningful when we consider that the kinases selected in our custom panel represent some of the most common off-target kinases inhibited by the parent compounds. Gratifyingly, unlike the published compounds from the BX and MRT series that elicited potent inhibition of nearly all kinases in the panel, our compounds have cleaned-up profiles, and we were able to dial out inhibition of certain kinases through structural modification. We were pleased to observe potent inhibition of several understudied kinases by analogs that inhibited fewer kinases in this panel, including BMP2K by **6**; AAK1, DRAK1, DRAK2, and MARK1 by **7**; AAK1 and BMP2K by **13**; and MARK1, MARK3, MARK4, MLK1, and NUA1 by **14**.



Table 2. NanoBRET Profiling of Entire Aminopyrimidine Library

compound	IC <sub>50</sub> values (nM)			
	DRAK1 <sup>b</sup>	MARK3 <sup>c</sup>	MARK4 <sup>c</sup>	TBK1 <sup>b</sup>
3	>10000	>10000	>10000	>10000
4	874 ± 103	>10000	>10000	2680 ± 230
5	>10000	>10000	>10000	7456
6	>10000	>10000	>10000	>10000
7	126 ± 27.6	>10000	3537	321 ± 2.49
8	>10000	>10000	>10000	>10000
9	638 ± 91.1	872	214	>10000
10	>10000	>10000	8445	>10000
11	>10000	>10000	>10000	2050 ± 196
12	>10000	>10000	>10000	>10000
13	>10000	>10000	>10000	6170 ± 2190
14	3622	4015	808	>10000
15	>10000	>10000	>10000	>10000
16	>10000	>10000	>10000	>10000
17	2311	>10000	>10000	>10000
18	4.47 ± 0.406	137	72	338 ± 22.5
19	>10000	>10000	>10000	>10000
20	>10000	>10000	>10000	>10000
21	>10000	>10000	>10000	>10000
22	58.2 ± 3.21	2001	509	2580 ± 215
MRT67307	43.2 ± 2.69	328 ± 38.5	319	N.T. <sup>a</sup>
MRT68921	N.T. <sup>a</sup>	95	N.T. <sup>a</sup>	N.T. <sup>a</sup>
BX-795	N.T. <sup>a</sup>	515	N.T. <sup>a</sup>	N.T. <sup>a</sup>
BX-912	N.T. <sup>a</sup>	3333	338 ± 4.5	2327
GSK8612	>10000	>10000	>10000	339 ± 39.5

<sup>a</sup>N.T.: not tested. <sup>b</sup>C Compounds tested in singlicate ( $n = 1$ ) in dose–response where error not shown, and compounds with SEM tested in triplicate ( $n = 3$ ) in dose–response. <sup>c</sup>C Compounds tested in singlicate ( $n = 1$ ) in dose–response where error not shown, and compounds with SEM tested in duplicate ( $n = 2$ ) in dose–response.

When we examined the data generated via screening in the Eurofins kinase panel versus compound structures for our synthetic library, we noticed some predominating trends. When varying the 5-position (X in Figure 2), more kinases were tolerant of the bromo substituent, and thus those analogs bearing X = Br inhibited the most kinases in this panel. When X = Br, an average of 6.4 kinases (range of 0–16 kinases) were inhibited  $\geq 90\%$ . The average number of kinases inhibited was calculated by adding the number of kinases inhibited  $\leq 10$  percent of control (PoC) in the enzyme panel (Table 1, column 2) and dividing by the total number of compounds. For X = Br, this works out to be a sum of 45, divided by 7 total compounds for an average of 6.4 kinases. We will use this equation to calculate and report average kinase inhibition throughout this section. Switching to X = H resulted in compounds that inhibited the fewest kinases in the series, with an average of only 0.1 kinases (range of 0–1 kinase), demonstrating  $\geq 90\%$  inhibition in the Eurofins panel at 1  $\mu\text{M}$ . Finally, cyclopropyl at position X was somewhere between H and Br in terms of number of kinases inhibited, with an average of 2.7 kinases (range of 0–9 kinases) inhibited  $\geq 90\%$ . When considering the amine side chains in the 2- and 4-positions, some general inhibition trends were also observed. Incorporation of the sulfonamide-bearing side chain in the pyrimidine 4-position (R<sub>1</sub> position, Scheme 1) resulted in compounds that inhibited the fewest number of kinases: an average of 1.3 kinases (range of 0–4 kinases)  $\geq 90\%$  at 1  $\mu\text{M}$ . In the pyrimidine 2-position, the substituted pyrazole is the R<sub>2</sub> substituent that resulted in aminopyrimidines with the narrowest inhibition profiles: an average of 1.1 kinases

(range of 0–7 kinases)  $\geq 90\%$ . The *ortho*-methyl group on the pyrazole ring likely contributes to this enhanced inhibition profile when compared to other side chains at the R<sub>2</sub> position. While some of the analogs in our library, including those with a 5-position H and/or 4-position sulfonamide, did not inhibit any kinases in our smaller panel, it is difficult to extrapolate whether this translates to loss of all kinase inhibitory activity or a narrower selectivity profile unless broader kinome-wide screening is executed.

#### Library-Wide Cellular Target Engagement Studies.

The data generated by screening our aminopyrimidine analogs in the panel of kinases at Eurofins motivated follow-up cell-based studies. We used cellular target engagement assays to determine whether potent enzyme inhibition corresponded with potent binding in cells. The NanoBRET assay offers a method through which cellular penetrance and binding of a compound to its kinase target in cells can be simultaneously assessed.<sup>30</sup> Given the consistently potent inhibition of TBK1 by many compounds in our library (Table S1) and our interest in this kinase, we profiled the entire library using the TBK1 NanoBRET assay in dose–response format (Table 2). We found that potent enzymatic inhibition of TBK1 did not always translate to potent engagement of TBK1 in cells. We note that orthogonal assay formats, such as an enzymatic and cellular target engagement assay, can sometimes yield different results and, for this reason, that it's best to assess kinase inhibition via multiple methods. All compounds that demonstrated at least 50% inhibition at 10  $\mu\text{M}$  when tested using the TBK1 NanoBRET assay in the first dose–response experiment were followed up with two additional replicates. Two members of

our library, **7** and **18**, and GSK8612 demonstrated submicromolar  $IC_{50}$  values in the TBK1 NanoBRET assay. These three compounds demonstrated PoC values  $\leq 6$  in the TBK1 enzymatic assay (Table S1), making them among the most potent inhibitors tested in this assay of those that we synthesized. The validation of GSK8612 as a potent, cell-active compound targeting TBK1 aligns well with the recent publication that described its development and characterization, including validation of its activity in multiple cell-based assays.<sup>25</sup> Further, submicromolar activity in a NanoBRET assay has translated to phenotypic results for multiple chemical probes and is one part of the chemical probe criteria defined for SGC-nominated chemical probes.<sup>17,31,32</sup>

Shifting our attention to understudied kinases, we also observed that some of our compounds potently inhibited DRAK1, MARK3, and MARK4 (Table S1). As part of the IDG program, we have interest in developing high-quality chemical tools to help elucidate the function of these poorly characterized kinases. For our aminopyrimidine series, dose-response NanoBRET analysis yielded five analogs (**4**, **7**, **9**, **18**, and **22**) and MRT67307 with submicromolar activity in the DRAK1 NanoBRET assay. We repeated the NanoBRET assay in dose-response for these six compounds and found all to maintain activity over three replicates. Gratifyingly, **7**, **9**, **18**, **22**, and MRT67307 were the most potent compounds in the DRAK1 enzymatic assay (Table S1), and all demonstrated PoC  $\leq 9$ . Finally, the entire series was tested in the MARK3 and MARK4 NanoBRET assays. We found four compounds (**9**, **14**, **18**, and **22**) with submicromolar  $IC_{50}$  values in the MARK4 NanoBRET assay, two of which (**9** and **18**) also demonstrated submicromolar  $IC_{50}$  values in the MARK3 NanoBRET assay. Several of the parent compounds also had submicromolar  $IC_{50}$  values in the MARK3/4 NanoBRET assays. For MARK3, the four most potent compounds in the MARK3 enzymatic assay, all with PoC  $\leq -1$  (Table S1), were the most efficacious in the MARK3 NanoBRET assay (Table 2). For MARK4, compounds **9**, **18**, MRT67307, and BX-912 were among the most potent compounds in the MARK4 enzymatic assay (Table S1, PoC  $\leq 5$ ), and all demonstrated MARK4 NanoBRET  $IC_{50}$  values  $< 400$  nM. In general, we noted very good correlation between the orthogonal enzymatic (Table S1) and cellular target engagement (Table 2) assay formats for these understudied kinases. Based on our 16-kinase enzyme inhibition panel, we felt confident that some of these understudied kinase chemical leads inhibited fewer kinases than their parent compounds, and we chose to assess their kinome-wide selectivities to determine whether they require further optimization in our pursuit of high-quality chemical tools.

**Assessment of Kinome-Wide Selectivity.** The promising inhibition profiles of our aminopyrimidine series in the custom enzymatic assay panel motivated a broader survey to ascertain the kinome-wide selectivity of our library. All 21 novel analogs were screened at  $1 \mu\text{M}$  via the DiscoverX scanMAX platform, which includes 403 wild-type (WT) human kinases. A selectivity score ( $S_{10}$ ) for each compound is included in Table 1, representative of the percentage of kinases that exhibit binding with a percent of control (PoC)  $< 10$  at  $1 \mu\text{M}$ . A final column is included in Table 1 that converts this  $S_{10}$  ( $1 \mu\text{M}$ ) value into the number of kinases bound with a PoC  $< 10$  in the DiscoverX panel. Figure S1 details the specific WT kinases that bound with a PoC  $< 10$  at  $1 \mu\text{M}$  in the DiscoverX scanMAX panel for each aminopyrimidine analog.

This more comprehensive analysis of selectivity surfaced many findings. We learned that trends within our smaller curated enzymatic kinase panel (16 kinases) were generally maintained in this larger profiling effort. Compounds that inhibited the fewest kinases in the Eurofins enzymatic panel were largely those that demonstrated the most favorable selectivity profile in the DiscoverX scanMAX screening. We identified several pyrimidine-based kinase inhibitors with useful selectivity. To provide some context on a useful selectivity threshold for tool compounds, we include kinase inhibitors with an  $S_{10}$  ( $1 \mu\text{M}$ )  $< 0.04$  in our kinase chemogenomic set (KCGS) since they are the compounds that when screened can be more easily used to correlate phenotype with kinase target.<sup>33,34</sup> Based on their selectivity scores, 14 of 21, or 67%, of our novel inhibitors were found to be KCGS eligible. We confirmed that kinases potently inhibited in the smaller, biased enzymatic panel were also inhibited in the DiscoverX profiling and identified additional kinases that were differentially inhibited by certain analogs, providing fodder for future projects.

When comparing the results from our smaller enzymatic screening with kinome-wide screening, it is apparent that results do not correlate perfectly. It is not unexpected that these orthogonal assay types, enzymatic and binding, would yield slightly different results. General structural trends observed when analyzing the smaller kinase panel, however, were generally conserved in broader profiling. The most selective compounds, inhibiting an average of 2.6 of 403 WT kinases, bear a 5-position H (**8**, **12**, **15**, **16**, **17**, **19**, **20**). As described for the smaller enzyme panel, average kinase inhibition here is being calculated by summing the number of kinases with PoC  $< 10$  in the kinome-wide profiling for each compound (Table 1, column 4) and then dividing by the total number of compounds. For 5-position H, this works out to be 18 divided by 7, which is equal to an average of 2.6 kinases inhibited. The 5-position cyclopropyl aminopyrimidines (**3**, **4**, **5**, **11**, **14**, **21**, and **22**) inhibited an average of 10.9 of 403 WT kinases, making them the next most selective when considering just the 5-position substituent. Finally, the remaining compounds (**6**, **7**, **9**, **10**, **13**, **18**, and GSK8612) with a 5-position bromo are among the least selective compounds when screened broadly, inhibiting an average of 44.7 of 403 WT kinases. Moving to the 4-position amine side chain, the aminopyrimidine analogs bearing a sulfonamide side chain (**5**, **6**, **11**, **12**, **13**, **16**, **19**, **21**, and GSK8612) were among the most selective compounds profiled and only inhibited an average of 5.6 of 403 WT kinases. Similarly, the 2-position pyrazole side chain imparted some selectivity to analogs **3**, **4**, **5**, **7**, **8**, **10**, **12**, **15**, and GSK8612, resulting in inhibition of an average of 12.8 of 403 WT kinases when broadly screened.

Taken together, our NanoBRET profiling (Table 2) and kinome-wide screening (Table 1) enabled us to confirm that GSK8612 is the most potent in cells, selective ( $S_{10}$  ( $1 \mu\text{M}$ ) = 0.02), and the most useful TBK1 inhibitor from all that we tested. We did not improve upon the activity of this published compound through these synthetic efforts. Next, of the DRAK1 active compounds in the NanoBRET assay, only **4** was selective enough to be considered a valuable tool molecule. Given its  $S_{10}$  ( $1 \mu\text{M}$ ) = 0.027 and submicromolar  $IC_{50}$  value in the DRAK1 NanoBRET assay, compound **4** was nominated as a dark kinase tool that can be used to help illuminate the function of DRAK1. Information for compound **4** has been posted on the Dark Kinase Knowledgebase.<sup>35</sup> Finally,



Table 3. Combined Enzymatic Data

compound	potently active <sup>a</sup>	moderately active <sup>b</sup>	weakly active <sup>c</sup>
15		MYLK2 = 479 nM	DRAK2: 91%
8			MKNK2 = 2866 nM, DRAK2: 60%, YANK2 > 10000 nM
12		CSF1R = 233 nM	
16	TYK2 = 33 nM	CSF1R = 305 nM	JAK2: 62%
21		TBK1 = 128 nM, TRKA = 477 nM	BMP2K = 2918 nM, AURKB: 61%, JAK2: 107%
3	LRRK2 = 89 nM		DRAK2: 59%, NIM1 = 4398 nM, MYLK2 = 1119 nM
5		TBK1 = 149 nM	IKK $\epsilon$ = 1199 nM
11		TBK1 = 187 nM, TRKA = 153 nM	JAK2: 87%, IKK $\epsilon$ = 1314 nM, AURKB: 51%
17		DRAK1 = 325 nM, DRAK2 = 161 nM, AAK1 = 390 nM, SIK2 = 481 nM	MKNK2 = 769 nM, TYK2 = 720 nM, JAK2 > 10000 nM, BMP2K: 56%
19	CSF1R = 91 nM	TYK2 = 276 nM	JAK2: 54%, ERBB2 > 10000 nM, TBK1 = 2737 nM
GSK8612	TBK1 = 37 nM	LRRK2 = 159 nM, MAP2K5: 11%, CSF1R = 264 nM	IKK $\epsilon$ = 552 nM, DAPK3 > 10000 nM, NUAK2 = 1151 nM, ULK3 = 946 nM, MKNK2 = 1369 nM
20	AURKB: 5%	NUAK1 = 176 nM, SIK2 = 185 nM	BMP2K: 58%, DRAK1: 78%, DRAK2: 65%, JAK2: 81%, ACVR1 = 537 nM, BMPR1B = 9028 nM
4	LRRK2 = 19 nM, DRAK2 = 62 nM	IKK $\epsilon$ = 216 nM, DRAK1 = 202 nM, ULK3 = 343 nM, MKNK2 = 380 nM, TBK1 = 192 nM, MAP2K5: 12%	ULK2 = 1742 nM, ULK1: 58%
13	AURKB: 6%, BMP2K = 40 nM, AAK1 = 74 nM, TYK2 = 48 nM, STK16 = 82 nM	TBK1 = 192 nM, JAK2: 12%, BMP2K = 488 nM, TRKA = 283 nM, NUAK1 = 317 nM	NUAK2 = 900 nM, CSNK2A2 = 2269 nM, PIP5K1A > 10000 nM, MKNK2 = 1009 nM
6	TBK1 = 66 nM, JAK2: 3%, BMP2K = 38 nM, STK16 = 88 nM, TYK2 = 67 nM, AURKB: 7%, AAK1 = 80 nM	CSF1R = 192 nM, TRKA = 158 nM, NUAK1 = 171 nM	PRP4 > 10000 nM, PIP5K1A > 10000 nM, CSNK2A2 = 2304 nM, CSNK2A1 > 10000 nM, ULK3 = 1371 nM

<sup>a</sup>Potently active: IC<sub>50</sub> value < 100 nM or < 10% control at 1  $\mu$ M (Table S1). All IC<sub>50</sub> values determined in duplicate. <sup>b</sup>Moderately active: IC<sub>50</sub> value 200–500 nM or 10–49% control at 1  $\mu$ M (Table S1). All IC<sub>50</sub> values determined in duplicate. <sup>c</sup>Weakly active: IC<sub>50</sub> value > 500 nM or > 49% control at 1  $\mu$ M (Table S1). All IC<sub>50</sub> values determined in duplicate.

selectivity profiling shows that all compounds with sub-micromolar IC<sub>50</sub> values in the MARK3/4 NanoBRET assays require further optimization to reduce the number of off-target kinases that are potently inhibited in addition to MARK3/4 ( $S_{10}$  (1  $\mu$ M) = 0.067–0.233). Efforts are ongoing to improve the selectivity of analogs we identified as cell-active in the MARK3/4 NanoBRET assays. The weak cellular potency of **4** for DRAK1 and **14/22** for MARK4 make it difficult to judge the selectivity window offered by these compounds. They should be considered chemical starting points in need of further optimization to improve upon this potency while maintaining or improving kinome-wide selectivity.

**Orthogonal Validation of scanMAX Results.** The scanMAX assay identifies potential targets for our compounds across the kinome. We chose to follow up and validate the scanMAX kinase binding results by further testing of selected actives in enzyme inhibition assays. Our choice of kinases for follow-up varied depending on the selectivity of the compound in question, as measured by  $S_{10}$  (1  $\mu$ M). Highly selective compounds that are also potent on their kinase target have the potential to be chemical probe candidates, and, as such, we chose to execute thorough enzyme profiling to validate or invalidate potential off-targets as well as further quantify potency. Thus, for the five compounds in our library with an  $S_{10}$  (1  $\mu$ M) < 0.002 (**15**, **8**, **12**, **16**, and **21**), we followed-up on all kinases with PoC < 35% at 1  $\mu$ M in the scanMAX platform and/or PoC < 50% in our initial custom enzymatic profiling panel at Eurofins (Table S1). One exception to this was exclusion of AURKA follow-up for **21**. For the six compounds in our library with an  $S_{10}$  (1  $\mu$ M) = 0.005–0.02 (**3**, **5**, **11**, **17**, **19**, and GSK8612), we carried out enzymatic assays on all kinases with PoC < 20% at 1  $\mu$ M in the scanMAX platform and/or PoC < 50% in our initial enzymatic profiling at Eurofins (Table S1). Given our interest in identifying chemical

leads, a few additional understudied kinases with PoC < 35% at 1  $\mu$ M in the scanMAX platform for these six compounds were also selected for follow-up. Lastly, for a final four compounds (**20**, **4**, **13**, and **6**) with  $S_{10}$  (1  $\mu$ M) = 0.022–0.047, we selected only certain kinases with PoC < 20% at 1  $\mu$ M in the scanMAX platform and/or PoC < 50% in our initial profiling at Eurofins (Table S1) for targeted follow-up, with a bias toward kinases that were frequently inhibited by other analogs in the series as well as understudied kinases of interest. All follow-up enzymatic assays were executed at the  $K_m$  = ATP for each respective kinase. Results from these studies combined with the single-concentration enzymatic results from Table S1 are displayed in Table 3. Compounds in Table 3 are listed in order of their kinome-wide selectivity scores from most (**15**) to least (**6**) selective.

In examining the data generated and collected in Table 3, some interesting trends emerge. The most selective compounds ( $S_{10}$  (1  $\mu$ M) < 0.02: **15**, **8**, **12**, **16**, and **21**) that were comprehensively profiled via enzymatic assays potently inhibited 0–1 kinase (potently active, Table 3). We classify the kinases potently inhibited by these compounds as more well-studied. Except for **17** and GSK8612, the same group of most selective compounds ( $S_{10}$  (1  $\mu$ M) < 0.02) inhibited 0–2 kinases with moderate potency (Table 3). Some less selective compounds (**13** and **6**) for which we did selective enzymatic follow-up were found to be potent inhibitors of 5–7 kinases, including members of the understudied NAK family (AAK1, BMP2K, and STK16).<sup>17</sup> Several of the aminopyrimidines tested demonstrated IC<sub>50</sub> values of 200–500 nM or inhibition equal to 10–49% control at 1  $\mu$ M for understudied kinases. Given their kinome-wide selectivity scores and modest potency, these compounds represent potential chemical leads for the development of chemical tools to study these poorly characterized kinases. Many kinases were assigned the weakly

Table 4. Selected NanoBRET Follow-Up

compound	IC <sub>50</sub> values (nM) <sup>a</sup>					
	BMP2K	CSF1R	LRRK2	MYLK2	NUAK1	TYK2
3			>10000			
6	1020				7010	
12		>10000				
13	3000				>10000	
15				3670		
16		>10000				>10000
19		5060				>10000
GSK8612		>10000	>10000			

<sup>a</sup>Compounds tested in singlicate ( $n = 1$ ) in dose–response.

active designation based on weak potency in the respective enzymatic assays. In some cases, such as with compounds **5** and **13**, two kinases that share high structural homology were inhibited with differential potencies. For compound **5**, there is an 8-fold difference in potency for TBK1 and IKK $\epsilon$ , and for compound **13**, there is a nearly 3-fold difference between NUA1 and NUA2.

Importantly, we see that the compounds with submicromolar IC<sub>50</sub> values in the respective NanoBRET assays corresponded with enzymatic inhibition IC<sub>50</sub> values < 250 nM for GSK8612 (TBK1 = 37 nM) and compound **4** (DRAK1 = 202 nM). TBK1, LRRK2, DRAK1/2, CSF1R, TYK2, and TRKA were identified as frequently inhibited kinases by our aminopyrimidine series. This list is comprised of some kinases that pyrimidines are known to potently inhibit (TBK1 and TYK2)<sup>36,37</sup> as well as kinases that represent new targets for optimization. Analysis of the compounds that inhibit these kinases could inform next steps in new chemistry to develop specific SAR for these kinases. Before embarking on next synthetic steps, the narrow selectivity profiles of exemplars within our series coupled with potent enzymatic data motivated interrogation of the cell-based activity of some of these compounds in the respective NanoBRET assays.

**Selective NanoBRET Assay Follow-Up.** For compounds in Table 3 that inhibited kinases with potency < 500 nM, we elected to determine their cellular target engagement via the NanoBRET assay. No more than two kinases were evaluated per compound. Several single digit micromolar inhibitors of specific kinases were identified among these selective aminopyrimidine compounds. Table 4 shows that these compounds were most cell-active in the BMP2K NanoBRET assay. We were excited to identify that weaker inhibition of MYLK2 in the enzymatic assay (IC<sub>50</sub> value = 479 nM) translated to single digit micromolar activity in the MYLK2 NanoBRET assay. Compound **15** potently inhibits the fewest kinases of the compounds that we synthesized (Tables 1 and 3), but demonstrates modest MYLK2 inhibitory potency. Given the paucity of literature around MYLK2 and the distinct lack of compound optimization efforts directed at MYLK2, **15** represents one of the most promising chemical starting points for MYLK2 chemical probe development. The single digit micromolar activity in cells will need to be improved upon via medicinal chemistry optimization to yield analogs with a better selectivity window versus off-target kinases. We also observed that compounds that exhibited potent activity in the LRRK2 enzyme assay (**3** and GSK8612, IC<sub>50</sub> values < 160 nM) and in the TYK2 enzyme assay (**16** and **19**, IC<sub>50</sub> values < 280 nM) did not have any activity in the respective NanoBRET assays when tested at concentrations up to 10  $\mu$ M. The disparity

between our enzymatic potencies and NanoBRET IC<sub>50</sub> values prompted us to further investigate compound properties that might impact cell permeability.

**Assessment of Compound Properties.** With exceptions, we observed > 30–300-fold losses in potency when considering enzymatic versus NanoBRET activities. This was true for NanoBRET values reported both in Tables 2 and 4. A < 10-fold loss in potency was only observed in four cases: GSK8612 for TBK1, **15** for MYLK2, and **4** and **17** for DRAK1. The overall trend of biochemical activity not translating to cellular potency made us curious about the physicochemical properties of our aminopyrimidines. To address this, we evaluated the kinetic solubility and permeability (PAMPA) of our library of compounds and included the parent compounds as well (Table 5).

Results in Table 5 demonstrated that our compounds were generally very soluble. With the exception of **5**, **6**, **7**, **11**, **13**, **16**, **18**, and **21**, the measured solubility was estimated to be > 75% of the dose concentration, and thus the actual solubility may be higher than Table 5 reflects. As nearly all compounds

Table 5. Kinetic Solubility and PAMPA Assay Results

compound	kinetic solubility ( $\mu$ M)	P <sub>e</sub> (cm/s)
3	171.0	3.89 $\times 10^{-7}$
4	190.1	5.08 $\times 10^{-6}$
5	33.2	<LOQ <sup>a</sup>
6	4.7	<LOQ <sup>a</sup>
7	40.3	3.73 $\times 10^{-6}$
8	174.6	2.39 $\times 10^{-6}$
9	159.0	1.30 $\times 10^{-6}$
10	195.2	1.51 $\times 10^{-6}$
11	118.7	7.09 $\times 10^{-7}$
12	167.7	<LOQ <sup>a</sup>
13	20.0	<LOQ <sup>a</sup>
14	173.6	5.61 $\times 10^{-7}$
15	176.9	6.23 $\times 10^{-8}$
16	147.0	<LOQ <sup>a</sup>
17	169.3	8.24 $\times 10^{-8}$
18	135.6	8.85 $\times 10^{-7}$
19	176.5	4.56 $\times 10^{-7}$
20	199.7	1.66 $\times 10^{-7}$
21	85.6	2.60 $\times 10^{-6}$
22	164.0	5.97 $\times 10^{-7}$
MRT67307	164.6	2.60 $\times 10^{-6}$
BX-912	155.5	1.39 $\times 10^{-7}$
GSK8612	173.1	<LOQ <sup>a</sup>

<sup>a</sup><LOQ: Below limit of quantitation.

demonstrated solubility > 10  $\mu\text{M}$ , they were not considered poorly soluble, and this was eliminated from consideration as driving their poor cellular potency. The permeability data, however, were a bit more varied for this aminopyrimidine library. Six compounds (**5**, **6**, **12**, **13**, **16**, and GSK8612) were below the limit of quantitation (LOQ) and/or precipitated in the assay media, making it impossible to determine their permeability. Several of these compounds were among the analogs with the lowest kinetic solubility concentrations as well. For reference,  $P_e$  (permeability coefficient) values <  $1.50 \times 10^{-6}$  cm/s correlate with the human fraction absorbed < 80% and is a generally accepted cutoff for low permeability. In addition to the compounds already mentioned that were below the LOQ, this cutoff adds the majority of our library as well as some parent compounds to a low permeability category: **3**, **9**, **11**, **14**, **15**, **17–20**, **22**, and BX-912.

If we start to consider which structural elements could be compromising the solubility and/or permeability of our compounds, some trends emerge. The sulfonamide side chain is present in most of the least soluble compounds (**5**, **6**, **11**, **13**, **16**, and **21**) and all poorly permeable compounds (**5**, **6**, **12**, **13**, **16**, and GSK8612). As compounds with suboptimal solubility (**7**) or poor permeability (GSK8612) still proved active in our NanoBRET assays, just looking at half of the data is not sufficient. None of the compounds with both problematic solubility and permeability (**5**, **6**, **13**, and **16**) were active in our NanoBRET assays, leading us to conclude that these two factors together point to compounds that are poorly cell permeable. Since the majority of compounds did not fall into this final category, consideration of physicochemical properties did not explain our cell-based results.

It is worth noting for compounds/kinases where enzymatic data has been published, the control compounds used in the NanoBRET assays can be considered as a benchmark. For CSF1R, dasatinib has a published enzymatic  $\text{IC}_{50} = 0.57$  nM, and we determined its NanoBRET  $\text{IC}_{50}$  to be 18.3 nM. For NUA1, BX-795 has a published  $\text{IC}_{50} = 5$  nM, and we determined its NanoBRET  $\text{IC}_{50}$  to be 187 nM.<sup>19</sup> In both cases, single digit or subnanomolar enzymatic  $\text{IC}_{50}$  values translated to submicromolar NanoBRET  $\text{IC}_{50}$  values, and a  $\sim 34$ -fold loss in potency was observed when moving to the cell-based assay. While not universal, it appears that for this set of compounds and kinase targets, exceptional enzymatic potency is key to achieving cellular potency to overcome the more than 30-fold drop-off in cellular potency.

**Structural Studies and Lead Optimization Plan for MARK Subfamily.** The MARK3 cocrystal structure with **9** corroborates the high affinity that this compound demonstrates in the MARK3 NanoBRET assay (Table 2). Figure 3 shows that the activation segment of MARK3 folds back and packs against compound **9** via residue V205, while maintaining a DFG-in conformation. Several key hydrogen bonds are made between **9** and the binding pocket. In addition, several hydrogen bonds are present between the binding pocket and the 2- and 4-position side chains of **9**. The imidazole nitrogen(s) can interact with the main chain carbonyl of I62 in the G-rich loop as well as E182 in the catalytic loop and E139 in the  $\alpha\text{D}$  helix. It has also been suggested that, although weak, C–H–O hydrogen bonds can exist.<sup>38</sup> While inhibitor conformations have been synchronized, the free rotation of the 4-position side chain allows the imidazole to rotate, which perturbs some of these interactions. These hydrogen bonds, therefore, do not simultaneously coexist, but rather different

hydrogen-bond patterns emerge due to free rotation of the imidazole ring. With respect to the 2-position side chain, K60 (not shown) is at a distance of 3.4 Å and Y134 is at a distance of 3.2 Å from the morpholine ring. Since the morpholine ring is highly flexible, these distances represent the proximity of the mentioned residues to the ring rather than to a particular atom within it. Unsupported geometries as well as the flexibilities of both residues and the morpholine ring, however, suggest that K60 and Y134 do not form strong hydrogen bonds with the morpholine ring. A weak and likely transient interaction between Y134 and the morpholine ring on **9** is shown in the Figure 3 pose. Essential interactions are made between the 3-position nitrogen of the pyrimidine core and 2-position NH with A135 in the MARK3 hinge. Importantly, the 5-position bromo is oriented such that it makes an interaction with the sulfur within gatekeeper residue M132.

It is interesting to consider this cocrystal structure versus those solved for MRT67307 with TBK1 (PDB codes: 4IM0 and 4IWQ) and ULK2 (PDB code: 6QAU), and BX-320, a close structural analog of BX-912, with PDK1 (PDB code: 1Z5M).<sup>23,39,40</sup> The gatekeeper in TBK1 and ULK2, like in MARK3, is a methionine (M86 in TBK1 and M85 in ULK2), while in PDK1 the gatekeeper is a leucine (L86).<sup>23,39,40</sup> The proximity of the cyclopropyl group in MRT67307 or bromine in BX-320 to the gatekeeper residue varies, supporting this position influences binding preference and excludes molecules that bear a group that is too large at the 5-position of the pyrimidine ring. Furthermore, the discussion around M85 in ULK2 noted some flexibility of this residue, suggesting a certain degree of plasticity of the back pocket when accommodating bulky hydrophobic residues such as the cyclopropyl group in MRT67307.<sup>40</sup> Hinge-binding interactions are maintained in all cases between the pyrimidine nitrogen at position 1 and the amino side chain NH at position 2, supporting that this essential part of the molecule cannot be modified without substantial losses in binding affinity. When MRT67307 binds to ULK2, the pendant morpholine on the 2-position side chain makes hydrogen-bonding interactions via a water molecule with D95 of ULK2.<sup>40</sup> The morpholine is not shown to hydrogen bond in TBK1 structures with MRT67307, which could partially explain the loss of affinity of **9** for TBK1 (Table 2) and potent binding of **9** to ULK2 (Figure S1).<sup>39</sup> Although the interactions between the morpholine ring and K60/Y134 of MARK3 are weak, these residues may be key in the development of more specific MARK3 binders. If the flexibilities of this 2-position side chain and/or morpholine ring are reduced, it may allow for formation of stronger hydrogen bonds and increase MARK3 binding affinity.

Also, in comparing the structure of **9** bound to MARK3 versus both the ULK2 and TBK1 structures with MRT67307, we observe that the binding mode of **9** induced a “folded” conformation of the activation segment that partially protrudes into the ATP binding pocket. Comparison of the various cocrystal structures suggests that this could be due to a more compact structure of **9**, in which the 2-position imidazole stacks onto the 4-position phenyl ring. MRT67307, in comparison, adopts a more elongated binding conformation that likely prevents this “folded” conformation. Six compounds from our library have the 4-position imidazole side chain: **3**, **9**, **10**, **14**, **15**, and **20**. Of these, only **9** and **14** demonstrate submicromolar affinity for MARK3 and/or MARK4 in the corresponding NanoBRET assays. In addition to the 2-position imidazole, both **9** and **14** share the 4-position phenyl ring in



their structures. It is possible that the 2-position imidazole cannot efficiently stack with the 4-position pyrazole shared by **3**, **10**, and **15** to allow for binding in the MARK3 pocket created when the activation segment folds. This unique compact binding mode that seems to be tied to inhibitor side chain substituents should be considered in future design efforts.

If we examine and compare the residues that line or surround the active sites of these kinases (TBK1, ULK2, and PDK1) versus some of our understudied kinases of interest (DRAK1, MARK3/4, and BMP2K; Figure 4), we observe that

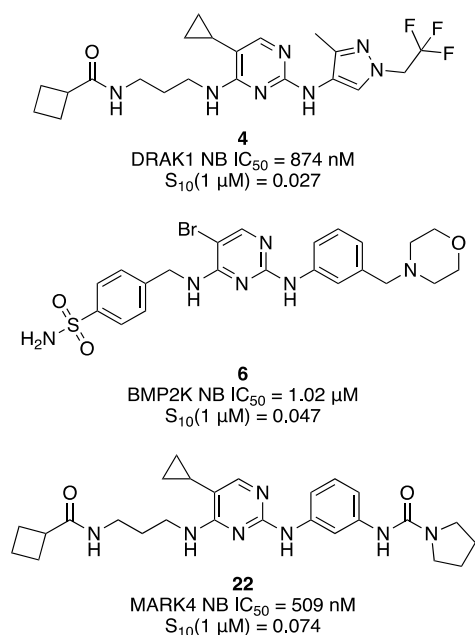


Figure 4. Promising chemical leads for understudied kinases.

the gatekeeper is either a methionine or leucine in all cases (gatekeeper, Figure S2). The key hinge-binding residue in all these kinases is maintained as either a cysteine or alanine (hinge donor and outer hydrogen-bond acceptor, Figure S2). Finally, the morpholine-anchoring residue is coming from the  $\alpha D$  helix in ULK2 rather than the conserved hinge tyrosine (hinge, Figure S2) utilized to anchor the morpholine in our MARK3 structure, supporting that this residue may be key to the design of MARK-family specific molecules.

Using the MARK3 cocrystal structure as our guide, we will build on the subfamily selectivity observed for compounds **14** and **22** versus **9** and **18**. Given that the 5-position of these compounds seems to dictate both subfamily and kinome-wide selectivity, we hypothesize that further exploration of this position is warranted. Y134 within the hinge of MARK family members is not maintained by all kinases, and thus adding interactions with this residue may impart additional selectivity through precluding binding with other kinases where it is another residue (phenylalanine in TBK1, for example). We aim to use these learnings to develop chemical tools that demonstrate specificity within the MARK family in addition to improved kinome-wide selectivity.

## CONCLUSIONS

In summary, we provide details related to the synthesis and extensive biological evaluation of a library of aminopyrimidines. We have shown that selectivity can be built into the

pyrimidine scaffold through design. Several cell-active compounds were discovered that exhibit submicromolar NanoBRET cellular target engagement  $IC_{50}$  values against kinases including TBK1, DRAK1, MARK3, and MARK4. Three of these kinases (DRAK1, MARK3, and MARK4) are understudied, IDG kinases that need high-quality chemical tools to be able to characterize their function. Examples of compounds with sub- or nearly submicromolar activities for understudied kinases and modest kinome-wide selectivity are included in Figure 4. These aminopyrimidines represent promising chemical starting points in our campaign to identify chemical probes to enable elucidation of the biological function(s) of lesser studied kinases. The cellular potency of these compounds will need to be improved via chemical optimization to furnish compounds more suitable for interrogating the biology of these understudied kinases. The aminopyrimidine represents an alternative chemotype to our recently disclosed AAK1/BMP2K chemical probe and, as such, inhibits a different panel of off-target kinases.<sup>17,18</sup> Development of this chemotype is expected to yield a chemical probe with a different kinome-wide inhibition profile and thus slightly different biological activities. Results here reiterate the need to employ orthogonal biochemical and cell-based assays to understand the actual selectivity and potency of kinase inhibitors more fully. The methods described herein offer a path for others to identify and develop high-quality inhibitors for understudied kinases to facilitate illumination of the entire druggable kinome.

## EXPERIMENTAL SECTION

**Chemistry. General Information.** Reagents were purchased from commercial suppliers and used without further characterization or purification. Temperatures are given in degrees Celsius ( $^{\circ}C$ ), and unless otherwise stated, operations were carried out at room or ambient temperature (r.t.), typically around  $25^{\circ}C$ . Evaporation of solvent was carried out using a rotary evaporator under reduced pressure with a bath temperature not exceeding  $60^{\circ}C$ . Thin-layer chromatography (TLC) was used to follow the course of reactions. Intermediates and products exhibited satisfactory  $^1H$  NMR and/or microanalytical data. The following conventional abbreviations are also used: equivalents (equiv), mmol (millimoles), mg (milligrams), and h (hours). Reactions were carried out under a blanket of nitrogen unless otherwise stated. Compounds were visualized using a UV (ultraviolet) lamp (254 nm).  $^1H$  and  $^{13}C$  NMR spectra were collected in DMSO- $d_6$ , acetonitrile- $d_4$ , chloroform- $d$ , or methanol- $d_4$  and recorded on Varian Inova 400 Megahertz (MHz), Bruker DRX 500 MHz, Bruker Avance III 400 MHz, Varian VNMRs 500 MHz, or Agilent ProPulse 600 MHz spectrometers, noting the magnet strength in all cases. Peak positions are given in parts per million (ppm) and calibrated based upon the shift of the indicated solvent. Coupling constants ( $J$  values) are expressed in hertz (Hz), and multiplicities are reported as follows: singlet (s), doublet (d), doublet(s) of doublets (dd/ddd) or triplets (dt) or quartets (dq), triplet (t), triplet(s) of doublets (td/ttd), quartet (q), pentet (p), pentet of doublets (pd), heptet (h), and multiplet (m). An asterisk (\*) was added after the line listing of spectral data for compounds where a single peak could not be unambiguously assigned in the  $^{13}C$  spectrum. Double asterisks (\*\*) were added after the line listing of spectral data for compounds where a single peak as part of a multiplet could not be unambiguously assigned in the  $^{13}C$  spectrum. Purity was assessed via LC-MS using an Agilent mass spectrometer (column: Agilent Poroshell 120 SB-C18, 4.6 mm  $\times$  30 mm, 2.7  $\mu m$  with UHPLC Guard Infinity Lab Poroshell 120 SB-C18, 4.6 mm  $\times$  5 mm, 2.7  $\mu m$ ). Syntheses of key intermediates and several final products were performed by ChemSpace LLC. Identity and purity of all final products were confirmed upon arrival.

**General Procedure for the Synthesis of Compound B: Procedure A.** To a solution of compound **1** (1 equiv) in ethanol (10–20 mL) were added dropwise DIPEA (2 mL) and amine **1** (1 equiv) at  $-10^{\circ}\text{C}$ . The resulting mixture was heated to r.t. then stirred at  $50^{\circ}\text{C}$  for 16 h. Solvent was next evaporated from the reaction mixture and to the resulting material was added water (30 mL). The obtained precipitate was filtered, washed with water, isopropanol, and hexane, and dried under vacuum at  $50^{\circ}\text{C}$  to give compounds **2a–2g** (amount, yield, purity), which were used in the next step without further purification.

*N*-(3-((2-Chloropyrimidin-4-yl)amino)propyl)cyclobutanecarboxamide (**2a**). 330 mg, 50% yield, 95% purity by LC–MS.

*N*-(3-((5-Bromo-2-chloropyrimidin-4-yl)amino)propyl)cyclobutanecarboxamide (**2b**). 2.20 g, 50% yield, 95% purity by LC–MS.

*N*-(3-((2-Chloro-5-cyclopropylpyrimidin-4-yl)amino)propyl)cyclobutanecarboxamide (**2c**). 570 mg, 67% yield, 95% purity by LC–MS.

4-(((5-Bromo-2-chloropyrimidin-4-yl)amino)methyl)benzenesulfonamide (**2d**). 6.40 g, 55% yield, 95% purity by LC–MS.

4-(((2-Chloro-5-cyclopropylpyrimidin-4-yl)amino)methyl)benzenesulfonamide (**2e**). 850 mg, 50% yield, 95% purity by LC–MS.

*N*-(2-(1*H*-Imidazol-4-yl)ethyl)-5-bromo-2-chloropyrimidin-4-amine (**2f**). 2.50 g, 25% yield, 95% purity by LC–MS.

*N*-(2-(1*H*-Imidazol-4-yl)ethyl)-2-chloro-5-cyclopropylpyrimidin-4-amine (**2g**). 420 mg, 50% yield, 95% purity by LC–MS.

**General Procedure for the Synthesis of Compounds 3–11, 13, 14, 17, 18, 21, 22, and GSK8612: Procedure B.** To a solution of compound **2** (1 equiv) and amine **2** (1 equiv) in butanol (2–5 mL) was added dioxane  $\times$  HCl (10%w/w) (0.5–2 mL), and the resulting mixture was stirred at  $80^{\circ}\text{C}$  for 16 h. The reaction mixture was next neutralized with aqueous ammonia and concentrated under vacuum. The resulting material was purified by preparative HPLC (2–7 min, 35–70% methanol (0.1% ammonium hydroxide), 30 mL/min; column: YMC-ACTUS TRIART C18, 20 mm  $\times$  100 mm, 5  $\mu\text{m}$ ) to give final compounds **3–11, 13, 14, 17, 18, 21, 22**, and GSK8612 (amount, yield).

*N*<sup>4</sup>-(2-(1*H*-Imidazol-4-yl)ethyl)-5-cyclopropyl-*N*<sup>2</sup>-(3-methyl-1-(2,2,2-trifluoroethyl)-1*H*-pyrazol-4-yl)pyrimidine-2,4-diamine (**3**). 71.0 mg, 36% yield. <sup>1</sup>H NMR (400 MHz, DMSO-*d*<sub>6</sub>)  $\delta$  11.86 (s, 1H), 8.11 (s, 2H), 7.56 (s, 2H), 6.84 (d, *J* = 16.5 Hz, 2H), 5.02–4.91 (m, 2H), 3.63 (q, *J* = 6.8 Hz, 2H), 2.81 (t, *J* = 7.4 Hz, 2H), 2.16 (s, 3H), 1.41 (td, *J* = 10.7, 8.6, 5.9 Hz, 1H), 0.78 (d, *J* = 8.0 Hz, 2H), 0.40 (t, *J* = 5.1 Hz, 2H). <sup>13</sup>C NMR (151 MHz, acetonitrile-*d*<sub>3</sub>)  $\delta$  160.51, 156.33, 150.93, 138.16, 134.55\*, 132.59, 121.60\*\* (q, *J* = 280.0 Hz), 120.39, 120.11, 113.02\*, 107.40, 49.73 (q, *J* = 33.9 Hz), 38.56, 24.68, 8.17, 5.05, 1.84. HPLC purity: 95.0%. HRMS (ESI) ([M + H]<sup>+</sup>) Calcd for C<sub>18</sub>H<sub>23</sub>F<sub>3</sub>N<sub>5</sub>: 407.1920, found: 407.1918.

*N*-(3-((5-Cyclopropyl-2-((3-methyl-1-(2,2,2-trifluoroethyl)-1*H*-pyrazol-4-yl)amino)pyrimidin-4-yl)amino)propyl)cyclobutanecarboxamide (**4**). 57.0 mg, 11% yield. <sup>1</sup>H NMR (400 MHz, chloroform-*d*)  $\delta$  8.01 (s, 1H), 7.70 (s, 1H), 6.21 (s, 1H), 5.94 (s, 1H), 5.59 (s, 1H), 4.62 (q, *J* = 8.5 Hz, 2H), 3.53 (q, *J* = 5.9 Hz, 2H), 3.36 (q, *J* = 6.3 Hz, 2H), 2.96 (p, *J* = 8.2 Hz, 1H), 2.31–2.19 (m, 5H), 2.18–2.10 (m, 2H), 2.03–1.82 (m, 2H), 1.77 (p, *J* = 6.7 Hz, 2H), 1.51–1.40 (m, 1H), 1.25 (s, 1H), 0.91 (dq, *J* = 5.7, 3.9 Hz, 2H), 0.53–0.45 (m, 2H). <sup>13</sup>C NMR (101 MHz, chloroform-*d*)  $\delta$  175.72, 162.75, 157.86, 152.71, 140.54, 123.13 (q, *J* = 280 Hz), 122.38, 121.92, 110.04, 52.97 (q, *J* = 34.7 Hz), 39.91, 37.24, 36.04, 29.84, 25.43, 18.09, 10.99, 7.41, 4.56. HPLC purity: 100%. HRMS (ESI) ([M + H]<sup>+</sup>) Calcd for C<sub>21</sub>H<sub>29</sub>F<sub>3</sub>N<sub>5</sub>O: 452.2386, found: 452.2385.

4-(((5-Cyclopropyl-2-((3-methyl-1-(2,2,2-trifluoroethyl)-1*H*-pyrazol-4-yl)amino)pyrimidin-4-yl)amino)methyl)benzenesulfonamide (**5**). 74.0 mg, 15% yield. <sup>1</sup>H NMR (400 MHz, DMSO-*d*<sub>6</sub>)  $\delta$  8.01 (s, 1H), 7.79–7.70 (m, 3H), 7.59 (s, 1H), 7.46 (d, *J* = 8.0 Hz, 2H), 7.38–7.33 (m, 1H), 7.26 (s, 2H), 4.87 (q, *J* = 9.2 Hz, 2H), 4.68 (d, *J* = 6.1 Hz, 2H), 2.08 (s, 3H), 1.52 (s, 1H), 0.83 (d, *J* = 8.0 Hz, 2H), 0.48 (d, *J* = 5.0 Hz, 2H). <sup>13</sup>C NMR (151 MHz, acetonitrile-*d*<sub>3</sub>)  $\delta$  160.37, 156.47, 151.51, 143.05, 139.49, 138.98, 125.27, 123.81, 123.0

(q, *J* = 279 Hz), 120.72, 119.89, 107.57, 49.90 (q, *J* = 34.0 Hz), 41.03, 8.12, 5.08, 1.98. HPLC purity: 100%. HRMS (ESI) ([M + H]<sup>+</sup>) Calcd for C<sub>20</sub>H<sub>23</sub>F<sub>3</sub>N<sub>7</sub>O<sub>2</sub>S: 482.1588, found: 482.1582.

4-(((5-Bromo-2-((3-(morpholinomethyl)phenyl)amino)pyrimidin-4-yl)amino)methyl)benzenesulfonamide (**6**). 128 mg, 24% yield. <sup>1</sup>H NMR (400 MHz, DMSO-*d*<sub>6</sub>)  $\delta$  9.19 (s, 1H), 8.06 (s, 1H), 7.73 (dd, *J* = 15.3, 7.0 Hz, 4H), 7.60 (s, 1H), 7.50 (d, *J* = 8.0 Hz, 2H), 7.43 (d, *J* = 8.2 Hz, 1H), 7.26 (s, 2H), 7.10 (t, *J* = 7.8 Hz, 1H), 6.81 (d, *J* = 7.4 Hz, 1H), 4.70 (d, *J* = 6.1 Hz, 2H), 3.52 (d, *J* = 4.8 Hz, 4H), 3.17 (d, *J* = 5.2 Hz, 2H), 2.28 (s, 4H). <sup>13</sup>C NMR (126 MHz, acetonitrile-*d*<sub>3</sub>)  $\delta$  158.62, 156.44, 145.33\*, 144.50, 141.96\*, 140.19, 133.48, 128.40, 127.58, 126.11, 122.70, 121.44, 119.72, 93.03\*, 66.46, 62.67, 60.58, 53.36, 43.67, 24.26\*. HPLC purity: 98.4%. HRMS (ESI) ([M + H]<sup>+</sup>) Calcd for C<sub>22</sub>H<sub>26</sub>BrN<sub>6</sub>O<sub>3</sub>S: 533.0970, found: 533.0955.

*N*-(3-((5-Bromo-2-((3-methyl-1-(2,2,2-trifluoroethyl)-1*H*-pyrazol-4-yl)amino)pyrimidin-4-yl)amino)propyl)cyclobutanecarboxamide (**7**). 83.0 mg, 17% yield. <sup>1</sup>H NMR (400 MHz, chloroform-*d*)  $\delta$  7.95 (s, 2H), 6.34 (s, 1H), 6.04–5.99 (m, 1H), 5.58–5.53 (m, 1H), 4.64 (q, *J* = 8.5 Hz, 2H), 3.49 (q, *J* = 6.2 Hz, 2H), 3.35 (q, *J* = 6.4 Hz, 2H), 2.98 (p, *J* = 8.5 Hz, 1H), 2.33–2.20 (m, 5H), 2.19–2.08 (m, 2H), 2.04–1.80 (m, 2H), 1.76 (p, *J* = 6.3 Hz, 2H). <sup>13</sup>C NMR (151 MHz, acetonitrile-*d*<sub>3</sub>)  $\delta$  173.06, 156.65, 156.48, 153.76, 138.90, 121.50\*\* (q, *J* = 279.8), 120.99, 119.51, 119.43, 49.88 (q, *J* = 34.2 Hz), 37.32, 35.47, 33.62, 26.93, 22.78, 15.55, 8.19. HPLC purity: 97.8%. HRMS (ESI) ([M + H]<sup>+</sup>) Calcd for C<sub>18</sub>H<sub>24</sub>BrF<sub>3</sub>N<sub>7</sub>O: 490.1178, found: 490.1176.

*N*-(3-((2-((3-Methyl-1-(2,2,2-trifluoroethyl)-1*H*-pyrazol-4-yl)amino)pyrimidin-4-yl)amino)propyl)cyclobutanecarboxamide (**8**). 75.0 mg, 15% yield. <sup>1</sup>H NMR (400 MHz, chloroform-*d*)  $\delta$  7.98 (s, 1H), 7.83 (d, *J* = 5.9 Hz, 1H), 6.33 (s, 1H), 5.82 (d, *J* = 5.6 Hz, 1H), 5.56 (s, 2H), 4.59 (q, *J* = 8.5 Hz, 2H), 3.41–3.25 (m, 4H), 2.95 (p, *J* = 8.6 Hz, 1H), 2.31–2.18 (m, 5H), 2.13 (q, *J* = 9.1, 8.3 Hz, 2H), 2.01–1.79 (m, 3H), 1.72 (p, *J* = 6.3 Hz, 2H). <sup>13</sup>C NMR (151 MHz, acetonitrile-*d*<sub>3</sub>)  $\delta$  172.67, 161.10, 157.78, 153.04\*, 138.64\*, 125.45\*, 121.63\*\* (q, *J* = 280), 120.78, 119.87, 118.98, 49.87 (q, *J* = 34.0 Hz), 37.31, 33.92, 26.98, 22.74, 15.56, 8.19. HPLC purity: 100%. HRMS (ESI) ([M + H]<sup>+</sup>) Calcd for C<sub>18</sub>H<sub>23</sub>F<sub>3</sub>N<sub>7</sub>O: 412.2073, found: 412.2069.

*N*<sup>4</sup>-(2-(1*H*-Imidazol-4-yl)ethyl)-5-bromo-*N*<sup>2</sup>-(3-(morpholinomethyl)phenyl)pyrimidine-2,4-diamine (**9**). 190 mg, 11% yield. <sup>1</sup>H NMR (400 MHz, DMSO-*d*<sub>6</sub>)  $\delta$  11.83 (s, 1H), 9.21 (s, 1H), 8.01 (s, 1H), 7.75 (s, 1H), 7.63–7.54 (m, 2H), 7.14 (t, *J* = 7.8 Hz, 2H), 6.83 (d, *J* = 7.5 Hz, 2H), 3.68 (q, *J* = 6.9 Hz, 2H), 3.54 (t, *J* = 4.6 Hz, 4H), 3.31 (s, 2H), 2.87–2.78 (m, 2H), 2.29 (s, 4H). <sup>13</sup>C NMR (101 MHz, methanol-*d*<sub>4</sub>)  $\delta$  163.42\*, 158.65, 158.56, 155.08, 140.37, 137.30, 134.65, 128.08, 122.67, 120.21, 118.15, 116.24\*, 92.60, 66.28, 63.13, 53.22, 40.58, 26.34. HPLC purity: 95.9%. HRMS (ESI) ([M + H]<sup>+</sup>) Calcd for C<sub>20</sub>H<sub>25</sub>BrN<sub>7</sub>O: 458.1304, found: 458.1300.

*N*<sup>4</sup>-(2-(1*H*-Imidazol-5-yl)ethyl)-5-bromo-*N*<sup>2</sup>-(3-methyl-1-(2,2,2-trifluoroethyl)-1*H*-pyrazol-4-yl)pyrimidine-2,4-diamine (**10**). 325 mg, 17% yield. <sup>1</sup>H NMR (400 MHz, DMSO-*d*<sub>6</sub>)  $\delta$  11.84 (s, 1H), 8.55 (s, 1H), 8.09 (s, 1H), 7.95 (s, 1H), 7.55 (s, 1H), 7.08 (s, 1H), 6.87 (s, 1H), 4.98 (s, 2H), 3.60 (q, *J* = 6.9, 6.5 Hz, 2H), 2.78 (t, *J* = 7.1 Hz, 2H), 2.16 (s, 3H). <sup>13</sup>C NMR (151 MHz, acetonitrile-*d*<sub>3</sub>)  $\delta$  156.58, 156.46, 153.77, 144.88\*, 143.51\*, 138.62, 132.63, 121.54 (q, *J* = 279.9 Hz), 120.99, 120.99, 119.43, 117.93, 49.74 (q, *J* = 34.1 Hz), 38.91, 24.47, 8.21. HPLC purity: 96.6%. HRMS (ESI) ([M + H]<sup>+</sup>) Calcd for C<sub>15</sub>H<sub>17</sub>BrF<sub>3</sub>N<sub>5</sub>: 445.0712, found: 445.0709.

4-(((5-Cyclopropyl-2-((3-(morpholinomethyl)phenyl)amino)pyrimidin-4-yl)amino)methyl)benzenesulfonamide (**11**). 18.0 mg, 4% yield. <sup>1</sup>H NMR (400 MHz, DMSO-*d*<sub>6</sub>)  $\delta$  8.83 (s, 1H), 7.75 (d, *J* = 8.1 Hz, 2H), 7.66 (s, 2H), 7.52 (d, *J* = 8.0 Hz, 2H), 7.50–7.42 (m, 3H), 7.25 (s, 2H), 7.06 (t, *J* = 7.9 Hz, 1H), 6.75 (d, *J* = 7.7 Hz, 1H), 4.75 (d, *J* = 5.9 Hz, 2H), 3.57–3.50 (m, 5H), 3.17 (d, *J* = 5.5 Hz, 2H), 2.32–2.25 (m, 4H), 1.61–1.50 (m, 1H), 0.88–0.83 (m, 2H), 0.52 (d, *J* = 4.7 Hz, 2H). <sup>13</sup>C NMR (101 MHz, methanol-*d*<sub>4</sub>)  $\delta$  162.60, 158.31, 152.19, 144.97, 142.02, 140.52, 137.00, 128.03, 127.12, 125.89, 122.35, 120.11, 118.04, 110.30, 66.24, 63.12, 53.13,



43.32, 39.00, 7.14, 3.92. HPLC purity: 100%. HRMS (ESI) ( $[M + H]^+$ ) Calcd for  $C_{25}H_{31}N_6O_3S$ :495.2178, found: 495.2162.

*N*-(3-((5-Bromo-4-((4-sulfamoylbenzyl)amino)pyrimidin-2-yl)amino)phenyl)pyrrolidine-1-carboxamide (**13**). 383 mg, 5% yield.  $^1H$  NMR (500 MHz, methanol- $d_4$ )  $\delta$  7.95 (d,  $J = 2.2$  Hz, 1H), 7.80 (dd,  $J = 8.4, 2.2$  Hz, 2H), 7.71 (d,  $J = 2.4$  Hz, 1H), 7.49–7.43 (m, 2H), 7.08 (dt,  $J = 4.6, 1.8$  Hz, 2H), 6.95 (td,  $J = 4.3, 1.8$  Hz, 1H), 4.77 (d,  $J = 2.0$  Hz, 2H), 3.42 (dt,  $J = 6.8, 3.5$  Hz, 4H), 1.94 (h,  $J = 2.5$  Hz, 4H).  $^{13}C$  NMR (101 MHz, methanol- $d_4$ )  $\delta$  158.61, 156.19, 155.36, 153.60, 144.23, 141.95, 140.23, 139.55, 128.02, 127.27, 125.75, 114.94, 114.62, 112.77, 92.26, 45.57, 43.56, 25.01. HPLC purity: 92.6%. HRMS (ESI) ( $[M + H]^+$ ) Calcd for  $C_{22}H_{23}BrN_7O_3S$ :546.0923, found: 546.0914.

*N*<sup>4</sup>-(2-(1*H*-imidazol-4-yl)ethyl)-5-cyclopropyl-*N*<sup>2</sup>-(3-(morpholinomethyl)phenyl)pyrimidine-2,4-diamine (**14**). 73.0 mg, 24% yield.  $^1H$  NMR (400 MHz, DMSO- $d_6$ )  $\delta$  11.82 (s, 1H), 8.85 (s, 1H), 7.81 (s, 1H), 7.64–7.54 (m, 3H), 7.11 (t,  $J = 7.8$  Hz, 1H), 6.90–6.81 (m, 2H), 6.77 (d,  $J = 7.5$  Hz, 1H), 3.69 (q,  $J = 6.7$  Hz, 2H), 3.54 (t,  $J = 4.6$  Hz, 4H), 3.30–3.20 (m, 1H), 3.17 (d,  $J = 3.9$  Hz, 1H), 2.85 (t,  $J = 7.2$  Hz, 2H), 2.29 (d,  $J = 4.8$  Hz, 4H), 1.44 (q,  $J = 4.8, 2.9$  Hz, 1H), 0.79 (dt,  $J = 8.3, 3.1$  Hz, 2H), 0.51–0.38 (m, 2H).  $^{13}C$  NMR (151 MHz, acetonitrile- $d_3$ )  $\delta$  160.24, 156.35, 150.71, 139.02, 136.45, 132.53, 126.05, 119.42, 116.81, 115.42, 114.90, 108.19, 64.35, 60.97, 51.28, 38.46, 24.40, 5.12, 1.85. HPLC purity: 100%. HRMS (ESI) ( $[M + H]^+$ ) Calcd for  $C_{23}H_{30}N_7O$ :420.2512, found: 420.2506.

*N*-(3-((4-(3-(Cyclobutanecarboxamido)propyl)amino)pyrimidin-2-yl)amino)phenyl)pyrrolidine-1-carboxamide (**17**). 19.0 mg, 10% yield.  $^1H$  NMR (400 MHz, chloroform- $d$ )  $\delta$  7.94 (s, 1H), 7.82 (s, 1H), 7.24 (s, 1H), 7.22–7.03 (m, 3H), 6.95 (d,  $J = 8.2$  Hz, 1H), 6.13 (s, 2H), 5.80 (d,  $J = 6.5$  Hz, 1H), 5.56 (s, 1H), 3.41 (m, 6H), 3.26 (m, 2H), 2.95–2.78 (m, 1H), 2.19 (d,  $J = 9.8$  Hz, 2H), 2.07–1.89 (m, 9H), 1.68 (d,  $J = 6.7$  Hz, 1H).  $^{13}C$  NMR (101 MHz, DMSO- $d_6$ )  $\delta$  174.29, 162.95, 160.25, 154.80, 154.49, 141.70, 140.83, 128.16, 113.36, 113.15, 111.41, 98.08, 55.31, 46.08, 39.17, 36.78, 29.55, 25.47, 25.11, 18.22. HPLC purity: 100%. HRMS (ESI) ( $[M + H]^+$ ) Calcd for  $C_{23}H_{32}N_7O_2$ : 438.2617, found: 438.2617.

*N*-(3-((5-Bromo-4-((3-(cyclobutanecarboxamido)propyl)amino)pyrimidin-2-yl)amino)phenyl)pyrrolidine-1-carboxamide (**18**). 335 mg, 13% yield.  $^1H$  NMR (400 MHz, DMSO- $d_6$ )  $\delta$  9.07 (s, 1H), 7.97 (s, 1H), 7.87 (t,  $J = 2.1$  Hz, 1H), 7.62 (t,  $J = 5.4$  Hz, 1H), 7.25 (d,  $J = 8.1$  Hz, 1H), 7.06 (t,  $J = 8.0$  Hz, 1H), 7.00–6.91 (m, 2H), 3.42 (q,  $J = 6.6$  Hz, 2H), 3.33 (d,  $J = 6.4$  Hz, 4H), 3.07 (q,  $J = 6.5$  Hz, 2H), 2.93 (p,  $J = 8.4$  Hz, 1H), 2.14–2.02 (m, 4H), 1.96 (q,  $J = 9.8$  Hz, 2H), 1.90–1.79 (m, 4H), 1.78–1.60 (m, 3H).  $^{13}C$  NMR (101 MHz, methanol- $d_4$ )  $\delta$  176.54, 158.67, 158.61, 155.60, 155.03, 140.53, 139.71, 128.13, 114.73, 114.19, 112.40, 92.61, 45.63, 39.47, 37.91, 36.26, 28.86, 25.06, 24.84, 17.58. HPLC purity: 98.1%. HRMS (ESI) ( $[M + H]^+$ ) Calcd for  $C_{23}H_{31}BrN_7O_2$ : 516.1723, found: 516.1707.

*N*-(3-((5-Cyclopropyl-4-((4-sulfamoylbenzyl)amino)pyrimidin-2-yl)amino)phenyl)pyrrolidine-1-carboxamide (**21**). 16.0 mg, 8% yield.  $^1H$  NMR (400 MHz, methanol- $d_4$ )  $\delta$  7.80 (d,  $J = 8.3$  Hz, 2H), 7.70 (t,  $J = 2.1$  Hz, 1H), 7.47–7.41 (m, 3H), 7.22 (t,  $J = 8.0$  Hz, 1H), 7.15 (dt,  $J = 8.0, 1.5$  Hz, 1H), 6.97 (dt,  $J = 8.0, 1.6$  Hz, 1H), 4.82 (s, 2H), 3.46–3.41 (m, 4H), 1.98–1.92 (m, 4H), 1.57 (td,  $J = 7.9, 4.0$  Hz, 1H), 1.02–0.97 (m, 2H), 0.61–0.56 (m, 2H).  $^{13}C$  NMR (101 MHz, methanol- $d_4$ )  $\delta$  163.32, 155.39, 152.73, 142.84, 142.38, 140.50, 139.89, 136.96, 128.85, 127.60, 125.88, 117.51, 117.11, 115.24, 112.53, 45.66, 43.99, 25.01, 23.61, 6.92, 4.27. HPLC purity: 100%. HRMS (ESI) ( $[M + H]^+$ ) Calcd for  $C_{23}H_{30}N_7O_3S$ :508.2131, found: 508.2116.

*N*-(3-((4-(3-(Cyclobutanecarboxamido)propyl)amino)-5-cyclopropyl)pyrimidin-2-yl)amino)-phenyl)pyrrolidine-1-carboxamide (**22**). 16.0 mg, 5% yield.  $^1H$  NMR (400 MHz, methanol- $d_4$ )  $\delta$  7.81 (t,  $J = 2.1$  Hz, 1H), 7.55 (d,  $J = 1.1$  Hz, 1H), 7.25 (ddd,  $J = 8.1, 2.2, 1.1$  Hz, 1H), 7.15 (t,  $J = 8.1$  Hz, 1H), 6.97 (ddd,  $J = 8.0, 2.1, 1.0$  Hz, 1H), 3.58 (t,  $J = 6.6$  Hz, 2H), 3.47–3.42 (m, 5H), 3.24 (t,  $J = 6.7$  Hz, 2H), 2.96 (pd,  $J = 8.6, 1.0$  Hz, 1H), 2.24–2.14 (m, 2H), 2.10–2.01 (m, 2H), 1.98–1.93 (m, 5H), 1.84–1.75 (m, 3H), 1.46 (tt,  $J = 8.1, 5.2, 1.1$  Hz, 1H), 0.92–0.87 (m, 2H), 0.49–0.44 (m, 2H).  $^{13}C$  NMR (101

MHz, methanol- $d_4$ )  $\delta$  176.49, 162.67, 158.29, 155.62, 151.52, 140.97, 139.70, 128.11, 114.28, 113.88, 112.08, 110.40, 45.61, 39.47, 39.00, 37.37, 36.13, 29.14, 25.06, 24.83, 17.57, 7.07, 3.81. HPLC purity: 100%. HRMS (ESI) ( $[M + H]^+$ ) Calcd for  $C_{26}H_{36}N_7O_2$ :478.2930, found: 478.2914.

4-(((5-Bromo-2-((3-methyl-1-(2,2,2-trifluoroethyl)-1*H*-pyrazol-4-yl)amino)pyrimidin-4-yl)amino)methyl)benzenesulfonamide (GSK8612). 379 mg, 73% yield.  $^1H$  NMR (400 MHz, DMSO- $d_6$ )  $\delta$  8.43 (s, 1H), 7.98 (s, 1H), 7.73 (d,  $J = 8.0$  Hz, 3H), 7.62–7.53 (m, 1H), 7.41 (s, 2H), 7.27 (s, 2H), 4.90 (q,  $J = 9.1$  Hz, 2H), 4.61 (s, 2H), 2.08 (s, 3H).  $^{13}C$  NMR (151 MHz, acetonitrile- $d_3$ )  $\delta$  156.82, 156.44, 154.25, 142.15, 139.72, 139.67, 125.39, 123.87, 123.25 (q,  $J = 28.1$  Hz), 121.58, 119.20, 49.92 (q,  $J = 34.0$  Hz), 41.30, 8.17. HPLC purity: 100%. HRMS (ESI) ( $[M + H]^+$ ) Calcd for  $C_{17}H_{18}BrF_3N_7O_2S$ : 520.0378, found: 520.0378.

**General Procedure for the Synthesis of Compounds 12, 15, 16, 19, and 20: Procedure C.** To a solution of **6**, **9**, **10**, **13**, or GSK8612 (1 equiv) in methanol (20 mL) were added 5% Pd/C (0.5 equiv) and triethylamine (TEA, 3 equiv). The resulting mixture was stirred under  $H_2$  (hydrogen) atmosphere at r.t. for 16 h. Next the reaction mixture was filtered, and the filtrate was concentrated in vacuo. The crude product was purified via preparative HPLC (2–7 min, 30–55% acetonitrile, 30 mL/min; column: SunFire C18, 19 mm  $\times$  100 mm, 5  $\mu$ m) to give **12**, **15**, **16**, **19**, and **20** (amount, yield).

4-(((2-((3-Methyl-1-(2,2,2-trifluoroethyl)-1*H*-pyrazol-4-yl)amino)pyrimidin-4-yl)amino)methyl)benzenesulfonamide (**12**). 108 mg, 36% yield.  $^1H$  NMR (400 MHz, DMSO- $d_6$ )  $\delta$  8.18 (s, 1H), 7.87 (s, 1H), 7.77 (dd,  $J = 8.9, 6.9$  Hz, 3H), 7.66 (s, 1H), 7.46 (d,  $J = 8.0$  Hz, 2H), 7.30 (s, 2H), 5.92 (s, 1H), 4.90 (q,  $J = 9.1$  Hz, 2H), 4.57 (s, 2H), 2.11 (s, 3H).  $^{13}C$  NMR (151 MHz, acetonitrile- $d_3$ )  $\delta$  161.02, 157.98, 153.76, 142.49, 139.69, 139.23, 125.44, 125.24, 123.88, 123.79, 121.45 (q,  $J = 27.9$  Hz), 121.16, 119.67, 94.31\*, 49.96 (q,  $J = 34.4$  Hz), 41.30, 8.11. HPLC purity: 96.6%. HRMS (ESI) ( $[M + H]^+$ ) Calcd for  $C_{17}H_{19}F_3N_7O_2S$ :442.1273, found: 442.1270.

*N*<sup>4</sup>-(2-(1*H*-imidazol-5-yl)ethyl)-*N*<sup>2</sup>-(3-methyl-1-(2,2,2-trifluoroethyl)-1*H*-pyrazol-4-yl)pyrimidine-2,4-diamine (**15**). 86.0 mg, 10% yield.  $^1H$  NMR (400 MHz, DMSO- $d_6$ )  $\delta$  11.81 (s, 1H), 8.15 (d,  $J = 35.4$  Hz, 2H), 7.73 (s, 1H), 7.53 (s, 1H), 7.18 (s, 1H), 6.83 (s, 1H), 5.85 (d,  $J = 5.8$  Hz, 1H), 4.95 (q,  $J = 9.2$  Hz, 2H), 3.51 (s, 2H), 2.75 (t,  $J = 7.5$  Hz, 2H), 2.16 (s, 3H).  $^{13}C$  NMR (151 MHz, acetonitrile- $d_3$ )  $\delta$  161.05, 157.72, 153.16\*, 138.57\*, 132.48, 122.48, 121.55 (q,  $J = 28.0$  Hz), 120.74, 119.80, 116.93\*, 114.19, 49.77 (q,  $J = 32.4$  Hz), 38.55, 24.75, 8.19. HPLC purity: 100%. HRMS (ESI) ( $[M + H]^+$ ) Calcd for  $C_{15}H_{18}F_3N_8$ :367.1607, found: 367.1596.

*N*-(3-((4-((4-Sulfamoylbenzyl)amino)pyrimidin-2-yl)amino)phenyl)pyrrolidine-1-carboxamide (**16**). 23.0 mg, 8% yield.  $^1H$  NMR (400 MHz, DMSO- $d_6$ )  $\delta$  8.82 (s, 1H), 7.93 (s, 1H), 7.88 (s, 1H), 7.80 (d,  $J = 5.8$  Hz, 1H), 7.74 (m, 3H), 7.48 (d,  $J = 8.3$  Hz, 2H), 7.26 (s, 2H), 7.18 (s, 1H), 6.99 (t,  $J = 8.0$  Hz, 1H), 6.92 (d,  $J = 8.7$  Hz, 1H), 5.97 (s, 1H), 4.63 (s, 2H), 3.31 (d,  $J = 7.5$  Hz, 4H), 1.82–1.78 (m, 4H).  $^{13}C$  NMR (101 MHz, DMSO- $d_6$ )  $\delta$  162.86, 160.14, 155.30\*, 154.46, 144.67, 142.92, 141.44, 140.84, 128.18, 127.94, 126.07, 113.46, 113.27, 111.51, 97.85\*, 46.09, 40.86, 25.46. HPLC purity: 95.0%. HRMS (ESI) ( $[M + H]^+$ ) Calcd for  $C_{22}H_{26}N_7O_3S$ :468.1818, found: 468.1814.

4-(((2-((3-(Morpholinomethyl)phenyl)amino)pyrimidin-4-yl)amino)methyl)benzenesulfonamide (**19**). 18.8 mg, 38% yield.  $^1H$  NMR (400 MHz, methanol- $d_4$ )  $\delta$  7.84 (d,  $J = 8.4$  Hz, 2H), 7.77 (d,  $J = 6.0$  Hz, 1H), 7.59 (t,  $J = 2.0$  Hz, 1H), 7.52–7.47 (m, 2H), 7.36 (d,  $J = 8.2$  Hz, 1H), 7.14 (t,  $J = 7.8$  Hz, 1H), 6.90 (dt,  $J = 2.5, 1.4$  Hz, 1H), 6.01 (d,  $J = 6.0$  Hz, 1H), 4.70 (s, 2H), 3.61 (t,  $J = 4.7$  Hz, 4H), 3.35 (s, 2H), 2.36 (t,  $J = 4.5$  Hz, 4H).  $^{13}C$  NMR (101 MHz, methanol- $d_4$ )  $\delta$  163.16, 159.74, 154.25, 144.48, 142.16, 140.34, 137.04, 128.07, 127.30, 125.95, 122.68, 120.45, 118.38, 97.18, 66.23, 63.11, 53.14, 43.26. HPLC purity: 100%. HRMS (ESI) ( $[M + H]^+$ ) Calcd for  $C_{22}H_{27}N_6O_3S$ : 455.1865, found: 455.1851.

*N*<sup>4</sup>-(2-(1*H*-imidazol-5-yl)ethyl)-*N*<sup>2</sup>-(3-(morpholinomethyl)phenyl)pyrimidine-2,4-diamine (**20**). 21.0 mg, 19% yield.  $^1H$  NMR (400 MHz, DMSO- $d_6$ )  $\delta$  11.81 (s, 1H), 8.92 (s, 1H), 7.80 (d,  $J = 16.9$  Hz, 2H), 7.61 (s, 1H), 7.54 (s, 1H), 7.24 (s, 1H), 7.12 (t,  $J = 7.8$  Hz, 1H), 6.79 (d,  $J = 10.4$  Hz, 2H), 5.92 (d,  $J = 5.8$  Hz, 1H), 3.54 (m,



6H), 3.31 (s, 2H), 2.79 (m, 2H), 2.29 (s, 4H).  $^{13}\text{C}$  NMR (101 MHz, Methanol- $d_4$ )  $\delta$  163.14, 159.75, 153.70, 140.60, 137.24, 134.91, 134.58, 128.07, 122.50, 120.29, 118.18, 116.44, 97.18, 66.28, 63.20, 53.24, 40.31, 26.50. HPLC purity: 100%. HRMS (ESI) ( $[\text{M} + \text{H}]^+$ ) Calcd for  $\text{C}_{20}\text{H}_{26}\text{N}_7\text{O}$ : 380.2199, found: 380.2186.

**Biological Evaluation: Enzymatic Assays.** Eurofins kinase enzymatic radiometric assays were carried out at the  $K_m = \text{ATP}$  at a single concentration (1  $\mu\text{M}$ ) in duplicate for each kinase in Table S1. Eurofins kinase enzymatic radiometric assays were carried out at the  $K_m = \text{ATP}$  in dose–response (9-pt curve in duplicate) for each kinase with an  $\text{IC}_{50}$  value listed in Table 3. Details about the substrate used, protein constructs, controls, and assay protocol for each kinase assay can be found at the Eurofins Web site: <https://www.eurofinsdiscoveryservices.com>.

**Library-Wide NanoBRET Assays.** Human embryonic kidney (HEK293) cells (hypotriploid, female, fetal) were purchased from ATCC and grown in Dulbecco's modified Eagle's medium (DMEM, Gibco) supplemented with 10% (v/v) fetal bovine serum (FBS, Corning). Cells were incubated in 5%  $\text{CO}_2$  at 37  $^\circ\text{C}$  and passaged every 72 h with trypsin. They were not allowed to reach confluency.

Constructs for NanoBRET measurements of DRAK1 (DRAK1-NLuc), MARK3 (NLuc-MARK3), MARK4 (NLuc-MARK4), and TBK1 (NLuc-TBK1) included in Table 2 were kindly provided by Promega. NanoBRET assays were executed as described previously.<sup>17</sup> Preferred NLuc orientations are indicated in parentheses after each construct. Assays were carried out in dose–response as described by the manufacturer using 0.5  $\mu\text{M}$  of tracer K-9 for DRAK1 and MARK3 and 0.5  $\mu\text{M}$  of tracer K-5 for MARK4 and TBK1. Respective tracer titration curves that we generated for DRAK1, MARK3, and MARK4 can be found at <https://darkkinome.org/data>.<sup>35</sup> Tracer titration curves for MARK3, MARK4, and TBK1 can also be found on the Promega Web site.

**Kinome Screening.** The scanMAX assay platform was used to assess the selectivity of each aminopyrimidine analog at 1  $\mu\text{M}$  at Eurofins DiscoverX Corporation. As described previously, this commercial assay platform screens against 403 WT human kinases and provides percent of control values.<sup>19</sup> These percent of control values are captured in Table 1.

**Specific NanoBRET Assay Follow-Up.** NanoBRET assays for the six kinases in Table 4 were carried out in dose–response in singlicate by Carna Biosciences. Assays were carried out according to the manufacturer's protocol.

**Kinetic Solubility and Permeability (PAMPA).** Kinetic solubility analysis was carried out from 10 mM DMSO stocks of compounds in phosphate buffered saline solution (PBS) at pH 7.4 by Analiza, Inc. Following 24 h incubation in a Millipore solubility filter plate, samples were vacuum filtered, and the filtrates collected for analysis. Filtrates were injected into the nitrogen detector for quantification via total chemiluminescent nitrogen determination (CLND). Filtrates were quantified with respect to a calibration curve generated using standards that span the dynamic range of the instrument. Calculated solubility values are corrected for background nitrogen present in the DMSO and the media.

PAMPA analysis was carried out by Analiza, Inc. using a Corning Gentest Precoated PAMPA plate. DMSO stocks of compound diluted in PBS at pH 7.4 were added to the donor compartment of the plate, PBS at pH 7.4 was added to the acceptor compartment, and the plate was left to incubate for 5h. Both the donor and acceptor compartments were collected and analyzed by CLND. Donor and acceptor samples were quantified using the calibration curve generated using standards that span the dynamic range of the instrument. Measured concentrations are corrected for background nitrogen present in the DMSO and the media. Concentration values from the donor and acceptor compartment are used in the calculation of the effective permeability of the compound. Solubility of the compound is determined experimentally rather than assuming full solubility.

**Statistics.** Standard error of the mean (SEM) was calculated for NanoBRET assays executed more than once. Calculated SEM is included alongside  $\text{IC}_{50}$  values in Table 2.

**Crystallization and Structure Determination.** The coding sequence for the MARK3 residues 48–366 was cloned into the vector pNIC-CT10HF. Accordingly, the expressed construct comprised a TEV-cleavable His<sub>6</sub> tag in its C-terminus. Expression in *E. coli* Rosetta (DE3) was performed as previously described.<sup>41</sup> For purification, the pellet was resuspended in lysis buffer (50 mM HEPES/NaOH pH 7.4, 500 mM NaCl, 0.5 mM TCEP, 5% glycerol), and the cells lysed by sonication. After clearance by centrifugation, the lysate was loaded onto a Ni-NTA column. The bound His<sub>6</sub>-tagged protein was eluted in lysis buffer containing 300 mM imidazole. TEV cleavage was performed while dialyzing the sample overnight at 4  $^\circ\text{C}$ . The cleaved tag, TEV, and contaminating proteins were removed by another Ni-NTA step. Finally, MARK3 was subjected to gel filtration using an AKTA Xpress system combined with an S200 column in KGF150 buffer (20 mM HEPES/NaOH pH 7.4, 150 mM NaCl, 0.5 mM TCEP, 5% glycerol).

100 nL of a solution containing the protein–ligand complex (14 mg/mL MARK3<sub>48–366</sub>, 500  $\mu\text{M}$  **9**) was transferred to a 3-well crystallization plate (Swissci), mixed with 50 nL of precipitant solution (0.1 M sodium formate pH 7.0, 24% PEG3350), and incubated at 4  $^\circ\text{C}$ . Crystals were spotted after 3 days and did not change appearance after 6 days. They were mounted in precipitant solution cryoprotected with additional 25% ethylene glycol. Data were collected at Swiss Light Source (SLS) X06SA and analyzed, scaled, and merged with the SLS automated data processing (adp) pipeline.<sup>42</sup> The structure was solved by molecular replacement with Phaser<sup>43</sup> using a MARK3 model as a template (PDB code: 2QNJ)<sup>44</sup> and refined with Phenix.<sup>45</sup> The model and structure factors have been deposited to the PDB with the code 7P1L (crystallographic parameters are included in Table S2).

## ■ ASSOCIATED CONTENT

### SI Supporting Information

The Supporting Information is available free of charge at <https://pubs.acs.org/doi/10.1021/acs.jmedchem.1c00440>.

Eurofins 16-kinase panel enzymatic data, an additional figure that details kinome-wide selectivities of all compounds, sequence alignment of kinases potentially inhibited by aminopyrimidines, X-ray crystallographic data, LC chromatograms, and NMR spectra are included (PDF)

Molecular formula strings (CSV)

## ■ AUTHOR INFORMATION

### Corresponding Author

Alison D. Axtman – Structural Genomics Consortium, UNC Eshelman School of Pharmacy and Division of Chemical Biology and Medicinal Chemistry, UNC Eshelman School of Pharmacy, University of North Carolina at Chapel Hill, Chapel Hill, North Carolina 27599, United States; [orcid.org/0000-0003-4779-9932](https://orcid.org/0000-0003-4779-9932); Email: [alison.axtman@unc.edu](mailto:alison.axtman@unc.edu)

### Authors

David H. Drewry – Structural Genomics Consortium, UNC Eshelman School of Pharmacy, Division of Chemical Biology and Medicinal Chemistry, UNC Eshelman School of Pharmacy, and UNC Lineberger Comprehensive Cancer Center, School of Medicine, University of North Carolina at Chapel Hill, Chapel Hill, North Carolina 27599, United States; [orcid.org/0000-0001-5973-5798](https://orcid.org/0000-0001-5973-5798)

Joel K. Annor-Gyamfi – Structural Genomics Consortium, UNC Eshelman School of Pharmacy and Division of Chemical Biology and Medicinal Chemistry, UNC Eshelman School of Pharmacy, University of North Carolina at Chapel

Hill, Chapel Hill, North Carolina 27599, United States;

orcid.org/0000-0001-8510-2951

**Carrow I. Wells** – Structural Genomics Consortium, UNC Eshelman School of Pharmacy and Division of Chemical Biology and Medicinal Chemistry, UNC Eshelman School of Pharmacy, University of North Carolina at Chapel Hill, Chapel Hill, North Carolina 27599, United States;

orcid.org/0000-0003-4799-6792

**Julie E. Pickett** – Structural Genomics Consortium, UNC Eshelman School of Pharmacy and Division of Chemical Biology and Medicinal Chemistry, UNC Eshelman School of Pharmacy, University of North Carolina at Chapel Hill, Chapel Hill, North Carolina 27599, United States;

orcid.org/0000-0002-9535-8528

**Verena Dederer** – Institute for Pharmaceutical Chemistry, Johann Wolfgang Goethe-University, 60438 Frankfurt am Main, Germany; Structural Genomics Consortium, Buchmann Institute for Molecular Life Sciences, Johann Wolfgang Goethe-University, 60438 Frankfurt am Main, Germany

**Franziska Preuss** – Institute for Pharmaceutical Chemistry, Johann Wolfgang Goethe-University, 60438 Frankfurt am Main, Germany; Structural Genomics Consortium, Buchmann Institute for Molecular Life Sciences, Johann Wolfgang Goethe-University, 60438 Frankfurt am Main, Germany

**Sebastian Mathea** – Institute for Pharmaceutical Chemistry, Johann Wolfgang Goethe-University, 60438 Frankfurt am Main, Germany; Structural Genomics Consortium, Buchmann Institute for Molecular Life Sciences, Johann Wolfgang Goethe-University, 60438 Frankfurt am Main, Germany; orcid.org/0000-0001-8500-4569

Complete contact information is available at:

<https://pubs.acs.org/10.1021/acs.jmedchem.1c00440>

## Notes

The authors declare no competing financial interest.

## ACKNOWLEDGMENTS

Constructs for NanoBRET measurements of DRAK1, MARK3, MARK4, and TBK1 were kindly provided by Promega. Coral was used to make the kinome tree depicted in our Table of Contents graphic. Coral was developed in the Phanstiel Lab at UNC: <http://phanstiel-lab.med.unc.edu/CORAL>.<sup>46</sup> We used the TREEspot kinase interaction mapping software to prepare the kinome trees in Figure 1<sup>1</sup>, and Supplemental Information: <http://treespot.discoverx.com>. We thank ChemSpace LLC for synthetic support and Stefan Knapp for guidance on x-ray crystallographic studies. We thank the Department of Chemistry Mass Spectrometry Core Laboratory at the University of North Carolina for their assistance with mass spectrometry analysis. The Structural Genomics Consortium is a registered charity (number 1097737) that receives funds from AbbVie, Bayer Pharma AG, Boehringer Ingelheim, Canada Foundation for Innovation, Eshelman Institute for Innovation, Genome Canada, Genentech, Innovative Medicines Initiative (EU/EFPIA) [ULTRA-DD grant no. 115766], Janssen, Merck KGaA Darmstadt Germany, MSD, Novartis Pharma AG, Ontario Ministry of Economic Development and Innovation, Pfizer, São Paulo Research Foundation-FAPESP, Takeda, and Wellcome [106169/ZZ14/Z]. Research reported in this publication was

supported in part by the NC Biotechnology Center Institutional Support grant 2018-IDG-1030, NIH 1U24DK116204 and U54AG065187, DoD ALSRP award AL190107, and ALS Association grant ID wa1127.

## ABBREVIATIONS USED

DIPEA, *N,N*-diisopropylethylamine; DMSO, dimethyl sulfoxide; HCl, hydrochloric acid; HPLC, high-performance liquid chromatography; IC<sub>50</sub>, half maximal inhibitory concentration; LC–MS, liquid chromatography–mass spectrometry; *K<sub>m</sub>*, Michaelis constant; LINCS, Library of Integrated Network-Based Cellular Signatures; NanoBRET, bioluminescence resonance energy transfer using nanoluciferase; Nluc, nanoluciferase; NMR, nuclear magnetic resonance; PAMPA, parallel artificial membrane permeability assay; Pd/C, palladium on carbon; v/v, volume for volume; w/w, weight for weight

## REFERENCES

- (1) Meeta, S.; Nadeem, S. A review on biological importance of pyrimidines in the new era. *Int. J. Pharm. Pharm. Sci.* **2016**, *8*, 8–21.
- (2) Roskoski, R., Jr Properties of FDA-approved small molecule protein kinase inhibitors: A 2020 update. *Pharmacol. Res.* **2020**, *152*, 104609.
- (3) Richters, A.; Basu, D.; Engel, J.; Ercanoglu, M. S.; Balke-Want, H.; Tesch, R.; Thomas, R. K.; Rauh, D. Identification and further development of potent TBK1 inhibitors. *ACS Chem. Biol.* **2015**, *10*, 289–298.
- (4) Llona-Minguez, S.; Baiget, J.; Mackay, S. P. Small-molecule inhibitors of IκB kinase (IKK) and IKK-related kinases. *Pharm. Pat. Anal.* **2013**, *2*, 481–498.
- (5) Perrior, T. R.; Newton, G. K.; Stewart, M. R.; Aquil, R. Pyrimidine compounds as inhibitors of protein kinases IKK epsilon and/or TBK-1, processes for their preparation, and pharmaceutical compositions containing them. International Patent WO2012010826A1, 2012.
- (6) Muvaffak, A.; Pan, Q.; Yan, H.; Fernandez, R.; Lim, J.; Dolinski, B.; Nguyen, T. T.; Strack, P.; Wu, S.; Chung, R.; Zhang, W.; Hulton, C.; Ripley, S.; Hirsch, H.; Nagashima, K.; Wong, K.-K.; Jänne, P. A.; Seidel-Dugan, C.; Zawel, L.; Kirschmeier, P. T.; Middleton, R. E.; Morris, E. J.; Wang, Y. Evaluating TBK1 as a therapeutic target in cancers with activated IRF3. *Mol. Cancer Res.* **2014**, *12*, 1055–1066.
- (7) Hutti, J. E.; Porter, M. A.; Cheely, A. W.; Cantley, L. C.; Wang, X.; Kireev, D.; Baldwin, A. S.; Janzen, W. P. Development of a high-throughput assay for identifying inhibitors of TBK1 and IKKε. *PLoS One* **2012**, *7*, No. e41494.
- (8) Crew, A. P.; Raina, K.; Dong, H.; Qian, Y.; Wang, J.; Vigil, D.; Serebrenik, Y. V.; Hamman, B. D.; Morgan, A.; Ferraro, C.; Situ, K.; Neklesa, T. K.; Winkler, J. D.; Coleman, K. G.; Crews, C. M. Identification and characterization of von Hippel-Lindau-recruiting proteolysis targeting chimeras (PROTACs) of TANK-binding kinase 1. *J. Med. Chem.* **2018**, *61*, 583–598.
- (9) Oakes, J. A.; Davies, M. C.; Collins, M. O. TBK1: a new player in ALS linking autophagy and neuroinflammation. *Mol. Brain* **2017**, *10*, 5.
- (10) Freischmidt, A.; Wieland, T.; Richter, B.; Ruf, W.; Schaeffer, V.; Müller, K.; Marroquin, N.; Nordin, F.; Hubers, A.; Weydt, P.; Pinto, S.; Press, R.; Millecamps, S.; Molko, N.; Bernard, E.; Desnuelle, C.; Soriani, M. H.; Dorst, J.; Graf, E.; Nordstrom, U.; Feiler, M. S.; Putz, S.; Boeckers, T. M.; Meyer, T.; Winkler, A. S.; Winkelmann, J.; de Carvalho, M.; Thal, D. R.; Otto, M.; Brannstrom, T.; Volk, A. E.; Kursula, P.; Danzer, K. M.; Lichtner, P.; Dikic, I.; Meitinger, T.; Ludolph, A. C.; Strom, T. M.; Andersen, P. M.; Weishaupt, J. H. Haploinsufficiency of TBK1 causes familial ALS and fronto-temporal dementia. *Nat. Neurosci.* **2015**, *18*, 631–636.
- (11) Hegde, R. N.; Chiki, A.; Petricca, L.; Martufi, P.; Arbez, N.; Mouchiroud, L.; Auwerx, J.; Landles, C.; Bates, G. P.; Singh-Bains, M.



- K.; Dragunow, M.; Curtis, M. A.; Faull, R. L.; Ross, C. A.; Caricasole, A.; Lashuel, H. A. TBK1 phosphorylates mutant Huntingtin and suppresses its aggregation and toxicity in Huntington's disease models. *EMBO J.* **2020**, *39*, No. e104671.
- (12) Verheijen, J.; van der Zee, J.; Gijselincx, I.; Van den Bossche, T.; Dillen, L.; Heeman, B.; Gómez-Tortosa, E.; Lladó, A.; Sanchez-Valle, R.; Graff, C.; Pastor, P.; Pastor, M. A.; Benussi, L.; Ghidoni, R.; Binetti, G.; Clarimon, J.; de Mendonça, A.; Gelpi, E.; Tsolaki, M.; Diehl-Schmid, J.; Nacmias, B.; Almeida, M. R.; Borroni, B.; Matej, R.; Ruiz, A.; Engelborghs, S.; Vandenbergh, R.; De Deyn, P. P.; Cruts, M.; Van Broeckhoven, C.; Sleegers, K.; et al. Common and rare TBK1 variants in early-onset Alzheimer disease in a European cohort. *Neurobiol. Aging* **2018**, *62*, 245.e1–245.e7.
- (13) Rodgers, G.; Austin, C.; Anderson, J.; Pawlyk, A.; Colvis, C.; Margolis, R.; Baker, J. Glimmers in illuminating the druggable genome. *Nat. Rev. Drug Discovery* **2018**, *17*, 301–302.
- (14) Krahn, A. I.; Wells, C.; Drewry, D. H.; Beitel, L. K.; Durcan, T. M.; Axtman, A. D. Defining the neural kinome: strategies and opportunities for small molecule drug discovery to target neurodegenerative diseases. *ACS Chem. Neurosci.* **2020**, *11*, 1871–1886.
- (15) Annadurai, N.; Agrawal, K.; Džubák, P.; Hajdúch, M.; Das, V. Microtubule affinity-regulating kinases are potential druggable targets for Alzheimer's disease. *Cell. Mol. Life Sci.* **2017**, *74*, 4159–4169.
- (16) Katz, J. D.; Haidle, A.; Childers, K. K.; Zabierek, A. A.; Jewell, J. P.; Hou, Y.; Altman, M. D.; Szewczak, A.; Chen, D.; Harsch, A.; Hayashi, M.; Warren, L.; Hutton, M.; Nuthall, H.; Su, H. P.; Munshi, S.; Stanton, M. G.; Davies, I. W.; Munoz, B.; Northrup, A. Structure guided design of a series of selective pyrrolopyrimidinone MARK inhibitors. *Bioorg. Med. Chem. Lett.* **2017**, *27*, 114–120.
- (17) Wells, C.; Couñago, R. M.; Limas, J. C.; Almeida, T. L.; Cook, J. G.; Drewry, D. H.; Elkins, J. M.; Gileadi, O.; Kapadia, N. R.; Lorente-Macias, A.; Pickett, J. E.; Riemen, A.; Ruela-de-Sousa, R. R.; Willson, T. M.; Zhang, C.; Zuercher, W. J.; Zutshi, R.; Axtman, A. D. SGC-AAK1-1: A chemical probe targeting AAK1 and BMP2K. *ACS Med. Chem. Lett.* **2020**, *11*, 340–345.
- (18) Agajanian, M. J.; Walker, M. P.; Axtman, A. D.; Ruela-de-Sousa, R. R.; Serafin, D. S.; Rabinowitz, A. D.; Graham, D. M.; Ryan, M. B.; Tamir, T.; Nakamichi, Y.; Gammons, M. V.; Bennett, J. M.; Counago, R. M.; Drewry, D. H.; Elkins, J. M.; Gileadi, C.; Gildadi, O.; Godoi, P. H.; Kapadia, N.; Muller, S.; Santiago, A. S.; Sorrell, F. J.; Wells, C. I.; Fedorov, O.; Willson, T. M.; Zuercher, W. J.; Major, M. B. WNT activates the AAK1 kinase to promote clathrin-mediated endocytosis of LRP6 and establish a negative feedback loop. *Cell Rep.* **2019**, *26*, 79–93.e8.
- (19) Davis, M. I.; Hunt, J. P.; Herrgard, S.; Ciceri, P.; Wodicka, L. M.; Pallares, G.; Hocker, M.; Treiber, D. K.; Zarrinkar, P. P. Comprehensive analysis of kinase inhibitor selectivity. *Nat. Biotechnol.* **2011**, *29*, 1046–1051.
- (20) Clark, K.; Peggie, M.; Plater, L.; Sorcek, R. J.; Young, E. R. R.; Madwed, J. B.; Hough, J.; McIver, E. G.; Cohen, P. Novel cross-talk within the IKK family controls innate immunity. *Biochem. J.* **2011**, *434*, 93–104.
- (21) McIver, E. G.; Bryans, J.; Birchall, K.; Chugh, J.; Drake, T.; Lewis, S. J.; Osborne, J.; Smiljanic-Hurley, E.; Tsang, W.; Kamal, A.; Levy, A.; Newman, M.; Taylor, D.; Arthur, J. S. C.; Clark, K.; Cohen, P. Synthesis and structure-activity relationships of a novel series of pyrimidines as potent inhibitors of TBK1/IKKε kinases. *Bioorg. Med. Chem. Lett.* **2012**, *22*, 7169–7173.
- (22) Petherick, K. J.; Conway, O. J.; Mpamhanga, C.; Osborne, S. A.; Kamal, A.; Saxty, B.; Ganley, I. G. Pharmacological inhibition of ULK1 kinase blocks mammalian target of rapamycin (mTOR)-dependent autophagy. *J. Biol. Chem.* **2015**, *290*, 11376–11383.
- (23) Feldman, R. I.; Wu, J. M.; Polokoff, M. A.; Kochanny, M. J.; Dinter, H.; Zhu, D.; Biroc, S. L.; Alicke, B.; Bryant, J.; Yuan, S.; Buckman, B. O.; Lentz, D.; Ferrer, M.; Whitlow, M.; Adler, M.; Finster, S.; Chang, Z.; Arnaiz, D. O. Novel small molecule inhibitors of 3-phosphoinositide-dependent kinase-1. *J. Biol. Chem.* **2005**, *280*, 19867–19874.
- (24) Stathias, V.; Turner, J.; Koleti, A.; Vidovic, D.; Cooper, D.; Fazel-Najafabadi, M.; Pilarczyk, M.; Terryn, R.; Chung, C.; Umeano, A.; Clarke, D. J. B.; Lachmann, A.; Evangelista, J. E.; Ma'ayan, A.; Medvedovic, M.; Schürer, S. C. LINCS Data Portal 2.0: next generation access point for perturbation-response signatures. *Nucleic Acids Res.* **2020**, *48*, D431–D439.
- (25) Thomson, D. W.; Poeckel, D.; Zinn, N.; Rau, C.; Strohmmer, K.; Wagner, A. J.; Graves, A. P.; Perrin, J.; Bantscheff, M.; Duempelfeld, B.; Kasparcova, V.; Ramanjulu, J. M.; Pesiridis, G. S.; Muelbaier, M.; Bergamini, G. Discovery of GSK8612, a highly selective and potent TBK1 inhibitor. *ACS Med. Chem. Lett.* **2019**, *10*, 780–785.
- (26) Faisal, M.; Kim, J. H.; Yoo, K. H.; Roh, E. J.; Hong, S. S.; Lee, S. H. Development and therapeutic potential of NUAks inhibitors. *J. Med. Chem.* **2021**, *64*, 2–25.
- (27) Drewes, G.; Ebnet, A.; Preuss, U.; Mandelkow, E.-M.; Mandelkow, E. MARK, a novel family of protein kinases that phosphorylate microtubule-associated proteins and trigger microtubule disruption. *Cell* **1997**, *89*, 297–308.
- (28) Lasagna-Reeves, C. A.; de Haro, M.; Hao, S.; Park, J.; Rousseaux, M. W.; Al-Ramahi, I.; Jafar-Nejad, P.; Vilanova-Velez, L.; See, L.; De Maio, A.; Nitschke, L.; Wu, Z.; Troncoso, J. C.; Westbrook, T. F.; Tang, J.; Botas, J.; Zoghbi, H. Y. Reduction of Nuak1 decreases tau and reverses phenotypes in a tauopathy mouse model. *Neuron* **2016**, *92*, 407–418.
- (29) Shi, B.; Conner, S. D.; Liu, J. Dysfunction of endocytic kinase AAK1 in ALS. *Int. J. Mol. Sci.* **2014**, *15*, 22918–22932.
- (30) Vasta, J. D.; Corona, C. R.; Wilkinson, J.; Zimprich, C. A.; Hartnett, J. R.; Ingold, M. R.; Zimmerman, K.; Machleidt, T.; Kirkland, T. A.; Huwiler, K. G.; Ohana, R. F.; Slater, M.; Otto, P.; Cong, M.; Wells, C. I.; Berger, B. T.; Hanke, T.; Glas, C.; Ding, K.; Drewry, D. H.; Huber, K. V. M.; Willson, T. M.; Knapp, S.; Muller, S.; Meisenheimer, P. L.; Fan, F.; Wood, K. V.; Robers, M. B. Quantitative, wide-spectrum kinase profiling in live cells for assessing the effect of cellular ATP on target engagement. *Cell Chem. Biol.* **2018**, *25*, 206–214.
- (31) Asquith, C. R. M.; Berger, B.-T.; Wan, J.; Bennett, J. M.; Capuzzi, S. J.; Crona, D. J.; Drewry, D. H.; East, M. P.; Elkins, J. M.; Fedorov, O.; Godoi, P. H.; Hunter, D. M.; Knapp, S.; Müller, S.; Torrice, C. D.; Wells, C. I.; Earp, H. S.; Willson, T. M.; Zuercher, W. J. SGC-GAK-1: A chemical probe for cyclin G associated kinase (GAK). *J. Med. Chem.* **2019**, *62*, 2830–2836.
- (32) Wells, C. I.; Drewry, D. H.; Pickett, J. E.; Tjaden, A.; Krämer, A.; Müller, S.; Gyenis, L.; Menyhart, D.; Litchfield, D. W.; Knapp, S.; Axtman, A. D. Development of a potent and selective chemical probe for the pleiotropic kinase CK2. *Cell Chem. Biol.* **2021**, *28*, 546–558.
- (33) Wells, C. I.; Al-Ali, H.; Andrews, D. M.; Asquith, C. R. M.; Axtman, A. D.; Dikic, I.; Ebner, D.; Etmayer, P.; Fischer, C.; Frederiksen, M.; Futrell, R. E.; Gray, N. S.; Hatch, S. B.; Knapp, S.; Lücking, U.; Michaelides, M.; Mills, C. E.; Müller, S.; Owen, D.; Picado, A.; Saikatendu, K. S.; Schröder, M.; Stolz, A.; Tellechea, M.; Turunen, B. J.; Vilar, S.; Wang, J.; Zuercher, W. J.; Willson, T. M.; Drewry, D. H. The Kinase Chemogenomic Set (KCGS): An open science resource for kinase vulnerability identification. *Int. J. Mol. Sci.* **2021**, *22*, 566.
- (34) Drewry, D. H.; Wells, C. I.; Andrews, D. M.; Angell, R.; Al-Ali, H.; Axtman, A. D.; Capuzzi, S. J.; Elkins, J. M.; Etmayer, P.; Frederiksen, M.; Gileadi, O.; Gray, N.; Hooper, A.; Knapp, S.; Laufer, S.; Luecking, U.; Michaelides, M.; Muller, S.; Muratov, E.; Denny, R. A.; Saikatendu, K. S.; Treiber, D. K.; Zuercher, W. J.; Willson, T. M. Progress towards a public chemogenomic set for protein kinases and a call for contributions. *PLoS One* **2017**, *12*, No. e0181585.
- (35) Berginski, M. E.; Moret, N.; Liu, C.; Goldfarb, D.; Sorger, P. K.; Gomez, S. M. The Dark Kinase Knowledgebase: an online compendium of knowledge and experimental results of understudied kinases. *Nucleic Acids Res.* **2021**, *49*, D529–D535.
- (36) Fensome, A.; Ambler, C. M.; Arnold, E.; Banker, M. E.; Clark, J. D.; Dowty, M. E.; Efremov, I. V.; Flick, A.; Gerstenberger, B. S.; Gifford, R. S.; Gopalsamy, A.; Hegen, M.; Jussif, J.; Limburg, D. C.; Lin, T. H.; Pierce, B. S.; Sharma, R.; Trujillo, J. I.; Vajdos, F. F.

Vincent, F.; Wan, Z.-K.; Xing, L.; Yang, X.; Yang, X. Design and optimization of a series of 4-(3-azabicyclo[3.1.0]hexan-3-yl)-pyrimidin-2-amines: Dual inhibitors of TYK2 and JAK1. *Bioorg. Med. Chem.* **2020**, *28*, 115481.

(37) Fensome, A.; Ambler, C. M.; Arnold, E.; Banker, M. E.; Brown, M. F.; Chrencik, J.; Clark, J. D.; Dowty, M. E.; Efremov, I. V.; Flick, A.; Gerstenberger, B. S.; Gopalsamy, A.; Hayward, M. M.; Hegen, M.; Hollingshead, B. D.; Jussif, J.; Knafels, J. D.; Limburg, D. C.; Lin, D.; Lin, T. H.; Pierce, B. S.; Saiah, E.; Sharma, R.; Symanowicz, P. T.; Telliez, J.-B.; Trujillo, J. I.; Vajdos, F. F.; Vincent, F.; Wan, Z.-K.; Xing, L.; Yang, X.; Yang, X.; Zhang, L. Dual inhibition of TYK2 and JAK1 for the treatment of autoimmune diseases: Discovery of ((S)-2,2-difluorocyclopropyl)((1R,5S)-3-(2-((1-methyl-1H-pyrazol-4-yl)-amino)pyrimidin-4-yl)-3,8-diazabicyclo[3.2.1]octan-8-yl)methanone (PF-06700841). *J. Med. Chem.* **2018**, *61*, 8597–8612.

(38) Gu, Y.; Kar, T.; Scheiner, S. Fundamental Properties of the CH...O Interaction: Is It a True Hydrogen Bond? *J. Am. Chem. Soc.* **1999**, *121*, 9411–9422.

(39) Larabi, A.; Devos, J. M.; Ng, S. L.; Nanao, M. H.; Round, A.; Maniatis, T.; Panne, D. Crystal structure and mechanism of activation of TANK-binding kinase 1. *Cell Rep.* **2013**, *3*, 734–746.

(40) Chaikuad, A.; Koschade, S. E.; Stolz, A.; Zivkovic, K.; Pohl, C.; Shaid, S.; Ren, H.; Lambert, L. J.; Cosford, N. D. P.; Brandts, C. H.; Knapp, S. Conservation of structure, function and inhibitor binding in UNC-51-like kinase 1 and 2 (ULK1/2). *Biochem. J.* **2019**, *476*, 875–887.

(41) Burgess-Brown, N. A.; Mahajan, P.; Strain-Damerell, C.; Gileadi, O.; Graslund, S. Medium-throughput production of recombinant human proteins: protein production in *E. coli*. *Methods Mol. Biol.* **2014**, *1091*, 73–94.

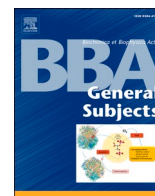
(42) Wojdyla, J. A.; Kaminski, J. W.; Panepucci, E.; Ebner, S.; Wang, X.; Gabadinho, J.; Wang, M. DA+ data acquisition and analysis software at the Swiss Light Source macromolecular crystallography beamlines. *J. Synchrotron Radiat.* **2018**, *25*, 293–303.

(43) McCoy, A. J.; Grosse-Kunstleve, R. W.; Storoni, L. C.; Read, R. J. Likelihood-enhanced fast translation functions. *Acta Crystallogr., Sect. D: Biol. Crystallogr.* **2005**, *61*, 458–464.

(44) Murphy, J. M.; Korzhnev, D. M.; Ceccarelli, D. F.; Briant, D. J.; Zarrine-Afsar, A.; Sicheri, F.; Kay, L. E.; Pawson, T. Conformational instability of the MARK3 UBA domain compromises ubiquitin recognition and promotes interaction with the adjacent kinase domain. *Proc. Natl. Acad. Sci. U. S. A.* **2007**, *104*, 14336–14341.

(45) Liebschner, D.; Afonine, P. V.; Baker, M. L.; Bunkoczi, G.; Chen, V. B.; Croll, T. I.; Hintze, B.; Hung, L. W.; Jain, S.; McCoy, A. J.; Moriarty, N. W.; Oeffner, R. D.; Poon, B. K.; Prisant, M. G.; Read, R. J.; Richardson, J. S.; Richardson, D. C.; Sammito, M. D.; Sobolev, O. V.; Stockwell, D. H.; Terwilliger, T. C.; Urzhumtsev, A. G.; Videau, L. L.; Williams, C. J.; Adams, P. D. Macromolecular structure determination using X-rays, neutrons and electrons: recent developments in Phenix. *Acta Crystallogr. D Struct. Biol.* **2019**, *75*, 861–877.

(46) Metz, K. S.; Deoudes, E. M.; Berginski, M. E.; Jimenez-Ruiz, I.; Aksoy, B. A.; Hammerbacher, J.; Gomez, S. M.; Phanstiel, D. H. Coral: Clear and customizable visualization of human kinome data. *Cell Syst* **2018**, *7*, 347–350.



## Characterizing the role of the dark kinome in neurodegenerative disease – A mini review

Alison D. Axtman\*

UNC Eshelman School of Pharmacy, Division of Chemical Biology and Medicinal Chemistry, Structural Genomics Consortium, Chapel Hill, NC, USA

### ARTICLE INFO

#### Keywords:

Kinase  
Neurodegeneration  
Small molecule  
Dark kinome  
Chemical probe  
Drug discovery

### ABSTRACT

**Background:** Drugs that modulate previously unexplored targets could potentially slow or halt the progression of neurodegenerative diseases. Several candidate proteins lie within the dark kinome, those human kinases that have not been well characterized. Much of the kinome (~80%) remains poorly studied, and these targets likely harbor untapped biological potential.

**Scope of review:** This review highlights the significance of kinases as mediators of aberrant pathways in neurodegeneration and provides examples of published high-quality small molecules that modulate some of these kinases.

**Major conclusions:** There is a need for continued efforts to develop high-quality chemical tools to illuminate the function of understudied kinases in the brain. Potent and selective small molecules enable accurate pairing of an observed phenotype with a protein target.

**General significance:** The examples discussed herein support the premise that validation of therapeutic hypotheses surrounding kinase targets can be accomplished via small molecules and they can serve as the basis for disease-focused drug development campaigns.

### 1. Background

Kinases are highly druggable protein targets [1,2]. With more than 500 protein kinases encoded by the human genome, the 67 FDA-approved drugs targeting kinases have established these proteins as a highly tractable and therapeutically important class of drug targets. The number of publications on the human form of a kinase defines how well-studied or how correspondingly "dark" a particular kinase is considered. Remarkably, at least one kinase target of the 67 FDA-approved small molecule inhibitors is in the top 100 most studied kinases (~20%) annotated in 2019 [3,4]. Thus, all kinase-targeting drugs have resulted from research centered around a small fraction of the human kinome. This preponderance of research focused on a small fraction of the human kinome has resulted in the full potential of human kinases not yet being fully realized, especially since most kinases remain understudied and are assigned to the dark kinome. With additional effort devoted to characterizing the dark kinome, the unexplored biological potential of these kinases can be realized. While a comprehensive review of the types of kinases, classified by substrate(s), and the distribution of dark kinases within the larger kinome is out of scope, these topics have been analyzed

by others [5,6].

While most therapeutic interest in kinases has centered in oncology, kinases play essential roles in the regulation of signaling pathways in the brain and changes in their function are associated with neurodegeneration [7,8]. With few currently available drugs for these disorders and a growing demand as the aging population increases, there is a need for new drugs and targets to treat chronic neurodegenerative diseases. Despite the established proficiency of the research community to convert kinase inhibitors into approved drugs, kinase tractability has not yet been exploited to the fullest in neuroscience.

Several kinases are either overactive or overexpressed in specific brain regions associated with neurodegenerative diseases [9–11]. In many cases enhanced signaling leads to hyperphosphorylation of proteins prone to aggregation, such as tau in Alzheimer's disease (AD) or TDP-43 in amyotrophic lateral sclerosis (ALS) or  $\alpha$ -synuclein in Parkinson's disease (PD) [11–13]. Other disease propagating phenotypes, such as neuroinflammation and neuronal death, also result from this aberrant signaling [14,15]. In contrast, kinase loss-of-function (LoF) has been identified as the genetic cause and a key driver of several neurodegenerative diseases. In most patients, homozygous LoF kinase

\* Corresponding author at: University of North Carolina at Chapel Hill, 120 Mason Farm Road, Chapel Hill, NC 27599-7356, USA.

E-mail address: [alison.axtman@unc.edu](mailto:alison.axtman@unc.edu).

<https://doi.org/10.1016/j.bbagen.2021.130014>

Received 28 June 2021; Received in revised form 26 August 2021; Accepted 14 September 2021

Available online 20 September 2021

0304-4165/© 2021 The Author(s).

Published by Elsevier B.V. This is an open access article under the CC BY-NC-ND license

(<http://creativecommons.org/licenses/by-nc-nd/4.0/>).

mutations result in impaired signaling from which the patient cannot adapt [1]. In other cases, heterozygous LoF variants result in loss of kinase expression and are reported as disease causative via haploinsufficiency [16].

## 2. Scope of review

This review discusses published high-quality small molecules that modulate specific kinases with described roles in neurodegeneration. These compounds modulate kinases in divergent manners, resulting in either activation or inhibition as the endpoint. High-quality chemical tools are defined as being potent, cell-active molecules having a limited spectrum of kinase activity (potently inhibiting ~10% or less of all kinases screened) [8]. Achieving this level of potency and selectivity often requires significant time and investment in medicinal chemistry. High-throughput biochemical platforms, such as the Eurofins KINOMEScan panel and kinobeads, offer methods by which to assess kinome-wide small molecule kinase binding affinity [17,18]. The literature is confounded by sub-optimal, poorly characterized kinase modulators that have been used to ascribe various phenomena to a specific kinase [19–22]. In 2017, Klaeger et al provided an analysis of over 243 clinically evaluated kinase inhibitors that supports this claim and provides a comprehensive landscape of the polypharmacology of these kinase-targeting drugs [17]. In contrast, high-quality chemical tools offer dynamic, reversible, and tunable perturbations of a particular target protein, resulting in modulation of its function and/or interactions. Importantly, molecules of this caliber represent potential leads for drug development. Some of the chemical tools discussed herein have been used to validate novel targets and disease models, while others represent best-in-class tools to characterize disease-propagating pathways for the first time. The development and use of high-quality small molecules that target kinases will create new avenues for the discovery of novel treatments for neurodegenerative diseases and expand the portfolio of putative drug targets to include members of the dark kinome.

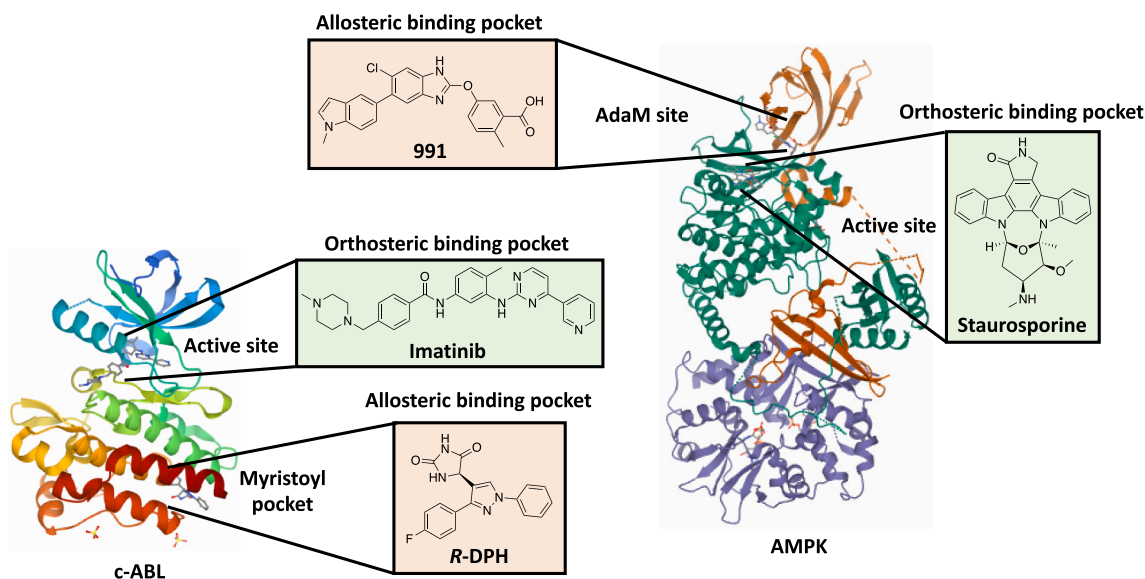
## 3. Kinase inhibition

Kinase inhibitors are most often designed to bind to the orthosteric ATP site (Fig. 1) that all kinases have in common. The high homology among the binding sites, however, is both an advantage and a challenge. This shared site makes kinases highly tractable but introduces the

challenge of achieving selectivity for one kinase. Kinases like BTK demonstrate that non-covalent as well as covalent small molecules can bind to this site and result in inhibition [23]. As an alternative approach, allosteric binding of a small molecule has been observed to result in kinase inhibition for kinases including ABL, AKT, AMPK, CDK2/8, CHK1, FAK, IGF1R, IKK, IRE1, ITK, JNK1, LIMK2, MEK1/2, mTOR, PAK1, PDK1, PKC $\zeta$ , PI3K, RIPK1, and SYK [24–26]. Targeting a pseudokinase domain, such as in the case of BMS-986165 for TYK2, can also elicit kinase inhibition [27]. Fig. 1 shows examples of two kinases (c-ABL and AMPK) that bind ligands in both their orthosteric and allosteric sites. Ligands that bind to the orthosteric site, which also binds ATP, are shaded green, while those that bind at a proximal (AMPK) or distal (c-ABL) allosteric site are shaded orange [28,29]. The success that has been realized around development of kinase inhibitors has made kinase inhibition a common therapeutic approach, especially in oncology. The observation that specific kinases are either overactive or overexpressed in patient brains supports kinase inhibition as a therapeutic approach for multiple neurodegenerative diseases (Fig. 2). As examples, kinase inhibition has been explored to reduce toxic protein aggregation, prevent death of neurons, reduce neuroinflammation, and/or slow disease progression in diseases like AD, ALS, and PD [30–36].

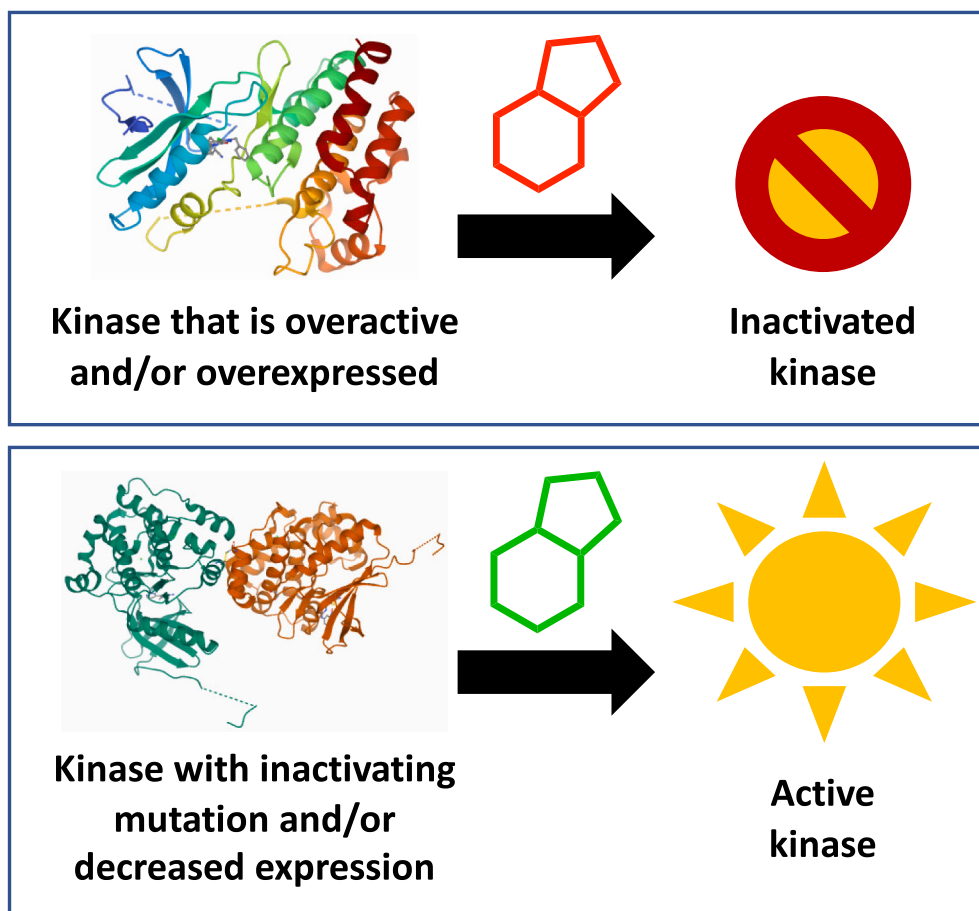
## 4. Kinase activation

Compounds capable of activating kinases have been identified for <1% of the human kinome. Selectivity for individual kinases among highly homologous family members is more easily achieved with small molecule activators than with ATP-site competitive inhibitors [37], as these allosteric sites or alternative domains are unique to a particular kinase rather than shared by all. Indirect methods to activate kinases have yielded some success but can carry with them unintended side effects due to indiscriminate activation of many signaling pathways [37]. There are specific examples of kinases that have been activated via a unique structural feature that is not common across the kinome, such as an allosteric site (myristoyl binding site of ABL, ADaM site of AMPK, allosteric site of AURKA, HM/PIF pocket of PDK1) or an alternative domain that binds ligands (the regulatory domain of PKC, the ligand-binding domain of EphA2/A4, the  $\gamma$ -subunit of AMPK, the intracellular region of IR) [26,37–39]. Fig. 1 shows c-ABL with an activator bound to its myristoyl pocket and AMPK with an activator bound to a pocket formed at the interface between the kinase domain and carbohydrate-



**Fig. 1.** Co-crystal structures of human c-ABL (left, PDB code: 3PPY) bound to imatinib in its orthosteric site and R-DPH in an allosteric (myristoyl) pocket and human AMPK (right, PDB code: 4CFE) bound to staurosporine in its orthosteric site and 991 in an allosteric (ADaM) site.





**Fig. 2.** Kinase perturbations associated with neurodegenerative diseases. RIPK1 (top, PDB code: 6C4D) is shown as an example of an overactive kinase for which inhibition is a strategy in ALS and AD. NEK1 (bottom, PDB code: 4B9D) is shown as an example of a kinase that harbors inactivating mutations in ALS for which restoring activity is a therapeutic strategy.

binding module known as the ADaM site [28,29,40]. As noted in the previous section, however, allosteric binding most often results in kinase inhibition and may not be the best strategy to elicit kinase activation. Kinases that demonstrate decreased expression in the brain when examined post-mortem or for which inactivating variants have been observed in the genomes of patients compared with age-matched controls lend support for strategies that restore function via kinase activation (Fig. 2). Generally, kinases involved in altered active kinase networks that are disrupted by disease are targets for gain-of-function drug discovery.

## 5. High-quality tools that have helped to interrogate neurodegenerative biologies

There are several examples in the literature of high-quality small molecules that have been developed and are being used to explore disease-propagating biologies in the brain. Examples in this section have advanced to clinical trials, demonstrating that chemical tools can be used to launch drug discovery campaigns, and this has happened in the neurodegenerative space. As more than 400 publications have reported findings related to the human forms of each of the kinases in this section and dedicated programs have identified chemical lead compounds, these would not be classified as understudied kinases.

### 5.1. RIPK1 inhibition

Given its roles in regulating inflammation, cytokine release, and necroptotic cell death, RIPK1 has been implicated in the pathogenesis of

ALS, AD, and multiple sclerosis (MS) [41–43]. When activated, RIPK1 becomes phosphorylated and interacts with a complex of other proteins, including RIPK3 and MLKL, triggering the pathogenic cellular responses described [41]. Multiple studies have demonstrated that inhibition of RIPK1 activity protects against inflammation and cell death in animal models [41,44–47]. Importantly, increased RIPK1 activity has also been observed in human diseases such as AD, ALS, and MS [41,48–50]. DNL104 is a potent, selective, and brain-penetrant RIPK1 inhibitor that dose-dependently inhibits RIPK1 phosphorylation in cells [41]. In a Phase I clinical trial designed to test its safety and tolerability, DNL104 showed good brain penetration and did not elicit any central nervous system toxicities, supporting continued development of CNS-penetrant RIPK1 inhibitors to treat neurodegenerative diseases [41]. While trials around DNL104 have been terminated, Phase Ib/IIa clinical trials with DNL747, another brain-penetrant RIPK1 inhibitor from Denali, were completed for AD (NCT03757325) and terminated for ALS (NCT03757351) [51]. Potential dose-limiting toxicities of DNL747 have motivated the introduction of another brain-penetrant RIPK1 inhibitor, DNL788, into Phase Ia trials in 2021 [51]. Structures of these compounds remain unpublished. Finally, GSK developed a potent and highly selective RIPK1 inhibitor (GSK2982772) that is currently in Phase II clinical studies for psoriasis, rheumatoid arthritis, and ulcerative colitis [52].

### 5.2. LRRK2 inhibition

Denali has also developed highly selective inhibitors of LRRK2 for PD. Kinase-activating mutations in the LRRK2 gene are the most

frequent cause of inherited PD [53]. Other gene variants are associated with higher risk of sporadic PD and there is some evidence that supports LRRK2 activation in idiopathic PD [54]. Increased LRRK2 kinase activity impairs vesicle trafficking and lysosomal function and promotes neuroinflammation to exacerbate PD pathology [55,56]. Reducing LRRK2 activity via small molecule inhibitors or via genetic knockdown in rodent models of PD reduces  $\alpha$ -synuclein aggregation, neuroinflammation, and dopaminergic neuron loss, encouraging clinical investigation of LRRK2 inhibitors [57,58]. Denali was the first to begin clinical testing of small molecules targeting LRRK2. DNL151 is an orally available, brain-penetrant inhibitor of LRRK2 that completed a Phase 1b clinical trial for PD (NCT04056689) and met target and pathway engagement goals. Two additional trials are planned for 2021.

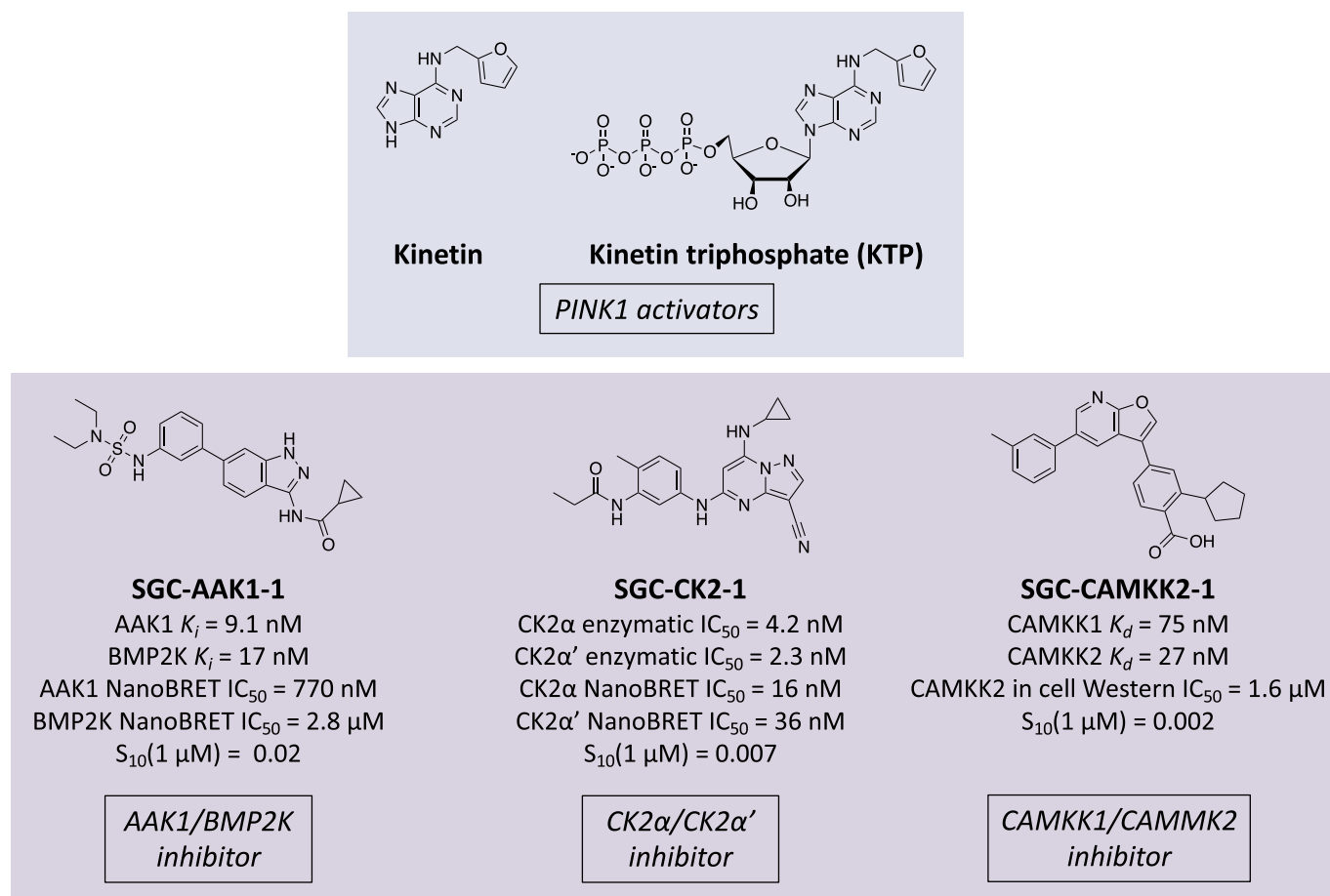
DNL201, another orally available, brain-penetrant LRRK2 inhibitor, will serve as the back-up compound to DNL151. This compound successfully completed a Phase 1b study for PD (NCT03710707). Structures of these compounds remain unpublished.

### 5.3. PINK1 activation

Mutations in PINK1 that reduce its kinase activity are associated with mitochondrial defects and result in an autosomal-recessive form of PD [59,60]. PINK1 mediates repair of mitochondrial dysfunction via responding to damage at the level of individual mitochondria and has been linked to the reduction of mitochondria-induced apoptosis in neurons [59,61–63]. Individuals homozygous for PINK1 LoF mutations can develop a form of early-onset PD that results from highly selective

dopaminergic neuronal loss and that can share the Lewy body pathology of sporadic PD [34,62,64–68]. There are 17 clinically relevant PINK1 mutations. Those mutants that impact its catalytic activity only, including PINK1 G309D, have demonstrated the most dramatic effect on neuron viability, further supporting the hypothesis that PINK activation could be neuroprotective [62,69,70]. Finally, the reduced catalytic activity observed with PINK1 G309D can be rescued by overexpression of wild-type PINK1, suggesting that increasing PINK1 activity could be an effective therapeutic strategy for PD [59].

As an approach for enhancing PINK1 activity, a neosubstrate involving the ATP analog kinetin triphosphate (KTP, Fig. 3) was developed [59]. This small molecule was designed based on the hypothesis that PINK1 exhibits altered substrate specificity [71]. KTP, which binds with higher catalytic efficiency than ATP, can be used to increase the activity of both PD-related mutant PINK1 (G309D) and wild-type PINK1 [59]. Importantly, no wild-type kinase has shown the ability to accept N<sup>6</sup>-modified ATP analogs, of which KTP is an example. This finding suggests that this compound specifically binds to PINK1. Furthermore, cells treated with the KTP precursor kinetin (Fig. 3) demonstrate higher levels of Parkin recruitment to depolarized mitochondria, reduced mitochondrial motility in axons, and lower levels of apoptosis [59]. This example supports kinase activation as a strategy for neurodegenerative disease therapy.



**Fig. 3.** Structures and associated data for high-quality kinase modulating small molecules discussed herein. Kinetin and KTP are examples of validated kinase activators targeting PINK1. SGC-AAK1-1 is a dual chemical probe that elicits AAK1 and BMP2K inhibition and a putative chemical tool for ALS- and PD-focused research. SGC-CK2-1 is a chemical probe that inhibits both catalytic subunits of CK2, a kinase implicated in AD. SGC-CAMKK2-1 is a chemical probe that inhibits both CAMKK1 and CAMMK2, the latter of which has a described role in AD.

## 6. Neurodegenerative pathways where newly disclosed chemical probes are available

There are key pathways that drive pathogenic processes in neurodegenerative diseases that are not fully understood. This incomplete characterization is partially due to a biased focus on other kinases and partially due to a lack of available reagents, including high-quality small molecule tools. In some cases, this has forced investigators to use sub-optimal tool molecules in their studies. CX-4945, one of the most commonly employed CK2 inhibitors in published studies, demonstrates sub-optimal kinome-wide selectivity, significantly inhibiting several kinases with IC<sub>50</sub> values <100 nM, and thus confounds efforts to attribute observed results to CK2 [72]. STO-609 is a comparable example that inhibits a significant number of kinases but is used in studies directed at understanding CAMKK2 function [73]. For understudied kinases like AAK1, only recently have high-quality small molecules become available to the research community [74–76].

### 6.1. SGC-AAK1-1 for AAK1 inhibition

AAK1 is widely expressed in the brain and spinal cord. Dysfunction of AAK1 is implicated in ALS, in which its increased co-localization with aggregated proteins is observed. AAK1 is misdirected into aggregates containing mutant SOD1 and neurofilament proteins in rodent models of ALS [8,77]. Expression of AAK1 protein is also decreased in human ALS spinal cords [77]. AAK1, which shows increased expression in PD patient brains, has been identified as a candidate risk factor gene for PD associated with age of onset, based on validated genome-wide association studies (GWAS) [78,79]. Its essential role in endocytosis and lysosomal sorting is suggested to contribute to PD pathogenesis [78]. In addition, AAK1 regulates  $\alpha$ -synuclein aggregation and resultant neurodegeneration in *C. elegans*, leading to the hypothesis that AAK1 inhibition would be therapeutically advantageous in PD [8,30,31].

A demonstrated role of AAK1 inhibition in enhancement of neuregulin-1-induced neuritogenesis and observation of AAK1 upregulation in postmortem cerebellum of schizophrenic patients support a role for AAK1 in the pathogenesis of schizophrenia [80]. Finally, AAK1 has potential as a novel therapeutic target for neuropathic pain [81]. An AAK1 inhibitor known as LP-935509 recapitulated AAK1 knockout in mice, resulting in dose-dependent reduction of the nociceptive behavioral response in rodent models of neuropathic pain [74]. SGC-AAK1 (Fig. 3) is a recently disclosed selective chemical probe for studying AAK1 biology that was released alongside a structurally related negative control compound that does not inhibit AAK1 [75,76]. The availability of this chemical probe set enables research aimed at illuminating the roles of AAK1 in the brain and the ability to determine whether AAK1 inhibition is therapeutically beneficial for diseases like ALS, PD, schizophrenia, and neuropathic pain.

### 6.2. SGC-CK2-1 for CK2 inhibition

Until recently, CK2 was believed to be a kinase especially required for cell cycle progression in non-neural cells [82]. This notion was challenged by the finding that CK2 is much more abundant in the mammalian brain than in any other tissue [82,83]. Accordingly, a multitude of CK2 substrates that influence neuronal and glial homeostasis exist in both the synaptic and nuclear compartments with clear implications in neuritogenesis, synaptic transmission, synaptic plasticity, and survival [82,83]. CK2 is especially important in the hippocampus, where it is associated with mechanisms underlying long-term potentiation and where neurotrophins stimulate CK2 activity [82]. CK2 is highly activated in AD and regulates many pathogenic processes [84]. Furthermore, the distribution of CK2 in brain sections of AD patients is altered [85]. CK2 is present at a significantly higher concentration in the AD particulate fraction of the brain cortex relative to an age-matched control [86]. Increased levels of CK2 have been detected in the

hippocampus and temporal cortex of AD patients compared to non-demented controls [35]. AD hippocampal neurons bearing neurofibrillary tangles (NFT) stain very strongly for CK2 [85–87]. Certainly, the known importance of CK2 and its reported overabundance in the hippocampus could contribute to the vulnerability of this brain region in AD.

CK2 regulates several pathways of pathological importance in AD, including neuroinflammation and protein aggregation. CK2 immunoreactive astrocytes are increased in AD versus non-demented controls and surround A $\beta$  deposits, suggesting a role of CK2 in the neuro-inflammatory response [35]. With respect to protein aggregation, CK2 has been shown to phosphorylate and co-localize with  $\alpha$ -synuclein in Lewy bodies found in PD and AD patient brains and to contribute to the formation of TDP-43 aggregates in ALS, frontotemporal dementia (FTD), and AD [83,88–90]. Finally, tau is a substrate of CK2 and CK2 has been suggested to play a role in its hyperphosphorylation and resultant accumulation [35,84,91]. Further, CK2 activity increases due to the presence of A $\beta$ , and thus AD may accelerate tau phosphorylation [92]. Pharmacological experiments aimed at discerning the role of CK2 in AD specific to neuroinflammation and protein aggregation (TDP-43 and tau) have been executed using sub-optimal molecules, such as CX-4945 and TBB [35,84,93,94]. These experiments can now be done using the exquisitely selective, cell-active chemical probe, SGC-CK2-1 (Fig. 3), alongside its structurally similar negative control compound [72].

### 6.3. SGC-CAMKK2-1 for CAMKK2 inhibition

CAMKK2 is an extremely abundant protein in the brain that plays a fundamental role in synaptic plasticity and memory formation [95,96]. Highlighting its essential role in the brain, CAMKK2 has been implicated in the pathogenesis of schizophrenia, bipolar disease, and neurodegeneration [97]. In the case of AD, dysregulation of CAMKK2 contributes to toxicity resulting from aberrant calcium signaling, synapse and neuronal loss, and impaired memory [95]. CAMKK2 overactivation is sufficient to induce dendritic spine loss. Inhibition of CAMKK2 activity protects hippocampal neurons against synaptotoxic effects in response to A $\beta$  oligomers in vitro and against loss of dendritic spines observed in a transgenic mouse model of AD [98,99]. Aberrant CAMKK2 in AD results in abnormal phosphorylation of transferrin, which leads to increased accumulation of iron and/or deregulated calcium homeostasis [97]. Mouse models of AD and postmortem human cerebrospinal fluid and serum samples from both early and late-stage AD patients corroborate these claims [97].

Optimized inhibitors of CAMKK2 that outperform commonly used and less selective inhibitors like STO-609 have emerged in the recent literature [73,100]. Given its enhanced selectivity profile and potency, the newly disclosed furopyridine SGC probe known as SGC-CAMKK2-1 (Fig. 3) is the best available tool molecule to study CAMKK2 biology in AD [101]. The chemical probe is offered alongside a structurally similar negative compound that should be used in parallel. Pharmacological inhibition of CAMKK2 is proposed to ameliorate the deficits caused by failed calcium homeostasis and thus be a putative treatment for AD.

## 7. Dark kinases implicated in neurodegenerative disease without high-quality chemical tools

Other recognized targets that hold promise have suffered from a dearth of tools and thus their full characterization hindered. These understudied kinases have been implicated via genetic studies as causal of neurodegenerative diseases. Two examples of understudied kinases with therapeutic potential are described here, one requires inhibition for the desired therapeutic response (MARK4) and the other would require activation (NEK1). These kinases represent two where chemical tools could be hugely impactful and could enable pivotal studies to validate underexplored targets to treat AD or ALS. Another brain-specific dark

kinase with implications in tau phosphorylation and thus neurodegeneration is BRSK2 [102]. Although potent chemical starting points have been identified that elicit BRSK2 inhibition, there is a need to improve the kinome-wide selectivity to improve their utility [103].

### 7.1. MARK4 in AD

MARK4, specifically the MARK4-S isoform, is predominantly expressed in the brain and has been characterized as a neuron-specific marker in the CNS [104–107]. Described roles in regulating synaptic function and dendritic spine morphogenesis, axonemal extension, tau phosphorylation and aggregation, and microtubule organization in neuronal cells have motivated pursuit of MARK4 inhibition as an AD therapeutic strategy [104,106,108]. MARK4 phosphorylates tau at Ser262 and causes its dissociation from microtubules and its over-expression in cells leads to tau hyperphosphorylation, resulting in morphological changes and cell death [109,110]. In AD patients, tau phosphorylation by MARK4 causes formation of NFT, a primary biomarker of the disease [111]. Due to its critical roles in AD, MARK4 was nominated as a novel target for AD as part of the Accelerating Medicines Partnership AD (AMP-AD) program, and Merck has published several papers directed at the development of MARK kinase inhibitors for AD therapy [112–115]. Significant GWAS variants associated with AD have been found surrounding the MARK4 locus [116–118]. A recent report demonstrated that mutations to the MARK4 gene can cause the properties of tau to change, making it more likely to aggregate and become insoluble [109]. Unlike the other three MARK paralogs (MARK1–3) that exhibit cytoplasmic localization, MARK4 colocalizes with the centrosome and with microtubules in cells [106]. Furthermore, a phosphorylated form of MARK4 colocalizes with phosphorylated tau in granulovacuolar degeneration bodies that progressively accumulate in AD [119]. A strong and significant elevation of MARK4 expression and MARK4-tau interactions in AD hippocampal tissue have been found in postmortem AD brains, correlating with the Braak stages of disease [120].

MARK inhibition was validated by Merck as a method for reducing both phosphorylated and total soluble tau species [113–115]. The Merck program, however, was not devoted to development of MARK4-specific inhibitors but rather inhibitors of the MARK family of kinases. MARK4 inhibition with a non-selective small molecule, methylene blue, has been shown to rescue synaptic toxicity in an animal model over-expressing this kinase and dose-dependently decrease MARK4-mediated tau phosphorylation in cells [121]. There is a need for a focused effort aimed at the development of potent and selective chemical tools targeting MARK4 to provide the reagents to be able to interrogate the importance of this kinase in mediating AD pathology.

### 7.2. NEK1 in ALS/ALS-FTD

NEK1 is an understudied kinase that is highly expressed in motor neurons and genetically associated with ALS and ALS-FTD [8,122,123]. NEK1 variants confer susceptibility to ALS/ALS-FTD, and a significant association has been identified between more than 20 heterozygous LoF NEK1 variants and both familial and sporadic ALS risk [71,124,125]. The role of NEK1 in ALS/ALS-FTD has not been well characterized. NEK1 regulates many processes, including primary ciliary and centrosome functions, the cell cycle, mitochondrial membrane permeability, apoptosis, and DNA damage responses, which may contribute to ALS/ALS-FTD pathology when its function is lost [123,126,127]. When subjected to DNA damage via  $\gamma$ -irradiation, motor neurons harboring a NEK1 variant (c.2434A > T) demonstrated significantly increased DNA damage and impaired DNA damage repair versus controls, mechanisms that could accelerate motor neuron death in ALS/ALS-FTD [128]. NEK1 also associates with other ALS-associated genes, including *ALS2*, *VAPB*, and *C21ORF2* [124,129]. *C21ORF2* codes for another protein with a role in DNA damage repair [129].

Like PINK1, since LoF is causative, restoration rather than inhibition of the NEK1 cellular role is required in ALS/ALS-FTD patients harboring mutant NEK1. Its understudied nature, however, has left NEK1 without high-quality chemical tools to enable study of its role in ALS/ALS-FTD [122]. Targeting the ATP-competitive site elicits NEK1 inhibition [130] and should phenocopy the LoF disease state. Alternative strategies, including targeting its interaction(s) with partner protein(s) via one of its many domains, must be pursued to rescue NEK1 function and restore its activity in ALS/ALS-FTD patients, possibly promoting recovery from these diseases [126,131].

## 8. Major conclusions

The scientific community has realized incredible success related to the development of kinase inhibitors, resulting in 67 FDA-approved drugs. Repurposing efforts of these kinase-targeting drugs for neurodegenerative diseases have been largely unsuccessful, as the majority of CNS-penetrant kinase inhibitors were optimized for peripheral exposure and lack the brain penetrance needed for CNS use [132,133]. GSK3 $\beta$  has been implicated as a driver of tau hyperphosphorylation in AD and examples of repurposed GSK3 inhibitors are currently in the clinic, while others are in advanced AD animal models of neuroprotection [134]. Further, in some cases such as for sarcatinib or nilvadipine in AD, the drug is being pursued due to its off-target kinase inhibition rather than inhibition of the target for which it was designed [8,135]. Finally, kinase inhibitor programs in oncology have typically not had to address species differences because they employ human xenograft animal models. Species differences will need to be considered when animal models are used in development of kinase-targeting drugs for CNS applications. Only via focused programs aimed at delivering brain-penetrant molecules for a specific neurological indication will a kinase-targeting compound advance through the clinic and be approved as a drug. Physical properties that kinase inhibitors need for CNS indications are stringent and have been reviewed [133]. Examples of these types of programs at Denali were highlighted, aimed at RIPK1 and LRRK2. While these examples focused on development of inhibitors of more well-studied kinases, they serve as proof-of-principle that kinase inhibition is a viable strategy for treating neurodegenerative diseases and is clinically tolerated when properly designed.

Most kinases discussed require therapeutic intervention in the form of inhibition to offer benefit to patients suffering from specific neurodegenerative diseases. In the case of PINK1 and NEK1, however, LoF is disease causative. The AMP-AD program and literature reports discuss many additional kinases where in neurodegenerative diseases LoF has been observed and results in disease progression [8,112]. As many kinases remain in the poorly characterized dark kinome and their putative role in disease has only been suggested, it is possible that inhibition of these kinases could also be beneficial for some patients with specific mutations or in related diseases. A high-quality inhibitor could also provide a way to transiently phenocopy the specific disease caused by the LoF variant. The PINK1 example illustrates that only through innovative approaches can kinase activation be realized and that it has utility in neurodegenerative diseases.

An overarching theme throughout has been the need to develop high-quality molecules to enable illumination of the role of kinase targets in propagating neurodegeneration. Examples of chemical tools that meet these criteria were discussed and shown (Fig. 3). As mentioned with respect to drug repurposing, the chemical probes for AAK1/BMP2K, CK2, and CAMKK1/2 were not developed for CNS diseases and are only validated for cell-based studies. As such, efforts to develop brain-penetrant molecules with appropriate in vivo exposure for advanced studies related to neurodegeneration are required. These probes demonstrate what is lacking for MARK4 and NEK1: chemical tools that definitively connect kinase inhibition with a specific phenotype. As kinases are highly druggable targets, there is undoubtedly vast untapped biological potential within the dark kinome for neurodegenerative



diseases and beyond.

## 9. General significance

Neurodegenerative diseases such as ALS, AD, and PD suffer from a lack of effective treatment options. Available therapeutic options offer patients late-stage symptom relief but fail to slow or halt disease progression [8]. Rather than continuing to pursue targets that have yielded clinical failures or duplicating efforts, there is a need to explore new therapeutically relevant targets in the pathology of neurodegenerative diseases. If they represent causative mediators of disease, these new targets could yield revolutionary disease-altering therapies. Several kinases, whether well-studied or within the dark kinome, have the potential to fall into this category and are thus promising leads in the pursuit of druggable targets for neurodegenerative disease therapy.

Supplementary data to this article can be found online at <https://doi.org/10.1016/j.bbagen.2021.130014>.

## Declaration of Competing Interest

The author declares no known competing financial interests or personal relationships that could have appeared to influence the work reported in the paper.

## Acknowledgements

The Structural Genomics Consortium is a registered charity (number 1097737) that receives funds from AbbVie, Bayer Pharma AG, Boehringer Ingelheim, Germany, Canada Foundation for Innovation, Eshelman Institute for Innovation, Genome Canada, Genentech, Innovative Medicines Initiative (EU/EFPIA), Janssen, Merck KGaA Darmstadt Germany, MSD, Novartis Pharma AG, Ontario Ministry of Economic Development and Innovation, Pfizer, São Paulo Research Foundation-FAPESP, Takeda, and Wellcome. Research reported in this publication was supported in part by NIH U24DK116204 and U54AG065187, DoD AL190107, and ALS wa1127.

## References

- [1] P. Lahiry, A. Torkamani, N.J. Schork, R.A. Hegele, Kinase mutations in human disease: interpreting genotype-phenotype relationships, *Nat. Rev. Genet.* 11 (2010) 60–74.
- [2] A.L. Hopkins, C.R. Groom, The druggable genome, *Nat. Rev. Drug Discov.* 1 (2002) 727–730.
- [3] M. Zwick, O. Kraemer, A.J. Carter, Dataset of the frequency patterns of publications annotated to human protein-coding genes, their protein products and genetic relevance, *Data Brief* 25 (2019) 104284.
- [4] P. Cohen, D. Cross, P.A. Jänne, Kinase drug discovery 20 years after imatinib: progress and future directions, *Nat. Rev. Drug Discov.* 20 (2021) 551–569.
- [5] G. Manning, D.B. Whyte, R. Martinez, T. Hunter, S. Sudarsanam, The protein kinase complement of the human genome, *Science* 298 (2002) 1912–1934.
- [6] N. Moret, C. Liu, B.M. Gyori, J.A. Bachman, A. Steppi, R. Taujale, L.-C. Huang, C. Hug, M. Berginski, S. Gomez, N. Kannan, P.K. Sorger, A resource for exploring the understudied human kinome for research and therapeutic opportunities, *BioRxiv* (2020), <https://doi.org/10.1101/2020.04.02.022277>.
- [7] Z. Xie, X. Yang, Y. Duan, J. Han, C. Liao, Small-molecule kinase inhibitors for the treatment of nononcologic diseases, *J. Med. Chem.* 64 (2021) 1283–1345.
- [8] A.I. Krahn, C. Wells, D.H. Drewry, L.K. Beitel, T.M. Durcan, A.D., Axtman defining the neural kinome: strategies and opportunities for small molecule drug discovery to target neurodegenerative diseases, *ACS Chem. Neurosci.* 11 (2020) 1871–1886.
- [9] W.S. Liang, T. Dunckley, T.G. Beach, A. Grover, D. Mastroeni, K. Ramsey, R. J. Caselli, W.A. Kukull, D. McKeel, J.C. Morris, C.M. Hulette, D. Schmechel, E. M. Reiman, J. Rogers, D.A. Stephan, Altered neuronal gene expression in brain regions differentially affected by Alzheimer's disease: a reference data set, *Physiol. Genomics* 33 (2008) 240–256.
- [10] W. Guo, T. Vandoorne, J. Steyaert, K.A. Staats, L. Van Den Bosch, The multifaceted role of kinases in amyotrophic lateral sclerosis: genetic, pathological and therapeutic implications, *Brain* 143 (2020) 1651–1673.
- [11] N. Dzamko, J. Zhou, Y. Huang, G.M. Halliday, Parkinson's disease-implicated kinases in the brain; insights into disease pathogenesis, *Front. Mol. Neurosci.* 7 (2014) 57.
- [12] P.J. Dolan, G.V.W., Johnson the role of tau kinases in Alzheimer's disease *curr. Opin. Drug Discov. Devel.* 13 (2010) 595–603.
- [13] T.R. Suk, M.W.C., Rousseaux the role of TDP-43 mislocalization in amyotrophic lateral sclerosis, *Mol. Neurodegener.* 15 (2020) 45.
- [14] S.-H. Lee, K., Suk kinase-based taming of brain microglia toward disease-modifying therapy front, *Cell. Neurosci.* 12 (2018) 474.
- [15] S. Tenreiro, K. Eckermann, T.F. Outeiro, Protein phosphorylation in neurodegeneration: friend or foe? *Front. Mol. Neurosci.* 7 (2014) 42.
- [16] A. Freischmidt, T. Wieland, B. Richter, W. Ruf, V. Schaeffer, K. Müller, N. Marroquin, F. Nordin, A. Hubers, P. Weydt, S. Pinto, R. Press, S. Millicamps, N. Molko, E. Bernard, C. Desnuelle, M.H. Soriani, J. Dorst, E. Graf, U. Nordstrom, M.S. Feiler, S. Putz, T.M. Boeckers, T. Meyer, A.S. Winkler, J. Winkelmann, M. de Carvalho, D.R. Thal, M. Otto, T. Brannstrom, A.E. Volk, P. Kursula, K.M. Danzer, P. Lichtner, I. Dikic, T. Meitinger, A.C. Ludolph, T.M. Strom, P.M. Andersen, J. H. Weishaupt, Haploinsufficiency of TBK1 causes familial ALS and fronto-temporal dementia, *Nat. Neurosci.* 18 (2015) 631–636.
- [17] S. Kläeger, S. Heinzlmeir, M. Wilhelm, H. Polzer, B. Vick, P.-A. Koenig, M. Reinecke, B. Ruprecht, S. Petzoldt, C. Meng, J. Zecha, K. Reiter, H. Qiao, D. Helm, H. Koch, M. Schoof, G. Canevari, E. Casale, S.R. Depaolini, A. Feuchtinger, Z. Wu, T. Schmidt, L. Rueckert, W. Becker, J. Huenges, A.-K. Garz, B.-O. Gohlke, D.P. Zolg, G. Kayser, T. Voorder, R. Preissner, H. Hahne, N. Tönisson, K. Kramer, K. Götze, F. Bassermann, J. Schlegl, H.-C. Ehrlich, S. Aiche, A. Walch, P.A. Greif, S. Schneider, E.R. Felder, J. Ruland, G. Médard, I. Zuerias, K. Spiekermann, B. Kuster, The target landscape of clinical kinase drugs, *Science* 358 (2017) eaan4368.
- [18] M.I. Davis, J.P. Hunt, S. Herrgard, P. Ciceri, L.M. Wodicka, G. Pallares, M. Hocker, D.K. Treiber, P.P. Zarrinkar, Comprehensive analysis of kinase inhibitor selectivity, *Nat. Biotechnol.* 29 (2011) 1046–1051.
- [19] S.V. Frye, The art of the chemical probe, *Nat. Chem. Biol.* 6 (2010) 159–161.
- [20] C.H. Arrowsmith, J.E. Audia, C. Austin, J. Baeli, J. Bennett, J. Blagg, C. Bountra, P.E. Brennan, P.J. Brown, M.E. Bunnage, C. Buser-Doepner, R.M. Campbell, A. J. Carter, P. Cohen, R.A. Copeland, B. Cravatt, J.L. Dahlin, D. Dhanak, A. M. Edwards, M. Frederiksen, S.V. Frye, N. Gray, C.E. Grimshaw, D. Hepworth, T. Howe, K.V.M. Huber, J. Jin, S. Knapp, J.D. Kotz, R.G. Kruger, D. Lowe, M. Mader, B. Marsden, A. Mueller-Fahrnow, S. Müller, R.C. O'Hagan, J. P. Overington, D.R. Owen, S.H. Rosenberg, R. Ross, B. Roth, M. Schapira, S. L. Schreiber, B. Shoichet, M. Sundström, G. Superti-Furga, J. Taunton, L. Toledo-Sherman, C. Walpole, M.A. Walters, T.M. Willson, P. Workman, R.N. Young, W. J. Zuercher, The promise and peril of chemical probes, *Nat. Chem. Biol.* 11 (2015) 536–541.
- [21] P. Workman, I. Collins, Probing the probes: fitness factors for small molecule tools, *Chem. Biol.* 17 (2010) 561–577.
- [22] A.A. Antolin, P. Workman, B. Al-Lazikani, Public resources for chemical probes: the journey so far and the road ahead, *Future Med. Chem.* 13 (2021) 731–747.
- [23] R. Zain, M. Vihinen, Structure-function relationships of covalent and non-covalent BTK inhibitors, *Front. Immunol.* 12 (2021) 694853.
- [24] J. Hall, A. Aulabaugh, F. Rajamohan, S. Liu, N. Kaila, Z.-K. Wan, M. Ryan, R. Magyar, X. Qiu, Biophysical and mechanistic insights into novel allosteric inhibitor of spleen tyrosine kinase, *J. Biol. Chem.* 287 (2012) 7717–7727.
- [25] P. Wu, M.H. Clausen, T.E. Nielsen, Allosteric small-molecule kinase inhibitors, *Pharmacol. Ther.* 156 (2015) 59–68.
- [26] S. Olivier, M. Foretz, B. Viollet, Promise and challenges for direct small molecule AMPK activators, *Biochem. Pharmacol.* 153 (2018) 147–158.
- [27] J.R. Burke, L. Cheng, K.M. Gillooly, J. Strnad, A. Zupa-Fernandez, I.M. Catlett, Y. Zhang, E.M. Heimrich, K.W. McIntyre, M.D. Cunningham, J.A. Carman, X. Zhou, D. Banas, C. Chaudhry, S. Li, C. D'Arienzo, A. Chimalakonda, X. Yang, J. H. Xie, J. Pang, Q. Zhao, S.M. Rose, J. Huang, R.M. Moslin, S.T. Wroblewski, D. S. Weinstein, L.M. Salter-Cid, Autoimmune pathways in mice and humans are blocked by pharmacological stabilization of the TYK2 pseudokinase domain, *Sci. Transl. Med.* 11 (2019) eaaw1736.
- [28] J. Yang, N. Campobasso, M.P. Biju, K. Fisher, X.-Q. Pan, J. Cottom, S. Galbraith, T. Ho, H. Zhang, X. Hong, P. Ward, G. Hofmann, B. Siegfried, F. Zappacosta, Y. Washio, P. Cao, J. Qu, S. Bertrand, D.-Y. Wang, M.S. Head, H. Li, S. Moores, Z. Lai, K. Johanson, G. Burton, C. Erickson-Miller, G. Simpson, P. Tummino, R. A. Copeland, A. Oliff, Discovery and characterization of a cell-permeable, small-molecule c-Abl kinase activator that binds to the myristoyl binding site, *Chem. Biol.* 18 (2011) 177–186.
- [29] B. Xiao, M.J. Sanders, D. Carmena, N.J. Bright, L.F. Haire, E. Underwood, B. R. Patel, R.B. Heath, P.A. Walker, S. Hallen, F. Giordanetto, S.R. Martin, D. Carling, S.J. Gamblin, Structural basis of AMPK regulation by small molecule activators, *Nat. Commun.* 4 (2013) 3017.
- [30] M. Usenovic, A.L. Knight, A. Ray, V. Wong, K.R. Brown, G.A. Caldwell, K. A. Caldwell, I. Stajlgjar, D. Krainc, Identification of novel ATP13A2 interactors and their role in  $\alpha$ -synuclein misfolding and toxicity, *Hum. Mol. Genet.* 21 (2012) 3785–3794.
- [31] A.F. Abdel-Magid, Inhibitors of adaptor-associated kinase 1 (AAK1) may treat neuropathic pain, schizophrenia, Parkinson's disease, and other disorders, *ACS Med. Chem. Lett.* 8 (2017) 595–597.
- [32] L. Martin, X. Latypova, C.M. Wilson, A. Magnaudeix, M.L. Perrin, C. Yardin, F. Ferro, Tau protein kinases: involvement in Alzheimer's disease, *Ageing Res. Rev.* 12 (2013) 289–309.
- [33] M.H. Flight, New kinase targets for Alzheimer's disease, *Nat. Rev. Drug Discov.* 12 (2013) 739.
- [34] Y. Zhang, W. Gao, K. Yang, H. Tao, H. Yang, Salt-inducible kinase 1 (SIK1) is induced by alcohol and suppresses microglia inflammation via NF- $\kappa$ B signaling, *Cell. Physiol. Biochem.* 47 (2018) 1411–1421.
- [35] A.F.N. Rosenberger, T.H.J. Morrema, W.H. Gerritsen, E.S. van Haastert, H. Snkhchyan, R. Hilhorst, A.J.M. Rozemuller, P. Scheltens, S.M. van der Vies, J.



- J.M. Hoozemans, Increased occurrence of protein kinase CK2 in astrocytes in Alzheimer's disease pathology, *J. Neuroinflamm.* 13 (2016) 4.
- [36] H. Qin, W. Yang, Z. Yan, E. Benveniste, Function of protein kinase CK2 in innate immune cells in neuroinflammation, *J. Immunol.* 202 (2019).
- [37] G.L. Simpson, J.A. Hughes, Y. Washio, S.M. Bertrand, Direct small-molecule kinase activation: novel approaches for a new era of drug discovery, *Curr. Opin. Drug Discov. Devel.* 12 (2009) 585–596.
- [38] J. Yang, N. Campobasso, M.P. Biju, K. Fisher, X.-Q. Pan, J. Cottom, S. Galbraith, T. Ho, H. Zhang, X. Hong, P. Ward, G. Hofmann, B. Siegfried, F. Zappacosta, Y. Washio, P. Cao, J. Qu, S. Bertrand, D.-Y. Wang, M.S. Head, H. Li, S. Moores, Z. Lai, K. Johanson, G. Burton, C. Erickson-Miller, G. Simpson, P. Tummino, R. A. Copeland, A. Oliff, Discovery and characterization of a cell-permeable, small-molecule c-Abl kinase activator that binds to the myristoyl binding site, *Chem. Biol.* 18 (2011) 177–186.
- [39] A. Petty, E. Myshkin, H. Qin, H. Guo, H. Miao, G.P. Tochtrop, J.-T. Hsieh, P. Page, L. Liu, D.J. Lindner, C. Acharya, A.D. MacKerell, E. Ficker, J. Song, B. Wang, A small molecule agonist of EphA2 receptor tyrosine kinase inhibits tumor cell migration in vitro and prostate cancer metastasis in vivo, *PLoS One* 7 (2012) e42120.
- [40] X. Gu, M.D. Bridges, Y. Yan, P.W. de Waal, X.E. Zhou, K.M. Suino-Powell, H.E. Xu, W.L. Hubbell, K. Melcher, conformational heterogeneity of the allosteric drug and metabolite (ADaM) site in AMP-activated protein kinase (AMPK), *J. Biol. Chem.* 293 (2018) 16994–17007.
- [41] H.W. Grievink, J. Heuberger, F. Huang, R. Chaudhary, W.A.J. Birkhoff, G. R. Tonn, S. Mosesova, R. Erickson, M. Moerland, P.C.G. Haddick, K. Searce-Levie, C. Ho, G.J. Groeneveld, DNL104, a centrally penetrant RIPK1 inhibitor, inhibits RIP1 kinase phosphorylation in a randomized Phase I ascending dose study in healthy volunteers, *Clin. Pharmacol. Ther.* 107 (2020) 406–414.
- [42] M.A. Kelliher, D.C. Seldin, P. Leder, Tal-1 induces T cell acute lymphoblastic leukemia accelerated by casin kinase I $\alpha$ , *EMBO J.* 15 (1996) 5160–5166.
- [43] A.T. Ting, F.X. Pimentel-Muinos, B. Seed, RIP mediates tumor necrosis factor receptor 1 activation of NF- $\kappa$ B but not Fas/APO-1-initiated apoptosis, *EMBO J.* 15 (1996) 6189–6196.
- [44] L. Mifflin, D. Ofengeim, J. Yuan, Receptor-interacting protein kinase 1 (RIPK1) as a therapeutic target, *Nat. Rev. Drug Discov.* 19 (2020) 553–571.
- [45] A. Degtarev, Z. Huang, M. Boyce, Y. Li, P. Jagtap, N. Mizushima, G.D. Cuny, T. J. Mitchison, M.A. Moskowitz, J. Yuan, Chemical inhibitor of nonapoptotic cell death with therapeutic potential for ischemic brain injury, *Nat. Chem. Biol.* 1 (2005) 112–119.
- [46] J.R. Lukens, P. Vogel, G.R. Johnson, M.A. Kelliher, Y. Iwakura, M. Lamkanfi, T. D. Kanneganti, RIP1-driven autoinflammation targets IL-1 $\alpha$  independently of inflammasomes and RIP3, *Nature* 498 (2013) 224–227.
- [47] X. Su, H. Wang, D. Kang, J. Zhu, Q. Sun, T. Li, K. Ding, Necrostatin-1 ameliorates intracerebral hemorrhage-induced brain injury in mice through inhibiting RIP1/RIP3 pathway, *Neurochem. Res.* 40 (2015) 643–650.
- [48] D. Ofengeim, Y. Ito, A. Najafov, Y. Zhang, B. Shan, J.P. DeWitt, J. Ye, X. Zhang, A. Chang, H. Vakifahmetoglu-Norberg, J. Geng, B. Py, W. Zhou, P. Amin, J. Berlink Lima, C. Qi, Q. Yu, B. Trapp, J. Yuan, Activation of necroptosis in multiple sclerosis, *Cell Rep.* 10 (2015) 1836–1849.
- [49] D. Ofengeim, S. Mazzitelli, Y. Ito, J.P. DeWitt, L. Mifflin, C. Zou, S. Das, X. Adiconis, H. Chen, H. Zhu, M.A. Kelliher, J.Z. Levin, J. Yuan, RIPK1 mediates a disease-associated microglial response in Alzheimer's disease, *Proc. Natl. Acad. Sci. U. S. A.* 114 (2017) E8788–E8797.
- [50] A. Degtarev, D. Ofengeim, J. Yuan, Targeting RIPK1 for the treatment of human diseases, *Proc. Natl. Acad. Sci. U. S. A.* 116 (2019) 9714–9722.
- [51] L. Mifflin, D. Ofengeim, J. Yuan, Receptor-interacting protein kinase 1 (RIPK1) as a therapeutic target, *Nat. Rev. Drug Discov.* 19 (2020) 553–571.
- [52] P.A. Harris, S.B. Berger, J.U. Jeong, R. Nagilla, D. Bandyopadhyay, N. Campobasso, C.A. Capriotti, J.A. Cox, L. Dare, X. Dong, P.M. Eidam, J. N. Finger, S.J. Hoffman, J. Kang, V. Kasparcova, B.W. King, R. Lehr, Y. Lan, L. K. Leister, J.D. Lich, T.T. MacDonald, N.A. Miller, M.T. Ouellette, C.S. Pao, A. Rahman, M.A. Reilly, A.R. Rendina, E.J. Rivera, M.C. Schaeffer, C.A. Sehon, R. R. Singhaus, H.H. Sun, B.A. Swift, R.D. Totoritis, A. Vossenkämper, P. Ward, D. D. Wisnoski, D. Zhang, R.W. Marquis, P.J. Gough, J. Bertin, Discovery of a first-in-class receptor interacting protein 1 (RIP1) kinase specific clinical candidate (GSK2982772) for the treatment of inflammatory diseases, *J. Med. Chem.* 60 (2017) 1247–1261.
- [53] S.A. Schneider, R.N. Alcalay, Precision medicine in Parkinson's disease: emerging treatments for genetic Parkinson's disease, *J. Neurol.* 267 (2020) 860–869.
- [54] R.Di Maio, E.K. Hoffman, E.M. Rocha, M.T. Keeney, L.H. Sanders, B.R. De Miranda, A. Zharikov, A. Van Laar, A.F. Stepan, T.A. Lanz, J.K. Kofler, E. A. Burton, D.R. Alessi, T.G. Hastings, J.T. Greenamyre, LRRK2 activation in idiopathic Parkinson's disease, *Sci. Transl. Med.* 10 (2018) eaar5429.
- [55] M. Taylor, D.R. Alessi, Advances in elucidating the function of leucine-rich repeat protein kinase-2 in normal cells and Parkinson's disease, *Curr. Opin. Cell Biol.* 63 (2020) 102–113.
- [56] B. Shutinoski, M. Hakimi, I.E. Harmsen, M. Lunn, J. Rocha, N. Lengacher, Y. Zhou, J. Khan, A. Nguyen, Q. Hake-Volling, D. El-Kodsi, J. Li, A. Alikashani, C. Beauchamp, J. Majithia, K. Coombs, D. Shimshek, P.C. Marcogliese, D.S. Park, J.D. Rioux, D.J. Philpott, J.M. Woulfe, S. Hayley, S. Sad, J.J. Tomlinson, E. G. Brown, M.G. Schlossmacher, Lrrk2 alleles modulate inflammation during microbial infection of mice in a sex-dependent manner, *Sci. Transl. Med.* 11 (2019) eaas9292.
- [57] J.P. Daher, L.A. Volpicelli-Daley, J.P. Blackburn, M.S. Moehle, A.B. West, Abrogation of  $\alpha$ -synuclein-mediated dopaminergic neurodegeneration in LRRK2-deficient rats, *Proc. Natl. Acad. Sci. U. S. A.* 111 (2014) 9289–9294.
- [58] J.P. Daher, H.A. Abdelmotilib, X. Hu, L.A. Volpicelli-Daley, M.S. Moehle, K. B. Fraser, E. Needle, Y. Chen, S.J. Steyn, P. Galatsis, W.D. Hirst, A.B. West, Leucine-rich repeat kinase 2 (LRRK2) pharmacological inhibition abates  $\alpha$ -synuclein gene-induced neurodegeneration, *J. Biol. Chem.* 290 (2015) 19433–19444.
- [59] Nicholas T. Hertz, A. Berthet, Martin L. Sos, Kurt S. Thorn, Al L. Burlingame, K. Nakamura, M. Kevan, Shokat a neo-substrate that amplifies catalytic activity of Parkinson's-disease-related kinase PINK1, *Cell* 154 (2013) 737–747.
- [60] E.M. Valente, P.M. Abou-Sleiman, V. Caputo, M.M. Muqit, K. Harvey, S. Gispert, Z. Ali, D. Del Turco, A.R. Bentivoglio, D.G. Healy, A. Albanese, R. Nussbaum, R. González-Maldonado, T. Deller, S. Salvi, P. Cortelli, W.P. Gilks, D.S. Latchman, R.J. Harvey, B. Dallapiccola, G. Auburger, N.W. Wood, Hereditary early-onset Parkinson's disease caused by mutations in PINK1, *Science* 304 (2004) 1158–1160.
- [61] H. Deng, J. Jankovic, Y. Guo, W. Xie, W. Le, Small interfering RNA targeting the PINK1 induces apoptosis in dopaminergic cells SH-SY5Y, *Biochem. Biophys. Res. Commun.* 337 (2005) 1133–1138.
- [62] A. Petit, T. Kawarai, E. Paitel, N. Sanjo, M. Maj, M. Scheid, F. Chen, Y. Gu, H. Hasegawa, S. Salehi-Rad, L. Wang, E. Rogaeva, P. Fraser, B. Robinson, P. St George-Hyslop, A. Tandon, Wild-type PINK1 prevents basal and induced neuronal apoptosis, a protective effect abrogated by Parkinson disease-related mutations, *J. Biol. Chem.* 280 (2005) 34025–34032.
- [63] X. Wang, D. Winter, G. Ashrafi, J. Schlehe, Y.L. Wong, D. Selkoe, S. Rice, J. Steen, M.L. LaVoie, T.L. Schwarz, PINK1 and Parkin target Miro for phosphorylation and degradation to arrest mitochondrial motility, *Cell* 147 (2011) 893–906.
- [64] C.A. Gautier, T. Kitada, J. Shen, Loss of PINK1 causes mitochondrial functional defects and increased sensitivity to oxidative stress, *Proc. Natl. Acad. Sci. U. S. A.* 105 (2008) 11364–11369.
- [65] S. Geisler, K.M. Holmström, A. Treis, D. Skujat, S.S. Weber, F.C. Fiesel, P.J. Kahle, W. Springer, The PINK1/Parkin-mediated mitophagy is compromised by PD-associated mutations, *Autophagy* 6 (2010) 871–878.
- [66] M.E. Haque, K.J. Thomas, C. D'Souza, S. Callaghan, T. Kitada, R.S. Slack, P. Fraser, M.R. Cookson, A. Tandon, D.S. Park, Cytoplasmic Pink1 activity protects neurons from dopaminergic neurotoxin MPTP, *Proc. Natl. Acad. Sci. U. S. A.* 105 (2008) 1716–1721.
- [67] C. Henchcliffe, M.F. Beal, Mitochondrial biology and oxidative stress in Parkinson disease pathogenesis, *Nat. Clin. Pract. Neurol.* 4 (2008) 600–609.
- [68] L. Samaranch, O. Lorenzo-Betancor, J.M. Arbelo, I. Ferrer, E. Lorenzo, J. Irigoyen, M.A. Pastor, C. Marrero, C. Isla, J. Herrera-Henriquez, P. Pastor, PINK1-linked parkinsonism is associated with Lewy body pathology, *Brain* 133 (2010) 1128–1142.
- [69] S. Song, S. Jang, J. Park, S. Bang, S. Choi, K.-Y. Kwon, X. Zhuang, E. Kim, J. Chung, Characterization of PINK1 (PTEN-induced putative kinase 1) mutations associated with Parkinson disease in mammalian cells and Drosophila, *J. Biol. Chem.* 288 (2013) 5660–5672.
- [70] J.W. Pridgeon, J.A. Olzmann, L.S. Chin, L. Li, PINK1 protects against oxidative stress by phosphorylating mitochondrial chaperone TRAP1, *PLoS Biol.* 5 (2007) e172.
- [71] K.P. Kenna, P.T. van Doornmaal, A.M. Dekker, N. Ticozzi, B.J. Kenna, F. P. Diekstra, W. van Rheenen, K.R. van Eijk, A.R. Jones, P. Keagle, A. Shatunov, W. Sproviero, B.N. Smith, M.A. van Es, S.D. Topp, A. Kenna, J.W. Miller, C. Fallini, C. Tiloca, R.L. McLaughlin, C. Vance, C. Troakes, C. Colombrita, G. Mora, A. Calvo, F. Verde, S. Al-Sarraj, A. King, D. Calini, J. de Belleroche, F. Baas, A.J. van der Kooij, M. de Visser, A.L. Ten Asbroek, P.C. Sapp, D. McKenna-Yasek, M. Polak, S. Asress, J.L. Munoz-Blanco, T.M. Strom, T. Meitinger, K. E. Morrison, G. Lauria, K.L. Williams, P.N. Leigh, G.A. Nicholson, I.P. Blair, C. S. Leblond, P.A. Dion, G.A. Rouleau, H. Pall, P.J. Shaw, M.R. Turner, K. Talbot, F. Taroni, K.B. Boylan, M. Van Blitterswijk, R. Rademakers, J. Esteban-Perez, A. Garcia-Redondo, P. Van Damme, W. Robberecht, A. Chio, C. Gellera, C. Drepper, M. Sendtner, A. Ratti, J.D. Glass, J.S. Mora, N.A. Basak, O. Hardiman, A.C. Ludolph, P.M. Andersen, J.H. Weishaupt, R.H. Brown Jr., A. Al-Chalabi, V. Silani, C.E. Shaw, L.H. van den Berg, J.H. Veldink, J.E. Landers, NEK1 variants confer susceptibility to amyotrophic lateral sclerosis, *Nat. Genet.* 48 (2016) 1037–1042.
- [72] C.I. Wells, D.H. Drewry, J.E. Pickett, A. Tjaden, A. Krämer, S. Müller, L. Geyens, D. Menyhard, D.W. Litchfield, S. Knapp, A.D. Axtman, Development of a potent and selective chemical probe for the pleiotropic kinase CK2, *Cell Chem. Biol.* 28 (2021).
- [73] S.N. O'Byrne, J.W. Scott, J.R. Pilotte, A.D.S. Santiago, C.G. Langendorf, J. S. Oakhill, B.J. Edulful, R.M. Couñago, C.I. Wells, W.J. Zuercher, T.M. Willson, D. H. Drewry, In depth analysis of kinase cross screening data to identify CAMKK2 inhibitory scaffolds, *Molecules* 25 (2020) 325.
- [74] W. Kostich, B.D. Hamman, Y.-W. Li, S. Naidu, K. Dandapani, J. Feng, A. Easton, C. Bourin, K. Baker, J. Allen, K. Savelieva, J.V. Louis, M. Dokania, S. Elavazhagan, P. Vattikundala, V. Sharma, M.L. Das, G. Shankar, A. Kumar, V.K. Holenarsipur, M. Gulianello, T. Molski, J.M. Brown, M. Lewis, Y. Huang, Y. Lu, R. Pieschl, K. O'Malley, J. Lippy, A. Nouraldein, T.H. Lanthorn, G. Ye, A. Wilson, A. Balakrishnan, R. Denton, J.E. Grace, K.A. Lentz, K.S. Santone, Y. Bi, A. Main, J. Swaffield, K. Carson, S. Mandlekar, R.K. Vikramadithyan, S.J. Nara, C. Dzierba, J. Bronson, J.E. Macor, R. Zaczek, R. Westphal, L. Kiss, L. Bristow, C.M. Conway, B. Zambrowicz, C.F. Albright, Inhibition of AAK1 kinase as a novel therapeutic approach to treat neuropathic pain, *J. Pharmacol. Exp. Ther.* 358 (2016) 371–386.
- [75] C. Wells, R.M. Couñago, J.C. Limas, T.L. Almeida, J.G. Cook, D.H. Drewry, J. M. Elkins, O. Gileadi, N.R. Kapadia, A. Lorente-Macias, J.E. Pickett, A. Riemen, R. R. Ruela-de-Sousa, T.M. Willson, C. Zhang, W.J. Zuercher, R. Zutshi, A.

- D. Axtman, SGC-AAK1-1: a chemical probe targeting AAK1 and BMP2K, *ACS Med. Chem. Lett.* 11 (2019) 340–345.
- [76] M.J. Agajanian, M.P. Walker, A.D. Axtman, R.R. Ruela-de-Sousa, D.S. Serafin, A. D. Rabinowitz, D.M. Graham, M.B. Ryan, T. Tamir, Y. Nakamichi, M. V. Gammons, J.M. Bennett, R.M. Counago, D.H. Drewry, J.M. Elkins, C. Gileadi, O. Gildadi, P.H. Godoi, N. Kapadia, S. Muller, A.S. Santiago, F.J. Sorrell, C. I. Wells, O. Fedorov, T.M. Willson, W.J. Zuercher, M.B., Major WNT activates the AAK1 kinase to promote clathrin-mediated endocytosis of LRP6 and establish a negative feedback loop, *Cell Rep.* 26 (2019) 79–83.
- [77] B. Shi, S.D. Conner, J. Liu, Dysfunction of endocytic kinase AAK1 in ALS, *Int. J. Mol. Sci.* 15 (2014) 22918–22932.
- [78] C. Progeni Investigators, L. Molecular Genetic, C. GenePd Investigators, L. J. C. Latourelle, N. Pankratz, A. Dumitriu, J.B. Wilk, S. Goldwurm, G. Pezzoli, C. B. Mariani, A.L. DeStefano, C. Halter, J.F. Gusella, W.C. Nichols, R.H. Myers, T. Foroud, Molecular Genetic Genomewide association study for onset age in Parkinson disease, *BMC Med. Genet.* 10 (2009) 98.
- [79] Y. Zhang, M. James, F.A. Middleton, R.L. Davis, ranscriptional analysis of multiple brain regions in Parkinson's disease supports the involvement of specific protein processing, energy metabolism, and signaling pathways, and suggests novel disease mechanisms, *Am. J. Med. Genet. B Neuropsychiatr. Genet.* 137b (2005) 5–16.
- [80] L. Kuai, S.-E. Ong, J.M. Madison, X. Wang, J.R. Duvall, T.A. Lewis, C.J. Luce, S. D. Conner, D.A. Pearlman, J.L. Wood, S.L. Schreiber, S.A. Carr, E.M. Scolnick, S. J. Haggarty, AAK1 identified as an inhibitor of neuregulin-1/ErbB4-dependent neurotrophic factor signaling using integrative chemical genomics and proteomics, *Chem. Biol.* 18 (2011) 891–906.
- [81] D. Dubuisson, S.G. Dennis, The formalin test: a quantitative study of the analgesic effects of morphine, meperidine, and brain stem stimulation in rats and cats, *Pain* 4 (1977) 161–174.
- [82] P.R. Blanquet, Casein kinase 2 as a potentially important enzyme in the nervous system, *Prog. Neurobiol.* 60 (2000) 211–246.
- [83] J. Castello, A. Ragnauth, E. Friedman, H. Rebholz, CK2—an emerging target for neurological and psychiatric disorders, *Pharmaceuticals* 10 (2017) 7.
- [84] Q. Zhang, Y. Xia, Y. Wang, Y. Shentu, K. Zeng, Y.A.R. Mahaman, F. Huang, M. Wu, D. Ke, Q. Wang, B. Zhang, R. Liu, J.-Z. Wang, K. Ye, X. Wang, CK2 phosphorylating I2PP2A/SET mediates tau pathology and cognitive impairment, *Front. Mol. Neurosci.* 11 (2018) 146.
- [85] D.S. Iimoto, E. Masliah, R. DeTeresa, R.D. Terry, T. Saitoh, Aberrant casein kinase II in Alzheimer's disease, *Brain Res.* 507 (1990) 273–280.
- [86] L. Baum, E. Masliah, D.S. Iimoto, L.A. Hansen, W.C. Halliday, T. Saitoh, Casein kinase II is associated with neurofibrillary tangles but is not an intrinsic component of paired helical filaments, *Brain Res.* 573 (1992) 126–132.
- [87] E. Masliah, D.S. Iimoto, M. Mallory, T. Albright, L. Hansen, T. Saitoh, Casein kinase II alteration precedes tau accumulation in tangle formation, *Am. J. Pathol.* 140 (1992) 263–268.
- [88] M.Y. Ryu, D.W. Kim, K. Arima, M.M. Mouradian, S.U. Kim, G. Lee, Localization of CKII beta subunits in Lewy bodies of Parkinson's disease, *J. Neurol. Sci.* 266 (2008) 9–12.
- [89] M. Hasegawa, T. Arai, T. Nonaka, F. Kametani, M. Yoshida, Y. Hashizume, T. G. Beach, E. Buratti, F. Baralle, M. Morita, I. Nakano, T. Oda, K. Tsuchiya, H. Akiyama, Phosphorylated TDP-43 in frontotemporal lobar degeneration and amyotrophic lateral sclerosis, *Ann. Neurol.* 64 (2008) 60–70.
- [90] A. Ishii, T. Nonaka, S. Taniguchi, T. Saito, T. Arai, D. Mann, T. Iwatsubo, S.-I. Hisanaga, M. Goedert, M. Hasegawa, Casein kinase 2 is the major enzyme in brain that phosphorylates Ser129 of human  $\alpha$ -synuclein: Implication for  $\alpha$ -synucleinopathies, *FEBS Lett.* 581 (2007) 4711–4717.
- [91] J. Avila, L. Ulloa, J. González, F. Moreno, J. Díaz-Nido, Phosphorylation of microtubule-associated proteins by protein kinase CK2 in neurogenesis, *Cell. Mol. Biol. Res.* 40 (1994) 573–579.
- [92] D.I. Perez, C. Gil, A. Martinez, Protein kinases CK1 and CK2 as new targets for neurodegenerative diseases, *Med. Res. Rev.* 31 (2011) 924–954.
- [93] D. Moujalled, J.L. James, S.J. Parker, G.E. Lidgerwood, C. Duncan, J. Meyerowitz, T. Nonaka, M. Hasegawa, K.M. Kanninen, A. Grubman, J.R. Liddell, P.J. Crouch, A.R. White, Kinase inhibitor screening identifies cyclin-dependent kinases and glycogen synthase kinase 3 as potential modulators of TDP-43 cytosolic accumulation during cell stress, *PLoS One* 8 (2013) e67433.
- [94] H. Yadikar, I. Torres, G. Aiello, M. Kurup, Z. Yang, F. Lin, F. Kobeissy, R. Yost, K. K. Wang, Screening of tau protein kinase inhibitors in a tauopathy-relevant cell-based model of tau hyperphosphorylation and oligomerization, *PLoS One* 15 (2020) e0224952.
- [95] A. Ghosh, K.P. Giese, Calcium/calmodulin-dependent kinase II and Alzheimer's disease, *Mol. Brain* 8 (2015) 78.
- [96] P.I. Hanson, H. Schulman, Neuronal Ca<sup>2+</sup>/calmodulin-dependent protein kinases, *Annu. Rev. Biochem.* 61 (1992) 559–601.
- [97] M.G. Sabbir, Loss of Ca(2+)/calmodulin dependent protein kinase kinase 2 leads to aberrant transferrin phosphorylation and trafficking: a potential biomarker for Alzheimer's disease, *Front. Mol. Biosci.* 5 (2018) 99.
- [98] G. Mairet-Coello, J. Courchet, S. Pieraut, V. Courchet, A. Maximov, F. Polleux, The CAMKK2-AMPK kinase pathway mediates the synaptotoxic effects of A $\beta$  oligomers through tau phosphorylation, *Neuron* 78 (2013) 94–108.
- [99] C. Thornton, Nicola J. Bright, M. Sastre, J. Phillip, D. Muckett, Carling AMP-activated protein kinase (AMPK) is a tau kinase, activated in response to amyloid  $\beta$ -peptide exposure, *Biochem. J.* 434 (2011) 503–512.
- [100] B.J. Edful, S.N. O'Byrne, L. Temme, C.R.M. Asquith, Y. Liang, A. Picado, J. R. Pilotte, M.A. Hossain, C.I. Wells, W.J. Zuercher, C.M.C. Catta-Preta, P. Z. Ramos, A.D.S. Santiago, R.M. Counago, C.G. Langendorf, K. Nay, J.S. Oakhill, T.L. Pulliam, C. Lin, D. Awad, T.M. Willson, D.E. Frigo, J.W. Scott, D.H. Drewry, Hinge binder scaffold hopping identifies potent calcium/calmodulin-dependent protein kinase-2 (CAMKK2) inhibitor chemotypes, *J. Med. Chem.* 64 (2020) 10849–10877.
- [101] <https://www.thesgc.org/chemical-probes/SGC-CAMKK2-1>.
- [102] N.J. Bright, D. Carling, C. Thornton, Investigating the regulation of brain-specific kinases 1 and 2 by phosphorylation, *J. Biol. Chem.* 283 (2008) 14946–14954.
- [103] T.Y. Tamir, D.H. Drewry, C. Wells, M.B. Major, A.D. Axtman, PKIS deep dive yields a chemical starting point for dark kinases and a cell active BRSK2 inhibitor, *Sci. Rep.* 10 (2020) 15826.
- [104] H.-S. Gong, Y. Guo, C. Tian, W.-L. Xie, Q. Shi, J. Zhang, Y. Xu, S.-B. Wang, B.-Y. Zhang, C. Chen, Y. Liu, X.-P. Dong, Reduction of protein kinase MARK4 in the brains of experimental scrapie rodents and human prion disease correlates with deposits of PrP<sup>Sc</sup>, *Int. J. Mol. Med.* 30 (2012) 569–578.
- [105] R.F. Moroni, S.De Biasi, P. Colapietro, L. Larizza, A. Beghini, Distinct expression pattern of microtubule-associated protein/microtubule affinity-regulating kinase 4 in differentiated neurons, *Neuroscience* 143 (2006) 83–94.
- [106] B. Trinczek, M. Brajenovic, A. Ebneth, G. Drewes, MARK4 is a novel microtubule-associated proteins/microtubule affinity-regulating kinase that binds to the cellular microtubule network and to centrosomes, *J. Biol. Chem.* 279 (2004) 5915–5923.
- [107] F. Naz, F. Anjum, A. Islam, F. Ahmad, M.I. Hassan, Microtubule affinity-regulating kinase 4: structure, function, and regulation, *Cell Biochem. Biophys.* 67 (2013) 485–499.
- [108] S. Kuhns, K.N. Schmidt, J. Reymann, D.F. Gilbert, A. Neuner, B. Hub, R. Carvalho, P. Wiedemann, H. Zentgraf, H. Erfle, U. Klingmüller, M. Boutros, G. Pereira, The microtubule affinity regulating kinase MARK4 promotes axoneme extension during early ciliogenesis, *J. Cell Biol.* 200 (2013) 505–522.
- [109] T. Oba, T. Saito, A. Asada, S. Shimizu, K.M. Iijima, K. Ando, Microtubule affinity-regulating kinase 4 with an Alzheimer's disease-related mutation promotes tau accumulation and exacerbates neurodegeneration, *J. Biol. Chem.* 295 (2020) 17138–17147.
- [110] G. Drewes, A. Ebneth, U. Preuss, E.-M. Mandelkow, E. Mandelkow, MARK, a novel family of protein kinases that phosphorylate microtubule-associated proteins and trigger microtubule disruption, *Cell* 89 (1997) 297–308.
- [111] J.Y. Chin, R.B. Knowles, A. Schneider, G. Drewes, E.M. Mandelkow, B.T. Hyman, Microtubule-affinity regulating kinase (MARK) is tightly associated with neurofibrillary tangles in Alzheimer brain: a fluorescence resonance energy transfer study, *J. Neurobiol. Exp. Neurol.* 59 (2000) 966–971.
- [112] R.J. Hodes, N. Buckholtz, Accelerating Medicines Partnership: Alzheimer's Disease (AMP-AD) knowledge portal aids Alzheimer's drug discovery through open data sharing, *Expert Opin. Ther. Targets* 20 (2016) 389–391.
- [113] J.D. Katz, A. Haidle, K.K. Childers, A.A. Zabierek, J.P. Jewell, Y. Hou, M. D. Altman, A. Szewczak, D. Chen, A. Harsch, M. Hayashi, L. Warren, M. Hutton, H. Nuthall, H.P. Su, S. Munshi, M.G. Stanton, I.W. Davies, B. Munoz, A. Northrup, Structure guided design of a series of selective pyrrolopyrimidinone MARK inhibitors, *Bioorg. Med. Chem. Lett.* 27 (2017) 114–120.
- [114] D.L. Sloman, N. Noutci, M.D. Altman, D. Chen, A.C. Mislak, A. Szewczak, M. Hayashi, L. Warren, T. Dellovade, Z. Wu, J. Marcus, D. Walker, H.P. Su, S. C. Edavettal, S. Munshi, M. Hutton, H. Nuthall, M.G. Stanton, Optimization of microtubule affinity regulating kinase (MARK) inhibitors with improved physical properties, *Bioorg. Med. Chem. Lett.* 26 (2016) 4362–4366.
- [115] A.M. Haidle, K.K. Childers, A.A. Zabierek, J.D. Katz, J.P. Jewell, Y. Hou, M. D. Altman, A. Szewczak, D. Chen, A. Harsch, M. Hayashi, L. Warren, M. Hutton, H. Nuthall, M.G. Stanton, I.W. Davies, B. Munoz, A. Northrup, MARK inhibitors: declaring a No-Go decision on a chemical series based on extensive DMPK experimentation, *Bioorg. Med. Chem. Lett.* 27 (2017) 109–113.
- [116] G.A. Pathak, Z. Zhou, T.K. Silzer, R.C. Barber, N.R. Phillips, Two-stage Bayesian GWAS of 9576 individuals identifies SNP regions that are targeted by miRNAs inversely expressed in Alzheimer's and cancer, *Alzheimers Dement.* 16 (2020) 162–177.
- [117] J. Schwartztruber, S. Cooper, J.Z. Liu, I. Barrio-Hernandez, E. Bello, N. Kumasaka, A.M.H. Young, R.J.M. Franklin, T. Johnson, K. Estrada, D. J. Gaffney, P. Beltrao, A. Bassett, Genome-wide meta-analysis, fine-mapping and integrative prioritization implicate new Alzheimer's disease risk genes, *Nat. Genet.* 53 (2021) 392–402.
- [118] C. Bellenguez, F. Küçükali, I. Jansen, V. Andrade, S. Moreno-Grau, N. Amin, A. Naj, B. Grenier-Boley, R. Campos-Martin, P. Holmans, A. Boland, L. Kleiheidam, V. Damotte, S. van der Lee, T. Kuulasmaa, Q. Yang, I. de Rojas, J. Bis, A. Yaqub, I. Prokic, M. Costa, J. Chapuis, S. Ahmad, V. Giedraitis, M. Boada, D. Aarsland, P. Garcia-González, C. Abdelnour, E. Alarcón-Martín, M. Alegret, I. Alvarez, V. Álvarez, N. Armstrong, A. Tsolaki, C. Antúnez, I. Appollonio, M. Arcaro, S. Archetti, A.A. Pastor, B. Arosio, L. Athanasiu, H. Bailly, N. Banaj, M. Baquero, A. Belén Pastor, L. Benussi, C. Berr, C. Besse, V. Bessi, G. Binetti, A. Bizzarro, D. Alcolea, R. Blesa, B. Borroni, S. Boschi, P. Bossù, G. Bråthen, C. Bresner, K. Brookes, L.I. Brusco, K. Bürger, M. Bullido, V. Burholt, W. Bush, M. Calero, C. Dufouil, A. Carracedo, R. Cecchetti, L. Cervera-Carles, C. Charbonnier, C. Chillotti, H. Brodaty, S. Ciccone, J.A.H.R. Claassen, C. Clark, E. Conti, A. Corma-Gómez, E. Costantini, C. Custodero, D. Daian, M. C. Dalmaso, A. Daniele, E. Dardiotis, J.-F. Dartigues, P.P. de Deyn, K. de Paiva Lopes, L. de Witte, S. Debette, J. Deckert, T. del Ser, N. Denning, A. DeStefano, M. Dichgans, J. Diehl-Schmid, M. Diez-Fairen, P.D. Rossi, S. Djurovic, E. Duron, E. Düzel, S. Engelborghs, V. Escott-Price, A. Espinosa, D. Buiza-Rueda, M. Ewers, F. Tagliaivini, S.F. Nielsen, L. Farotti, C. Fenoglio, M. Fernández-Fuertes, J. Hardy, R. Ferrari, C. Ferreira, E. Ferri, B. Fin, P. Fischer, T. Fladby, K. Fließbach, J. Fortea, S. Postinelli, N. Fox, E. Franco-Macias, A. Frank-García, L. Froelich,

- D. Galimberti, J.M. García-Alberca, S. Garcia-Madrone, G. García-Ribas, G. Chene, R. Ghidoni, I. Giegling, G. Giaccone, O. Goldhardt, A. González-Pérez, C. Graff, G. Grande, E. Green, T. Grimmer, E. Grünblatt, T. Guetta-Baranes, A. Haapasalo, G. Hadjigeorgiou, J. Haines, K. Hamilton-Nelson, H. Hampel, O. Hanon, A. Hartmann, L. Hausner, J. Harwood, S. Heilmann-Heimbach, S. Helisalmi, M. Heneka, I. Hernández, M. Herrmann, P. Hoffmann, C. Holmes, H. Holstege, R.H. Vilas, M. Hulsman, J. Humphrey, G.J. Biessels, C. Johansson, P. Kehoe, L. Kilander, A.K. Ståhlbom, M. Kivipelto, A. Koivisto, J. Kornhuber, M. Kosmidis, P. Kuksa, B. Kunkle, C. Lage, E. Laukka, A. Lauria, C.-Y. Lee, J. Lehtisalo, C. Satizabal, O. Lerch, A. Lleó, R. Lopez, O. Lopez, A.L. de Munain, S. Love, M. Löwemark, L. Luckcuck, J. Macías, C. MacLeod, W. Maier, F. Mangialasche, M. Spallazzi, M. Marquié, R. Marshall, E. Martin, A. Martín Montes, C.M. Rodríguez, C. Masullo, R. Mayeux, S. Mead, P. Mecocci, M. Medina, A. Meggy, S. Mendoza, M. Menéndez-González, P. Mir, M.T. Perinán, M. Mol, L. Molina-Porcel, L. Montreuil, L. Morelli, F. Moreno, K. Morgan, M. Nöthen, C. Muchnik, B. Nacmias, T. Ngandu, G. Nicolas, B. Nordestgaard, R. Orlaso, A. Orellana, M. Orsini, G. Ortega, A. Padovani, P. Caffarra, G. Papenberg, L. Parnetti, F. Pasquier, P. Pastor, A. Pérez-Cordón, J. Pérez-Tur, P. Pericard, O. Peters, Y.A.L. Pijnenburg, J.A. Pineda, G. Piñol-Ripoll, C. Pisanu, T. Polak, J. Popp, D. Posthuma, J. Priller, R. Puerta, O. Quenez, I. Quintela, J. Q. Thomassen, A. Rábano, I.Ramakers Rainero, L.M. Real, M.J.T. Reinders, S. Riedel-Heller, P. Riederer, E. Rodríguez-Rodríguez, A. Rongve, I.R. Allende, M. Rosende-Roca, J.L. Royo, E. Rubino, D. Rujescu, M.E. Sáez, P. Sakka, I. Saltvedt, A. Sanabria, M.B. Sánchez-Arjona, F. Sanchez-García, S. Mehrabian, P. Sánchez-Juan, R. Sánchez-Valle, S.B. Sando, M. Scamosci, N. Scarmeas, E. Scarpini, P. Scheltens, N. Scherbaum, M. Scherer, M. Schmid, A. Schneider, J. M. Schott, G. Selbæk, J. Sha, A.A. Shadrin, O. Skrobot, G.J.L. Snijders, H. Soininen, V. Solfrizzi, A. Solomon, S. Sorbi, O. Sotolongo-Grau, G. Spalletta, A. Spottke, A. Squassina, J.P. Tartari, L. Tárraga, N. Tesí, A. Thalamuthu, T. Tegos, L. Traykov, L. Tremolizzo, A. Tybjærg-Hansen, A. Uitterlinden, A. Ullgren, I. Ulstein, S. Valero, C. Van Broeckhoven, A. van der Lugt, J. Van Dongen, J. van Rooij, J. van Swieten, R. Vandenberghe, F. Verhey, J.-S. Vidal, J. Vogelgsang, M. Vyhnaek, M. Wagner, D. Wallon, L.-S. Wang, R. Wang, L. Weinhold, J. Wiltfang, G. Windle, B. Woods, M. Yannakoulia, Y. Zhao, M. Zulaica, M. Serrano-Rios, D. Seripa, E. Stordal, L.A. Farrer, B.M. Psaty, M. Ghanbari, T. Raj, P. Sachdev, K. Mather, F. Jessen, M.A. Ikram, A. de Mendonça, J. Hort, M. Tsolaki, M.A. Pericak-Vance, P. Amouyel, J. Williams, R. Frikke-Schmidt, J. Clarimon, J.-F. Deleuze, G. Rossi, S. Seshadri, O. A. Andreassen, M. Ingelsson, M. Hiltunen, K. Sleegers, G.D. Schellenberg, C. M. van Duijn, R. Sims, W.M. van der Flier, A. Ruiz, A. Ramirez, J.-C. Lambert, New insights on the genetic etiology of Alzheimer's and related dementia, *medRxiv* (2020), <https://doi.org/10.1101/2020.10.01.20200659>.
- [119] H. Lund, E. Gustafsson, A. Svensson, M. Nilsson, M. Berg, D. Sunnemark, G. von Euler, MARK4 and MARK3 associate with early tau phosphorylation in Alzheimer's disease granulovacuolar degeneration bodies, *Acta Neuropathol. Commun.* 2 (2014) 22.
- [120] G.J. Gu, H. Lund, D. Wu, A. Blokzijl, C. Classon, G. von Euler, U. Landegren, D. Sunnemark, M. Kamali-Moghaddam, Role of individual MARK isoforms in phosphorylation of tau at Ser262 in Alzheimer's disease, *Neuromolecular Med.* 15 (2013) 458–469.
- [121] W. Sun, S. Lee, X. Huang, S. Liu, M. Inayathullah, K.-M. Kim, H. Tang, J. W. Ashford, J. Rajadas, Attenuation of synaptic toxicity and MARK4/PAR1-mediated Tau phosphorylation by methylene blue for Alzheimer's disease treatment, *Sci. Rep.* 6 (2016) 34784.
- [122] C.I. Wells, N.R. Kapadia, R.M. Couñago, D.H. Drewry, In depth analysis of kinase cross screening data to identify chemical starting points for inhibition of the Nek family of kinases, *Med. Chem. Comm.* 9 (2018) 44–66.
- [123] H.P. Nguyen, S. Van Mossevelde, L. Dillen, J.L. De Bleeker, M. Moisse, P. Van Damme, C. Van Broeckhoven, J. van der Zee, S. Engelborghs, R. Crols, P.P. De Deyn, P. De Jonghe, J. Baets, P. Cras, R. Mercelis, R. Vandenberghe, A. Sieben, P. Santens, A. Ivanou, O. Deryck, L. Vanopdenbosch, J. Delbeck, NEK1 genetic variability in a Belgian cohort of ALS and ALS-FTD patients, *Neurobiol. Aging* 61 (2018), pp. 255.e251–255.e257.
- [124] E.T. Cirulli, B.N. Lasseigne, S. Petrovski, P.C. Sapp, P.A. Dion, C.S. Leblond, J. Couthouis, Y.-F. Lu, Q. Wang, B.J. Krueger, Z. Ren, J. Keebler, Y. Han, S. E. Levy, B.E. Boone, J.R. Wimbish, L.L. Waite, A.L. Jones, J.P. Carulli, A.G. Day-Williams, J.F. Staropoli, W.W. Xin, A. Chesi, A.R. Raphael, D. McKenna-Yasek, J. Cady, J.M.B. Vianney de Jong, K.P. Kenna, B.N. Smith, S. Topp, J. Miller, A. Gkazi, A. Al-Chalabi, L.H. van den Berg, J. Veldink, V. Silani, N. Ticozzi, C. E. Shaw, R.H. Baloh, S. Appel, E. Simpson, C. Lagier-Tourenne, S.M. Pulst, S. Gibson, J.Q. Trojanowski, L. Elman, L. McCluskey, M. Grossman, N. A. Schneider, W.K. Chung, J.M. Ravits, J.D. Glass, K.B. Sims, V.M. Van Deerlin, T. Maniatis, S.D. Hayes, A. Ordeurau, S. Swarup, J. Landers, F. Baas, A.S. Allen, R. S. Bedlack, J.W. Harper, A.D. Gitler, G.A. Rouleau, R. Brown, M.B. Harms, G. M. Cooper, T. Harris, R.M. Myers, D.B. Goldstein, Exome sequencing in amyotrophic lateral sclerosis identifies risk genes and pathways, *Science* 347 (2015) 1436–1441.
- [125] D. Brenner, K. Müller, T. Wieland, P. Weidt, S. Böhm, D. Lulé, A. Hübers, C. Neuwirth, M. Weber, G. Borck, M. Wahlqvist, K.M. Danzer, A.E. Volk, T. Meitinger, T.M. Strom, M. Otto, J. Kassubek, A.C. Ludolph, P.M. Andersen, J. H. Weishaupt, NEK1 mutations in familial amyotrophic lateral sclerosis, *Brain* 139 (2016) e28.
- [126] M.J. Surpili, T.M. Delben, J. Kobarg, Identification of proteins that interact with the central coiled-coil region of the human protein kinase NEK1, *Biochemistry* 42 (2003) 15369–15376.
- [127] P. Amin, M. Florez, A. Najafov, H. Pan, J. Geng, D. Ofengeim, S.A. Dziedzic, H. Wang, V.J. Barrett, Y. Ito, M.J. LaVoie, J. Yuan, Regulation of a distinct activated RIPK1 intermediate bridging complex I and complex II in TNF $\alpha$ -mediated apoptosis, *Proc. Natl. Acad. Sci. U. S. A.* 115 (2018) E5944–E5953.
- [128] J. Higelin, A. Catanese, L.L. Semelink-Sedlacek, S. Oeztuerk, A.K. Lutz, J. Bausinger, G. Barbi, G. Speit, P.M. Andersen, A.C. Ludolph, M. Demestre, T. M. Boeckers, NEK1 loss-of-function mutation induces DNA damage accumulation in ALS patient-derived motoneurons, *Stem Cell Res.* 30 (2018) 150–162.
- [129] Y. Watanabe, T. Nakagawa, T. Akiyama, M. Nakagawa, N. Suzuki, H. Warita, M. Aoki, K. Nakayama, An amyotrophic lateral sclerosis-associated mutant of C21ORF2 is stabilized by NEK1-mediated hyperphosphorylation and the inability to bind FBXO3, *iScience* 23 (2020) 101491.
- [130] G. Baumann, T. Meckel, K. Böhm, Y.-H. Shih, M. Dickhaut, T. Reichardt, J. Pilakowski, U. Pehl, B. Schmidt, Illuminating a dark kinase: Structure-guided design, synthesis, and evaluation of a potent Nek1 inhibitor and its effects on the embryonic zebrafish pronephros, *J. Med. Chem.* (2021), <https://doi.org/10.1021/acs.jmedchem.0c02118>.
- [131] M.J. Surpili, T.M. Delben, J. Kobarg, Identification of proteins that interact with the central coiled-coil region of the human protein kinase NEK1, *Biochemistry* 42 (2003) 15369–15376.
- [132] T.P. Heffron, Small molecule kinase inhibitors for the treatment of brain cancer, *J. Med. Chem.* 59 (2016) 10030–10066.
- [133] Y. Shi, M. Mader, Brain penetrant kinase inhibitors: Learning from kinase neuroscience discovery, *Bioorg. Med. Chem. Lett.* 28 (2018) 1981–1991.
- [134] G. Griebel, J. Stemmelin, M. Lopez-Grancha, D. Boulay, G. Boquet, F. Slowinski, P. Pichat, S. Beeské, S. Tanaka, A. Mori, M. Fujimura, J. Eguchi, The selective GSK3 inhibitor, SAR502250, displays neuroprotective activity and attenuates behavioral impairments in models of neuropsychiatric symptoms of Alzheimer's disease in rodents, *Sci. Rep.* 9 (2019) 18045.
- [135] D. Paris, G. Ait-Ghezala, C. Bachmeier, G. Laco, D. Beaulieu-Abdelahad, Y. Lin, C. Jin, F. Crawford, M. Mullan, The spleen tyrosine kinase (Syk) regulates Alzheimer amyloid- $\beta$  production and Tau hyperphosphorylation, *J. Biol. Chem.* 289 (2014) 33927–33944.



**Alison Axtman, Ph.D.**, is a Principal Investigator in Medicinal Chemistry at SGC-UNC and Research Associate Professor in the Division of Chemical Biology and Medicinal Chemistry Department in the UNC Eshelman School of Pharmacy. Her interests lie at the interface of chemistry and biology, with a focus on using small molecules to explore and impact disease-propagating biological pathways, especially those that cause neurodegenerative diseases. Active projects are aimed at finding pre-clinical small molecule candidates that address the need for new therapeutics in the areas of amyotrophic lateral sclerosis (ALS) and Alzheimer's disease (AD), among others. She joined SGC-UNC after working at GlaxoSmithKline on the Chemical Biology team at the RTP site. Before that, Axtman completed her doctorate at the University of Kansas in the Department of Medicinal Chemistry with Brian Blagg and postdoctoral studies at Stanford University in the laboratory of Paul Wender. She is eager to enable the efforts of other investigators through sharing high-quality small molecule tools to speed the drug discovery process and more quickly help patients in need.